Viral infection and predation of phytoplankton residing in a turbulent environment

Thesis submitted in accordance
with the requirements of the
University of Liverpool
for the degree of
Doctor in Philosophy

by

Nicola Fairbank

January 2011

Abstract

This thesis investigates the spatial and temporal population dynamics of a coupled 3 component system (phytoplankton, virus and predator) in a turbulent environment. The scientific motivation for this is to understand the dynamics of harmful algal blooms in marine environments, in particular understanding the role of turbulence and swimming. The mathematical content combines small-scale fluid dynamics, models of turbulence, and population dynamics to develop a mean-field (PDE) model for the population dynamics which incorporates small-scale details of swimming and turbulence within relevant parameters. The main research is presented in 3 chapters.

Chapter 2 studies the contact rate of phytoplankton with viral particles and the encounter rate of phytoplankton with predators. Two distinct models are investigated: a diffusion model for viral concentration, based on previous models of nutrient uptake by phytoplankton, and a swept volume approach for the encounter rate between predator and prey, utilising a published encounter model for motile plankton in still fluid. The effect of swimming motion and turbulence on the contact rates is discussed with reference to published mathematical results. An investigation of how contact rates are affected by swimming and turbulence for realistic turbulent intensities and biologically realistic parameters for specific species is performed.

Chapter 3 presents and analyses a system of ODEs describing the population dynamics of a coupled phytoplankton-virus-predator system. Both long term dynamics and transient behaviours are investigated analytically and numerically, and specific species interactions are compared with published field and laboratory data. The plausibility of using a virus or predator as a method to control phytoplankton blooms is considered numerically. The results of Chapter 2 are incorporated into parameters of the ODEs to explore how the population dynamics are affected by swimming and turbulence. A comparison of how the choice of virus used affects the behaviour of the system is discussed.

Chapter 4 investigates spatial dynamics, extending the systems of ODEs presented in Chapter 3 to a coupled set of PDEs in which turbulence is modelled by spatial diffusion. Published data is utilised to allow realistic spatial variance to be incorporated into appropriate parameters. Long term and transient behaviours are investigated numerically and compared with the results of Chapter 3. The possibility of turbulence altering the outcome of competition between viruses and grazers is thus explored and the work of Chapter 3 on phytoplankton control is continued.

Contents

List of Figures

List of Tables

Chapter 1

Introduction

1.1 Motivation

The photosynthetic, microscopic, organisms known as phytoplankton can experience massive and prolonged overgrowth, known as an algal bloom (Dionysiou, 2010). The natural behaviour of these organisms is to bloom periodically during the year, particularly in the summer months, and then reduce to pre-bloom levels. Unfortunately, these blooms can be detrimental to our ecosystem, termed harmful algal blooms or HABs. Gunter et al. (1948) observed mass mortality of marine animals coincident with a phytoplankton bloom. It is now known that HABs can deplete oxygen levels in their surroundings and can also produce natural toxins (Dionysiou, 2010). Exposure to these toxins through skin contact or inhalation is now recognised to cause a range of illnesses in humans, which can be life threatening (Dionysiou, 2010). The economic impact of HABs has been estimated to be $50 million per year in the US, on average (Dionysiou, 2010).

Information regarding initiation, persistence and termination of HABS has thus been sought. Gunter et al. (1948) suggested that changes in meteorological conditions may have brought about increased supplies of nutrient salts, which may have been responsible for bloom initiation. Other factors such as increased light intensity, increased water temperature and selective grazing were also suggested as mechanisms potentially leading to phytoplankton blooms. Studies on the role of nutrient enrichment, grazers and light intensity, etc are still being performed (e.g. Yin et al., 2008; Buskey, 2008; Lanerolle et al., 2006). In terms of bloom termination, nutrient limitation is considered to be a factor, as is predator grazing (e.g. Holmes et al., 1967; Matsuyama et al., 1999; Strom et al., 2007). Even though virus-like particles were occasionally found in phytoplankton cells during early work (e.g. Dodds, 1979), it was Bergh et al. (1989) who first suggested that viral infection may be an important factor in controlling phytoplankton populations after finding the concentration of viral particles in natural water to be much higher than previously thought. Suttle et al. (1990) fully established

viral infection as a possible control mechanism after showing viruses could infect and lyse marine phytoplankton in the laboratory. Further work on the role of viruses in ceasing algal blooms and on estimating parameter values important in the interactions have been conducted over the last two decades (e.g. Bratbak et al., 1993; Nagasaki et al., 1999; Tarutani et al., 2000). Alongside this experimental research, population dynamics of phytoplankton-virus (e.g. Bratbak et al., 1998), phytoplankton-predator (e.g. Dubois, 1975) and phytoplankton-virus-predator (e.g. Beltrami and Carroll, 1994) systems have been considered mathematically. Vargo (2009) list the currently postulated mechanisms for bloom termination to be cyst formation, cell death, cell lysis due to lytic bacteria or viruses, nutrient limitation, grazing, advection, dilution or disruption of physical concentration mechanisms. The effectiveness of these mechanisms is also subject to other factors. For instance, grazers will themselves be predated upon and Rhodes and Martin (2010) found there to be a critical level of nutrient in a phytoplankton-virus-predator model above which the virus becomes extinct.

In this thesis, we have chosen to specifically consider bloom termination, comparing predator grazing and viral infection as control mechanisms. We consider a full phytoplankton-virus-predator model in different flow regimes in order to gauge the effects of spatial heterogeneity on the system. We tie in with current experimental research by considering specific species throughout and comparing the phytoplankton-virus model and phytoplankton-predator model against published observations from the field and mesocosms.

A free-living viral infection model and predator-prey model are combined and used to investigate how the incorporation of viral infection and predation alter the temporal population dynamics of phytoplankton. Small scale fluid dynamics are considered to establish how plankton swimming and turbulence will affect the rate at which the phytoplankton-virus and phytoplankton-predator achieve contact. The impact of spatial heterogeneity is then considered by adding a diffusion term into the population model, to represent turbulence, and allowing spatial variance of parameter values.

This chapter provides background information for the work in the thesis and a review of current literature. Section 1.2 introduces phytoplankton and the science of the environment in which they reside. Discussion of the specific phytoplankton species considered throughout the thesis is also included in the section. We then give background information on the population dynamics, including predation and viral infection, in section 1.3. The predator species used in the thesis is discussed, as are predator-prey models. The phytoplankton-predator contact rate is also discussed in the section. There is a discussion of viruses generally, before looking at a specific virus to be considered throughout. We also introduce viral infection models and the theory behind phytoplankton-virus contact. We then move on to the incorporation of spatial heterogeneity into the system in section 1.4. Turbulence and how to model it is considered, followed by a discussion of the PDE system used.

1.2 Phytoplankton

Phytoplankton are microscopic plants that live in the ocean. There are many species of phytoplankton, which have many different characteristics. For example, many are motile, which is a characteristic of the phytoplankton we will model. Collectively, phytoplankton grow abundantly in oceans around the world and are the foundation of the marine food chain (Boney, 1989). Phytoplankton are consumed as food by zooplankton, which in turn are eaten by fish. Phytoplankton require sunlight, water and nutrients for growth (Boney, 1989). They also contain the pigment chlorophyll, which is used for photosynthesis. Phytoplankton are good indicators of changes in their environment (Hays et al., 2005). Since phytoplankton depend upon certain conditions for growth, variance in any of these conditions (sunlight, water, nutrients, etc) over time for a given region will affect the phytoplankton concentrations there. It is this dependence of phytoplankton on key resources that prevents their populations from growing exponentially indefinitely. For any given quantity of resources in a particular location there will be a maximum phytoplankton population level, above which it can no longer sustain itself. This maximum level is called a carrying capacity. Phytoplankton also play a key role in climate change (Falkowski and Wilson, 1992) since, when they die, they can carry atmospheric carbon dioxide to the bottom layers of the ocean. However, if, for example, they are eaten by fish (who respire), the carbon returns to the atmosphere. Turbulence can aid phytoplankton growth by transporting essential nutrients from the deeper layers of the ocean to the upper sunlit layers. However, the mixing generated by turbulence also spreads the phytoplankton throughout the water column. Pingree et al. (1975) noted the understanding of primary production in the sea to be hampered by an inadequate knowledge of the turbulent environment in which the phytoplankton exist. Therefore, when modelling phytoplankton populations, population dynamics such as growth, predation, etc are important (considered in Chapter 3), as is the spatial position of the population (considered in Chapter 4).

1.2.1 *Heterosigma akashiwo*

We will consider general, theoretical information regarding the impact of predation, viral infection and spatial heterogeneity on phytoplankton populations, but we also wish to make specific calculations, requiring us to specify an example phytoplankton species. Since we are considering control of harmful algal blooms, we will choose a species known to be responsible for damaging our ecosystem. There are many such species of phytoplankton, so we have also taken into account the information available to us in the literature, which we intend to use in our models. We require a species that is thought to be controllable by a known virus and also by a known predator.

Heterosigma akashiwo is known to be responsible for the mass-mortality of cultured fish in the coastal seas of temperate and subarctic areas (Nagasaki, Ando, Itakura, Imai

and Ishida, 1994). The means by which *H. akashiwo* is toxic to fish is currently unclear (Clough and Strom, 2005), but at least three viruses known to infect *H. akashiwo* have been isolated. Observed population data of the interactions between *H. akashiwo* and one of these viruses is available in the literature (Tarutani et al., 2000). *H. akashiwo* also has a number of predators, one of which has been observed interacting with *H. akashiwo* and the results represented in a form to be used in a mathematical model (Jeong et al., 2003). Thus, *H. akashiwo* will be used as an example phytoplankton species throughout the thesis.

1.3 Population Dynamics

1.3.1 Predator grazing

Pennington (1941) observed small invertebrates to be capable of rapidly decreasing a phytoplankton population, thus acting as a control of the phytoplankton. Anderson et al. (1955) further presented data on the relationships between phytoplankton and zooplankton in two saline lakes in Central Washington, which indicated an inverse relationship between phytoplankton and zooplankton. There has since been growing evidence that grazing of phytoplankton by microzooplankton is one of the most important features controlling phytoplankton population levels. For example, Holmes et al. (1967) observed grazing to decimate a dinoflagellate bloom in California. However, consideration of *Daphnia magna* grazing on the alga *Sphaerocystis schroeteri* by Porter (1976) showed that most of the algal cells emerged from the predator intact. Enhanced algal growth was observed after gut passage, since viable algal cells take up nutrients when passing through the predator's gut. Also, study of the standing crop and production relationships of bacteria, phytoplankton and zooplankton by Coveney et al. (1977) found nongrazing losses of phytoplankton to outweigh grazing losses. Nevertheless, whilst current research also focuses on bottom-up control mechanisms such as nutrient limitation, grazing is still considered to be an important factor (e.g. Matsuyama et al., 1999; Strom et al., 2007; Rejas and Muylaert, 2010).

H. akashiwo predators

Graham and Strom (2010) found *H. akashiwo* to be harmful to a number of microzooplankton grazers and found some grazers to avoid *H. akashiwo* in favour of other non-toxic prey. However, in natural bloom samples, phytoplankton species other than *H. akashiwo* are often more abundant even though *H. akashiwo* appeared to be a better competitor for nutrients, suggesting mechanisms such as grazing may be reducing this competitive advantage of *H. akashiwo* (Demir et al., 2008). *H. akashiwo* has the potential to be good prey for protists and microzooplankton due to these grazers being known to consume phytoplankton of a similar size, form and structure (Clough

and Strom, 2005). Jeong et al. (2003) found the heterotrophic dinoflagellate *Oxyrrhis marina* to be the most dominant heterotrophic protist in blooms dominated by *H. akashiwo*. The authors measured the growth and grazing rates of *O. marina* on *H. akashiwo* in the lab. and mesocosms in nature, observing a decline in the *H. akashiwo* population to correspond with an increase in the *O. marina* population. Jeong et al. (2003) fitted their observations to grazing functions, described in the 'Modelling predation' section. Due to the availability of this parameterisation of *O. marina's* consumption of *H. akashiwo*, we will use *O. marina* as our example species here. Menden-Deuer and Grünbaum (2006) investigated the behaviour of *O. marina*, finding its swimming speed in the presence of prey *Isochrysis galbana* to have an average value of $339\mu\text{ms}^{-1}$. We will take this to also be the average swimming speed of *O. marina* in the presence of *H. akashiwo*.

Modelling predation

The first mathematical representation of predator-prey interactions were those of Lotka and Volterra (derived separately by each at around the same time):

$$\frac{dP}{dt} = P(a - bZ), \tag{1.1}$$

$$\frac{dZ}{dt} = Z(cP - d), \tag{1.2}$$

where P and Z represent the population density of prey and predator respectively, the quantities a, b and c being positive constants (Murray, 2003). From these equations, in the absence of predation, the growth of the prey is exponential. Removal of prey is via grazing only, a relationship that is also linear with no upper limit. Growth of the predator is solely through consumption of the prey species and the population decays via the death rate, d. Thus, in the absence of prey, the predator population becomes extinct. This simple model forms the basis of how predator-prey interactions are modelled today, but certain modifications are generally made. This is due to the coexistence equilibrium being neutrally stable, meaning that phase-plane trajectories are closed. Any small perturbation will move the solution onto another trajectory, which does not, everywhere, lie close to the original solution (Murray, 2003). However, small alterations to the system can make the model much more reasonable for real populations. Introducing self-regulation into the prey growth term is one such alteration, making the coexistence equilibrium stable rather than neutrally stable. Self-regulating growth is reasonable when considering phytoplankton since their growth is dependent on nutrient and light levels, for example. Another useful modification is to incorporate limitation into the predation rate. We therefore consider phytoplankton-predator interactions with a set of equations of the form:

$$\frac{dP}{dt} = rP\left(1 - \frac{P}{K}\right) - ZG(P), \tag{1.3}$$

$$\frac{dZ}{dt} = \gamma ZG(P) - \nu Z. \tag{1.4}$$

The first term in the phytoplankton population equation is called a logistic growth function. The maximum growth rate of the phytoplankton is r and K is the carrying capacity of the population, the maximum population level at which the phytoplankton population can sustain itself. The grazing function is $G(P)$, the growth of the predator being some proportion, γ, of this function. Finally, ν is the death rate of the predator. There are a wide choice of grazing functions. We will consider those described by Holling.

Holling (1959) describes the functional responses of predators to have three basic forms. Holling's Type I, represented by

$$G(P) = R_m P, \tag{1.5}$$

where R_m is a biological constant, is a linear function. This represents a predator whose pattern of searching is random and whose rate of searching remains constant at all prey densities. Thus, the number of prey consumed per predator would be directly proportional to prey density. This type of response was first noted by William Ricker in 1941. Note, Holling (1959) remarks that all functional responses must have an upper limit. Consumption cannot rise indefinitely.

Holling's Type II (or Michaelis-Menten), is of the form

$$G(P) = R_m \frac{P}{\alpha + P}, \tag{1.6}$$

where α, a biological constant, allows for the predators to become satisfied. Here, the rates of searching become progressively less as prey density increases. This more complex functional response seems first to have been noted by Paul De Bach and Harry Smith in 1941. Holling's Type III, represented by

$$G(P) = R_m \frac{P^2}{\alpha^2 + P^2}, \tag{1.7}$$

adds the feature that if the population of prey is very low, the predators may find it harder to catch them. This functional response was first demonstrated by Holling (1959).

All three predatory responses have been used to model the predator-prey dynamics of plankton. Truscott and Brindley (1994) model a plankton system where the prey grows logistically and the predator grazes with a Holling Type III response. They trigger "blooms" by setting initial conditions slightly away from equilibrium values.

Cropp and Norbury (2009) use a Holling Type II response to consider the predator-prey interactions in a plankton food web model. Carpenter et al. (1994) found the linear response to be the best grazing model when fitting models to time series of plankton in two lakes.

An alternative approach found in the literature is to separate the grazing response into predator ingestion rate, termed the functional response, $G(P)$, and predator growth rate, known as the numerical response, $H(P)$, rather than taking the predator growth rate to be a proportion of its ingestion rate as seen in model (1.3, 1.4). The model would then take the form:

$$\frac{dP}{dt} = rP\left(1-\frac{P}{K}\right) - ZG(P), \tag{1.8}$$

$$\frac{dZ}{dt} = ZH(P) - \nu Z. \tag{1.9}$$

Experimental investigations into the functional and numerical responses of micro-zooplankton have often found a Holling Type II (Michaelis-Menten) function of prey concentration to provide an adequate description (e.g. Heinbokel, 1978; Montagnes, 1996; Jeong et al., 2003; Kimmance et al., 2006). In the 1970s, it was suggested that there might be a threshold prey concentration beneath which the grazers reduce or cease grazing (Heinbokel (1978) and references therein). This type of behaviour can be incorporated into a grazing model when functional and numerical responses are considered separately. Montagnes (1996) believes establishing these threshold levels may be crucial when parameterising predator-prey models, as the predator can die from starvation as well as higher grazing. Heinbokel (1978) generated numerical response curves (predator growth rate against prey concentrations) for micro-zooplankton grazing on a variety of prey. The numerical response data was fitted to a Michaelis-Menten equation, which incorporates this threshold prey concentration. This numerical response is of the form:

$$H(P) = \frac{\mu_{\max}(P-p')}{K_{\mathrm{GR}} + (P-p')}, \tag{1.10}$$

where $\mu_{\max}$ is the maximum growth rate, p' is the threshold concentration (the prey concentration where $H(P) = 0$), K_{GR} is a half-saturation constant and P continues to represent prey concentration. Note that $P < p'$ represents mortality of the predator due to insufficient food supplies. Studies of *O. marina* grazing (e.g. Jeong et al., 2003; Kimmance et al., 2006) found *O. marina* to exhibit a threshold prey level, where its growth is zero. However, the studies were unable to detect a threshold level for *O. marina's* ingestion rate, thus determining the functional response to be best modelled by an unmodified Holling Type II equation. Jeong et al. (2003) determined the functional and numerical response for *O. marina* grazing upon *H. akashiwo* to be:

$$G(P) = \frac{I_{\max} P}{K_{\text{IR}} + P}, \tag{1.11}$$

$$H(P) = \frac{\mu_{\max}(P - p')}{K_{\text{GR}} + P - p'}, \tag{1.12}$$

where $I_{\max}$ is the maximum ingestion rate of the predator and K_{IR} is the prey concentration sustaining $\frac{1}{2} I_{\max}$. The parameter values specific to *H. akashiwo* and *O. marina* are provided in Jeong et al. (2003) and will be used in this thesis. The two studies conducted by Jeong et al. (2003) (to determine both functional and numerical responses) were consistent in terms of location and organism, *O. marina* grazing on cultured *H. akashiwo* in a mesocosm. We include logistic phytoplankton growth and a predator death rate, ν, to give the model:

$$\frac{dP}{dt} = rP\left(1 - \frac{P}{K}\right) - \frac{I_{\max} P Z}{K_{\text{IR}} + P}, \tag{1.13}$$

$$\frac{dZ}{dt} = \frac{\mu_{\max}(P - p')Z}{K_{\text{GR}} + P - p'} - \nu Z, \tag{1.14}$$

which will be used throughout this thesis to represent the phytoplankton-predator interactions.

Phytoplankton-predator contact

Gerritsen and Strickler (1977) constructed a model of predator-prey encounter rates in 3-dimensional space. They considered predation of zooplankton, where both the predator and prey are motile. The predator is assumed to "sweep" through the fluid and an encounter occurs when its prey is within some pre-defined distance of the predator. Gerritsen and Strickler's (1977) encounter rate model has been used extensively in the literature (e.g. Bailey and Batty, 1983; Stelzer, 1998; Uttieri et al., 2010).

The effect of small-scale turbulence on the plankton encounter rate was first established by Rothschild and Osborn (1988), by including a correction for turbulence in the Gerritsen and Strickler (1977) model. Evans (1989) noted that Gerritsen and Strickler (1977) assumed all individuals in a population to move at the same speed and the Rothschild and Osborn (1988) correction does not yield a constant speed. Evans (1989) instead suggested the use of a Gaussian velocity distribution with the amendment for turbulence. Models of the form presented by both Rothschild and Osborn (1988) and Evans (1989) have been widely used to model the encounter rate of motile plankton in turbulent fluid (e.g. Muelbert et al., 1994; Visser et al., 2009; Pecseli et al., 2010). Lewis and Pedley (2000) also consider, from first principles, the encounter rate of motile plankton in a turbulent fluid. They argue that the approach of Rothschild and Osborn (1988) is problematic due to their encounter rate differing to that

of Gerritsen and Strickler (1977) when both plankton species are non-motile. Lewis and Pedley (2000) also discuss confusion in the Rothschild and Osborn (1988) model regarding what a distance parameter present in the encounter model actually represents and also a lack of information present in the Gerritsen and Strickler (1977) and Rothschild and Osborn (1988) models about possible changes in swimming trajectory during the time period considered. However, Lewis and Pedley's (2000) model has currently received more limited usage in the literature (e.g. Metcalfe et al., 2004; Rhodes and Anderson, 2008).

1.3.2 Viral Infection

There are an estimated 10^{30} viruses in the ocean and, every second, approximately 10^{23} viral infections occur (Suttle, 2007). Viruses do not respire, move or grow. They are completely dependent on their host cells for multiplication (Brussaard, 2004). Viruses consist of DNA or RNA, which can be single-stranded or double-stranded. This is surrounded by a protective layer of protein called a capsid (Willey et al., 2007). Viruses are only 20 to 200 nanometres long (Nybakken and Bertness, 2005).

Viruses can exist in two states: outside of host cells and inside host cells. Virions are free-living virus particles which exist extracellularly and cannot reproduce independent of living host cells (Willey et al., 2007). These particles must pass through the water and be adsorbed by host cells if the virus is to spread, but during this stage the particles may be destroyed. The longer the delay in finding a new host, the greater the risk of destruction for the particle (Murray and Jackson, 1992).

In the intracellular phase, viruses exist within infected host cells where they either direct the hosts to produce progeny viruses, or integrate their nucleic acid with the hosts' genome. The former type of reproduction, which is what will be considered in this thesis, is called lytic infection and will result in lysis of the host and release of progeny viruses (virions). The burst size is the number of virions released per infected cell. The length of the lytic cycle (latent period) and the burst size are important in terms of spread of the infection. Also, the higher the abundance of the virus, the higher the phytoplankton-virus contact rate, discussed later in this section. The latter type of reproduction is referred to as lysogeny (or latency). The viral genome reproduces with the host genome until an induction event triggers the virus into lytic reproduction (Brussaard, 2004). A virus capable of both lytic and lysogenic reproduction is known as a temperate virus (Evans et al., 2007).

The existence of bacterial viruses was established in the early 20^{th} Century within the field of medicine (Willey et al., 2007). These viruses were named bacteriophages (or just phages). Evidence for viral infection of eukaryotic algae only began to emerge in the 1960's (see Suttle (2000) and references therein) and there is still much less known about viruses infecting phytoplankton than viruses infecting bacteria. Currently, only

one algal species has been found to contain lysogens (Tarutani et al., 2006). All other host-virus systems isolated to date are lytic (Thyrhaug et al., 2003), and we shall therefore only consider lytic viruses in this thesis. Lytic viruses are a major cause of marine phytoplankton mortality (Graham and Wilcox, 2000). There have been several reports that viruses are involved in the termination of algal blooms (e.g. Nagasaki et al. (1999); Tarutani et al. (2000);Bratbak et al. (1993)).

H. akashiwo viruses

As discussed in section 1.2.1, *H. akashiwo* will be used as an example phytoplankton species. We therefore require information regarding viruses infecting *H. akashiwo* so one can be chosen as an example virus species.

The first virus-like particles observed in *H. akashiwo* were documented by Nagasaki, Ando, Imai, Itakura and Ishida (1994). The link between these virus-like particles and the involvement of viral lysis in the final stage of a *H. akashiwo* bloom was suggested by Nagasaki, Ando, Itakura, Imai and Ishida (1994). In 1996, Nagasaki and Yamaguchi (1997) isolated a virus infecting *H. akashiwo* and named it HaV (*H. akashiwo* Virus). The same paper gave the diameter of the virus particle to be 202 ± 6nm. Nagasaki et al. (1999) estimated the latent period of HaV (clone 01) to be 30-33h and its burst size to be 7.7×10^2 lysis-causing units per infected cell. Nagasaki et al. (1999) also went on to suggest that, from the viewpoint of scale and cost, the use of HaV as a microbiological agent against *H. akashiwo* may be promising. Observations of *H. akashiwo* and HaV in the field were depicted in Tarutani et al. (2000) and will be used in Chapter 3 to compare the model results against.

So far, at least two other viruses have been reported to infect *H. akashiwo*. One is HaNIV (*H. akashiwo* Nuclear Inclusion Virus), described by Lawrence et al. (2001). The diameter is reported to be $\sim$ 30nm and they estimated the burst size to be 10^5 virions per cell lysis. The latent period was found to be in the region of 42h. The virus HaRNAV (*H. akashiwo* RNA Virus), the first reported single-stranded RNA virus causing lysis of phytoplankton, was presented by Tai et al. (2003). This virus was found to have a burst size of 21000 virions per cell and a latent period of 29h, by Lawrence et al. (2006).

Due to the largest volume of literature, and observed population data, being available for HaV, we chose to use this as our example virus throughout the thesis. However, the large variation in diameter and burst size for these three different viruses may be important in determining the phytoplankton-virus population dynamics. A comparison of how these three different viruses affect the population dynamics is therefore made in section 3.3.7.

Modelling viral infection

There appear to be two forms of model available when considering the spread of infection: those where the virus is considered explicitly and those where its presence is implicit. The former is referred to as a free-living model. The first model suggested to study the effects of viral infection on phytoplankton population dynamics was proposed by Beltrami and Carroll (1994), and is of the type where the virus is not considered explicitly:

$$\frac{dP}{dt} = rP\left(1-\frac{P+I}{K}\right) - aPZ - b\frac{PI}{P+I} \tag{1.15}$$

$$\frac{dI}{dt} = b\frac{PI}{P+I} - qIZ - \alpha I, \tag{1.16}$$

$$\frac{dZ}{dt} = aPZ + qIZ - dZ, \tag{1.17}$$

where P represents the population of phytoplankton susceptible to infection, I is the population of infected phytoplankton, K is the carrying capacity, b represents transmission of the infection between infected phytoplankton and susceptible phytoplankton and α is the pathogen induced death rate. The other terms correspond to a linear predation response: a being the rate of consumption of susceptibles, q the rate of consumption of infecteds and d the death rate of the predator. Beltrami and Carroll (1994) found that, for this model in the absence of viral infection, there is a single susceptible phytoplankton-predator stable steady state. The inclusion of infected phytoplankton, even in very small numbers, allows two possible long term behaviours: a point-stable (P, I, Z) equilibrium or a (P, I, Z) limit cycle. The behaviour achieved is dependent on parameter values. Models of this type have been widely used to study the spread of infection, some of which study the infection of phytoplankton specifically (e.g. Sieber et al., 2007; Malchow et al., 2005; Chattopadhyay and Pal, 2002). Singh et al. (2004) considered a similar system to Beltrami and Carroll (1994) for phytoplankton (split into susceptible and infected) and their predator, but with a linear viral transmission term and infected prey being more vulnerable to grazing than susceptibles. Singh et al. (2004) found a threshold of force of infection. Below this threshold the infection cannot be sustained. They found coexistence of the susceptible phytoplankton, infected phytoplankton and zooplankton predator, this coexistence being locally asymptotically stable in some region of parameter space and exhibiting limit cycle oscillations at some other regions.

Both the Beltrami and Carroll (1994) and Singh et al. (2004) models deal with viral contamination due to direct contact between susceptible and infected cells, but don't explicitly represent the interactions between free-living viral particles and susceptible phytoplankton cells. However, Beltrami and Carroll (1994) do highlight that this model is adequate if the number of viral particles is proportional to the number of infected

cells. It may also be reasonable to neglect the free-living virus population if the virions decay quickly compared to the timescale of other processes in the system (Rhodes et al., 2008). However, we here consider the virus explicitly so as to allow a better understanding of the phytoplankton-virus interactions and the relative importance of parameters such as burst size.

We consider the alternative approach to model the spread of infection of microparasites offered by Anderson and May (1981), where the free-living infective stages are included explicitly:

$$\frac{dP}{dt} = a(P+I) - \beta P - \nu PV + \mu I \tag{1.18}$$

$$\frac{dI}{dt} = \nu PV - (\alpha + \beta + \mu)I \tag{1.19}$$

$$\frac{dV}{dt} = \lambda I - (\gamma + \nu(P+I))V, \tag{1.20}$$

where P and I are once again the population of susceptible and infected phytoplankton respectively, V is the population of free-living virus particles, a is the reproductive rate of both susceptibles and infecteds, β is the natural death rate of phytoplankton, α is the pathogen induced death rate, μ is the rate at which infected recover to susceptibles, ν is the transmission rate, λ is the rate at which free-living infective stages are produced and γ is the decay rate of the free-living infective stages.

Bratbak et al. (1998) took a similar approach when modelling interactions between the marine alga *Phaeocystis pouchetii* and the lytic virus pVO1. They proposed the following delay differential equation model:

$$\frac{dP}{dt} = rP - \mathrm{c_v}\sigma_1\sigma_2 PV \tag{1.21}$$

$$\frac{dI}{dt} = \mathrm{c_v}\sigma_1\sigma_2 PV - \mathrm{c_v}\sigma_1\sigma_2 P_{t-\tau}V_{t-\tau} \tag{1.22}$$

$$\frac{dV}{dt} = m\mathrm{c_v}\sigma_1\sigma_2 P_{t-\tau}V_{t-\tau} - \mathrm{c_v}\sigma_1 V(P+I) - \gamma V. \tag{1.23}$$

Here P, I and V are the population of susceptible phytoplankton, infected phytoplankton and free-living virus particles respectively, r is the growth rate of susceptible phytoplankton, $\mathrm{c_v}$ is the volume clearance rate between virus and host cells (found using the method in Murray and Jackson (1992) and discussed later in this section), σ_1 is the fraction of viruses colliding with a host cell that actually adsorb to it, σ_2 is the fraction of adsorbed viruses that infected a host cell, τ is the time between infection and lysis of a cell (known as the length of the lytic cycle or latent period) and γ is the decay rate for the virus. This model has the advantage that parameters such as the burst size and contact rate feature explicitly.

Gons et al. (2006) used this Bratbak et al. (1998) model to simulate the host-virus dynamics of the cyanobacterium *Limnothrix* sp., with a hypothetical cyanophage.

They found that for low value burst sizes the virus had no significant effect on the host population level. For larger burst sizes, increasing the burst size decreased the maximum host population density. Also, the host population started to diminish sooner for larger burst sizes. In the model simulations, the host population would always recover after the first collapse, regardless of burst size.

The model as presented in Bratbak et al. (1998) predicts extinction of both the alga and its virus. However, coexistence between a host and its virus has been reported (e.g. Lawrence et al. (2006)). Thyrhaug et al. (2003) achieve coexistence in the model by adding an inhibiting factor, which could represent many decayable mechanisms that reduce the frequency of collisions leading to adsorption. Thyrhaug et al. (2003) propose the following:

$$\frac{dP}{dt} = rP - \mathrm{c_v}\frac{\sigma_1}{1+H}\sigma_2 PV \tag{1.24}$$

$$\frac{dV}{dt} = m\mathrm{c_v}\frac{\sigma_1}{1+H(t-\tau)}\sigma_2 P_{t-\tau}V_{t-\tau} - \mathrm{c_v}\frac{\sigma_1}{1+H}PV - \gamma V \tag{1.25}$$

$$\frac{dH}{dt} = k\mathrm{c_v}\frac{\sigma_1}{1+H(t-\tau)}\sigma_2 P(t-\tau)V(t-\tau) - \gamma_H H, \tag{1.26}$$

where H is an inhibiting factor, γ_H is the inhibitor decay rate and k is the amount of inhibitor released per lytic event. However, the inclusion of an inhibitor appears to be unnecessary. Simply replacing the linear phytoplankton growth term in Bratbak et al. (1998) with a logistic growth term will make phytoplankton-virus coexistence possible. Others, such as Singh et al. (2004) and Rhodes et al. (2008), have also found coexistence in prey-virus-predator models without the use of an inhibitor.

Rhodes et al. (2008) consider two models in their investigation into viral infection of phytoplankton. The first model is a nutrient-phytoplankton-zooplankton-detritus model, with the inclusion of viral infection (and separate free-living viral particle class). Here, only the susceptible phytoplankton reproduce. Phytoplankton grow with a Holling Type II response to nutrients and the zooplankton predation function is of Holling Type III form. This model addresses seasonal variance in phytoplankton populations, whilst the second model enables a bloom to be triggered, negating the need for more complex behaviour to be included to instigate a bloom. Two models were used in order to increase confidence in the results. The authors concluded the second model was less useful in modelling long-term behaviour since phytoplankton, virus and zooplankton could only coexist during plankton limit cycles, whereas observations suggest plankton and viruses stably coexist. Similarly to Singh et al. (2004), Rhodes et al. (2008) found a threshold value of the viral transmission rate, below which the virus decays to zero when introduced to the system and above which the virus persists at a stable level indefinitely. Rhodes et al. (2008) also found that presence of the virus stably suppressed the phytoplankton population, unlike what was seen in Beltrami and

Carroll (1994). High levels of the virus transmission rate saw the emergence of limit cycle behaviour of the plankton and virus in both Singh et al. (2004) and Rhodes et al. (2008). Rhodes et al. (2008) hypothesize that if a highly transmissible virus were to emerge, it would become extinct during a deep trough of the limit cycles.

In Chapter 3 we investigate phytoplankton-virus population dynamics, using a model based on that proposed by Bratbak et al. (1998). For simplicity, we will assume that the transition from susceptible phytoplankton to free-living virion is instantaneous. Elimination of an infected class would be acceptable if the length of the lytic cycle (latent period) was short compared with other processes in the model. This may be appropriate here since we take the phytoplankton growth rate, r, to be $2\mathrm{d}^{-1}$ throughout the thesis (the estimation of this parameter is given in section 3.2.2), which is larger than the typical latent period of 30-33 hours for the virus used as an example species, HaV. However, omission of an infected class won't always be acceptable as phytoplankton growth rate is highly variable and the latent period of the virus will vary between species. We also assume the phytoplankton to grow logistically, and couple in the predation model discussed in section 1.3.1 to give:

$$\frac{dP}{dt} = rP\left(1-\frac{P}{K}\right) - \mathrm{c_v}\sigma_1\sigma_2 PV - \frac{I_{\max}PZ}{K_{\mathrm{IR}}+P}; \tag{1.27}$$

$$\frac{dV}{dt} = m\mathrm{c_v}\sigma_1\sigma_2 PV - \mathrm{c_v}\sigma_1 PV - \gamma V = \lambda \mathrm{c_v}\sigma_1 PV - \gamma V; \tag{1.28}$$

$$\frac{dZ}{dt} = \frac{\mu_{\max}(P-p')}{K_{\mathrm{GR}}+P-p'}Z - \nu Z. \tag{1.29}$$

Phytoplankton-Virus Contact

In studying the use of a virus in controlling phytoplankton populations it is important to understand how a phytoplankton cell becomes infected. By modelling this interaction we can investigate how the rate of contact between the phytoplankton and virus is affected by turbulence and phytoplankton swimming, and find other factors important in determining the contact rate.

Murray and Jackson (1992) describe the transport of aquatic viruses to particles in terms of diffusive transport theory. The virus is treated as a solute, diffusing due to Brownian motion. The phytoplankton-virus contact rate is written in terms of the Sherwood number, a non-dimensional quantity representing the enhancement of virion flux across a phytoplankton cell wall due to fluid motions. The Sherwood number is related to the Péclet number, which is a non-dimensional quantity representing the relative importance of advection to diffusion. Murray and Jackson (1992) noted that fluid flow generated by particle motion or shear enhances viral transport to a particle more than it enhances transport of a small molecule, such as nutrients. They found transport to larger particles to be more influenced by particle motion than that to smaller particles. The paper also investigated the removal of viruses from solution.

Karp-Boss et al. (1996) conducted a thorough review of diffusive transport theory, applied to phytoplankton-nutrient interactions. They also added their own expressions for the Sherwood number, found by interpolation, to fill gaps in current knowledge. They considered four flow regimes: motile phytoplankton in still fluid, non-motile phytoplankton in shear flow, non-motile phytoplankton in turbulent flow and motile phytoplankton in turbulent flow. In Chapter 2 we follow this work by Karp-Boss et al. (1996), applying it to phytoplankton-virus interactions, considering the effects of turbulence as well as phytoplankton swimming.

1.4 Spatial Heterogeneity

So far we have discussed the population dynamics of phytoplankton and how to model fluctuations in their population over time. However, this ignores the spatial heterogeneity inherent in phytoplankton populations. In Chapter 4 we consider the effects of spatial heterogeneity on the population dynamics by incorporating turbulence into our phytoplankton-virus-predator model and by allowing some key parameters to vary with depth. Section 1.4.1 introduces the equations used to model fluid motion and introduces the Reynolds number, a dimensionless quantity representing the importance of inertial forces compared to viscous forces. Section 1.4.2 introduces some of the effects of turbulence on phytoplankton and discusses the different length scales involved in a turbulent environment. In section 1.4.3 we discuss how to model turbulence and section 1.4.4 then discusses incorporation of turbulence into our population model.

1.4.1 Equations of motion

Mathematically, fluid flow is modelled by the equations of motion, also known as the Navier-Stokes equations, of an incompressible fluid (Tennekes and Lumley, 1972):

$$\frac{\partial u_i'}{\partial t} + u_j' \frac{\partial u_i'}{\partial x_j} = -\frac{1}{\rho}\left(\frac{\partial p}{\partial x_i} - \mu \frac{\partial^2 u_i'}{\partial x_j \partial x_j}\right) \tag{1.30}$$

$$\nabla \cdot u_i' = 0, \tag{1.31}$$

where u_i' is the i^{th} component of the fluid velocity, ρ is the density (assumed constant) and p is the fluid pressure and μ is the dynamic, or molecular, viscosity. The kinematic viscosity is defined as $\nu = \frac{\mu}{\rho}$. The term $u_j' \frac{\partial u_i'}{\partial x_j}$ represents inertial forces, while $\frac{\mu}{\rho} \frac{\partial^2 u_i'}{\partial x_j \partial x_j}$ represents molecular dissipation of momentum. If we non-dimensionalise on a characteristic length L, e.g. the width of the domain, and a typical velocity U, e.g. the incoming flow, equation (1.30) becomes:

$$\frac{\partial u_i'}{\partial t} + u_j' \frac{\partial u_i'}{\partial x_j} = -\frac{\partial p}{\partial x_i} + \frac{1}{\mathrm{Re}} \frac{\partial u_i'}{\partial x_j \partial x_j}, \tag{1.32}$$

where $\mathrm{Re} = \frac{\rho LU}{\mu}$ is the Reynolds number. This is a dimensionless quantity equal to the inertial forces divided by viscous forces. The parameter was defined by Reynolds in 1883 when considering the transition of flow along a straight, smooth pipe from laminar (smooth, regular motion) to turbulent (chaotic, random motion) flow (Davidson, 2006). Consider the flow field around a swimming phytoplankton. The phytoplankton species *Heterosigma akashiwo* is $10 - 25 \times 10^{-6}$m in length (Smayda, 1998) with swimming speed $20-160\times10^{-6}\mathrm{ms}^{-1}$ (Smayda, 1998). If we use a characteristic length of $L = 15\times 10^{-6}$m and a characteristic swimming speed of $U = 100\times10^{-6}\mathrm{ms}^{-1}$, then the Reynolds number for this organism swimming in water [1] is of the order 10^{-3}. This value is much smaller than unity and thus viscous forces dominate locally to the phytoplankton. Phytoplankton swimming in still fluid will be modelled as the flow past a spherical phytoplankton cell in Stokes flow, that is zero-Reynolds number hydrodynamics, in section 2.3.1. A large Reynolds number signifies turbulent flow, which may be found when considering large scale oceanic motions, such as wind driven disturbance.

1.4.2 Turbulence

It is the presence of turbulence in water, the habitat of phytoplankton, that draws our attention to it here. Turbulence acts to mix and spread oceanic matter, working on a much faster timescale than molecular diffusion. Platt (1972) hypothesised that the local concentration of phytoplankton is largely controlled by turbulence. Kemp and Mitsch (1979) observed from their model that, in the absence of water motion, no two phytoplankton species were able to coexist. For advection in the absence of turbulence, two species were able to coexist. The introduction of turbulence allowed coexistence of all three phytoplankton species considered. The competitive exclusion principle, detailed by Hardin (1960), states that when two species compete for the same limited resources one of the species usually becomes extinct (Murray, 2003). Hutchinson (1961) notes the apparent paradox of plankton since many species of competitors are observed to coexist in a small volume of water. The results of Kemp and Mitsch (1979) suggest that turbulence may be a mechanism for coexistence between phytoplankton species.

Turbulence consists of eddies of many different sizes (Okubo and Levin, 2002). An eddy is a current moving contrary to the direction of the main current, especially in a circular motion. The separation between the largest and the smallest turbulent length scales (or eddy length scales) is determined by the Reynolds number. Energy is supplied to the larger length scales through external processes, for example, winds or currents. As these large eddies become unstable, they transfer their energy to smaller and smaller eddies. For large eddies, the effects of viscosity are negligible. However, smaller eddies finally reach a size where viscosity can no longer be ignored and at this point energy will begin to dissipate into heat (Lazier and Mann, 1989). These smallest

[1] At a temperature of 20 °C where $\rho = 998.2\mathrm{kg\ m}^{-3}$ and $\mu = 1.003 \times 10^{-3}\mathrm{kg\ ms}^{-1}$.

scales of turbulence are known as the Kolmogorov microscales, η and are dependent on the kinematic viscosity and the rate of dissipation (Abbott and Basco, 1989):

$$\eta = \left(\frac{\nu^3}{\epsilon}\right)^{\frac{1}{4}}. \tag{1.33}$$

In the oceanic upper mixed layer, the kinematic viscosity, $\nu \simeq 10^{-6}\mathrm{m}^2\mathrm{s}^{-1}$ and the dissipation rate, ϵ ranges from 10^{-6} to $10^{-9}\mathrm{m}^2\mathrm{s}^3$, which puts η roughly varying between 1 and 6mm. In comparison, energy generally first appears in eddies $1 - 10$m across (Lazier and Mann (1989) and references therein). More generally, length scales in the ocean can be much smaller than the $\sim 10^{-3}$m of Kolmogorov microscales. In particular, phytoplankton can be of the order 10^{-6}m whilst viruses and bacteria can be as small as 10^{-8}m. At these sub-Kolmogorov scales, shearing motion dominates. In section 2.3.2, when considering the interactions of phytoplankton with virus particles, which occur at the sub-Kolmogorov scales, we model advection due to small-scale turbulence as advection due to fluctuating shear flow.

1.4.3 Eddy diffusivity

Turbulence acts to mix passive contaminants, such as phytoplankton. Turbulence is often modelled by eddy diffusivity, of the form:

$$\frac{\partial C}{\partial t} = \kappa_z \frac{\partial^2 C}{\partial x_i \partial x_i}, \tag{1.34}$$

where κ_z is the eddy diffusivity (the amount of diffusion due to turbulence) and C is the concentration of some passive contaminant. Representing turbulence by eddy diffusivity is an ad-hoc process, but can be semi-justified as follows:

$$U_j \frac{\partial U_i}{\partial x_j} = \frac{1}{\rho}\frac{\partial}{\partial x_j}\left(\Sigma_{ij} - \overline{\rho u_i u_j}\right) \tag{1.35}$$

is equation (1.30) averaged over time with parameters decomposed into mean (denoted by an upper-case letter) and fluctuating (denoted by a lower-case letter) parts. The mean stress tensor is denoted by Σ_{ij}. The quantity $\overline{\rho u_i u_j}$, referred to as the Reynolds stress, represents the turbulent contribution to the dissipation of momentum. Boussinesq proposed that the effect of the turbulent mixing of momentum is analogous to the molecular transport of momentum (Davidson, 2006). Comparing equations (1.30) and (1.35), the Reynolds stress term is proposed to take the following form to represent mixing of momentum due to small-scale turbulence:

$$\frac{\partial}{\partial x_j}\left(\overline{\rho u_i u_j}\right) \equiv \rho \nu_{\mathrm{T}} \frac{\partial^2 U_i}{\partial x_j \partial x_j}, \tag{1.36}$$

where ν_{T} is the eddy viscosity (the amount of momentum transfer due to turbulence). Substituting into equation (1.35) gives:

$$U_j \frac{\partial U_i}{\partial x_j} = \frac{1}{\rho} \frac{\partial}{\partial x_j} \left(\Sigma_{ij} - \rho \nu_T \frac{\partial^2 U_i}{\partial x_j \partial x_j} \right). \tag{1.37}$$

Analogy can now be made between the way turbulence transports momentum and the way it transports passive contaminants, such as phytoplankton. Reynolds' analogy is based on the same eddies responsible for the transport of momentum being responsible for the transport of passive contaminants (Davidson, 2006), which leads to the introduction of the quantity eddy diffusivity. Comparing equation (1.37) with equation (1.30) and keeping only those terms representing mixing due to turbulence, we write the equation to represent diffusion of passive contaminants as:

$$\frac{\partial C}{\partial t} = \kappa_z \frac{\partial^2 C}{\partial x_i \partial x_i}, \tag{1.38}$$

where κ_z is the eddy diffusivity and C represents the passive contaminant.

An alternative approach is that of numerical simulation. A computational method, known as direct numerical simulation (DNS), attempts to explicitly solve the Navier-Stokes equations for eddies of all length scales. Orszag and Patterson (1972) were the first to demonstrate the feasibility of DNS models. However, over 30 years on, the computing power necessary to perform DNS for large Reynolds numbers is still not available. In order to facilitate relatively high Reynolds number, a small domain must be used (Davidson, 2006), which is inadequate for ocean-scale modelling.

Large eddy simulation (LES) models fall somewhere in between statistically averaged closure schemes (such as eddy diffusivity models) and DNS models. LES models can simulate flows of higher Reynolds number, compared with DNS models, since LES models only directly compute the large energy-containing eddies, whilst modelling the influence of the small scales (Moin and Mahesh, 1998). However, this method becomes problematic at the boundary, where eddies are small. A boundary layer can be incorporated in one of two ways. Either the resolution close to the boundary becomes so high that the LES model effectively becomes a DNS model, or the boundary layer can be considered separately (Davidson, 2006). In the latter case, the boundary layer could be modelled using a suitable closure scheme model and then patched back in to the full LES model (Davidson, 2006). Neither situation is ideal. LES models are attractive compared to DNS models since large scales are often more important (but not always). In DNS, virtually all effort goes into computing the small-to-intermediate scales (Davidson, 2006).

Both DNS and LES models have a high degree of accuracy, but they are still much more difficult to implement than statistically averaged closure schemes and are also computationally expensive. Eddy diffusivity, on the other hand, relies heavily on approximation, but is simpler and much less computationally expensive. The eddy diffusivity approach has been widely used when simulating phytoplankton (e.g. Bearon

et al., 2006; Ross and Sharples, 2004; Elliott and Thackeray, 2004), and will be used throughout this study.

1.4.4 A spatial population model

As discussed, turbulence will be modelled via a diffusion term with an eddy diffusivity parameter. However, this spreading and mixing component of turbulence isn't its only effect on the populations. For the case of non-motile phytoplankton residing in a turbulent environment considered in Chapter 4, both the $P-V$ and $P-Z$ contact rates depend on the energy dissipation rate. Data for the energy dissipation rate is used in Chapter 4 to calculate the eddy diffusivity. Thus, both contact rates will change with eddy diffusivity. Phytoplankton growth will also be affected by turbulence, although this isn't examined here. Since shearing motion is experienced at the smallest length scales considered, we are considering both shearing motion and large scale diffusion.

We embed spatial heterogeneity into spatially homogeneous population models. Our model is therefore a reaction-diffusion system of the form:

$$\frac{\partial \mathbf{C}}{\partial t} = \mathbf{f} + \nabla \cdot (\kappa_z \nabla \mathbf{C}), \tag{1.39}$$

where $\mathbf{C}$ is a vector of population concentrations. Each population is diffusing due to turbulence with a coefficient of eddy diffusivity, κ_z, as introduced in section 1.4.2. The reaction parts of the model, denoted by $\mathbf{f}$, encapsulate the population dynamics, as discussed in section 1.3. This approach, taking κ_z to be the diffusion coefficient of all three species, is a simplified approach that ignores possible correlation between the diffusing species. An alternative approach is explored by Pasquero (2005), who compared a reaction diffusion ecosystem model with an eddy diffusion parameterisation to one with an effective eddy diffusion parameterisation. An effective eddy diffusion coefficient is determined by Pasquero (2005), extending the work of Plumb (1979), based on the reaction time of the tracers considered. The effective diffusivity, κ_{eff}, is equal to the time-dependent single particle dispersion at the reaction time scale, T_{R} (Pasquero, 2005):

$$\kappa_{\text{eff}} = \frac{< [\mathbf{X}_j(t_0 + T_{\text{R}}) - \mathbf{X}_j(t_0)]^2 >}{2T_{\text{R}}}, \tag{1.40}$$

where $\mathbf{X}_j(t_0)$ is the position of the j^{th} particle at time t_0 and $<>$ represents ensemble average over all particles. The author found the effective eddy diffusion coefficient to be a better approximation, finding a non-modified eddy diffusion coefficient to overestimate the spreading of these tracers.

Model (1.39) is a population-level model. An alternative would be to use an individual-based model. However, numerical simulation of the movements of all individual cells in populations of phytoplankton on scales of metres and days is computationally unfeasible (Bearon and Grünbaum, 2008).

The boundary conditions used are no flux, signifying there will be no input or loss to the population from the surface or bottom of the water column:

$$\kappa_z \frac{\partial \mathbf{C}}{\partial z} = 0 \text{ at } z = 0, H, \tag{1.41}$$

where H is the height of the water column. No flux boundary conditions have been used previously in modelling phytoplankton (e.g. Huisman and Sommeijer, 2002). The virus and predator initial conditions are uniform throughout. Both uniform and non-uniform initial phytoplankton conditions are considered.

1.5 Thesis outline

This thesis investigates the use of viral infection and predation in controlling phytoplankton populations. Chapter 2 considers, separately, the contact rate between the phytoplankton and virus, and the phytoplankton and predator. The effects of a turbulent environment and motility of plankton are investigated. Firstly, the effects of swimming and turbulence on the phytoplankton-virus contact rate are compared. The work adapts that published by Karp-Boss et al. (1996) on nutrient uptake by phytoplankton, to consider virus 'uptake' by phytoplankton. The theory, which considers the effects of fluid motion on this 'uptake' rate, is based on classical theory for heat transfer to/from cells. Asymptotic results are verified, expressing the phytoplankton-virus contact rate explicitly as a function of biological parameters (virus and phytoplankton diameter, phytoplankton swimming speed) and of physical parameters (temperature, fluid viscosity). We extend the analysis of Murray and Jackson (1992) on phytoplankton-virus contact rates to include the effect of ambient flows, including steady shear and fluctuating shear (the latter being an appropriate approximation for turbulent flows at sufficiently small scales). The Sherwood number, Sh, (a measure of by how much particulate flux across the cell wall is enhanced due to fluid motion) is calculated, using asymptotic and interpolated expressions (which will be reviewed within the chapter), for motile cells in still water and non-motile cells in turbulent water.

For typical known size and swimming speeds of the phytoplankton species *H. akashiwo* and typical known size of HaV, phytoplankton swimming yields a larger Sherwood number than turbulence does. That is, compared to a pure molecular diffusion situation, phytoplankton swimming is found to increase the flux of viral particles into the cell by more than the introduction of a turbulent fluid flow. The effect of changing temperature and size of the phytoplankton and virus is also considered. An expression of Sherwood number for motile cells in turbulent water, when fluid motion is strong, is also available in Karp-Boss et al. (1996), originally derived by Batchelor (1980). The only component of phytoplankton swimming in this expression is the average swimming velocity parallel to the axis of rotation. However, in an isotropic

turbulent flow the average of this swimming velocity component is zero, leaving only the turbulence term in the Sherwood number equation. We thus investigate what happens when turbulence isn't so strong and quantify levels of turbulence intensity below which *H. akashiwo* swimming can affect the contact rate.

Secondly we study the effects of plankton swimming and turbulence on the phytoplankton-predator encounter rate. We review the study of Gerritsen and Strickler (1977) into how plankton swimming at fixed speeds affects the contact rate and then analyse the work of Lewis and Pedley (2000) to consider plankton swimming at fixed speeds in turbulent fluid. Limitations of the models when applied to a specific phytoplankton-predator system are established. Our calculations of the contact rate between the phytoplankter *H. akashiwo* and its predator *O. marina* found it to be unaffected by the inclusion of turbulence, for levels typically found in the upper oceanic mixed layer, to two significant figures. The ability of *H. akashiwo* to swim also doesn't significantly affect the phytoplankton-predator contact rate. In contrast, consideration of a larger example predator and faster swimming prey demonstrates how the contact rate can increase with increasing turbulence intensity and swimming speeds. We also consider how varying the contact radius of the predator alters the contact rate.

Chapter 3 explores the population dynamics of the phytoplankton, virus and predator via a three component ODE model, which contains parameters representing the phytoplankton-virus and phytoplankton-predator contact rates explored in Chapter 2. The focus of Chapter 3 is to compare the effectiveness of viral infection and predation as controls of phytoplankton blooms. To facilitate this, as in the previous chapter, specific phytoplankton, virus and predator species are considered. The phytoplankton are assumed to grow logistically whilst virus and predator populations can only increase in the presence of phytoplankton. The phytoplankton-virus interaction is modelled using a 'mass-action' (density dependent) approach as seen in Bratbak et al. (1998). The other aspect to the model is the inclusion of predation upon phytoplankton. Grazing is assumed to follow a Holling Type II response, the specific terms having been fitted to experimental data by Jeong et al. (2003), for *O. marina* grazing upon *H. akashiwo*. We suggest a modification to the phytoplankton-predator grazing model so as to include changes to the volume clearance rate.

The model is analysed analytically and numerically to show five possible long term dynamics, three of which occur at steady state. The virus and predator are considered to compete for phytoplankton and thus, due to the competitive exclusion principle, there is no steady state for non-trivial parametric conditions where all three species coexist. However, it should be noted that there are limitations to the competitive exclusion principle. For example, Hutchinson (1961) discovered two species existing on one resource in a time-varying situation and Haigh and Smith (1972) showed two species coexisting by utilising different life stages of the same prey species. Spatial heterogeneity is also suggested to contradict the competitive exclusion principle. For

our system, pressures on the virus and predator are not the same. The competitive exclusion built into our model may therefore give an unreliable result. Upon analysis of our model, we find all three species to coexist away from equilibrium. Also, phytoplankton-virus and phytoplankton-predator can exist at equilibrium and explicit expressions are computed for the concentration of virions or predators needed to reduce the phytoplankton population in the short term. There is also the possibility of phytoplankton-predator limit cycles. The regions in parameter space where these different outcomes occur are computed and displayed graphically in a two-dimensional bifurcation plot of viral decay rate and predator death rate parameter space. The model is solved numerically using the program Matlab. Figures depicting transient and long term dynamics are presented. We explore control of phytoplankton by the addition of virions or grazers to a phytoplankton community existing alone at carrying capacity, reducing the phytoplankton population to its coexistence equilibrium with the virus or predator respectively. We similarly show that the addition of a small quantity of virions to a phytoplankton-predator stable coexistence or stable limit cycle system can shift the long term behaviour to phytoplankton-virus stable coexistence. The importance of stochastic effects in possible bloom extinction is considered. For example, where the behaviour is cyclic in the long term, we find the trough concentrations may be sufficiently low for stochastic events to eliminate the phytoplankton population. Where possible, realistic parameter values found in the literature have been used and as such a comparison is made between model results and experimental data on population dynamics in the field and mesocosms. Numerical simulations compare well with the published data for the phytoplankton-virus or phytoplankton-predator system, but some discrepancies are identified which relate to limitations of the Jeong et al. (2003) grazing model for predation. The effects of varying the contact rates on the transient and long-term population dynamics are considered and a comparison between three types of *H. akashiwo* virus is also made within this chapter.

Chapter 4 investigates the effects of spatial heterogeneity on the population dynamics by extending the ODE population model of Chapter 3, leaving a one dimensional, three component, PDE model. The vertical spatial dimension is the one considered as it is viewed to be the most important dimension since it has the most rapid variation in key environmental conditions such as light, nutrients and turbulence. Having compared various turbulence models, turbulence is modelled here via a diffusion term with an eddy diffusivity coefficient. This was chosen largely to reduce computational cost. The population model of Chapter 3 is merged with the diffusion equation to form a reaction-diffusion model. This model has also been solved in Matlab, validating Matlab's PDE solver, pdepe, against one of its ODE solvers, ode45, for zero and large eddy diffusivity with uniform initial conditions. This is due to the ode solver within pdepe being less accurate than ode45. We find the results using pdepe to be reasonable and thus use it throughout the chapter. We analyse field data, supplied by

Prof. J. Sharples, at two time points to obtain depth profiles for the energy dissipation rate to estimate the phytoplankton-virus and phytoplankton-predator contact rates as a function of depth using results from Chapter 2 (assuming the phytoplankton to be non-motile). The field data is then re-analysed to give depth profiles of Brunt-Vaisala frequency (a measure of how stratified the system is), which is combined with the energy dissipation rate to obtain depth profiles for eddy diffusivity. The main difference between the two profiles is a more pronounced thermocline (a region of low turbulence) in one than the other.

When the phytoplankton, virus and predator are initially uniformly distributed, some spatial heterogeneity is introduced prior to the system stabilising to a long term equilibrium. This is due to the variation in contact rate with depth (due to a variable energy dissipation rate), as we find eddy diffusion alone is not able to generate heterogeneity from an initially uniform distribution. When the phytoplankton population is initially non-uniformly distributed, much more spatial heterogeneity is present. For a system tending to phytoplankton-virus stable in the absence of predation, we see several transient peaks of the predator population in the lower part of the water column prior to the system stabilising. Where the system tends to phytoplankton-predator stable in the absence of viral infection, a long transient period is seen where the viral population dominates in the upper part of the water column and the predators dominate in the lower part before the phytoplankton-predator equilibrium is realised. Finally, we calculate how the addition of viruses or predators to the surface layer could control a phytoplankton bloom, either shifting the long term dynamics away from phytoplankton existing alone at carrying capacity to phytoplankton-predator or phytoplankton-virus stable equilibrium, or shifting between phytoplankton-predator and phytoplankton-virus equilibria.

The conclusions of the thesis are presented in Chapter 5. Additional material relevant to Chapters 2 and 3 can be found in Appendices A and B respectively, whilst appropriate figure licenses are provided in Appendix C.

Chapter 2

Effects of swimming and turbulence on contact rates

2.1 Introduction

This chapter explores how turbulence and phytoplankton swimming affect the contact rates between phytoplankton and their viruses, and phytoplankton and their predators. We use the theory of a diffusing chemical being absorbed by a sphere, which Karp-Boss et al. (1996) applied to nutrient uptake by phytoplankton, and apply it here to virion adsorption to phytoplankton. We have laid out this classical theory in detail, writing it in our context of virion "uptake" by phytoplankton. We review contact rate expressions for three different flow regimes, which were previously summarised in Karp-Boss et al. (1996) for nutrient uptake. We then conduct a thorough analysis of these previously developed expressions to determine which parameters are most important in altering the phytoplankton-virus contact rate. We place particular emphasis on determining whether phytoplankton swimming or turbulence is most influential to this contact rate. The phytoplankton-predator contact rate is investigated using theory previously established by Lewis and Pedley (2000). We reiterate this theory here, making a new contribution by highlighting some drawbacks of the model when applied to our system. Again, we investigate the effects of individual parameters on the contact rate and compare the importance of phytoplankton swimming and turbulence. A further contribution is made by calculating these contact rates for specific phytoplankton, virus and predator species.

The phytoplankton-virus, $P - V$, and phytoplankton-predator, $P - Z$, contact rates are considered separately, using different methods. In calculating the $P - V$ contact rate, we assume the virions diffuse due to Brownian motion and take the contact rate between the phytoplankton and virus to be the flux of virions across the phytoplankton cell wall. This is analagous to classic work of diffusing chemical being absorbed by a sphere. The effect of fluid motion, either due to phytoplankton

swimming or turbulent motions, modifies the flux, which can be computed by solving the advection-diffusion equation for the viral concentration field in the vicinity of a phytoplankton cell. The dimensionless quantity known as the Péclet number, Pe, will be used in this chapter. Here, Pe is the ratio of the rate of advection of a species by the flow to the rate of diffusion of a species in the fluid regime considered. A large Pe implies the advective properties of the fluid dominate over the diffusive properties. In this chapter, we will define a Péclet number for phytoplankton swimming in still fluid, $\mathrm{Pe}_{\mathrm{swim}}$, and a Péclet number for non-motile phytoplankton in a turbulent fluid, $\mathrm{Pe}_{\mathrm{turb}}$. We separately consider motile phytoplankton in still fluid, non-motile phytoplankton in turbulent flow, where advection due to small-scale turbulence will be modelled as advection due to fluctuating shear flow, and motile cells in turbulent fluid. In the latter case it is found that swimming is unimportant in calculating the contact rate when the turbulent Péclet number is large. We then consider what 'critical' turbulent Péclet number is required for this to hold, and find the minimum swimming speed required for phytoplankton swimming to have a greater effect on the contact rate than turbulence. We consider expressions for the Sherwood number (a parameter showing by how much virion flux into a phytoplankton cell is increased by fluid motions) as a function of the Péclet number. Denoting $\mathrm{CR_v}$ to be the phytoplankton-virus contact rate, then $\mathrm{Sh(Pe)} = \dfrac{\mathrm{CR_v(Pe)}}{\mathrm{CR_v}(0)}$. This allows us to gauge the relative importance of parameters such as temperature, the size of both the virus and phytoplankton, swimming speed of the phytoplankton and energy dissipation rate in determining the $P - V$ contact rate. Realistic parameter values for *H. akashiwo* and HaV are used to calculate the $P - V$ contact rate, enabling us to compare the effects of phytoplankton swimming and turbulence on the contact rate.

Similarly, in calculating the $P - Z$ contact rate we compute the flux of phytoplankton into a sphere. The predator is assumed to have a perception field around it, which represents how close to the predator a phytoplankton cell must be for the predator to perceive its prey. Any phytoplankton entering the perception field is counted as an encounter or "contact". Assuming the perception field to be spherical in shape, the number of prey entering the perception field through some small section of the sphere per unit time is determined. The total flux of prey into the whole sphere per unit time is then computed. In contrast to the $P - V$ contact rate calculation where the virions are homogeneously distributed and enter the phytoplankton cell via diffusive transport, the $P - Z$ contact rate calculation considers individual interactions between the predator and phytoplankton (both of which are motile). A further difference in these approaches is that the $P - V$ contact rate calculation considers disturbance to the fluid due to the presence of the phytoplankton and treats it as a towed body problem, whereas these effects are ignored in the $P - Z$ contact rate calculation. The approach used to calculate the $P - V$ contact rate may become limited if the virions aren't

small enough compared to the phytoplankton or aren't in high enough abundance. As with the $P-V$ contact rate, the effect of fluid motion is considered. We calculate the contact rate for *H. akashiwo* and the predator *O. marina*, considering the effects of plankton swimming and turbulence. The effects on the $P-Z$ contact rate of varying some key parameters, such as the predator's perception radius, are considered.

In this chapter we use sophisticated fluid dynamical models to establish numerical values of the contact rates for the specific species considered. This allows us to identify which parameters are most influential and would therefore enable an informed choice if one were to choose a virus or predator to maximise its contact rate with the phytoplankton. In Chapter 3, these contact rate values are used in a population model. Unfortunately, not all parameters are known to this level of accuracy. However, some of these parameters may be determined in the future, making numerical values of the contact rates more useful in the model.

2.2 Methodology

2.2.1 Background

Phytoplankton-Virus

Here we follow the work of Karp-Boss et al. (1996), who considered nutrient uptake by phytoplankton. The phytoplankton-virus contact rate is modelled by assuming the virus behaves like a solute and is absorbed by phytoplankton through their cell wall. The work presented here extends that of Murray and Jackson (1992), who consider how size, shape and swimming speed of planktonic organisms affect the mass transfer rate of virions, to also investigate the effects of turbulence and specifically consider the phytoplankter *H. akashiwo*.

Initially, consider how the virus concentration changes over time via the advection-diffusion equation:

$$\frac{\partial V}{\partial t} = -\mathbf{U}\cdot\nabla V + D_v\nabla^2 V, \tag{2.1}$$

where V is the virus concentration, a quantity varying in space and time, and D_v is diffusivity of the virus (due to Brownian motion), assumed to be constant. The velocity field $\mathbf{U}$, which varies in time as well as space, can be due to fluid advection or phytoplankton swimming. The boundary conditions to be used are:

$$V = 0 \text{ at } r = r_0, \text{ and} \tag{2.2}$$

$$V = V_\infty \text{ for } r \to \infty. \tag{2.3}$$

The radius of the phytoplankton cell is denoted by r_0. Thus condition (2.2) sets the virus concentration to be zero at the host cell surface, i.e. we assume virions cross the

phytoplankton surface the instant they arrive. This is therefore a maximum contact rate. Condition (2.3) sets the virus concentration to ambient/far field concentration away from the host (r being radial distance from the centre of the host cell).

Non-dimensionalise by setting $\mathbf{U} = \mathbf{U}^* U$, $V = V^* V_\infty$ and $r = r^* r_0$ (Karp-Boss et al., 1996), where $*$ represents a non-dimensional quantity. Dropping the asterisk, the non-dimensional steady state equation is thus

$$\mathrm{Pe}\,(\mathbf{U} \cdot \nabla V) = \nabla^2 V, \tag{2.4}$$

where Péclet number, $\mathrm{Pe} = \frac{U r_0}{D_v}$. The corresponding boundary conditions are now:

$$V = 0 \text{ at } r = 1, \text{ and} \tag{2.5}$$

$$V = 1 \text{ for } r \to \infty. \tag{2.6}$$

The phytoplankton-virus contact rate, $\mathrm{CR_v}$, is defined as the total virion flux across the phytoplankton cell wall. We must therefore solve the advection-diffusion equation (2.4) for V and then find (Leal, 2007):

$$\mathrm{CR_v} = \int_S (\nabla V \cdot \mathbf{n})\,|_{r=1} dS, \tag{2.7}$$

where S is the complete phytoplankton body surface. The Sherwood number, Sh, represents the enhancement of flux across the phytoplankton cell wall due to fluid motion. It is found by dividing $\mathrm{CR_v}$, calculated in the presence of fluid motion, by the contact rate found for diffusion in the absence of fluid motion.

In order to solve the advection-diffusion equation we must specify $\mathbf{U}$. Equation (2.4) will thus be solved for three different fluid regimes: phytoplankton swimming in still fluid, non-motile phytoplankton in a turbulent environment, and phytoplankton swimming in a turbulent fluid. The solution for V in each case is then used to determine expressions of the form $\mathrm{Sh} = \mathrm{Sh(Pe)}$. The phytoplankton-virus contact rate is then equal to Sh multiplied by the purely diffusional flux. Obtaining an explicit relationship for Sh as a function of Pe allows us to clearly see how Pe changes Sh, thereby showing flux enhancement due to phytoplankton swimming and turbulent motions.

In order to express the contact rate in terms of Sh, we must calculate the purely diffusional flux. The steady state of the non-dimensional diffusion equation is $V = 1 - \frac{1}{r}$ (see Appendix A.1.1). The total flux is therefore:

$$\int \frac{\partial V}{\partial r} dS = 4\pi. \tag{2.8}$$

The phytoplankton-virus contact rate, in dimensional values, is:

$$\mathrm{CR_v} = 4\pi D_v r_0 V_\infty \mathrm{Sh}. \tag{2.9}$$

This contact rate represents the number of virions encountered by a single phytoplankton per unit time. The total number of contacts therefore involves multiplying CR_v by the number of phytoplankton. Later in this chapter we make calculations in terms of a volume clearance rate, c_v, rather than contact rate. The phytoplankton-virus volume clearance rate is equal to CR_v divided by V_∞. Consideration of the volume clearance rate allows us to investigate how fluid motions, temperature and size of the phytoplankton and virus affect their encounters, independent of the quantity of virions. The total number of contacts between the phytoplankton and virus populations can therefore be defined as:

$$\text{Total number of contacts } = PV_\infty c_v. \tag{2.10}$$

As mentioned previously, this will provide a maximal value since we made the assumption that all virions cross the phytoplankton cell wall the instant they arrive. Chapter 3 therefore sees the inclusion of this term in a population model, with adjustments to reduce it from a maximal value.

Phytoplankton-Predator

In calculating the phytoplankton-predator encounter rate we use an alternative modelling approach, that of swept volumes. This was described in Kubo (1965) to consider collisions between gas molecules and is now widely used in modelling planktonic predator-prey systems (e.g. Visser et al., 2009; Mariani et al., 2005; Mackenzie and Leggett, 1991). The theory will be used here to model encounters between phytoplankton and their predators, considering the effects of swimming and turbulence.

We consider the predator to have a spherical perception field with radius R and to be swimming with speed U_z, as depicted in Figure 2.1. Any phytoplankton cell up to a distance R away from the predator will be perceived by the predator and thus counted as an encounter.

For non-motile phytoplankton, the phytoplankton-predator encounter rate is found by calculating the volume "swept" by the predator. From Figure 2.1(b), this basic contact rate is therefore equal to the cross-sectional area of a sphere, πR^2, multiplied by the swimming speed of the predator, U_z, and the concentration of prey, P:

$$CR_z = \pi R^2 P U_z. \tag{2.11}$$

This contact rate represents the number of phytoplankton particles encountered by a single predator per unit time. Therefore, the total number of contacts is equal to CR_z multiplied by the predator density, Z. Again, we will make calculations later in this chapter in terms of the volume clearance rate, c_z, which is the contact rate, CR_z, divided by the phytoplankton density, P. Thus, the total number of contacts can be written:

$$\text{Total number of contacts } = PZc_z. \tag{2.12}$$

We will refer back to this equation in Chapter 3 when considering how changes in the phytoplankton-predator volume clearance rate affect population dynamics.

We follow Gerritsen and Strickler (1977) to consider the inclusion of phytoplankton swimming and then the work of Lewis and Pedley (2000) to consider phytoplankton swimming in a turbulent fluid. The number of phytoplankton entering the perception field through a surface element per unit time, which is the product of the cross-sectional area of the surface element, prey density, relative swimming speed of phytoplankton to predator and the probability of moving with this speed, is determined. We then integrate over the surface of the sphere and velocity fields of the plankton to give the total contact rate per predator.

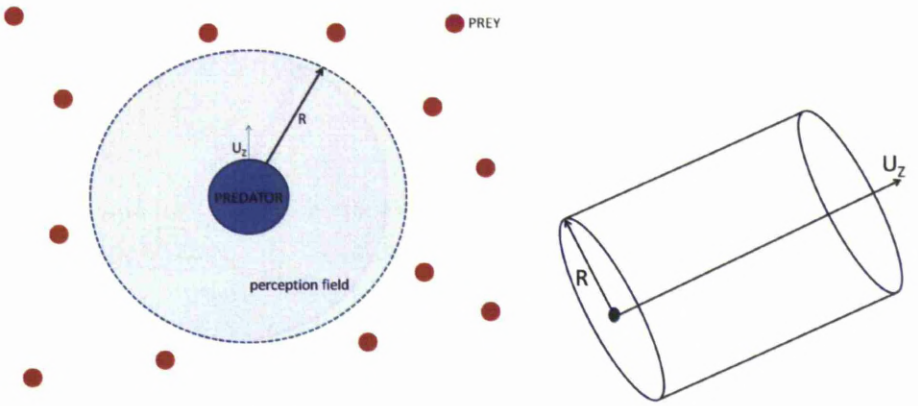

(a) Motile predator encountering non-motile prey. (b) Volume "swept" by the predator.

Figure 2.1: Predator-prey dynamics leading to the basic contact rate, equation (2.11).

2.2.2 Parameter Estimation

Parameter values for *H. akashiwo*, HaV and *O. marina* have been estimated from the literature and used in this thesis to calculate the $P-V$ and $P-Z$ volume clearance rates.

The $P-V$ volume clearance rate is dependent on the size of both the phytoplankton and virions. *H. akashiwo* is unicellular and $10-25\times10^{-6}$m in length (Smayda, 1998). As such, calculations of the *H. akashiwo*-HaV volume clearance rate are based on *H. akashiwo* having a diameter, d of 15×10^{-6}m. However, we will also investigate how varying phytoplankton diameter alters the volume clearance rate. Virion diameter can also be found in the literature. Tarutani et al. (2006) have observed HaV with a diameter, d_v of 200×10^{-9}m, which is the value used here. However, we do also consider

how changes in the virion diameter affect the volume clearance rate. The diffusivity of a spherical virus, D_v is found using the following equation stated in Murray and Jackson (1992):

$$D_v = \frac{kT}{3\pi\mu d_v}, \tag{2.13}$$

where k is Boltzmann's constant. We take $T = 293$K, the Kelvin temperature equivalent to 20°C as our primary value. However, we do also vary the temperature in some calculations to investigate how this affects the volume clearance rate. The dynamic viscosity of water at 20°C is $\mu = 1.002 \times 10^{-3}\text{kgm}^{-1}\text{s}^{-1}$ (Batchelor, 1967), thus the viral diffusivity is $D_v = 2.14 \times 10^{-12}\text{m}^2\text{s}^{-1}$. Other parameters involved in calculating the $P - V$ contact rate are those used to determine the effects of turbulence and phytoplankton swimming. The parameters characterising turbulence are the energy dissipation rate, ϵ, and kinematic viscosity of water, ν. Typical values of ϵ in the oceanic upper mixed layer range from 10^{-9} to $10^{-6}\text{m}^2\text{s}^{-3}$ and ν is approximately $10^{-6}\text{m}^2\text{s}^{-2}$ (Karp-Boss et al., 1996). Swimming speeds of *H. akashiwo*, U_{P}, have been observed in the range $20 - 160 \times 10^{-6}\text{ms}^{-1}$ (Smayda, 1998).

When considering the $P - Z$ volume clearance rate, the predator swims with speed U_{Z}. Menden-Deuer and Grünbaum (2006) observed *O. marina* to swim at $339\mu\text{ms}^{-1}$ in the presence of its prey *I. galbana*. We will therefore treat this as an estimation of its swimming speed in the presence of *H. akashiwo*. We will also consider how a predator larger and faster than *O. marina* would alter the volume clearance rate. Uttieri et al. (2008) estimated the copepod *C. furcatus* to have a contact radius of approximately $R = 400 \times 10^{-6}\text{m}$ and swim with speed 10^{-2}ms^{-1}. We will use this data to establish the difference in volume clearance rate for a predator of this size and speed compared to *O. marina*. Parameter values given in Jeong et al. (2003) have been used to estimate the *H. akashiwo* - *O. marina* contact rate (discussed further in section 3.2.2), from which we estimate the perception radius, R, of *O. marina* to be $4.3 \times 10^{-6}\text{m}$.

2.3 Phytoplankton-Virus Contact

Each of the sections 2.3.1, 2.3.2 and 2.3.3 use classical fluid dynamics theory to determine appropriate expressions for the Sherwood number, as summarised in Karp-Boss et al. (1996). The second part of each section uses these expressions to calculate the phytoplankton-virus volume clearance rate, which is equal to the contact rate without the inclusion of virus density, i.e. equation (2.9) without V_∞, and has units of volume per time. The effects on the volume clearance rate of varying phytoplankton swimming speed and parameters representing turbulence are then explored.

Symbol	Value	Source
Phytoplankton diameter, d	15×10^{-4}cm	Estimated from Smayda (1998) for *H. akashiwo*
Phytoplankton swimming speed, U_{P}	$20 - 160 \times 10^{-4}$cms^{-1}	Observed values for *H. akashiwo* summarised by Smayda (1998)
Virus diameter, d_v	0.2×10^{-4}cm	Observed for HaV by Tarutani et al. (2006)
Viral diffusivity, D_v	2.14×10^{-8}cm^{2}s^{-1}	Calculated for HaV at 20°C, using theory from Murray and Jackson (1992).
Boltzmann's constant, k	1.38×10^{-19}cm^{2}kg s^{-2}K^{-1}	Batchelor (1967).
Energy dissipation rate, ϵ	$10^{-5} - 10^{-2}$cm^2 s^{-3}	Karp-Boss et al. (1996)
Kinematic viscosity of water, ν	10^{-2}cm^2 s^{-2}	Karp-Boss et al. (1996)
Skewness factor of the rate of extension in a fixed direction, S	0.6	Lies in the range 0.3-1.0, Batchelor (1980)
Predator swimming speed, U_{Z}	339×10^{-4}cms^{-1} 1cms^{-1}	Observed by Menden-Deuer and Grünbaum (2006) for *O. marina* in the presence of prey. Observed by Uttieri et al. (2008) for *C. furcatus*
Perception radius, R	4.3×10^{-4}cm 400×10^{-4}cm	Estimated for *O. marina*, using data from Jeong et al. (2003) Observed for *C. furcatus* by Uttieri et al. (2008)
Structure function constant, Sc	2.411	Taken from Lewis and Pedley (2000)

Table 2.1: Parameter values used to investigate the *H. akashiwo*-HaV and *H. akashiwo*-*O. marina* volume clearance rates.

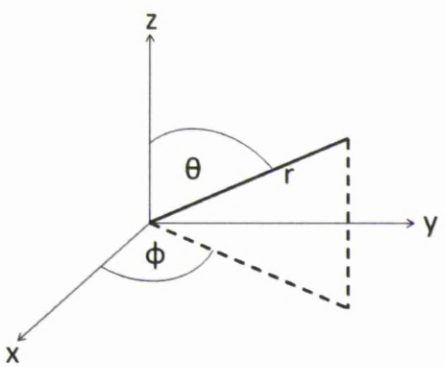

Figure 2.2: Spherical coordinate system, (r, ϕ, θ).

2.3.1 Motile cells, still water

This section follows theory from Leal (2007) for heat transfer from a solid sphere in uniform flow. Figure 2.2 depicts the spherical coordinate system used in this section. We will model phytoplankton swimming in still fluid as a stationary sphere in uniform flow, setting fluid velocity to zero at the sphere surface. At the phytoplankton scale, we expect viscous forces to be dominant over inertial forces and therefore model the flow past a spherical phytoplankton cell as uniform creeping flow (also known as Stokes flow). The velocity field, $\mathbf{U}$, is therefore defined as

$$\mathbf{U} = -\mathbf{V} + \mathbf{U}^{(T)}, \tag{2.14}$$

where $-\mathbf{V}$ is the uniform fluid velocity in the absence of the phytoplankton cell and $\mathbf{U}^{(T)}$ represents the disturbance to the fluid due to the presence of a rigid sphere (Batchelor, 1980). The velocity field will be represented by Stokes' solution for uniform creeping flow past a solid sphere, which has streamfunction:

$$\psi = \frac{1}{2}\left(r^2 - \frac{3r}{2} + \frac{1}{2r}\right)\sin^2\theta. \tag{2.15}$$

This streamfunction will be used to calculate the velocity components (Leal, 2007). The net force on the solid sphere in this flow field is Stokes drag, which represents the drag force that a sinking or towed object swimming steadily experiences when moving through a fluid. In contrast, a self-propelled low Reynolds number object experiences no net force, as drag and thrust forces must exactly balance. Stokes' solution (2.15) isn't therefore strictly valid for a self-propelled object (Visser, 2001). Velocity fields around swimming organisms have been proposed, e.g. Magar and Pedley (2005), however, the towed body Stokes solution is widely used as a first approximation for swimming phytoplankton and will be used here.

In axisymmetric flow, the velocity components (U_r, U_ϕ, U_θ) are all independent of ϕ (Batchelor, 1967). The non-zero flow velocity components are:

$$U_r = \frac{1}{r^2\sin\theta}\frac{\partial\psi}{\partial\theta} = \left(1 - \frac{3}{2r} + \frac{1}{2r^3}\right)\cos\theta, \tag{2.16}$$

$$U_\theta = -\frac{1}{r\sin\theta}\frac{\partial\psi}{\partial r} = \left(1 - \frac{3}{4r} - \frac{1}{4r^3}\right)\sin\theta. \tag{2.17}$$

Equation (2.4) can now be written in spherical coordinates with $\mathbf{U} = (U_r, 0, U_\theta)$ (see Appendix A.1.2):

$$\begin{aligned}&\frac{1}{r^2}\left[\frac{\partial}{\partial r}\left(r^2\frac{\partial V}{\partial r}\right) + \frac{1}{\sin\theta}\frac{\partial}{\partial\theta}\left(\sin\theta\frac{\partial V}{\partial\theta}\right)\right]\\ &= \mathrm{Pe}\left[\left(1 - \frac{3}{2r} + \frac{1}{2r^3}\right)\cos\theta\frac{\partial V}{\partial r} - \frac{\sin\theta}{r}\left(1 - \frac{3}{4r} - \frac{1}{4r^3}\right)\frac{\partial V}{\partial\theta}\right].\end{aligned} \tag{2.18}$$

Full solution of equation (2.18) requires numerical methods. However, we can gain useful insights by obtaining an approximate solution in the limits $\mathrm{Pe} \gg 1$ and $\mathrm{Pe} \ll 1$. It is shown in Appendix A.1.3 that:

$$V = \frac{\int_0^S e^{-t^3} dt}{\int_0^\infty e^{-t^3} dt}, \tag{2.19}$$

found using matched asymptotics. The denominator is equal to the gamma function, $\Gamma\left(\frac{4}{3}\right)$, which equals 0.8930 (Leal, 2007). Our objective is the relationship

$$\mathrm{Sh} = \mathrm{Sh}(\mathrm{Pe}),$$

where, from equation (2.7),

$$\begin{aligned} \mathrm{Sh} &= -\frac{1}{4\pi} \int_0^{2\pi} \int_0^{\pi} \left(r^2 \sin\theta \frac{\partial V}{\partial r} \right) \Big|_{r=1} d\theta d\phi \\ &= -\frac{1}{2} \int_0^{\pi} \sin\theta \frac{\partial V}{\partial r} \Big|_{r=1} d\theta. \end{aligned} \tag{2.20}$$

We know from formulation of the boundary-layer equations (shown in Appendix A.1.3) that:

$$\left(\frac{\partial V}{\partial r} \right)_{r=1} = \mathrm{Pe}^{\frac{1}{3}} \left(\frac{\partial V}{\partial Y} \right)_{Y=0}$$

where $(\partial V/\partial Y)_{Y=0}$ is $O(1)$ in magnitude and completely independent of Pe [1]. It follows from this and equation (2.20) that the correlation between Sh and Pe must take the form

$$\mathrm{Sh} = A\mathrm{Pe}^{\frac{1}{3}},$$

where

$$A \equiv -\frac{1}{2} \int_0^{\pi} \sin\theta \left(\frac{\partial V}{\partial Y} \right) \Big|_{Y=0} d\theta.$$

Leal (2007) calculates A, from equation (2.19), to be 0.6245 [2]. Thus, for $\mathrm{Pe} \gg 1$,

$$\mathrm{Sh} = 0.6245\mathrm{Pe}^{\frac{1}{3}} + o(\mathrm{Pe}^{\frac{1}{3}}), \tag{2.21}$$

where writing $f(x) = o(g(x))$ refers to f growing much more slowly than g.

However, it should be remembered that (2.21) only represents the leading order term in an asymptotic expansion as $\mathrm{Pe} \to \infty$. The next term is found by finding

[1] $\frac{\partial V}{\partial r} = \frac{\partial V}{\partial (r-1)} = \frac{\partial V}{\partial y} = \frac{\partial V}{\partial (\mathrm{Pe}^{-\frac{1}{3}} Y)} = \mathrm{Pe}^{\frac{1}{3}} \frac{\partial V}{\partial Y}$

[2] Note: Leal (2007) actually calculates A to be 1.249, but this is because Sh for pure diffusion is taken to be 2 rather than 1 as used here.

an additional term in the expansion. The Sherwood number expressions for motile phytoplankton in still fluid are:

$$\mathrm{Sh} = 0.6245\mathrm{Pe}^{\frac{1}{3}} + 0.461 + o(1) \qquad \mathrm{Pe} \gg 1, \tag{2.22}$$

$$\mathrm{Sh} = 1 + \frac{1}{2}\mathrm{Pe} + \frac{1}{2}\mathrm{Pe}^2 \ln(\mathrm{Pe}) + O(\mathrm{Pe}^2) \qquad \mathrm{Pe} \ll 1, \tag{2.23}$$

$$\mathrm{Sh} = \frac{1}{2}\left(1 + (1 + 2\mathrm{Pe})^{\frac{1}{3}}\right) \qquad 0.01 < \mathrm{Pe} < 100, \tag{2.24}$$

where O contains the less significant terms in the expression. Each expression was originally recorded by Acrivos and Goddard (1965), Acrivos and Taylor (1962), and Clift et al. (1978) respectively, as detailed in Karp-Boss et al. (1996). The expression for $\mathrm{Pe} \ll 1$, equation (2.23), was derived using asymptotic expansion, whereas the expression for intermediate values of Pe, equation (2.24), was found numerically.

Calculation of contact rate

Here we use realistic parameter values for *H. akashiwo* and its virus HaV, summarised in Table 2.1, to calculate values of the phytoplankton-virus volume clearance rate, which is equal to the contact rate without the inclusion of virus density, for motile phytoplankton in still fluid.

Denoting the phytoplankton characteristic swimming speed as U_{P} and the characteristic length scale of the phytoplankton to be its radius, the Péclet number for phytoplankton swimming in still fluid is defined as

$$\mathrm{Pe}_{\mathrm{swim}} = \frac{U_{\mathrm{P}} r_0}{D_v}, \tag{2.25}$$

where D_v is virus diffusivity. This Péclet number is used in one of equations (2.22, 2.23, 2.24) to find the Sherwood number, Sh, which is then used in

$$\mathrm{c_V} = 4\pi r_0 D_v \mathrm{Sh} \tag{2.26}$$

(as defined in section 2.2.1) to calculate the volume clearance rate.

Remember that, the diffusivity of a spherical virus can be given by the equation (Murray and Jackson (1992) and references therein):

$$D_v = \frac{kT}{3\pi\mu d_v}, \tag{2.27}$$

where k is the Boltzmann constant, T is temperature in Kelvins, μ is the dynamic viscosity of water (increasing temperature decreases μ) and d_v is virus diameter. Hence, viral diffusivity is influenced by temperature and virus diameter. If we take the temperature to be 20°C, then the diffusivity of HaV was found in section 2.2.2 to be $D_v = 2.14 \times 10^{-8}\mathrm{cm^2 s^{-1}}$. For non-motile phytoplankton in still fluid, the Sherwood

number is equal to 1. Hence, from equation (2.26), the purely diffusional volume clearance rate is $c_v = 1.7 \times 10^{-5}$ml d^{-1}.

The characteristic swimming speed of *H. akashiwo*, U_P, lies in the range $20 - 160 \times 10^{-4}$cms^{-1} (as given in Table 2.1). Therefore, using equation (2.25), Pe is in the range 70 to 561 and thus by using equations (2.22) and (2.24) we obtain Sh = 3.10 – 5.61. Hence, the *H. akashiwo* - HaV volume clearance rate is 3.10 and 5.61 times higher for *H. akashiwo* swimming at speeds 20×10^{-4}cms^{-1} and 160×10^{-4}cms^{-1} respectively, compared to if it was non-motile. The volume clearance rate for *H. akashiwo* and HaV is therefore estimated to be $c_v = 5.4$ to 9.8×10^{-5}ml d^{-1}, thus increasing the phytoplankton swimming speed by 8 times (from 20 to 160×10^{-4}cms^{-1}) almost doubles the contact rate.

This difference in the contact rate for *H. akashiwo* having the ability to swim is striking if we compare how the swimming speed of *H. akashiwo* would increase its contact rate with nutrients. Since nutrient diffusivity is of the order 10^{-5}cms^{-1} (Karp-Boss et al., 1996), three orders of magnitude larger than D_v, the Sherwood number for *H. akashiwo* and its nutrients, with *H. akashiwo* swimming in the range $20 - 160 \times 10^{-4}$cms^{-1}, would only be between 1.05 and 1.25. Therefore, the ability of *H. akashiwo* to swim within this range would increase its contact rate with a virus by more than its contact rate with nutrients. The level of swimming speed seems to have less of an effect on the nutrient contact rate, where swimming 8 times faster (increasing from 20×10^{-4}cms^{-1} to 160×10^{-4}cms^{-1}) increases Sh from 1.05 to 1.25, in contrast to the Sh for a virus increasing from 3.10 to 5.61 for the same *H. akashiwo* swimming speeds.

For Pe large, Sh is of the order $\mathrm{Pe}^{\frac{1}{3}}$ from equation (2.22). The volume clearance rate can thus be expressed as

$$\begin{aligned} c_v \approx 4\pi r_0 D_v \left(0.6245\mathrm{Pe}^{\frac{1}{3}}\right) &= 2.498\pi r_0 D_v \left(\frac{U_P r_0}{D_v}\right)^{\frac{1}{3}} \\ &= 2.498\pi r_0^{\frac{4}{3}} D_v^{\frac{2}{3}} U_P^{\frac{1}{3}}. \end{aligned} \tag{2.28}$$

Therefore, increasing D_v will increase c_v and hence increasing temperature increases the contact rate. Similarly, increasing virion diameter will decrease D_v and therefore decrease c_v . Since r_0 is of the highest order in equation (2.28), doubling phytoplankton radius for example would lead to a larger change in c_v than would doubling virus diffusivity or phytoplankton swimming speed.

As mentioned above, viral diffusivity is affected by temperature. Therefore changing temperature alters the contact rate. For example, if the temperature were to double to 40°C, the viral diffusivity increases by more than 1.5 times. Thus, the purely diffusional volume clearance rate increases from $c_v = 1.7 \times 10^{-5}$ml d^{-1} to $c_v = 2.6 \times 10^{-5}$ml d^{-1}. The change in c_v for motile phytoplankton would not be

quite as large since viral diffusivity acts to decrease Pe and therefore Sh. For *H. akashiwo* swimming at 20 to 160 $\times$ 10^{-4}cms^{-1}, the volume clearance rate at 40°C is c_v = 7.7 $\times$ 10^{-5} to 1.4 $\times$ 10^{-4}ml d^{-1}, compared to c_v = 5.4 to 9.8 $\times$ 10^{-5}ml d^{-1} at 20°C.

Other factors affecting the $P-V$ contact rate are the size of both the virus and the phytoplankton. As shown above, increasing the size of the phytoplankton increases the contact rate, both directly and through Pe, whereas increasing the size of the virus will decrease virus diffusivity and thus decrease the contact rate. A phytoplankton cell with double the radius of *H. akashiwo*, i.e. $r_0 = 15\times10^{-4}$cm, would have a purely diffusional volume clearance rate of c_v = 3.5 $\times$ 10^{-5}ml d^{-1}, more than double that found above for *H. akashiwo*. If this larger phytoplankton also had swimming speeds in the range 20 to 160 $\times$ 10^{-4}cms^{-1}, its volume clearance rate would be c_v = 1.3 to 2.4 $\times$ 10^{-4}ml d^{-1}. This is more than double that calculated above for *H. akashiwo*, where $r_0 = \frac{15}{2} \times 10^{-4}$cm. Conversely, for a virus with double the diameter of HaV, i.e. $d_v = 4\times10^{-5}$cm, infecting *H. akashiwo*, the purely diffusional volume clearance rate is $c_v = 8.7\times10^{-6}$ml d^{-1}, half of that for HaV. For motile *H. akashiwo*, this effect would be reduced since the smaller value of D_v would increase Pe and therefore Sh. The volume clearance rate for *H. akashiwo*, swimming with speeds in the range 20 to 160 $\times$ 10^{-4}cms^{-1}, and a virus with diameter $d_v = 4 \times 10^{-5}$cm is c_v = 3.2 to 6.0 $\times$ 10^{-5}ml d^{-1}.

It should be noted that some values of c_v calculated in this section use specific values for *H. akashiwo* radius and swimming speeds. Smayda (1998) describes *H. akashiwo* to be 10 to 25 $\times$ 10^{-4}cm in length, but we haven't explicitly considered this range. Also, the range of *H. akashiwo* swimming speeds used are those summarised in Smayda (1998), but swimming speeds of those organisms are difficult to measure and may be measured differently by different labs. Bearon et al. (2004) observed substantial variability in swimming speeds between strains of *H. akashiwo*. For example, under the same conditions, one strain had mean vertical swimming speeds in the range 51 to 103 $\times$ 10^{-4}cms^{-1}, whilst the speeds of another strain were in the range 35 to 60 $\times$ 10^{-4}cms^{-1}. Bearon et al. (2004) also found there to be a large difference in mean vertical swimming speeds for cells swimming at different times of day. However, the trends shown in the calculations of this section will hold for different *H. akashiwo* parameter values and different species. For example, when Pe is large, changing phytoplankton radius or swimming speed, or changing viral diffusivity, will alter c_v as shown in equation (2.28) for other species.

2.3.2 Non-motile cells, turbulent environment

We now calculate the enhancement of virion flux across a phytoplankton cell wall due to turbulence. For the time being, swimming will be ignored. We first consider non-motile phytoplankton in steady shear flow since, for sufficiently small scales, the steady

shear flow field can later be used to model a turbulent flow field.

Non-motile cells in steady shear flow

Steady shear flow is associated with viscous dissipation of small-scale turbulence and will be defined as:

$$\mathbf{U}(\mathbf{X}) = \boldsymbol{\Omega} \cdot \mathbf{X} + \mathbf{X} \cdot \mathbf{E} + \mathbf{U}^{(\mathrm{E})}, \tag{2.29}$$

where $\boldsymbol{\Omega}$ is the rate of rotation of the fluid (an antisymmetric tensor), $\mathbf{E}$ is the rate of strain of the fluid (a tensor), the flow field $\mathbf{U}^{(\mathrm{E})}$ represents disturbance to the fluid due to the presence of a rigid sphere (Batchelor, 1980) and $\cdot$ represents the dot-product.

The advection-diffusion system (2.4, 2.5, 2.6) is solved for the velocity field $\mathbf{U}$ as defined in equation (2.29). Similarly to section 2.3.1, asymptotic approximation is used to find the relationship Sh = Sh(Pe) in the limits of Pe.

The Péclet number is defined as $\frac{r_0}{D_v}$ multiplied by a velocity characteristic of the ambient flow, where r_0 is the characteristic length scale, taken to be sphere radius, and D_v continues to represent virus diffusivity. Batchelor (1979) finds the quantity $r_0 E$ to be an appropriate characteristic velocity, defining E to be a representative magnitude of the rate of strain tensor (also referred to as the shear rate) where:

$$E = |\mathbf{E}| = (E_{ij}E_{ij})^{\frac{1}{2}}. \tag{2.30}$$

Thus, the Péclet number is defined here as

$$\mathrm{Pe}_{\mathrm{shear}} = \frac{E r_0^2}{D_v}. \tag{2.31}$$

Batchelor (1979) investigate asymptotic expressions for the mass transfer rate, for $\mathrm{Pe} \ll 1$ and $\mathrm{Pe} \gg 1$. The asymptotic expressions for small Pe hold for any shaped particle and for any Reynolds number of the flow about the particle, whereas the asymptotic expressions for large Pe have assumed the cell to be spherical and the Reynolds number small (compared with unity). The following three expressions (2.32, 2.33, 2.34), which were derived by Batchelor (1979) and summarised in Karp-Boss et al. (1996), provide approximations, for $\mathrm{Pe} \ll 1$, of the Sherwood number. The first expression relates to a pure straining motion of the fluid, i.e. $\boldsymbol{\Omega} = 0$, whilst the second equation gives the enhancement of virion flux across the cell wall for a moderate level of rotation. Finally, Batchelor (1979) notes that when rotation is strong relative to strain there will be a suppression of flux enhancement (since strong rotation changes the form of the streamlines to closed circles rather than open curves extending to infinity) and thus equation (2.33) will be less accurate. Hence, a third expression was established by Batchelor (1979) for when rotation is strong.

$$\begin{aligned}
\mathrm{Sh} &= 1 + 0.36\mathrm{Pe}_{\mathrm{shear}}^{\frac{1}{2}} && \text{(pure straining motion)}, && (2.32)\\
\mathrm{Sh} &= 1 + 0.34\mathrm{Pe}_{\mathrm{shear}}^{\frac{1}{2}} && \text{(rotation less than or equal to strain)}, && (2.33)\\
\mathrm{Sh} &= 1 + 0.40\left(\frac{r_0^2|E_\omega|}{D_v}\right)^{\frac{1}{3}} \\
&\approx 1 + 0.23\mathrm{Pe}_{\mathrm{shear}}^{\frac{1}{2}} && \text{(strong rotation relative to strain)}. && (2.34)
\end{aligned}$$

The approximation in equation (2.34) uses the approach of Batchelor (1979) where he supposes the shear rate in the direction of the axis of rotation, E_ω, to be approximated by $E_\omega^2 \approx \frac{E^2}{9}$, which is based on there being 9 terms like E_ω^2 in the expression for E^2. In the limit $\mathrm{Pe} \gg 1$, the following expressions were derived by Batchelor (1979):

$$\begin{aligned}
\mathrm{Sh} &= 0.9\mathrm{Pe}_{\mathrm{shear}}^{\frac{1}{3}} && \text{(pure straining motion)}, && (2.35)\\
\mathrm{Sh} &= 0.97\left(\frac{r_0^2|E_\omega|}{D_v}\right)^{\frac{1}{3}} \approx 0.67\mathrm{Pe}_{\mathrm{shear}}^{\frac{1}{3}} && \text{(rotation and strain both acting)} && (2.36)
\end{aligned}$$

again using the relation $E_\omega^2 \approx \frac{E^2}{9}$ to approximate equation (2.36). For large Pe, a similar effect is seen as for small Pe, in that there will be significant suppression of the flux enhancement, but here it will happen for any non-small value of $\mathbf{\Omega}$ (rather than the strong rotation needed at small Pe). Hence, only one expression for the Sherwood number when both rotation and strain are acting is required (Batchelor, 1979).

Non-motile cells in turbulent fluid

Consider a fluid in statistically steady turbulent motion. The virion flux into a phytoplankton cell suspended in this fluid is determined by the flow field near the cell, where the Reynolds number is small. For sufficiently small length scales, the turbulent flow field is defined by equation (2.29), but where $\mathbf{\Omega}$ and $\mathbf{E}$ may fluctuate with time. Again, the advection-diffusion system (2.4, 2.5, 2.6) is solved for this flow field. For $\mathrm{Pe} \gg 1$,

$$\mathrm{Sh} = 0.97\left(\frac{r_0^2|<E_\omega>|}{D_v}\right)^{\frac{1}{3}}, \qquad (2.37)$$

a result given by Batchelor (1980) for mass transfer from particles in turbulent fluid, using results for steady ambient flow described in Batchelor (1979). The angle brackets denote a time average. Notice the similarity between equation (2.37) and equation (2.36). For locally homogeneous and isotropic turbulence (Batchelor (1980) and references therein),

$$<E_\omega> = 0.18\left(\frac{\epsilon}{\nu}\right)^{\frac{1}{2}}. \qquad (2.38)$$

Substituting equation (2.38) into equation (2.37) gives an expression for the Sherwood number in terms of the oceanic turbulent measures: energy dissipation rate, ϵ and kinematic viscosity, ν,

$$\mathrm{Sh} = 0.55 \left(\frac{r_0^2}{D_v} \left(\frac{\epsilon}{\nu} \right)^{\frac{1}{2}} \right)^{\frac{1}{3}}. \tag{2.39}$$

By defining the turbulent Péclet number to be

$$\mathrm{Pe}_{\mathrm{turb}} = \frac{r_0^2}{D_v} \left(\frac{\epsilon}{\nu} \right)^{\frac{1}{2}}, \tag{2.40}$$

equation (2.39) can be rewritten as

$$\mathrm{Sh} = 0.55 \mathrm{Pe}_{\mathrm{turb}}^{\frac{1}{3}}. \tag{2.41}$$

Currently, there don't appear to be any comparable solutions for small or intermediate values of Pe. However, Karp-Boss et al. (1996) do make an argument for an appropriate small Pe asymptotic solution and also found expressions for intermediate values of Pe by interpolation. They estimated Sh in the region $0.01 < \mathrm{Pe}_{\mathrm{turb}} < 100$ for the case of pure straining motion and the case of shearing motion in the presence of strong rotation. Their interpolations assume a function of the form $\mathrm{Sh} = a + b\mathrm{Pe}_{\mathrm{turb}}^{c}$. They found the lower limit for interpolation to be given by equation (2.43) and the upper limit by equation (2.44). Below are a list of Sherwood number expressions for mass transfer to cells in turbulent fluid:

$$\mathrm{Sh} = 1 + 0.29\mathrm{Pe}_{\mathrm{turb}}^{\frac{1}{2}} \quad \mathrm{Pe}_{\mathrm{turb}} \ll 1, \tag{2.42}$$

$$\mathrm{Sh} = 1.014 + 0.15\mathrm{Pe}_{\mathrm{turb}}^{\frac{1}{2}} \quad 0.01 < \mathrm{Pe}_{\mathrm{turb}} < 100, \text{ lower } \mathrm{Pe}_{\mathrm{turb}} \text{ limit}, \tag{2.43}$$

$$\mathrm{Sh} = 0.955 + 0.344\mathrm{Pe}_{\mathrm{turb}}^{\frac{1}{3}} \quad 0.01 < \mathrm{Pe}_{\mathrm{turb}} < 100, \text{ upper } \mathrm{Pe}_{\mathrm{turb}} \text{ limit}, \tag{2.44}$$

$$\mathrm{Sh} = 0.55\mathrm{Pe}_{\mathrm{turb}}^{\frac{1}{3}} \quad \mathrm{Pe}_{\mathrm{turb}} \gg 1. \tag{2.45}$$

Calculation of contact rate

We now use parameter values from Table 2.1, which represent *H. akashiwo* and HaV, to calculate values of the phytoplankton-virus volume clearance rate for non-motile phytoplankton residing in a turbulent environment.

Consider the Péclet number for turbulence defined by equation (2.40):

$$\mathrm{Pe}_{\mathrm{turb}} = \frac{r_0^2}{D_v} \left(\frac{\epsilon}{\nu} \right)^{\frac{1}{2}}. \tag{2.46}$$

Typical values of the energy dissipation rate, ϵ, in the oceanic upper mixed layer range from 10^{-5} to $10^{-2}\mathrm{cm}^2\mathrm{s}^{-3}$ and the kinematic viscosity, ν, is approximately $10^{-2}\mathrm{cm}^2\mathrm{s}^{-2}$ (Karp-Boss et al., 1996). Continuing to take phytoplankton radius, $r_0 = \frac{15}{2} \times 10^{-4}\mathrm{cm}$

and viral diffusivity, $D_v = 2.14 \times 10^{-8}\text{cm}^2\text{s}^{-1}$ gives the Péclet number, using equation (2.46), for non-motile *H. akashiwo* in turbulent water to be in the range 0.83 to 26.3. Therefore, equation (2.43) can be used to calculate the Sherwood number, which lies in the range 1.15 to 1.78. It should be remembered that equation (2.43) was found by Karp-Boss et al. (1996) by interpolation rather than asymptotic approximation. Using

$$\text{c}_\text{v} = 4\pi r_0 D_v \text{Sh}, \tag{2.47}$$

the phytoplankton-virus volume clearance rate for non-motile phytoplankton in turbulent fluid is $\text{c}_\text{v} = 2.0 \times 10^{-5}\text{ml d}^{-1}$ for $\epsilon = 10^{-5}\text{cm}^2\text{s}^{-3}$ and $\text{c}_\text{v} = 3.1 \times 10^{-5}\text{ml d}^{-1}$ for $\epsilon = 10^{-2}\text{cm}^2\text{s}^{-3}$. This is a rather small change in the volume clearance rate given the three orders of magnitude difference in ϵ.

The Sherwood number represents enhancement of virion flux across a phytoplankton cell wall due to fluid motion. Comparing the values of Sherwood number found here ($\text{Sh} = 1.15 - 1.78$) with those found for motile phytoplankton in stagnant water ($\text{Sh} = 3.10 - 5.61$), it is clear that the phytoplankton-virus volume clearance rate will be increased by more when there are motile phytoplankton in still fluid as opposed to non-motile phytoplankton in turbulent fluid, for the typical values of ϵ found in the natural environment compared to *H. akashiwo* swimming.

The calculations above suggest that the Péclet number for non-motile *H. akashiwo* and HaV in a turbulent fluid is fairly small, making equation (2.43) the appropriate choice for finding Sh, as used above. The volume clearance rate can therefore be expressed as:

$$\begin{aligned}
\text{c}_\text{v} &= 4\pi r_0 D_v \left(1.014 + 0.15\text{Pe}_\text{turb}^{\frac{1}{2}}\right) \\
&= 4.056\pi r_0 D_v + 0.6\pi r_0 D_v \left(\frac{r_0^2}{D_v}\left(\frac{\epsilon}{\nu}\right)^{\frac{1}{2}}\right)^{\frac{1}{2}} \\
&= 4.056\pi r_0 D_v + 0.6\pi r_0^2 D_v^{\frac{1}{2}} \left(\frac{\epsilon}{\nu}\right)^{\frac{1}{4}}.
\end{aligned} \tag{2.48}$$

Therefore, increasing r_0, D_v or ϵ will increase c_v, whilst increasing ν will decrease c_v. Also, since increasing D_v increases c_v, increasing temperature or decreasing the size of the virus will increase c_v.

Changing the temperature causes the viral diffusivity to change via the Kelvin temperature parameter, T, and the dynamic viscosity, μ. If, for example, we increase the temperature to 40°C, the viral diffusivity increases to $3.51 \times 10^{-8}\text{cm}^2\text{s}^{-1}$. The Péclet number is in the range 0.625 to 19.756 (3dp) for the energy dissipation rate between 10^{-5} and $10^{-2}\text{cm}^2\text{s}^{-3}$. The kinematic viscosity, ν, has decreased from $1 \times 10^{-2}\text{cm}^2\text{s}^{-1}$ at $20°C$ to $0.658 \times 10^{-2}\text{cm}^2\text{s}^{-1}$ at $40°C$. The volume clearance rate for non-motile *H. akashiwo* and HaV in a turbulent fluid at 40°C is then $\text{c}_\text{v} = 3.2$ to $4.8 \times$

10^{-5}ml d^{-1}, compared to between $c_v = 2.0$ and 3.1×10^{-5}ml d^{-1} at 20°C. The volume clearance rate is 1.5 times larger at 40°C than at 20°C. This is a slightly larger difference than was seen for motile phytoplankton in still fluid.

Let's now consider the effect of doubling the phytoplankton radius to $r_0 = 15 \times 10^{-4}$cm. The Péclet number would then be in the range 3.32 to 105.14. The volume clearance rate corresponding to the lower value of $\mathrm{Pe}_{\mathrm{turb}}$ is found via equation (2.43) for Sh, whereas the volume clearance rate corresponding to the higher value of $\mathrm{Pe}_{\mathrm{turb}}$ is found via equation (2.45) for Sh, giving $c_v = 4.49 - 9.05 \times 10^{-5}$ml d^{-1}. This is around 3 to 4 times larger than the volume clearance rate of a phytoplankter of half the size. Again, the difference made to this volume clearance rate by doubling the phytoplankton radius is more pronounced than was seen for the volume clearance rate of motile cells in stagnant fluid. However, if we double the diameter of the virus to $d_v = 4 \times 10^{-5}$cm, and keep the phytoplankton radius at $\frac{15}{2} \times 10^{-4}$cm, the contact rate will decrease. For this diameter, the viral diffusivity halves to become $D_v = 1.07 \times 10^{-8}\mathrm{cm}^2\mathrm{s}^{-1}$. The Péclet number is then between 1.66 and 52.57, thus the Sherwood number will be computed using equation (2.43) for the lower value of Pe and equation (2.44) for the higher value of Pe. The phytoplankton-virus volume clearance rate is then in the range $c_v = 1.1$ to 2.0×10^{-5}ml d^{-1} for $d_v = 4 \times 10^{-5}$cm, compared to $c_v = 2.0$ to 3.1×10^{-5}ml d^{-1} for $d_v = 2 \times 10^{-5}$cm.

2.3.3 Motile cells, turbulent fluid

Here, the work of Batchelor (1980) on mass transfer from particles in turbulent fluid is followed to consider the $P - V$ contact rate for motile phytoplankton residing in a turbulent fluid. This flow is a superposition of the creeping flow of section 2.3.1 and the small-scale turbulence flow of section 2.3.2 (Batchelor, 1980). The flow is thus defined as:

$$\mathbf{U}(\mathbf{X}) = -\mathbf{V} + \mathbf{U}^{(\mathrm{T})} + \boldsymbol{\Omega} \cdot \mathbf{X} + \mathbf{X} \cdot \mathbf{E} + \mathbf{U}^{(\mathrm{E})}. \tag{2.49}$$

Recall that $-\mathbf{V}$ is the uniform fluid velocity field (corresponding to a phytoplankton swimming velocity of $\mathbf{V}$), $\boldsymbol{\Omega}$ is the rate of rotation of the fluid and $\mathbf{E}$ the rate of strain tensor. The flow fields $\mathbf{U}^{(\mathrm{T})}$ and $\mathbf{U}^{(\mathrm{E})}$ represent disturbance to the fluid due to the presence of a rigid sphere. Specifically, as we are modelling phytoplankton swimming as a stationary particle in a uniform creeping flow, $\mathbf{U}^{(\mathrm{T})}$ represents the disturbance to the uniform flow due to the presence of a stationary rigid sphere and $\mathbf{U}^{(\mathrm{E})}$ represents the disturbance due to a rigid sphere being unable to follow the straining motion of the ambient flow field (Batchelor, 1980). The flow will be modelled using equation (2.49), where the parameters $\mathbf{V}, \mathbf{E}$ and $\boldsymbol{\Omega}$ are functions of time.

A concentration boundary layer is the mechanism by which virions are transported around the sphere surface. Batchelor (1980) considered the advection-diffusion system

(2.4, 2.5, 2.6) with **U** as defined in equation (2.49) within the concentration boundary layer (since it is assumed that variations in concentration of virions occurs mainly within the boundary layer) for Pe $\gg$ 1. Again, we are not aware of any comparable results for small or intermediate values of Pe. Define the velocity component in the direction of the axis of rotation to be $-V_\omega$ and the component of the rate of strain in the direction of the axis of rotation to be E_ω. For a statistically steady flow, Batchelor (1980) found that, relative to the particle surface, the mean motion of fluid elements in the concentration boundary layer is the same as for a stationary cell suspended in a steady ambient flow with a uniform streaming flow of velocity V_ω and a pure straining motion with rate of strain E_ω. All other components of **V** and **E** have a mean value of zero. He was then able to conclude that mass transfer is due only to the components V_ω and E_ω, and their fluctuations, for Pe $\gg$ 1. Batchelor (1980) determined the Sherwood number for motile cells in turbulent fluid when $\mathrm{Pe}_{\mathrm{turb}}$ large to be:

$$\mathrm{Sh} = 0.404L(\beta)\left\{\frac{r_0\left(2.25 < V_\omega >^2 + 56.25 r_0^2 < E_\omega >^2\right)^{\frac{1}{2}}}{D_v}\right\}^{\frac{1}{3}}, \tag{2.50}$$

where L is a dimensionless function of $\beta = \frac{5r_0 < E_\omega >}{< V_\omega >}$. The straining component $< E_\omega >$ is given by equation (2.38). When $< V_\omega >= 0$, $\beta \to \infty$ and $L = 1.225$ (Batchelor, 1980). The Sherwood number in the absence of phytoplankton swimming is therefore:

$$\mathrm{Sh} = 0.968\left(\frac{r_0^2 | < E_\omega > |}{D_v}\right)^{\frac{1}{3}} \approx 0.55\mathrm{Pe}_{\mathrm{turb}}^{\frac{1}{3}}, \tag{2.51}$$

which is consistent with equation (2.45), for $S = 0.6$. Similarly, when $< E_\omega >= 0$, $\beta = 0$ and $L = 1.351$ (Batchelor, 1980), giving the Sherwood number for motile phytoplankton in the absence of straining motion to be

$$\mathrm{Sh} = 0.625\left(\frac{r_0 | < V_\omega > |}{D_v}\right)^{\frac{1}{3}}. \tag{2.52}$$

If the vorticity vector were constant, we could say $< V_\omega >= U_{\mathrm{P}}$ and reduce equation (2.52) to

$$\begin{aligned} \mathrm{Sh} &= 0.625\left(\frac{r_0 U_{\mathrm{P}}}{D_v}\right)^{\frac{1}{3}} \\ &= 0.625\mathrm{Pe}_{\mathrm{swim}}^{\frac{1}{3}}, \end{aligned} \tag{2.53}$$

which is the leading order expression given in equation (2.22).

In isotropic turbulence, the vorticity vector is continually being reoriented because it doesn't have a preferred direction. If we assume the phytoplankton to always swim in one fixed direction, the mean swimming speed in the direction of the vorticity vector will be zero due to the vorticity vector being reoriented. Therefore, since $< V_\omega >= 0$,

the Sherwood number expression (2.50) reduces to equation (2.51), which is independent of phytoplankton swimming. This leads us to the conclusion that phytoplankton swimming is unimportant, to leading order, when $\mathrm{Pe}_{\mathrm{turb}}$ is large. However, it should be noted that, if there are any interactions between the phytoplankton cell and vorticity vector such that the swimming direction aligns with the vorticity vector, this may not be the case (see the work of Thorn and Bearon (2010), for example).

We will now consider what 'critical' value of $\mathrm{Pe}_{\mathrm{turb}}$ is required for this to hold, and find the minimum swimming speed required for phytoplankton swimming to have a greater effect on the contact rate than turbulence. Consider motile cells in still fluid swimming upwards with speed U_{P}, where the Sherwood expression (2.53) applies. We consider $\mathrm{Pe}_{\mathrm{swim}}$ to be $\frac{r_0 U_{\mathrm{P}}}{D_v}$ and $\mathrm{Pe}_{\mathrm{turb}}$ to be zero. If stirring is applied to this system, $\mathrm{Pe}_{\mathrm{turb}}$, which is equal to $\frac{r_0^2}{D_v}\left(\frac{\epsilon}{\nu}\right)^{\frac{1}{2}}$, will increase and at some critical point become so large that expression (2.52) is no longer applicable and thus replaced by expression (2.51). By examining the validity of intermediary steps in the asymptotic calculations, Batchelor (1980) determined this switch to occur when the r.m.s vorticity in the stirring motion is of the order:

$$\Omega = \frac{U_{\mathrm{P}} \mathrm{Pe}_{\mathrm{swim}}^{-\frac{1}{3}}}{r_0}. \tag{2.54}$$

Using $\Omega = \left(\frac{\epsilon}{\nu}\right)^{\frac{1}{2}}$, equation (2.54) rearranges to give the critical swimming speed, above which swimming dominates the enhancement of flux and below which $\mathrm{Pe}_{\mathrm{turb}}$ is sufficiently large that equation (2.51) is the correct expression:

$$\begin{aligned} \left(\frac{\epsilon}{\nu}\right)^{\frac{1}{2}} &= \frac{U_{\mathrm{P}}^{\frac{4}{3}}}{r_0^{\frac{2}{3}} D_v^{\frac{1}{3}}}, \\ \therefore U_{\mathrm{P}} = U_{\mathrm{crit}} &= \left(\frac{r_0^2}{\sqrt{D_v}}\right)\left(\frac{\epsilon}{\nu}\right)^{\frac{3}{4}}, \end{aligned} \tag{2.55}$$

a result used in Figure 7 of Karp-Boss et al. (1996). Figure 2.3 plots U_{crit}, as a function of phytoplankton radius and swimming speed, for values of ϵ ranging from 10^{-5} to $10^{-2}\mathrm{cm}^2\mathrm{s}^{-3}$, and depicts the regions where swimming or turbulence dominate the flux.

Investigation of phytoplankton swimming dominating flux

Since equation (2.50), valid for large Pe, predicts swimming to have no influence on the $P-V$ contact rate, any calculation for *H. akashiwo* and HaV using this equation for Sh would only give the same results as section 2.3.2. However, we can use equation (2.55) to explore what values of ϵ allow *H. akashiwo* swimming to dominate the enhancement of virion flux into the cell.

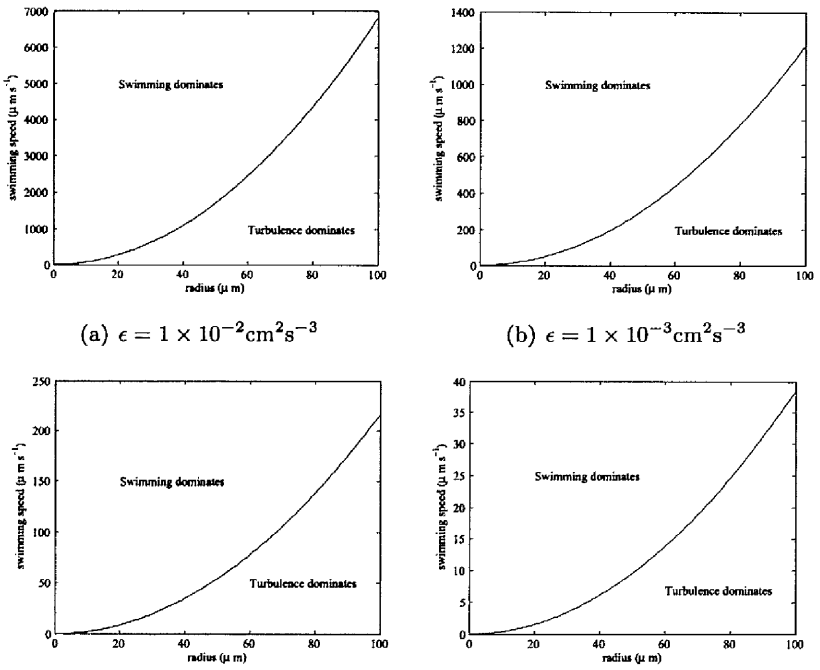

(a) $\epsilon = 1 \times 10^{-2}\text{cm}^2\text{s}^{-3}$ (b) $\epsilon = 1 \times 10^{-3}\text{cm}^2\text{s}^{-3}$

(c) $\epsilon = 1 \times 10^{-4}\text{cm}^2\text{s}^{-3}$ (d) $\epsilon = 1 \times 10^{-5}\text{cm}^2\text{s}^{-3}$

Figure 2.3: Plot showing for which values of phytoplankton radius and phytoplankton swimming speed the $P-V$ contact rate is dominated by swimming or turbulence. Plot (a) uses the highest value of ϵ, which is used in Figure 7 of Karp-Boss et al. (1996).

For swimming to dominate, the phytoplankton swimming speed must be greater than the critical velocity, U_{crit}. Therefore,

$$\left(\frac{r_0^2}{\sqrt{D_v}}\right)\left(\frac{\epsilon}{\nu}\right)^{\frac{3}{4}} < U_{\text{P}}, \tag{2.56}$$

which rearranges to show that swimming dominates when

$$\epsilon < \frac{U_{\text{P}}^{\frac{4}{3}} D_v^{\frac{2}{3}} \nu}{r_0^{\frac{8}{3}}}. \tag{2.57}$$

Therefore, for *H. akashiwo* of radius $r_0 = \frac{15}{2} \times 10^{-4}$cm, swimming at $U_{\text{P}} = 20$ to $160 \times 10^{-4}\text{cms}^{-1}$ and a virus with diffusivity $D_v = 2.14 \times 10^{-8}\text{cm}^2\text{s}^{-1}$, swimming dominates when the energy dissipation rate, $\epsilon < 4.18 \times 10^{-3}\text{cm}^2\text{s}^{-3}$ (for $U_{\text{P}} = 20 \times 10^{-4}\text{cms}^{-1}$) or $\epsilon < 6.69 \times 10^{-2}\text{cm}^2\text{s}^{-3}$ (for $U_{\text{P}} = 160 \times 10^{-4}\text{cms}^{-1}$). Since the energy dissipation rate in the oceanic upper mixed layer is typically in the range 10^{-5} to $10^{-2}\text{cm}^2\text{s}^{-3}$, the motility of *H. akashiwo* is likely to be influential in increasing its probability of being infected by HaV.

More generally, increasing phytoplankton swimming speed or virus diffusivity increases the threshold above which turbulence dominates. However, increasing the radius of the phytoplankton decreases this threshold. Therefore, there will be values of ϵ for which turbulence may dominate the flux enhancement of a larger cell, but not a smaller one, if the two are swimming at the same speed. If we were to assume swimming speed to be directly proportional to cell radius, the flux enhancement of larger organisms would still be dominated by turbulence for lower values of ϵ than smaller organisms because r_0 has twice the order of U_{P} in equation (2.57), when keeping D_v and ν constant. The relationship between cell size and swimming speed is slightly more complex than this. Kamykowski et al. (1992) observed lab. cultures of six dinoflagellate species and found good agreement with the relationship proposed by Okubo in 1987: swimming velocity (U) increases with cell length (L) in the form (Kamykowski et al., 1992):

$$U = 2.69L^{0.86}. \tag{2.58}$$

However, Kamykowski et al. (1992) also found some evidence to suggest that maximum swimming velocities were present for intermediate cell sizes.

According to Karp-Boss et al. (1996), the diffusivity of nutrients is of the order $10^{-5}\text{cm}^2\text{s}^{-1}$. For motile *H. akashiwo*, the enhancement of nutrient flux will be dominated by swimming when $\epsilon < 25 \times 10^{-8}\text{cm}^2\text{s}^{-3}$ (for $U_{\text{P}} = 20 \times 10^{-4}\text{cms}^{-1}$) or $\epsilon < 4 \times 10^{-6}\text{cm}^2\text{s}^{-3}$ (for $U_{\text{P}} = 160 \times 10^{-4}\text{cms}^{-1}$). It therefore appears that there may be situations where *H. akashiwo* motility will increase its uptake of virions, but not that of nutrients.

2.4 Phytoplankton-Zooplankton contact

The simplest assumption is that a planktonic predator possesses a three-dimensional, spherical, perception field of radius R within which any potential prey particle is likely to be perceived. Such a perception will be termed a 'contact' or encounter. The aim of this section is to try and estimate the number of such encounters a predator swimming at relative speed U might make. We show the theory behind calculating the encounter rate of plankton swimming in still fluid, following Gerritsen and Strickler (1977), and calculating the encounter rate of plankton swimming in turbulent fluid, following Lewis and Pedley (2000). We then explore how changing some key parameters will affect the encounter rate and make some calculations of the volume clearance rate for *H. akashiwo* and its predator *O. marina*, and the copepod *Clausocalanus furcatus*. Grazing studies of *C. furcatus* consuming dinoflagellate cells have been performed (e.g. Mazzocchi and Paffenhofer, 1999; Uttieri et al., 2008), revealing swimming speed and perception radius data that will be utilised in this section.

2.4.1 Plankton swimming in still fluid

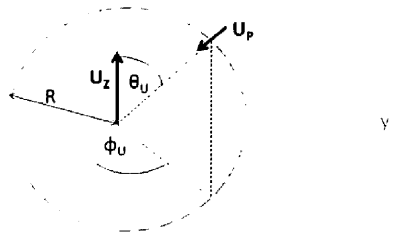

Figure 2.4: Depicting an encounter, as given in Gerritsen and Strickler (1977), between one prey and one predator in terms of the spherical coordinate system, (R, ϕ_U, θ_U), with the predator at the origin. The prey is swimming with speed U_P towards the predator at angles ϕ_U and θ_U with respect to the predator swimming speed U_Z.

Gerritsen and Strickler (1977) improved upon the basic encounter rate model, equation (2.11), by including prey swimming. The framework set up by Gerritsen and Strickler (1977) is to consider the predator and prey swimming with constant speeds, U_Z and U_P respectively, in a still fluid. The relative velocity of the prey with respect to the predator is $\mathbf{U} = \mathbf{U}_\mathrm{Z} - \mathbf{U}_\mathrm{P}$. They modelled an encounter by considering a prey

particle swimming towards a predator moving along the z-axis, as shown in Figure 2.4, where ϕ_U and θ_U are angles between the velocity vectors $\mathbf{U}_\mathrm{Z}$ and $\mathbf{U}_\mathrm{P}$.

Remember the basic encounter rate model:

$$\mathrm{CR}_\mathrm{z} = \pi R^2 P U_\mathrm{Z}. \tag{2.59}$$

Now, for motile prey, we need to consider relative speed as opposed to the predator swimming speed used in the basic model. Thus, we replace U_Z by:

$$\int U P(\omega) d\Omega. \tag{2.60}$$

Here, $U = |\mathbf{U}|$ is a function of θ_U and ϕ_U so we calculate the average value over all angles θ_U and ϕ_U and $P(\omega)$ is the probability of swimming with a track angle in the element of solid angle given by $d\Omega = \sin\theta_U d\theta_U d\phi_U$. The probability that a single prey swims towards the predator with a track angle ω in $d\Omega$ is proportional to $d\Omega$ (Gerritsen and Strickler, 1977):

$$P(\omega) d\Omega = k d\Omega = k \sin\theta_U d\theta_U d\phi_U. \tag{2.61}$$

The encounter rate of a predator with its motile prey in a still fluid is then given by (Gerritsen and Strickler, 1977):

$$\mathrm{CR}_\mathrm{z} = \pi P R^2 \frac{\left(U_\mathrm{P}^2 + 3U_\mathrm{Z}^2\right)}{3U_\mathrm{Z}} \qquad U_\mathrm{Z} \geq U_\mathrm{P}, \tag{2.62}$$

which is equal to equation (2.59) when $U_\mathrm{P} = 0$. The full derivation is shown in Appendix A.2.1. A similar expression for when $U_\mathrm{P} \geq U_\mathrm{Z}$ is given in Gerritsen and Strickler (1977).

2.4.2 Plankton swimming in a turbulent fluid

Lewis and Pedley (2000) developed an expression to calculate the encounter rate between a predator and prey swimming in turbulent fluid. We work through the derivation of this equation before using it to explore how key parameters, such as the energy dissipation rate and perception radius, affect the encounter rate. We also calculate some values of the volume clearance rate (CR_z without prey density) for our example phytoplankton species, *H. akashiwo*, and its predator *O. marina*.

Following the framework set up by Lewis and Pedley (2000), consider the predator at the origin of the spherical coordinate system (r, ϕ_R, χ_R), shown in Figure 2.5. Both the predator and its potential prey are motile, with velocities $\mathbf{U}_\mathrm{Z}$ and $\mathbf{U}_\mathrm{P}$ respectively. Let $\mathbf{U} = \mathbf{U}_\mathrm{Z} - \mathbf{U}_\mathrm{P}$ be the predator's relative velocity, directed without loss of generality, along the z-axis. We shall assume there is no preferred swimming direction (in contrast to the statement following equation (2.53)). We are now considering a reference frame where the prey is stationary and the predator is moving with a fixed velocity $\mathbf{U}$. One

can define a surface element of the spherical perception field to consist of the surface of the points on the sphere of radius R lying between χ_R and $\chi_R + \delta\chi_R$, and between ϕ_R and $\phi_R + \delta\phi_R$, as depicted by the shaded region in Figure 2.6(a). The encounter rate will be calculated for this small section of the perception field, which will then be integrated over the surface of the sphere and velocity fields of the plankton to give the total contact rate per predator. The encounter rate for the surface element per unit time is equal to the area of the surface element projected onto the $x - y$ plane multiplied by the prey density, relative speed U and the probability of moving with this speed.

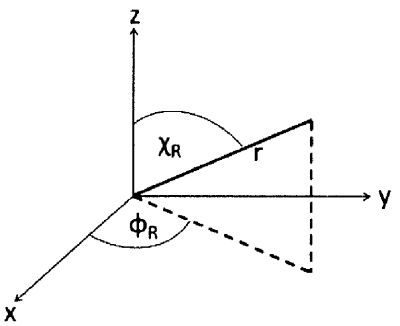

Figure 2.5: The spherical coordinate system used in considering the phytoplankton-predator contact rate, (r, ϕ_R, χ_R).

Figure 2.6(b) shows a projection of the surface element onto the $x - y$ plane (i.e. where $z = 0$). The area of the shaded region in Figure 2.6(b) is approximately equal to the cross-sectional area of the surface element, for small angles. Therefore, subtracting the area of the smaller sector in Figure 2.6(b) from the area of the whole sector gives an approximation of the cross-sectional area of the surface element to be:

$$A = \frac{R^2}{2}\left\{\sin^2(\chi_R + \delta\chi_R) - \sin^2(\chi_R)\right\}\delta\phi_R. \tag{2.63}$$

Providing the predator's 'line of sight' corresponds to its direction of motion, a hemisphere is equivalent to a sphere since, for a predator moving forwards along the z-axis towards a field of stationary prey, the prey can only enter the perception field through the upper surface of the sphere (Dr. D.M. Lewis, in personal communication). Therefore, Lewis and Pedley (2000) model the contact rate through a spherical perception field by calculating the contact rate through a hemisphere projected in the direction of predator motion. They integrate over χ_R for $0 < \chi_R < \frac{\pi}{2}$, thus eliminating

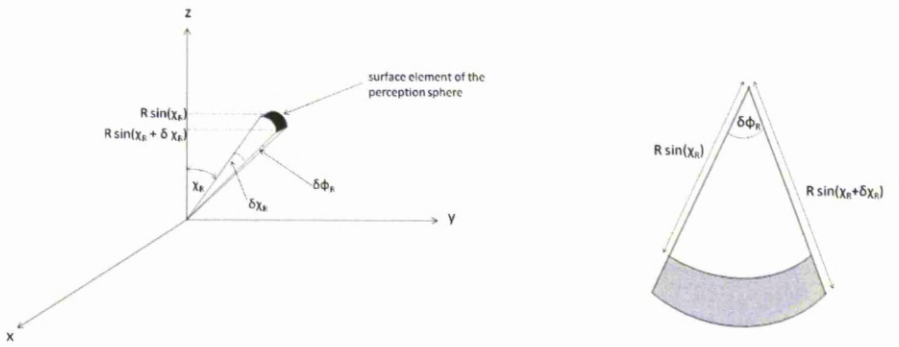

(a) Surface element

(b) Projection onto the $x - y$ plane.

Figure 2.6: The surface element of the perception field, through which phytoplankton must enter for an encounter to take place. The contact rate through this surface element is then used to find the total contact rate for the whole sphere.

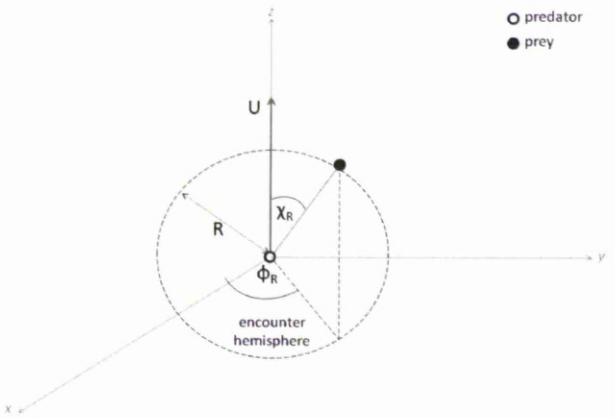

Figure 2.7: Depicting an encounter between one prey and one predator in terms of the spherical coordinate system, (R, ϕ_R, χ_R), where χ_R is an acute angle. The coordinate system is moving with the prey, so that the predator has relative speed U directed along the z-axis. The stationary prey particle is perceived by the predator as it enters the perception field at an angle χ_R to the z-axis and ϕ_R to the x-axis (Lewis and Pedley, 2000).

the negative z-axis.

Lewis and Pedley (2000) consider a coordinate system moving with the prey, so that the predator has relative speed U (where $\mathbf{U} = \mathbf{U}_Z - \mathbf{U}_P$) directed along the z-axis. A stationary phytoplankton cell enters the sphere at an angle χ_R to the direction of U (the z-axis) and ϕ_R to the x-axis, where $0 \leq \chi_R \leq \frac{\pi}{2}$ and $0 \leq \phi_R \leq 2\pi$, as in Figure 2.7. For this coordinate system, the cross-sectional area is as equation (2.63):

$$A = \frac{R^2}{2}\left\{\sin^2(\chi_R + \delta\chi_R) - \sin^2(\chi_R)\right\}\delta\phi_R \approx \frac{R^2}{2}\sin(2\chi_R)\, d\chi_R d\phi_R. \tag{2.64}$$

Letting $\theta_R = 2\chi_R$, this can also be written as:

$$A = \frac{R^2}{4}\sin\theta_R d\theta_R d\phi_R, \quad 0 < \theta_R < \pi. \tag{2.65}$$

For motile plankton in a turbulent flow, the plankton are able to move both by self-propelled swimming motions and through advection by the flow. Therefore, the total velocities of the plankton, $\mathbf{V}_Z$ for the predator and $\mathbf{V}_P$ for the phytoplankton, are defined as (Lewis and Pedley, 2000):

$$\mathbf{V}_Z(\mathbf{x}, t) = \mathbf{U}_Z(\mathbf{x}, t) + \mathbf{w}(\mathbf{x}, t), \tag{2.66}$$

$$\mathbf{V}_P(\mathbf{x} + \mathbf{r}, t) = \mathbf{U}_P(\mathbf{x} + \mathbf{r}, t) + \mathbf{w}(\mathbf{x} + \mathbf{r}, t), \tag{2.67}$$

where $\mathbf{w}$ is the velocity vector of the turbulent flow and the predator and prey are positioned at $\mathbf{x}$ and $\mathbf{x} + \mathbf{r}$ respectively. We assume the turbulence to be homogeneous and isotropic. The probability that the predator and its prey are moving with non-uniform velocities $\mathbf{V}_Z$ and $\mathbf{V}_P$ respectively when the prey enters the perception field, can be represented by the conditional joint probability density function of the velocities at a vector separation $\mathbf{R}$:

$$p_{P,Z}(\mathbf{V}_Z, \mathbf{V}_P|\mathbf{R}). \tag{2.68}$$

Multiplying the cross-sectional area by phytoplankton density, P, relative speed, $U_{(\mathbf{R})}$, and probability of plankton moving with that speed, $p_{P,Z}(\mathbf{V}_Z, \mathbf{V}_P|\mathbf{R})$, and integrating over the hemisphere and all possible swimming velocities gives the encounter rate at (or inward flux through) the "encounter hemisphere" for a single predator where plankton are swimming in turbulent fluid (Lewis and Pedley, 2000):

$$\mathrm{CR}_z = \frac{R^2 P}{4}\int_{\mathbf{V}_Z}\int_{\mathbf{V}_P}\int_0^{\pi}\int_0^{2\pi} U(\mathbf{R})\sin(\theta_R) p_{P,Z}(\mathbf{V}_Z, \mathbf{V}_P|\mathbf{R}) d\phi_R d\theta_R d\mathbf{V}_P d\mathbf{V}_Z. \tag{2.69}$$

Following two sets of change in variables and approximation of $p_{P,Z}(\mathbf{V}_Z, \mathbf{V}_P|\mathbf{R})$ (shown fully in Appendix A.2.2), the encounter rate reduces to the integral:

$$\mathrm{CR_z} = PR^2\sqrt{\frac{\pi}{2}}\int_0^{\pi}\left\{\sqrt{\frac{\pi}{2}}\mathrm{erf}\left(\frac{<U>}{\sigma_U\sqrt{2}}\right)\left[<U>+\frac{\sigma_U^2}{<U>}\right]\right.$$
$$\left.+\,\sigma_U\exp\left(-\frac{<U>^2}{2\sigma_U^2}\right)\right\}\sin\theta_R d\theta_R. \tag{2.70}$$

The average relative speed, for plankton swimming with uniform speeds, is given by

$$\begin{aligned} <U>^2 &= <\mathbf{U}>\cdot<\mathbf{U}> \\ &= (<\mathbf{U_Z}>-<\mathbf{U_P}>)\cdot(<\mathbf{U_Z}>-<\mathbf{U_P}>) \\ &= (\mathbf{U_Z}-\mathbf{U_P})\cdot(\mathbf{U_Z}-\mathbf{U_P}) \\ &= U_Z^2+U_P^2-2\mathbf{U_Z}\cdot\mathbf{U_P}. \end{aligned} \tag{2.71}$$

The quantity $\mathbf{U_P}\cdot\mathbf{U_Z}$ is equal to U_PU_Z multiplied by the cosine of the angle between the velocity vectors $\mathbf{U_P}$ and $\mathbf{U_Z}$, which corresponds to θ_U in section 2.4.1. Lewis and Pedley (2000) assume this angle to be equivalent to the θ_R used throughout this section, which is actually the angle between the position of the prey and the relative velocity of the predator. Lewis and Pedley (2000) demonstrate the equivalence of these two approaches in their appendix, showing that equating the angles θ_R and θ_U allows one to recover the Gerritsen and Strickler (1977) result, equation (2.62), with corrections due to the presence of turbulence. However, further work to consider how these two angles relate would be desirable.

We will follow Lewis and Pedley (2000) and use

$$<U>^2 = U_Z^2+U_P^2-2U_PU_Z\cos(\theta_R) \tag{2.72}$$

to calculate the encounter rate for plankton swimming in still fluids. The quantity $\sigma_U(\mathbf{R})$ is given by

$$\begin{aligned} \sigma_U^2(\mathbf{R}) &= \frac{<\mathbf{U}\cdot\mathbf{U}>-<\mathbf{U}>\cdot<\mathbf{U}>}{3}, \\ &= \frac{1}{3}\left[6W^2-2<\mathbf{w}(\mathbf{x},t)\cdot\mathbf{w}(\mathbf{x}+\mathbf{R},t)>+<\mathbf{U_Z}\cdot\mathbf{U_Z}>+<\mathbf{U_P}\cdot\mathbf{U_P}>\right. \\ &- \left.2<\mathbf{U_Z}\cdot\mathbf{U_P}>-(\mathbf{U_Z}-\mathbf{U_P})\cdot(\mathbf{U_Z}-\mathbf{U_P})\right], \end{aligned} \tag{2.73}$$

assuming the swimming motion is uncorrelated with the turbulent flow. The quantity $W^2=\frac{<\mathbf{w}(\mathbf{x},t)\cdot\mathbf{w}(\mathbf{x},t)>}{3}$ is a measure of turbulent intensity (Lewis and Pedley, 2000). The last terms cancel to leave (see Appendix A.2.6):

$$\begin{aligned}\sigma_U^2(\mathbf{R}) &= \frac{1}{3}\left[6W^2 - 2 < \mathbf{w}(\mathbf{x},t)\cdot\mathbf{w}(\mathbf{x}+\mathbf{R},t) >\right], \\ &= \frac{4}{3}\int_0^\infty E(k,t)\left(1-\frac{\sin(kR)}{kR}\right)dk, \\ &\approx < \epsilon >^{\frac{2}{3}} R^{\frac{2}{3}}\left[Sc - \frac{3\eta^{\frac{2}{3}}}{R^{\frac{2}{3}}} + 2\int_{\frac{R}{\eta}}^\infty \frac{\sin(x)}{x^{\frac{8}{3}}}dx\right], \end{aligned} \tag{2.74}$$

where k is the wavenumber and $E(k,t)$ is the energy spectrum (Davidson, 2006). The approximation in equation (2.74) is obtained by substituting $E(k,t) = \frac{3}{2} < \epsilon >^{\frac{2}{3}} k^{-\frac{5}{3}}$ and performing the integral where possible, experimental data suggesting the value of $\frac{3}{2}$ (Tennekes and Lumley, 1972), which corresponds to the general form observed in the inertial subrange of all turbulent flows. The full calculation of equation (2.74) is shown in Appendix A.2.6. This is appropriate for $R \gg \eta$, where η is the Kolmogorov microscale of equation (1.33). Lewis and Pedley (2001) discuss other options for $E(k,t)$ when $R \ll \eta$ and $R \sim \eta$ suggested by Monin and Yaglom in 1975. They suggested $E(k,t)$ is proportional to $< \epsilon > \frac{R^2}{\nu}$ when $R \ll \eta$ and proportional to $< \epsilon >^{\frac{2}{3}} R^{\frac{2}{3}}$ when $R \sim \eta$. From Lewis and Pedley (2000), $Sc = \frac{9}{10}\Gamma\left(\frac{1}{3}\right) = 2.411$. Note that, when studying equation (2.74), the energy dissipation rate, ϵ, also appears implicitly in η.

Example calculations of contact rates

Here we use realistic parameter values for *H. akashiwo* and its predator *O. marina*, summarised in Table 2.1, to calculate values of the phytoplankton-predator volume clearance rate, c_z. We will also consider how a larger zooplankter *C. furcatus* would alter c_z, compared to *O. marina*.

We have the result, derived by Lewis and Pedley (2000), that the phytoplankton-predator volume clearance rate (i.e. the contact rate without the inclusion of prey density) is given as a function of contact radius, R, average relative speed, $< U >$, and the average energy dissipation rate, $< \epsilon >$, given in equation (2.70):

$$\begin{aligned} c_z = R^2\sqrt{\frac{\pi}{2}}\int_0^\pi \left\{\sqrt{\frac{\pi}{2}}\mathrm{erf}\left(\frac{< U >}{\sigma_U\sqrt{2}}\right)\left[< U > + \frac{\sigma_U^2}{< U >}\right]\right. \\ \left. + \sigma_U \exp\left(-\frac{< U >^2}{2\sigma_U^2}\right)\right\}\sin\theta_R d\theta_R, \end{aligned} \tag{2.75}$$

where

$$\sigma_U^2(R) \approx < \epsilon >^{\frac{2}{3}} R^{\frac{2}{3}}\left[Sc - \frac{3\eta^{\frac{2}{3}}}{R^{\frac{2}{3}}} + 2\int_{\frac{R}{\eta}}^\infty \frac{\sin(x)}{x^{\frac{8}{3}}}dx\right]. \tag{2.76}$$

As discussed previously, we will use

$$< U >^2 = U_Z^2 + U_P^2 - 2U_P U_Z \cos(\theta_R) \tag{2.77}$$

to calculate c_z for constant swimming speeds, following Lewis and Pedley (2000).

Consider the *H. akashiwo* volume clearance rate specifically. We will calculate the $P - Z$ volume clearance rate as this will aid comparison with the $P - V$ work in section 2.3. The volume clearance rate is found by calculating the contact rate without the inclusion of prey density. The swimming speed of *H. akashiwo* is in the range $20 - 160 \times 10^{-4}\text{cms}^{-1}$. We will use $339 \times 10^{-4}\text{cms}^{-1}$ for the *O. marina* swimming speed and $R = 4.3 \times 10^{-4}\text{cm}$ for the perception radius. This perception radius is estimated in section 3.3.6, using data observed by Jeong et al. (2003).

We first calculate the basic volume clearance rate, which represents non-motile phytoplankton in still fluid, in order to determine the effects of introducing phytoplankton swimming and turbulence. The contact rate (2.75) reduces to that shown in equation (2.11) in the absence of phytoplankton swimming and turbulence. Thus, the basic volume clearance rate is:

$$c_z = \pi R^2 U_Z. \tag{2.78}$$

The volume clearance rate for non-motile *H. akashiwo* in still fluid is therefore 0.0017 ml d^{-1} (2sf). We determine how introducing phytoplankton motility will affect this clearance rate by using the Gerritsen and Strickler (1977) expression, given in equation (2.62), which the contact rate (2.70) reduces to in the absence of turbulence. The volume clearance rate is therefore now given by:

$$c_z = \pi R^2 \frac{(U_P^2 + 3U_Z^2)}{3U_Z} \qquad U_Z \geq U_P. \tag{2.79}$$

The volume clearance rate for motile *H. akashiwo* in still fluid is therefore calculated to be in the range 0.0017 to 0.0018 ml d^{-1} (2sf). Thus, the ability of *H. akashiwo* to swim in still fluid increases its contact rate with *O. marina*, but not substantially. Finally, we calculate the volume clearance rate of motile *H. akashiwo* in turbulent fluid using equations (2.75) and (2.76). This volume clearance rate has been calculated numerically in Matlab to be between 0.0017 and 0.0018 ml d^{-1} (2sf), for *H. akashiwo* swimming at speeds in the range 20 to $160 \times 10^{-4}\text{cms}^{-1}$ for all ϵ between 10^{-5} and $10^{-2}\text{cm}^2\text{s}^{-3}$. Thus, for these parameter values to 2sf, changing ϵ doesn't alter the volume clearance rate of *O. marina* and *H. akashiwo*. The Matlab code used to make this calculation is shown in Appendix A.2.7.

We now explore more generally how changing some key parameters will affect the phytoplankton-predator volume clearance rate. Figure 2.8 investigates the effects of turbulence, via variation of the energy dissipation rate, ϵ. This appears explicitly in equation (2.76) and implicitly via η. The volume clearance rate is calculated over a range of phytoplankton swimming speeds for two values of ϵ: $10^{-5}\text{cm}^2\text{s}^{-3}$ and $1\text{cm}^2\text{s}^{-3}$.

The former is the minimal value of ϵ typical in the upper oceanic mixed layer, whereas the latter value is outside of the range we have considered in this chapter. This is done to enable us to see the difference made by ϵ in Figure 2.8 more clearly. In each plot, $\epsilon = 1\text{cm}^2\text{s}^{-3}$ is represented by $\circ$ and $\epsilon = 10^{-5}\text{cm}^2\text{s}^{-3}$ is represented by $\diamond$. We take the kinematic viscosity, $\nu = 10^{-2}\text{cm}^2\text{s}^{-1}$. Four plots have been produced. Figure 2.8(a) shows how the volume clearance rate varies with prey swimming speeds for a non-motile predator, whilst Figure 2.8(b) represents *O. marina* swimming at $3.39 \times 10^{-2}\text{cms}^{-1}$, which is the swimming speed Menden-Deuer and Grünbaum (2006) observed for *O. marina* in the presence of a prey species. The largest value of prey swimming speed plotted ($U_{\text{P}} = 3 \times 10^{-2}\text{cms}^{-1}$) is comparable to that of the predator. The third plot, Figure 2.8(c), shows the volume clearance rate changing with prey swimming speed for the faster predator *C. furcatus*. The swimming speed used is 1cms^{-1}, which Uttieri et al. (2008) observed for *C. furcatus*. For comparison, the copepod is typically 10^{-1}cm in length (Uttieri et al., 2008) compared to *O. marina* typically 13×10^{-4}cm in length (Menden-Deuer and Grünbaum, 2006). The final plot, Figure 2.8(d), shows the volume clearance rate for *C. furcatus* swimming at 1cms^{-1}, as in Figure 2.8(c), over a larger range of prey swimming speeds. The largest value of U_{P} plotted is 1cms^{-1}, which is comparable to the swimming speed of the predator. The perception radius used in plots (a) and (b) is 4.3×10^{-4}cm. This is the value we have estimated for *O. marina* from data given in Jeong et al. (2003). This process is shown fully in section 3.3.6. Plots (c) and (d) use $R = 4 \times 10^{-2}$cm, the value Uttieri et al. (2008) estimated for *C. furcatus*. It should be noted that, for the ν and ϵ values in Table 2.1, the Kolmogorov length-scale given by equation (1.33) is in the range 10^{-1} to 5.6×10^{-1}cm. Therefore, since the approximation in equation (2.74) is applicable for $R \gg \eta$, the approximation that will be used throughout this section is not appropriate for the values of R used here. Lewis and Pedley (2000) use equations (2.75) and (2.76) to calculate the encounter rate of Herring fish larvae and their prey. Since a contact radius of $R = 3 \times 10^{-1}$cm was used in Lewis and Pedley (2000), their contact radius is approximately equal to η, depending on the energy dissipation rate being considered.

As expected, the larger value of ϵ yields a larger volume clearance rate, as does increasing predator or prey swimming speeds, although the difference is minimal in all but plot (c). Increasing the phytoplankton swimming speed makes a more noticeable difference than changing ϵ, for the values considered. Introducing motility to the predator, giving it a speed of $3.39 \times 10^{-2}\text{cms}^{-1}$ (i.e. the difference between Figure 2.8(a) and Figure 2.8(b)), has a marked improvement on the volume clearance rate, particularly at low phytoplankton swimming speeds. The gradient of the curve increases as swimming speed increases in Figure 2.8(b), meaning that, over this range of prey swimming speeds, larger U_{P} makes a more significant difference to the volume clearance rate. The vertical dashed lines in Figure 2.8(b) represent the swimming speed range of *H. akashiwo* (the left line being at $U_{\text{P}} = 20 \times 10^{-4}\text{cms}^{-1}$ and the line

on the right is at $U_P = 160 \times 10^{-4}\text{cms}^{-1}$) and demonstrate that the volume clearance rate increases from $1.7 \times 10^{-3}\text{ml d}^{-1}$ to $1.8 \times 10^{-3}\text{ml d}^{-1}$ (2sf), for $\epsilon = 10^{-5}\text{cm}^2\text{s}^{-3}$, and from $1.7 \times 10^{-3}\text{ml d}^{-1}$ to $1.8 \times 10^{-3}\text{ml d}^{-1}$ (2sf), for $\epsilon = 10^{-2}\text{cm}^2\text{s}^{-3}$ (2sf). Since for these parameter values, there is no difference in the volume clearance rate over the range of ϵ, to 2sf, increased access to nutrients and light achieved by the phytoplankton through motility may outweigh the increased probability of being grazed upon. Increasing predator swimming speed reduces the gradient of the curves, i.e. for larger predator swimming speeds, a larger prey swimming speed is needed before c_z will be altered. The volume clearance rate for the predator swimming at 1cms^{-1}, shown in Figure 2.8(c), is unchanged for prey swimming speeds in the range 0 to $3 \times 10^{-2}\text{cm s}^{-1}$. However, the volume clearance rate for a predator swimming at 1cms^{-1} with perception radius $R = 4 \times 10^{-2}\text{cm}$ is substantially larger than for a predator swimming at $3.39 \times 10^{-2}\text{cms}^{-1}$ with perception radius $R = 4.3 \times 10^{-4}\text{cm}$.

Figure 2.9 considers how the perception radius, R, affects the $P - Z$ volume clearance rate. From equation (2.75), R affects the volume clearance rate directly through increasing the size of the perception field, but also indirectly through changing the correlation in turbulent velocity. Three values of R are considered: $R = 4 \times 10^{-2}\text{cm}$, represented by $\diamond$ in each plot, $R = 4 \times 10^{-3}\text{cm}$, represented by $\circ$, and $R = 4 \times 10^{-4}\text{cm}$, represented by $\star$. The first value is approximately the perception radius of the copepod *C. furcatus* whilst the last value is approximately that of *O. marina*. The value of ϵ used is a mid-range value of those typically found in the upper oceanic mixed layer, $\epsilon = 10^{-3}\text{cm}^2\text{s}^{-3}$. All other values are consistent with Figure 2.8. Figure 2.9(a) shows the volume clearance rate for a non-motile predator, whilst Figure 2.9(b) shows the same plot zoomed in to see the curves $R = 4 \times 10^{-3}\text{cm}$ and $R = 4 \times 10^{-4}\text{cm}$ more clearly. Figures 2.9(c) and 2.9(d) show the volume clearance rate for *O. marina* swimming at $3.39 \times 10^{-2}\text{cms}^{-1}$ and, finally, Figures 2.9(e) and 2.9(f) show the volume clearance rate for *C. furcatus* swimming at 1cms^{-1}.

Increasing the perception radius, R, increases the volume clearance rate, as we expect from equation (2.75). The change to the volume clearance rate can be considerable. For example, Figures 2.9(e) and 2.9(f) show that increasing R from $4 \times 10^{-3}\text{cm}$ to $4 \times 10^{-2}\text{cm}$ increases c_z from ~ 4.5 to 450ml d^{-1}, for a predator swimming at 1cms^{-1}. As was seen in Figure 2.8, increasing phytoplankton swimming speed from 0 to $3 \times 10^{-2}\text{cms}^{-1}$ doesn't change the volume clearance rate significantly. Again, these phytoplankton swimming speeds have more of an impact on the volume clearance rate for lower predator swimming speeds. Conversely, the factor difference in the volume clearance rate by changing R is larger for larger predator swimming speeds. Thus, the faster a predator can swim, the more of an impact changing its perception radius would have. This wasn't seen when changing the energy dissipation rate. This may be because the mixing from turbulence may effectively reduce the distance travelled by the predator, even when its swimming speed has increased.

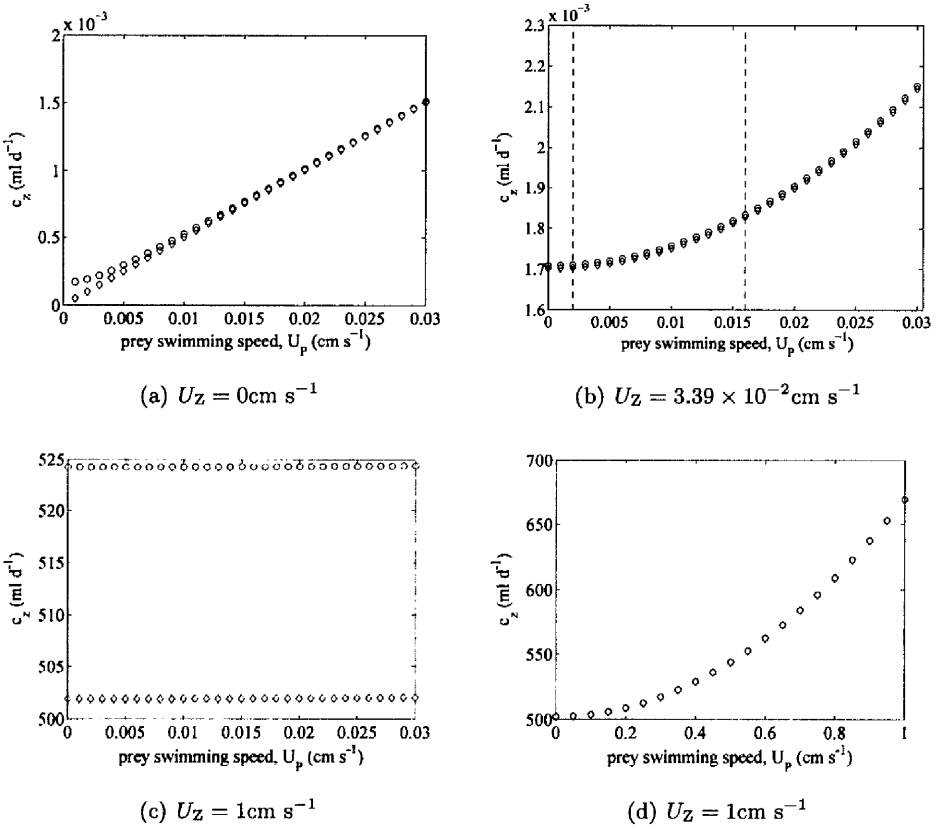

(a) $U_Z = 0\text{cm s}^{-1}$

(b) $U_Z = 3.39 \times 10^{-2}\text{cm s}^{-1}$

(c) $U_Z = 1\text{cm s}^{-1}$

(d) $U_Z = 1\text{cm s}^{-1}$

Figure 2.8: Plot of phytoplankton-predator volume clearance rate against phytoplankton swimming speed. The two sets of data on each graph represent the two values of ϵ used: $\epsilon = 10^{-2}\text{cm}^2\text{s}^{-3}$, represented by $\circ$ in each figure (the top data set) and $\epsilon = 10^{-5}\text{cm}^2\text{s}^{-3}$, represented by $\diamond$ in each figure (the bottom data set). Plot (a) represents a non-motile predator, (b) is for *O. marina* swimming at $3.39 \times 10^{-2}\text{cms}^{-1}$, (c) is for *C. furcatus* swimming at 1cm s^{-1} and (d) shows *C. furcatus* swimming at 1cm s^{-1} again, but for a larger range of prey swimming speeds. The vertical dashed lines in (b) represent the range of *H. akashiwo* swimming speeds considered throughout this chapter ($U_P = 20$ to $160 \times 10^{-4}\text{cms}^{-1}$). The perception radius used in plots (a) and (b) is $4.3 \times 10^{-4}\text{cm}$. That used in plots (c) and (d) is $R = 4 \times 10^{-2}\text{cm}$.

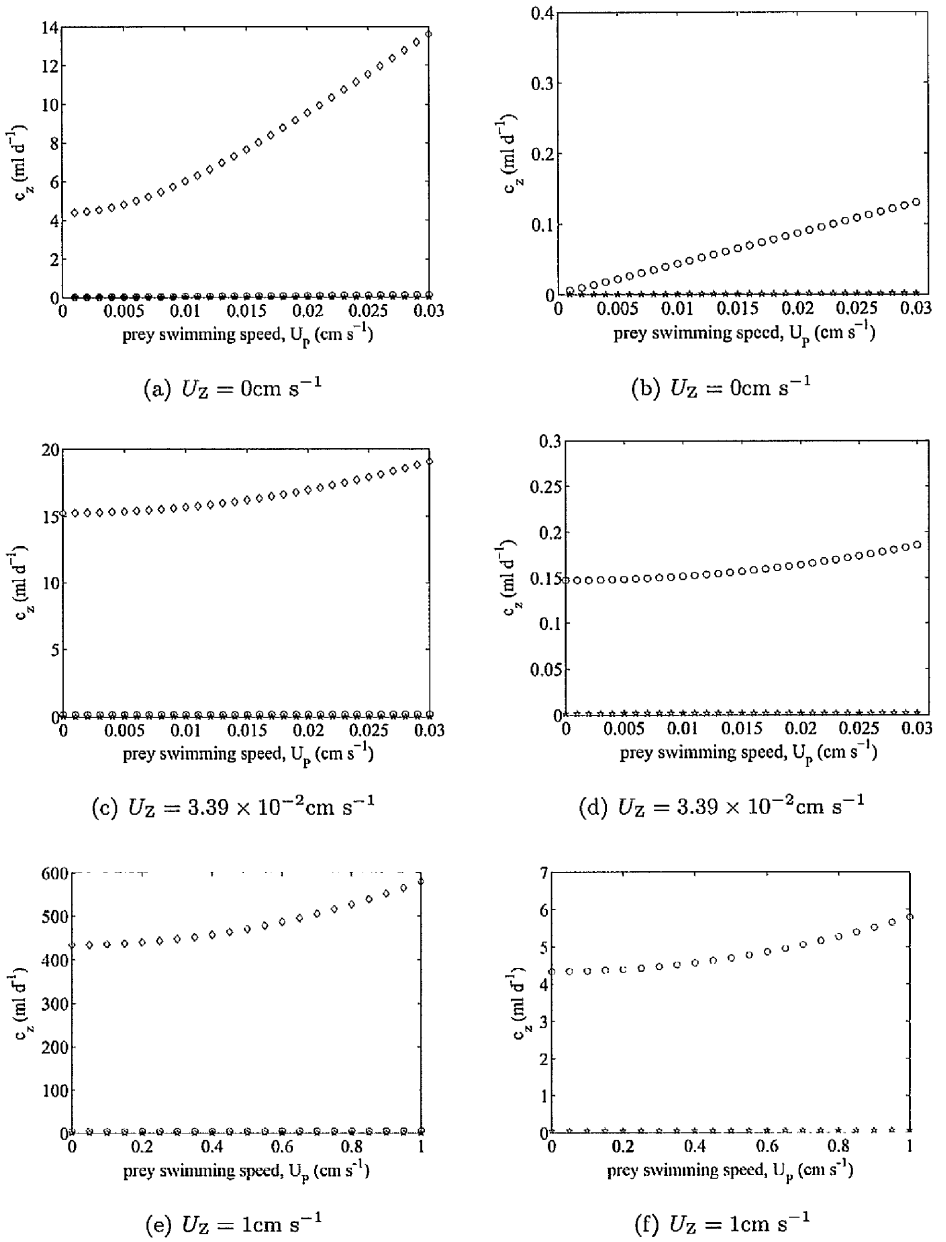

(a) $U_Z = 0\text{cm s}^{-1}$ (b) $U_Z = 0\text{cm s}^{-1}$

(c) $U_Z = 3.39 \times 10^{-2}\text{cm s}^{-1}$ (d) $U_Z = 3.39 \times 10^{-2}\text{cm s}^{-1}$

(e) $U_Z = 1\text{cm s}^{-1}$ (f) $U_Z = 1\text{cm s}^{-1}$

Figure 2.9: Plot of phytoplankton-predator volume clearance rate against phytoplankton swimming speed. The three sets of data on each graph represent the three values of R used: $R = 4 \times 10^{-2}$cm, represented by $\diamond$ in each figure (the top data set), $R = 4 \times 10^{-3}$cm, represented by $\circ$ in each figure (the middle data set) and $R = 4 \times 10^{-4}$cm, represented by $\star$ in each figure (the bottom data set). Plots (a) and (b) represent a non-motile predator, (c) and (d) *O. marina* swimming at 3.39×10^{-2}cm s^{-1} and (e) and (f) *C. furcatus* swimming at 1cm s^{-1}.

2.5 Discussion

The contact rate between a phytoplankton and its virus, and between a phytoplankton and its predator, has been considered. The derivation of each contact rate used differing approaches. For the $P-V$ contact rate, the work of Karp-Boss et al. (1996) has been followed. Karp-Boss et al. (1996) used fluid dynamics theory studying heat transfer from a sphere to determine the nutrient absorption rate by phytoplankton. We have then used this same theory, treating virions as solutes, to determine a volume clearance rate of virions by phytoplankton. This is equivalent to a maximum contact rate, i.e. it is assumed that every contact results in absorption.

We firstly studied motile cells in still fluid. We investigated expressions available for Sh in the limits of $\mathrm{Pe}_{\mathrm{swim}}$, derived by Acrivos and Taylor (1962) and Acrivos and Goddard (1965) by asymptotic approximation. This method was shown here for Pe large. An expression is also available for intermediate values of $\mathrm{Pe}_{\mathrm{swim}}$, found numerically by Clift et al. (1978). We discussed asymptotic approximations of Sh, derived by Batchelor (1979), for non-motile phytoplankton in steady shear flow in the limits of large and small $\mathrm{Pe}_{\mathrm{shear}}$. We then considered non-motile phytoplankton in a turbulent fluid, where advection due to small-scale turbulence was modelled as advection due to fluctuating shear flow. An asymptotic expansion for $\mathrm{Pe}_{\mathrm{turb}}$ large has been derived by Batchelor (1980), but not for $\mathrm{Pe}_{\mathrm{turb}}$ small. Karp-Boss et al. (1996) suggested an expression for $\mathrm{Pe}_{\mathrm{turb}}$ small to bridge this gap. Sherwood number expressions for intermediate values of $\mathrm{Pe}_{\mathrm{turb}}$ were also found by Karp-Boss et al. (1996), by interpolation, and included here. The final regime considered for the $P-V$ contact rate was that of motile cells in turbulent fluid. Again, an asymptotic approximation to Sh has been derived, by Batchelor (1980), for Pe large, but not Pe small. Consideration of this Sherwood number equation in the limit of large Pe leads to the conclusion that mass transfer to motile cells in turbulent fluid is independent of phytoplankton swimming. Following Batchelor (1980) we calculated the critical swimming velocity as a function of turbulence for which mass transfer is independent of swimming.

We then used the theory summarised for each of these flow regimes to gain an understanding of which parameters were important and the effects of altering them. We calculated the volume clearance rate for *H. akashiwo* and HaV under different temperature conditions, and also altering the size of each species. We found that, for the Péclet numbers calculated for *H. akashiwo* and HaV swimming in still fluid and not swimming in turbulent fluid, increasing phytoplankton radius or viral diffusivity increased the contact rate. Since increasing viral diffusivity increases the contact rate, increasing temperature or decreasing the diameter of the virus will increase the volume clearance rate. Changes in the phytoplankton radius led to a larger change in the volume clearance rate of the turbulent regime than the swimming regime, since the size of the phytoplankton contributed to the turbulent contact rate by $\alpha r_0 + \beta r_0^2$

whereas the contribution of r_0 to the swimming contact rate is proportional to $r_0^{\frac{4}{3}}$. Similarly, viral diffusivity contributes to the turbulent contact rate via $D_v + \sqrt{D_v}$ as opposed to the $D_v^{\frac{2}{3}}$ in the swimming regime. The swimming speed contributed to the swimming volume clearance rate by $U_{\mathrm{P}}^{\frac{1}{3}}$.

For the values of the energy dissipation rate and kinematic viscosity used here, the turbulent volume clearance rate was affected more by changes in phytoplankton radius and virus diffusivity than by the dissipation rate or kinematic viscosity. By calculating the volume clearance rate in both of these flow regimes, using the parameter values of Table 2.1, we found the flux of virions to *H. akashiwo* to be enhanced more by *H. akashiwo* swimming in still fluid than by being non-motile in turbulent fluid. We also found when comparing the Sherwood number for *H. akashiwo* with its virus compared to Sh for *H. akashiwo* with nutrients that there may be situations where the ability of *H. akashiwo* to swim will increase its uptake of virions by more than its uptake of nutrients. For the final case of motile phytoplankton in turbulent fluid, when $\mathrm{Pe}_{\mathrm{turb}}$ is large, the contact rate between *H. akashiwo* and HaV is the same as for non-motile phytoplankton in turbulent fluid since the Sherwood number expression used in this section predicted phytoplankton swimming to be unimportant in the mass transfer. However, we did use a formula, presented in Karp-Boss et al. (1996) following Batchelor (1980), to consider what values of the energy dissipation rate would allow *H. akashiwo* swimming to dominate over turbulence in terms of flux enhancement. We found that, for the parameter values listed in Table 2.1, *H. akashiwo* motility would dominate when $\epsilon < 4.18 \times 10^5 \mu\mathrm{m}^2\mathrm{s}^{-3}$, for *H. akashiwo* swimming at $20\mu\mathrm{ms}^{-1}$ and $\epsilon < 6.69 \times 10^6 \mu\mathrm{m}^2\mathrm{s}^{-3}$, for *H. akashiwo* swimming at $160\mu\mathrm{ms}^{-1}$. Since we are taking ϵ to typically lie in the range 10^3 to $10^6 \mu\mathrm{ms}^{-1}$, it is feasible that *H. akashiwo* motility will be influential in increasing its contact rate with HaV.

The calculation of the $P-Z$ contact rate followed the work of Lewis and Pedley (2000), who used a swept volume approach. The predator swims at a relative speed such that a stationary prey particle is perceived up to a distance R from the predator. The contact rate is equal to the flux of prey into the perception field. Similarly to the $P-V$ contact rate, the actual number of prey consumed by the predator will be some proportion of this contact rate and so our calculation gives an upper bound.

The effects of varying the energy dissipation rate, perception radius and predator and prey swimming speed on the $P-Z$ contact rate has been explored. Three species were considered: *H. akashiwo*, *O. marina* and *C. furcatus*. Increasing the energy dissipation rate, ϵ, increases the contact rate, but the effects are minimal, particularly for a predator with a lower swimming speed. The effects of ϵ, and thus turbulence, are also increased for larger prey swimming speeds. The effects of altering the perception radius, R, are however more substantial. We found that the faster a predator swims, the more of an impact changing its perception radius has. However, this wasn't seen

when varying ϵ. Calculations for *H. akashiwo* and *O. marina* showed plankton motility to be more influential to the contact rate than turbulence. However, the effects of phytoplankton motility on the contact rate weren't substantial and may mean that increased access to light and nutrients due to motility outweigh the increased chance of being consumed. Comparison of the predators *O. marina* and *C. furcatus* shows that the $P-Z$ contact rate is considerably larger for a predator swimming at a larger speed and with a larger perception radius, for a prey swimming with speeds in the range 0 to $300\mu\text{ms}^{-1}$.

Both the $P-V$ and $P-Z$ contact rates can be increased by the presence of phytoplankton motility or turbulence. For *H. akashiwo*, HaV and *O. marina*, phytoplankton motility is more influential than turbulence in altering the contact rates. However, both swimming and turbulence have more of an impact on the $P-V$ contact rate than the $P-Z$ contact rate for these species. The discrepancy may be in part due to the different modelling approaches used. Taking the characteristic length and swimming speed of *O. marina* to be 13×10^{-6}m and $3.39\times10^{-2}\text{ms}^{-1}$ respectively. This gives a Reynolds number of 4.4×10^{-3}, which is the same order of magnitude as that of *H. akashiwo*. At low Reynolds number, a swimming organism will transport a significant amount of fluid with them (e.g. Purcell, 1977) and so the swept volume approach may be inappropriate for explaining the effect of swimming at small scales.

Our calculations suggest that the ability of phytoplankton to swim does not significantly decrease the phytoplankton's encounter rate with its predator or increase its nutrient uptake rate. However, their motility increases the phytoplankton-virus contact rate, which is detrimental to the phytoplankton. This poses the question of why the phytoplankton can swim if it doesn't benefit them. However, phytoplankton motility does enable access to light near the surface of the water column and nutrients in the deeper layers, for example.

This chapter has often focussed on specific species, principally *H. akashiwo*, HaV and *O. marina*. However, the theory can be applied to a wide range of species, which could potentially make significant differences to the calculations performed here. It was mentioned in section 2.3.1 that there is a large variation in reported swimming speeds of *H. akashiwo*, a parameter we have found to be important in contact rate calculations. As may be expected, the variation in speeds and sizes of different species is even wider.

In terms of further work, plankton don't, in reality, swim with a constant speed, as has been investigated here. Incorporation of variable swimming velocity of the plankton would therefore be an interesting study. This could range in sophistication from swimming velocity varying with depth to changes in velocity due to perception of prey, for example. Lewis and Pedley (2000) considered plankton swimming with a Gaussian distribution in the encounter model described here and Lewis and Bala (2006) considered predators following an irregular trajectory (either through swimming

behaviour or changes in the flow). Inclusion of non-constant swimming seems to be pertinent for plankton. For example, Jiang et al. (2002) found that when copepods hovered or swam slowly they were more efficient in terms of relative capture volume compared to energy expended. Visser et al. (2009) noted for zooplankton that a predator's optimal swimming speed decreases with increasing prey concentration and that taking a convoluted path is more beneficial to the predator than a straight path. Alternative shapes of the perception field can also be considered. Work by Kiorboe and Visser (1999), amongst others, suggests that the perception field of copepods is not a perfect sphere. Lewis (2003) modelled the encounter between a predator with a conical perception field and its prey, and found differences in optimal swimming strategy dependent on perception field shape. Approximating equation (2.74) for the values of R appropriate to the planktonic species considered here would also be a good next step. Another key area for further work is that of the $P-V$ contact rate for motile phytoplankton in turbulent fluid. Ideally, more information regarding the enhancement of flux at low and intermediate Pe would be sought. Further consideration of the form Sh should take at small $\mathrm{Pe}_{\mathrm{turb}}$ for non-motile cells in turbulent fluid would also be desirable. Investigation of Sh at low values of Pe could be achieved via numerical simulation, such as direct numerical simulations. Incorporation of a velocity field applicable to swimming organisms could also be considered. For instance, the work of Magar et al. (2003) on nutrient uptake by a self-propelled steady squirmer, which showed a significant difference in Sh at large Pe when comparing a model for a squirmer with that for a rigid sphere, could be considered.

2.5.1 Summary

1. Studied the phytoplankton-virus contact rate:

   - Verified asymptotic results expressing $P - V$ contact rate explicitly as a function of biological parameters (virus and phytoplankton diameter, phytoplankton swimming speed) and of physical parameters (temperature, fluid viscosity)

   - Extended analysis of contact rates to include the effect of ambient flows including steady shear and fluctuating shear; the latter being an appropriate approximation for turbulent flows at sufficiently small scales

   - Quantified levels of turbulence intensity below which swimming can affect contact rate.

2. Studied the phytoplankton-predator contact rate:

- Re-examined two derivations for encounter rates for predators and prey moving at fixed speeds, explicitly noting limitations of the models when applied to a specific phytoplankton-predator system

- Re-examined how turbulence is included in the second model, again noting limitations when applied to a specific phytoplankton-predator system

3. Analyzed above results for a range of biological parameters relevant to example harmful algal bloom phytoplankton and known virus and predator:

   - Demonstrated that phytoplankton swimming ability can alter the $P - V$ contact rate. For example, in still fluid for typical parameters, the ability to swim can cause up to a five-fold increase in contact rate from that predicted for a stationary phytoplankton cell

   - In contrast, calculated that for typical values of turbulence, water motions do not have a significant effect on P-V contact rates for non-motile phytoplankton

   - Calculated that for relevant biological and physical parameters, there are turbulent regimes where swimming behaviour can still contribute to P-V contact rate

   - Noted several assumptions of P-Z contact model were either invalid or questionable for the primary P-Z species considered: The radius of the perception sphere was much smaller than the Kolmogorov microscale, an assumption necessary in equation (2.74); there was some discrepancy regarding co-ordinate systems we were unable to fully resolve, equation (2.72); it is not clear how appropriate the swept volume approach is at the low Reynolds numbers appropriate for the predator considered (in which the act of swimming drags a large quantity of fluid along with it)

   - Subject to the previous caveats, calculated that for typical parameters for *H. akashiwo* and *O. marina*: the ability of prey to swim doesn't significantly affect the P-Z contact rate and that typical turbulence intensities also don't affect the contact rate. However, in contrast, for an example larger zooplankton predator (as opposed to the micro-zooplankton predator *O. marina*) and faster swimming prey, demonstrated how contact rate

could increase with increasing turbulence intensity and swimming speeds

Chapter 3

Population Dynamics

3.1 Introduction

This chapter compares the use of viral infection and predation as controls of harmful algal blooms. A model, consisting of ordinary differential equations for the concentrations of phytoplankton, viral particles and predators, is developed based on previous theoretical models for free-living viral particles and experimentally determined functional and numeric responses for grazing as discussed in Chapter 1.

This full phytoplankton (P) - virus (V) - predator (Z) model displays five possible long-term dynamics which are described analytically as functions of the model parameters: point equilibria of phytoplankton alone, phytoplankton and predator, or phytoplankton and virus; limit cycles of phytoplankton and predator, or phytoplankton, predator and virus limit cycles. The regions in parameter space where these different outcomes occur are explicitly computed and displayed graphically in a two-dimensional plot of the parameter space of viral decay rate and predator death rate.

Numerical simulations of the temporal dynamics leading to these five outcomes are presented to compare how viruses and predators control the phytoplankton population. We have found that addition of virions or grazers to a phytoplankton population existing alone at carrying capacity can alter the long term dynamics, reducing the phytoplankton from carrying capacity to some lower equilibrium concentration. We suggest HaV to be a better control of *H. akashiwo* than *O. marina* since, for the parameter values used here, the *H. akashiwo* coexistence equilibrium with HaV is lower than that with *O. marina*. The long term behaviour achieved when adding grazers is dependent on the predator death rate, with the long term behaviour being that of predator-prey limit cycles if the death rate is too low. The long term behaviour can also be shifted between phytoplankton-virus stable, phytoplankton-predator stable and non-equilibrium solutions by careful consideration of the virion and predator death rates. We also find the quantity of virions or grazers needed to reduce a phytoplankton population in the short term, that is otherwise heading to equilibrium. This is done in

an attempt to reduce the phytoplankton population to such low concentrations that it may not recover due to stochasticity. However, the quantities required are very large. For smaller quantities of V or Z, the virus or predator will reduce the phytoplankton population naturally, it just may be allowed to bloom first.

Numerical simulations compare well with published data on measured population dynamics in the field and mesocosms for either the PZ or PV system, but some discrepancies are identified which relate to limitations of the Jeong et al. (2003) grazing model for predation. The implications of a change in the phytoplankton-virus or phytoplankton-predator volume clearance rates are explored. We find that changing the *H. akashiwo* - HaV volume clearance rate alters the population dynamics more than changing the *H. akashiwo* - *O. marina* volume clearance rate.

3.2 Methodology

3.2.1 Model

The model contains three classes: the population of phytoplankton susceptible to infection, P, the population of free-living virus particles (virions), V and the population of predators, Z. For simplicity, it is assumed that there is no time delay between a host becoming infected and bursting, thus there is no class of infected phytoplankton.

$$\frac{dP}{dt} = rP\left(1-\frac{P}{K}\right) - \mathrm{c_v}\sigma_1\sigma_2 PV - \frac{I_{\max}PZ}{K_{\mathrm{IR}}+P}; \tag{3.1}$$

$$\frac{dV}{dt} = m\mathrm{c_v}\sigma_1\sigma_2 PV - \mathrm{c_v}\sigma_1 PV - \gamma V = \lambda \mathrm{c_v}\sigma_1 PV - \gamma V; \tag{3.2}$$

$$\frac{dZ}{dt} = \frac{\mu_{\max}(P-p')}{K_{\mathrm{GR}}+P-p'}Z - \nu Z. \tag{3.3}$$

The susceptible phytoplankton are assumed to have a logistic growth rate, with maximum growth rate r, and carrying capacity K. The viral infection terms, which model lytic viruses, were taken from Bratbak et al. (1998). In order for the phytoplankton cell to lyse, a virus particle has to make contact with the cell, be adsorbed, and cause infection once adsorbed. The associated parameters for this process are: $\mathrm{c_v}$, the phytoplankton-virus volume clearance rate; σ_1, the fraction of contacts achieving adsorption; and σ_2, the fraction of adsorbed virions which are infective. The burst size, m, is the number of virions released when a phytoplankton cell bursts. In equation (3.2), the first term represents the production of virion particles following cell lysis, the second term represents removal of virions due to adsorption, and the final term is viral decay. For convenience, we introduce the parameter $\lambda = m\sigma_2 - 1$, which represents the increase in the number of infective virions during one cell lysis cycle and is assumed to be positive.

The predation terms, found by fitting Holling type II predation functions to observed data, were taken from Jeong et al. (2003), with an added death rate ν which could represent grazing by higher predators. The functional response involves the maximum ingestion rate $I_{\max}$ and K_{IR}, the prey concentration sustaining $\frac{1}{2}I_{\max}$. For prey concentrations greater than K_{IR}, the grazing term in equation (3.1) increases more slowly thus allowing for the predator to become satisfied. Jeong et al. (2003) fitted a numeric response with maximum growth rate of the predator given by $\mu_{\max}$, half saturation constant K_{GR}, and threshold prey concentration, p', that is the number of prey the predator must consume to achieve positive growth. We will assume that $p' < K$, so when $\nu = 0$ the predators will increase in number when introduced to a population of prey at carrying capacity.

3.2.2 Numerical methods and parameters

An analytical solution of model (3.1, 3.2, 3.3) can't be found and thus we seek an approximate solution of our non-linear system using numerical methods. Matlab has several ODE solvers and recommends ode45 as the one to use in most circumstances. The ode45 solver has been used throughout this chapter and is based on a Runge-Kutta formula, the Dormand-Prince pair. The Runge-Kutta methods of solving initial value problems are one-step methods (i.e. only an initial condition is required to begin), where only evaluations of the RHS of model (3.1, 3.2, 3.3) are used as opposed to computing derivatives of the RHS (Bradie, 2006). These are therefore relatively simple methods to use. Higher order Runge-Kutta methods are considerably more accurate than lower order methods (Sauer, 2006). Fourth order means that, for every halving of the step size, the error drops by approximately a factor of 2^4 (Sauer, 2006). Hence, the error of the ODE approximation at some fixed time t goes to zero, as the step size goes to zero, more quickly using a higher order method (Sauer, 2006). The Dormand-Prince pair are fourth and fifth order. The ode45 solver uses a variable time step. All phase portraits have been computed using Matlab's odephas2.

Parameter Estimation

Parameter values for *H. akashiwo*, HaV and *O. marina* have been estimated from the literature, some of which we discussed in Chapter 2. Viral burst size and diameter were taken directly from the literature. Nagasaki et al. (1999) found the burst size of HaV to be approximately 770 virions released per host cell. Nagasaki and Yamaguchi (1997) used electron microscopy to find the diameter of HaV to be $202 \pm 6 \times 10^{-7}$cm (average $\pm$ standard deviation). A value of $d_v = 2 \times 10^{-5}$cm is used here. *H. akashiwo* is unicellular, $10 - 25 \times 10^{-4}$cm in length with swimming speeds observed in the range $U_{\mathrm{P}} = 20 - 160 \times 10^{-4}\mathrm{cms}^{-1}$ (Smayda, 1998). As previously, we take *H. akashiwo* to have a diameter of $d = 15 \times 10^{-4}$cm. We can use these parameter values to estimate

the phytoplankton-virus volume clearance rate, c_v. In order to compare with observed data in section 3.3.5, we calculate the volume clearance rate for motile *H. akashiwo* residing in a still fluid (as calculated in section 2.3.1).

The phytoplankton-virus contact rate is a value found theoretically using the diffusive transport theory of Murray and Jackson (1992), which was discussed in detail in Chapter 2. The volume clearance rate here is calculated for phytoplankton moving through a still fluid with a temperature of $20°C$. Recall viral diffusivity, D_v:

$$D_v = \frac{kT}{3\pi\mu d_v}, \tag{3.4}$$

where $k = 1.38 \times 10^{-19}\text{cm}^2\text{kg s}^{-2}\text{K}^{-1}$ is the Boltzmann constant, $T = 293\text{K}$ is the Kelvin temperature equivalent to $20°C$, $\mu = 1.002 \times 10^{-5}\text{kg cm}^{-1}\text{s}^{-1}$ (Batchelor, 1967) is the dynamic viscosity of water at $20°C$ and d_v is the diameter of the virus, taken to be $2 \times 10^{-5}\text{cm}$ for HaV. The viral diffusivity is therefore $D_v = 2.14 \times 10^{-8}\text{cm}^2\text{s}^{-1}$. This can now be used to calculate the phytoplankton-virus volume clearance rate for motile *H. akashiwo* in still fluid, using theory from Chapter 2. The Péclet number here is:

$$\text{Pe}_{\text{swim}} = \frac{U_{\text{P}} r_0}{D_v}, \tag{3.5}$$

where U_{P} is the swimming speed of the phytoplankton and r_0 is the radius of the phytoplankton. Therefore, Pe_{swim} lies in the range 70 to 561. From Chapter 2, for $\text{Pe} \gg 1$, the Sherwood number, Sh, is given by equation (2.22):

$$\text{Sh} = 0.6245\text{Pe}^{\frac{1}{3}} + 0.461 + o(1) \qquad \text{Pe} \gg 1, \tag{3.6}$$

and, for $0.01 < \text{Pe} < 100$, the Sherwood number, Sh, is given by equation (2.24):

$$\text{Sh} = \frac{1}{2}\left(1 + (1 + 2\text{Pe})^{\frac{1}{3}}\right) \qquad 0.01 < \text{Pe} < 100. \tag{3.7}$$

Hence, Sh is between 3.10 and 5.61. Finally, the phytoplankton-virus volume clearance rate, c_v is given by:

$$c_v = 2\pi d D_v \text{Sh}, \tag{3.8}$$

and thus lies in the range $5.4 - 9.8 \times 10^{-5}\text{ml d}^{-1}$. A value of $c_v = 7 \times 10^{-5}\text{ml d}^{-1}$ is used throughout as an estimate of the volume clearance rate between *H. akashiwo* and its virus HaV, but section 3.3.6 investigates how changing this volume clearance rate alters the population dynamics.

Another viral parameter taken from the literature is that of σ_2, the fraction of adsorbed virions that are infectious. Tarutani et al. (2006) found that infectious viral particles only made up 3 to 4% of direct count estimates of HaV. We then make the assumption that this is also the percentage of adsorbed virions that are infectious and

thus take σ_2 to be 0.03. Unfortunately, an estimate of the quantity σ_1, the fraction of contacts resulting in adsorption, for HaV hasn't been found in the literature and we therefore use $\sigma_1 = 0.1$, which is the value used in Bratbak et al. (1998) to investigate viral infection of the alga *Phaeocystis pouchetii*. However, Tarutani et al. (2006) found only infectious HaV particles adsorbed to their host and caused infection. The value of σ_1 may therefore be closer to 1. Although, on inspection of model (3.1, 3.2, 3.3) we find that σ_1 is only present with c_v. Therefore, variance of c_v in section 3.3.6 may capture some of the σ_1 variance.

Values of maximum ingestion, I_{max}, and growth rates, μ_{max}, of *O. marina*, half saturation constants, K_{IR} and K_{GR}, and threshold prey concentration, p', are taken directly from Jeong et al. (2003), where they were found by fitting predation terms to observed data. By comparing the growth curve in Figure 3.12(a), taken from Jeong et al. (2003), representing the control experiment (i.e. growth of *H. akashiwo* in the absence of *O. marina*, labelled MC2(Hs)) with model

$$\frac{dP}{dt} = rP\left(1 - \frac{P}{K}\right), \tag{3.9}$$

we can estimate values of *H. akashiwo* growth and carrying capacity to be $r = 2\text{d}^{-1}$ and $K = 50000$ cells ml^{-1} respectively. These laboratory estimates will also be used to model Tarutani et al.'s (2000) field observations of *H. akashiwo* and HaV in section 3.3.5. However, these parameters will vary under different regimes. For instance, *H. akashiwo* growth can be affected by salinity (Shikata et al., 2008), irradiance (Gao et al., 2007) and both macro- and micro-nutrients (e.g. Tomas, 1979), amongst others, and the growth response can vary between strains (Martinez et al., 2010).

The phytoplankton-predator volume clearance rate, c_z, will be defined in section 3.3.6 in terms of the half-saturation constant, K_{IR}, and varied to explore how this affects the population dynamics.

All of the above parameters are given in Table 3.1. Values for viral decay rate, γ, and predator death rate, ν, are not included in the table since they are difficult to estimate from the literature and are expected to vary widely. They are therefore varied throughout this chapter to alter the long-term dynamics achieved.

3.3 Results

Following standard methods, e.g. Murray (2003), to analyze the non-linear dynamical system described by model (3.1, 3.2, 3.3), we first seek equilibrium solutions (found by setting the right hand side of the model to zero) and then compute the stability of these point equilibria, using linear stability analysis. There are four equilibria: the trivial unstable zero solution; the phytoplankton alone at carrying capacity; phytoplankton and viral particles alone; and phytoplankton and predator alone. This result

Symbol	Value	Source
r	2 d^{-1}	Estimated from Jeong et al. (2003)
K	5×10^4 cells ml^{-1}	Estimated from Jeong et al. (2003)
c_v	7×10^{-5} ml d^{-1}	Theoretical value, calculated in section 2.3.1 to be in the range $5.4 - 9.8 \times 10^{-5}$ml d^{-1}.
σ_1	0.1	Bratbak et al. (1998)
σ_2	0.03	Tarutani et al. (2006)
m	770 viruses $cell^{-1}$	Nagasaki et al. (1999)
$\lambda = m\sigma_2 - 1$	22.1 viruses $cell^{-1}$	Calculated from above
I_{max}	12.5 cells $grazer^{-1}$ d^{-1}	Jeong et al. (2003)
K_{IR}	7040 cells ml^{-1}	Jeong et al. (2003)
μ_{max}	1.43 d^{-1}	Jeong et al. (2003)
K_{GR}	1040 cells ml^{-1}	Jeong et al. (2003)
p'	80 cells ml^{-1}	Jeong et al. (2003)

Table 3.1: Parameter values used for phytoplankton-virus-predator model

is to be expected from the competitive exclusion principle; the virus and predator can be viewed as competing for one resource, the phytoplankton, and hence there is no coexistence point equilibria (May, 1974). A modification of Kolmogorov's Theorem is then used to examine the existence of a predator-prey limit cycle in the (P, Z) subsystem. We numerically analyze the long-term dynamics of the full parameter space, which reduces to considering the $\nu - \gamma$ parameter space, and show that a further long term solution, that of three species coexistence, is also possible. Using numerical simulations, we calculate the temporal dynamics of the system to make predictions about control mechanisms and compare with observed data. Stability conditions of the equilibria are used to explore how changes to the volume clearance rates, and the use of different viruses, may affect the long-term behaviour.

3.3.1 Linear stability analysis

Letting F, G and H equal the RHS of equation (3.1), (3.2) and (3.3) respectively, the Jacobian matrix of the model takes the form:

$$\mathbf{J} = \begin{pmatrix} \frac{\partial F}{\partial P} & \frac{\partial F}{\partial V} & \frac{\partial F}{\partial Z} \\ \frac{\partial G}{\partial P} & \frac{\partial G}{\partial V} & \frac{\partial G}{\partial Z} \\ \frac{\partial H}{\partial P} & \frac{\partial H}{\partial V} & \frac{\partial H}{\partial Z} \end{pmatrix}$$

$$= \begin{pmatrix} r - \frac{2rP}{K} - c_v\sigma_1\sigma_2 V - \frac{I_{max}K_{IR}Z}{(K_{IR}+P)^2} & -c_v\sigma_1\sigma_2 P & -\frac{I_{max}P}{K_{IR}+P} \\ \lambda c_v\sigma_1 V & \lambda c_v\sigma_1 P - \gamma & 0 \\ \frac{\mu_{max}K_{GR}Z}{(K_{GR}+P-p')^2} & 0 & \frac{\mu_{max}(P-p')}{(K_{GR}+P-p')} - \nu \end{pmatrix}.$$

This matrix will be used to find the stability of the equilibria of the system. We will write the stability criteria in terms of the viral decay rate, γ, and predator death rate, ν.

- Equilibrium 1: Prey alone at carrying capacity, $P = K, V = Z = 0$.

  This equilibrium is always feasible since P, V and Z are always non-negative. The Jacobian matrix here is:

$$\mathbf{J}(K,0,0) = \begin{pmatrix} -r & -c_v\sigma_1\sigma_2 K & -\frac{I_{max}K}{K_{IR}+K} \\ 0 & \lambda c_v\sigma_1 K - \gamma & 0 \\ 0 & 0 & \frac{\mu_{max}(K-p')}{K_{GR}+K-p'} - \nu \end{pmatrix}.$$

  The eigenvalues are:

$$\lambda_1 = -r, \lambda_2 = \lambda c_v\sigma_1 K - \gamma, \lambda_3 = \frac{\mu_{max}(K-p')}{K_{GR}+K-p'} - \nu. \tag{3.10}$$

  The steady state is stable when all eigenvalues are negative. Since the phytoplankton growth rate is strictly non-negative, this equilibrium is stable if the decay rate of the virus and death rate of the predator is larger than the 'growth' rates:

$$\gamma > c_v\sigma_1\lambda K = \gamma_1, \tag{3.11}$$

$$\nu > \frac{\mu_{max}(K-p')}{K_{GR}+K-p'} = \nu_1, \tag{3.12}$$

  where we have introduced the constants γ_1 and ν_1 for mathematical convenience.

- Equilibrium 2: Phytoplankton and viral particles alone, $P = P_2^*, V = V^*, Z = 0$.

  The equilibrium concentrations are given by:

$$P_2^* = \frac{\gamma}{c_v\sigma_1\lambda}, \quad V^* = \frac{r}{c_v\sigma_1\sigma_2}\left(1 - \frac{P_2^*}{K}\right). \tag{3.13}$$

  For this solution to be feasible, that is for $V^* > 0$, we require the phytoplankton concentration to be at less than the carrying capacity, that is $P_2^* < K$, which is equivalent to $\gamma < \gamma_1$, as defined in equation (3.11). Note that if equilibrium 2 is feasible, equilibrium 1 is unstable. The Jacobian matrix is now:

$$\mathbf{J}(P_2^*, V^*, 0) = \begin{pmatrix} -\frac{r\gamma}{K c_v \sigma_1 \lambda} & -\frac{\gamma\sigma_2}{\lambda} & -\frac{I_{\max} P_2^*}{K_{IR}+P_2^*} \\ \frac{r\lambda}{\sigma_2}\left(1-\frac{P_2^*}{K}\right) & 0 & 0 \\ 0 & 0 & \frac{\mu_{\max}(P_2^*-p')}{K_{GR}+P_2^*-p'} - \nu \end{pmatrix}.$$

One eigenvalue is:

$$\lambda_1 = \frac{\mu_{\max}(P_2^* - p')}{K_{GR} + P_2^* - p'} - \nu, \tag{3.14}$$

which is non-negative when $\nu > \frac{\mu_{\max}(P_2^* - p')}{K_{GR} + P_2^* - p'}$. The others are found from

$$\begin{vmatrix} -\frac{r\gamma}{K c_v \sigma_1 \lambda} - \lambda_{2,3} & -\frac{\gamma\sigma_2}{\lambda} \\ \frac{r\lambda}{\sigma_2}\left(1-\frac{P_2^*}{K}\right) & -\lambda_{2,3} \end{vmatrix} = 0.$$

The Routh-Hurwitz criteria state that the steady state is stable if (Edelstein-Keshet, 2005):

$$\frac{r\gamma}{K c_v \sigma_1 \lambda} > 0 \text{ and } \gamma r\left(1-\frac{P_2^*}{K}\right) > 0.$$

The former inequality is always satisfied since all the quantities involved are non-negative. Similarly, the latter inequality is satisfied provided $P_2^* < K$. Therefore, equilibrium 2 is stable when feasible provided the death rate of the predator is larger than the growth rate:

$$\nu > \frac{\mu_{\max}(P_2^* - p')}{K_{GR} + P_2^* - p'} = f(\gamma), \tag{3.15}$$

where we have introduced the function $f(\gamma)$ for mathematical convenience. The stability boundary $\nu = f(\gamma)$ crosses the axes at the point $(\gamma, \nu) = (0.012, 0)\text{d}^{-1}$.

- Equilibrium 3: Phytoplankton and predator alone, $P = P_3^*, V = 0, Z = Z^*$. The equilibrium concentrations are given by:

$$P_3^* = \frac{\nu K_{GR}}{\mu_{\max} - \nu} + p', \quad Z^* = \frac{r}{I_{\max}}(K_{IR} + P_3^*)(1 - \frac{P_3^*}{K}). \tag{3.16}$$

For this solution to be feasible, $Z^* > 0$, we require that $P_3^* < K$, which is equivalent to $\nu < \nu_1$, as defined in equation (3.12). The condition $\nu < \nu_1$ also ensures that the phytoplankton concentration is feasible, $P_3^* > 0$. Note that if equilibrium 3 is feasible, equilibrium 1 is unstable. The Jacobian matrix is:

$$\mathbf{J}(P_3^*, 0, Z^*) = \begin{pmatrix} r - \frac{2rP_3^*}{K} - \frac{I_{\max}K_{\text{IR}}Z^*}{(K_{\text{IR}}+P_3^*)^2} & -c_v\sigma_1\sigma_2P_3^* & -\frac{I_{\max}P_3^*}{K_{\text{IR}}+P_3^*} \\ 0 & \lambda c_v\sigma_1P_3^* - \gamma & 0 \\ \frac{\mu_{\max}K_{\text{GR}}Z^*}{(K_{\text{GR}}+P_3^*-p')^2} & 0 & \frac{\mu_{\max}(P_3^*-p')}{K_{\text{GR}}+P_3^*-p'} - \nu \end{pmatrix}.$$

The first eigenvalue is:

$$\lambda_1 = \lambda c_v\sigma_1P_3^* - \gamma, \tag{3.17}$$

which is negative when $\gamma > \lambda c_v\sigma_1P_3^*$. The other eigenvalues are found from: $\nu > \dfrac{\mu_{\max}(K - 2p' - K_{\text{IR}})}{2K_{\text{GR}} + K - 2p' - K_{\text{IR}}}$. The other eigenvalues are found from:

$$\begin{vmatrix} r - \frac{2rP_3^*}{K} - \frac{I_{\max}K_{\text{IR}}Z^*}{(K_{\text{IR}}+P_3^*)^2} - \lambda_{2,3} & -\frac{I_{\max}P_3^*}{K_{\text{IR}}+P_3^*} \\ \frac{\mu_{\max}K_{\text{GR}}Z^*}{(K_{\text{GR}}+P_3^*-p')^2} & -\lambda_{2,3} \end{vmatrix} = 0.$$

From the Routh-Hurwitz criteria, this equilibrium is stable when $\dfrac{I_{\max}P_3^*}{K_{\text{IR}}+P_3^*}\left(\dfrac{\mu_{\max}K_{\text{GR}}Z^*}{(K_{\text{GR}}+P_3^*-p')^2}\right) > 0$ and $r - \dfrac{2rP_3^*}{K} - \dfrac{I_{\max}K_{\text{IR}}Z^*}{(K_{\text{IR}}+P_3^*)^2} < 0$. Since all of the quantities involved are non-negative, the first inequality is satisfied. The second inequality is satisfied provided $\nu > \dfrac{\mu_{\max}(K - 2p' - K_{\text{IR}})}{2K_{\text{GR}} + K - 2p' - K_{\text{IR}}}$. Thus, equilibrium 3 is stable provided the decay rate of the virus is larger than the 'growth' rate, and an additional constraint on the death rate of the predator is satisfied:

$$\gamma > c_v\sigma_1\lambda P_3^* \Rightarrow \nu < f(\gamma), \tag{3.18}$$

$$\nu > \frac{\mu_{\max}(K - 2p' - K_{\text{IR}})}{2K_{\text{GR}} + K - 2p' - K_{\text{IR}}} = \nu_2. \tag{3.19}$$

For mathematical convenience, we have rewritten the constraint on γ to aid comparison with equation (3.15), and introduced the constant ν_2. Comparing equations (3.15) and (3.18) shows that when equilibrium 3 is stable equilibrium 2 is unstable, and vice versa.

- Equilibrium 4: Phytoplankton, virus and predator coexistence, $P = P_{4,5}^*, V = V^*, Z = Z^*$. The equilibrium concentrations are given by:

$$P_{4,5}^* = \frac{1}{2}\left[(P_3^* - K_{\text{IR}}) \pm \sqrt{(K_{\text{IR}} + P_3^*)^2 - 4(P_3^*K - P_3^{*2} - KK_{\text{IR}})}\right], \tag{3.20}$$

$$V^* = \frac{r}{c_v\sigma_1\sigma_2}\left(1 - \frac{P_2^*}{K}\right), \tag{3.21}$$

$$Z^* = \frac{r}{I_{\max}}(K_{\text{IR}} + P_3^*)\left(1 - \frac{P_3^*}{K}\right). \tag{3.22}$$

Note, the fixed points V^* and Z^* only occur together in the special case where

$$P_2^* = P_3^* \implies \nu = f(\gamma).$$

Feasibility conditions for V^* and Z^* have been stated in the previously: $\gamma < \gamma_1 \implies V^* > 0$ and $\nu < \nu_1 \implies Z^* > 0$. The steady states $P_{4,5}^*$ both require $(K_{\text{IR}} + P_3^*)^2 > 4(P_3^* K - P_3^{*2} - KK_{\text{IR}})$ for feasibility. Where

$$P_4^* = \frac{1}{2}\left[(P_3^* - K_{\text{IR}}) - \sqrt{(K_{\text{IR}} + P_3^*)^2 - 4(P_3^* K - P_3^{*2} - KK_{\text{IR}})}\right], \tag{3.23}$$

$P_3^* > K_{\text{IR}}$ and $(P_3^* - K_{\text{IR}}) > \sqrt{(K_{\text{IR}} + P_3^*)^2 - 4(P_3^* K - P_3 *^2 - KK_{\text{IR}})}$ are also required for feasibility. The condition that $(P_3^* - K_{\text{IR}}) < \sqrt{(K_{\text{IR}} + P_3^*)^2 - 4(P_3^* K - P_3^{*2} - KK_{\text{IR}})}$, if $P_3^* < K_{\text{IR}}$, is required for P_5^* to be feasible. Therefore, P_4^* is unfeasible when P_5^* is feasible and vice versa. Remembering from equations (3.1, 3.2, 3.3) that

$$r - \frac{rP}{K} - \mathrm{c_v}\sigma_1\sigma_2 V - \frac{I_{\max} Z}{K_{\text{IR}} + P} = 0,$$

$$\lambda \mathrm{c_v}\sigma_1 P - \gamma = 0,$$

$$\frac{\mu_{\max}(P - p')}{K_{\text{GR}} + P - p'} - \nu = 0,$$

at the (P, V, Z) coexistence equilibrium, the Jacobian matrix takes the form:

$$\mathbf{J}(P_{4,5}^*, V^*, Z^*) = \begin{pmatrix} \frac{I_{\max} Z}{K_{\text{IR}} + P_{4,5}^*}\left(1 - \frac{K_{\text{IR}}}{K_{\text{IR}} + P_{4,5}^*}\right) - \frac{rP_{4,5}^*}{K} & -\mathrm{c_v}\sigma_1\sigma_2 P_{4,5}^* & -\frac{I_{\max} P_{4,5}^*}{K_{\text{IR}} + P_{4,5}^*} \\ \lambda \mathrm{c_v}\sigma_1 V^* & 0 & 0 \\ \frac{\mu_{\max} K_{\text{GR}} Z^*}{(K_{\text{GR}} + P_{4,5}^* - p')^2} & 0 & 0 \end{pmatrix}.$$

Eigenvalues, $\lambda_{1,2,3}$, satisfy the characteristic equation:

$$a_1 \lambda_{1,2,3}^3 + a_2 \lambda_{1,2,3}^2 + a_3 \lambda_{1,2,3} + a_4 = 0. \tag{3.24}$$

Here $a_1 = 1, a_2 = \dfrac{rP_{4,5}^*}{K} - \dfrac{I_{\max} Z^*}{K_{\text{IR}} + P_{4,5}^*}\left(1 - \dfrac{K_{\text{IR}}}{K_{\text{IR}} + P_{4,5}^*}\right)$ and $a_3 = -{\mathrm{c_v}}^2 \sigma_1^2 \sigma_2 \lambda V^* P_{4,5}^* - \dfrac{I_{\max} P_{4,5}^*}{K_{\text{IR}} + P_{4,5}^*}\left(\dfrac{\mu_{\max} K_{\text{GR}} Z^*}{(K_{\text{GR}} + P_{4,5}^* - p')^2}\right)$. Parameters a_1 and a_3 must have opposing signs, thus steady state $(P_{4,5}^*, V^*, Z^*)$ is unstable.

In summary, the phytoplankton and virus are able to stably coexist in the absence of grazing by predators and the phytoplankton and predator can coexist at stable steady state in the absence of viral infection. Feasibility of either coexistence equilibrium forces the $(K, 0, 0)$ equilibrium to be unstable. Stability of either coexistence equilibrium forces the other coexistence equilibrium to be unstable. An equilibrium where the phytoplankton, virus and predator coexist emerges in the special case where $P_2^* = P_3^*$ and thus the parameter set satisfies $\nu = f(\gamma)$, however this equilibrium is always unstable. Equilibria are established by setting the RHS of the model equations (3.1,3.2, 3.3) to zero and rearranging to give P, V or Z. Figure 3.3 depicts these stability regions in $\gamma - \nu$ parameter space.

Consideration of the stability criteria uncovers a region of parameter space that doesn't contain any stable steady states. We will next consider what dynamics may be present in this region.

3.3.2 Limit Cycles

In this section we consider the existence of limit cycles. Only nonlinear systems can have stable limit cycles. It is worth noting that these stable limit cycles are not the neutrally stable oscillations of the Lotka-Volterra equations. The amplitude of oscillation in the neutrally stable case is determined by the initial conditions, whereas the amplitude and period of the stable limit cycle is determined by the model parameters (May, 1974). A limit cycle, in phase-space, is a curve trajectory that doesn't contain steady states, doesn't cross itself and must be closed, i.e. a point moving along the cycle must return to its starting position after some fixed time (Edelstein-Keshet, 2005). For two component systems, the existence of limit cycles can be found analytically. Kolmogorov formulated criteria, as described in May (1974), to determine the existence of limit cycles in predator-prey type systems. Stability analysis will establish the criterion for a point stable equilibrium. When these criteria are not met, but Kolmogorov's theorem holds, a stable limit cycle will occur. An informal reasoning for the Kolmogorov criteria can be seen in Edelstein-Keshet (2005). Cyclic behaviour of algae has been observed (e.g. Shertzer et al., 2002).

Considering the systems separately, the phytoplankton-virus and phytoplankton-predator models considered in this thesis are of the form:

$$\frac{dP}{dt} = PF(P, W) \tag{3.25}$$

$$\frac{dW}{dt} = WG(P). \tag{3.26}$$

These are similar to those considered by Kolmogorov, except G is only a function of P here rather than a function of P and W as studied by Kolmogorov. As such, not all of

Kolmogorov's criteria are satisfied. We shall therefore check informally if the theorem still holds for our models, following work in Britton (2003).

Suppose there is a coexistence equilibrium, (P^*, W^*), such that $F(P^*, W^*) = G(P^*) = 0$. The Jacobian matrix here is:

$$\mathbf{J}(P^*, W^*) = \begin{pmatrix} P\frac{\partial F}{\partial P} & P\frac{\partial F}{\partial W} \\ W\frac{\partial G}{\partial P} & 0 \end{pmatrix}.$$

Eigenvalues λ of the Jacobian matrix satisfy

$$\det(\mathbf{J} - \lambda\mathbf{I}) = 0$$

and thus, for a 2×2 Jacobian matrix,

$$\lambda^2 + a_1\lambda + a_2 = 0,$$

where $a_1 = -\text{trace}(\mathbf{J})$ and $a_2 = \text{determinant}(\mathbf{J})$. The equilibrium in question is therefore stable if $a_1 > 0$ and $a_2 > 0$, by the Routh-Hurwitz stability criterion. From $\mathbf{J}(P^*, W^*)$, $a_1 = -P\frac{\partial F}{\partial P}$ which is greater than zero when $\frac{\partial F}{\partial P} < 0$, and $a_2 = -PW\frac{\partial F}{\partial W}\frac{\partial G}{\partial P}$ which is greater than zero when one of $\frac{\partial F}{\partial W}$, $\frac{\partial G}{\partial P}$ are less than zero. Biologically, $a_2 > 0$ will be satisfied because removal of phytoplankton due to viral infection or predation will decrease growth of the phytoplankton population, whilst the virus or predator population will grow in the presence of prey, i.e. $\frac{\partial F}{\partial W} < 0$ and $\frac{\partial G}{\partial P} > 0$. The coexistence equilibrium is therefore unstable when $\frac{\partial F}{\partial P} > 0$. However, in the phytoplankton-virus system, $\dfrac{\partial F}{\partial P} = -\dfrac{r}{K}$. This is never greater than zero and the coexistence equilibrium is therefore always stable when feasible. We shall leave an analytical analysis of limit cycles in the $P-V$ system here and consider the $P-Z$ system solely. For the phytoplankton-predator system, $\dfrac{\partial F}{\partial P} = -\dfrac{r}{K} + \dfrac{I_{\max}W}{(K_{\text{IR}} + P)^2}$. Thus, providing $\dfrac{I_{\max}W}{(K_{\text{IR}} + P)^2} > \dfrac{r}{K}$, the phytoplankton-predator system can be unstable. The aim is now to establish the possibility of periodic oscillations when this equilibrium is unstable.

Consider the phase plane. The Poincaré-Bendixson theorem states that for (P, W) bounded as $t \to \infty$, then (P, W) either is or tends to a point equilibrium as $t \to \infty$, or it is or tends to a periodic solution (Britton, 2003). The system is bound for P via the condition $F(B, 0) = 0, B > 0$, i.e. there is a prey population size beyond which the prey can't increase further, even in the absence of predation (e.g. the phytoplankton carrying capacity). However, due to the $G = 0$ null-cline being a straight line, we don't have a condition to restrict the predator population size. However, due to the horizontal component (the prey), the phase trajectory is actually pulled around from right to left as it travels upwards. By plotting a trajectory starting from $P = B$ (the prey upper bound), we can see a closed "box" emerge. Thus, there is an absorbing

set $0 \leq P \leq B$ and $0 \leq W \leq A$ that includes the unstable phytoplankton-predator equilibrium. The Poincaré-Bendixson theorem implies the existence of periodic orbits inside this set. See Figure 3.1. Figure 3.2 shows an example stable limit cycle of the system (3.25, 3.26).

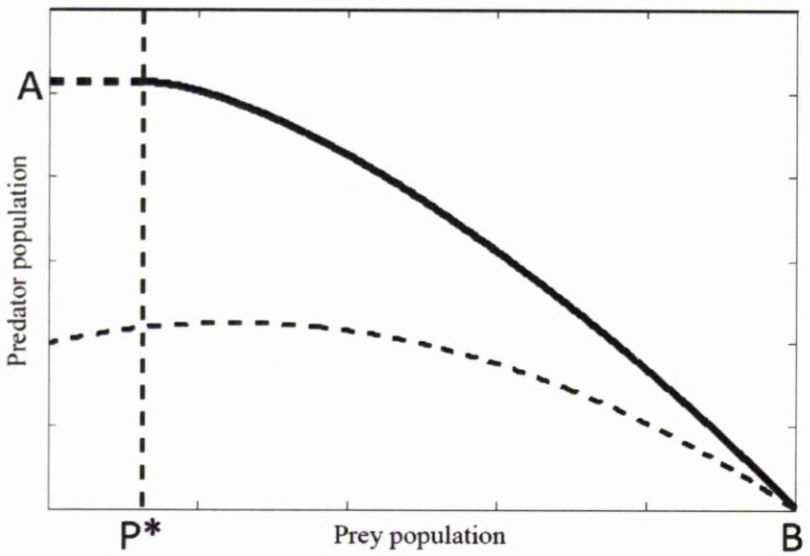

Figure 3.1: A trajectory initiating at the prey upper bound B, which depicts a predator upper bound, A, and thus enables the existence of periodic orbits for the system (3.25, 3.26). Again, the full line is the trajectory and it runs to the straight line null-cline (the dashed lines being the null-clines). To the left of the vertical null-cline the predator population is declining and so the thick dashed line that runs from the end of the trajectory to the predator axis represents the maximal predator population size. The prey coexistence equilibrium occurs at P^*.

Thus, the predator-prey system used throughout this thesis (equations (3.1) and (3.3) with $V = 0$) gives rise to a periodic solution when the equilibrium point is unstable. In the next section we will numerically consider the nature of these periodic orbits. The equilibrium point is stable when both equation (3.18) and equation (3.19) are satisfied. If equation (3.18) is satisfied, but equation (3.19) is not, a periodic solution exists, i.e. a predator-prey periodic solution exists when the lower bound of the predator death rate is zero rather than ν_2. When equation (3.18) isn't satisfied, equilibrium 2 is stable (from equation (3.15)). We can't perform this analysis for the three component system. As the decay rate of the virus reduces, we expect the virus may be able to invade, leading to some form of coexistence. We will investigate the long term behaviour of the three-component system numerically in the next section.

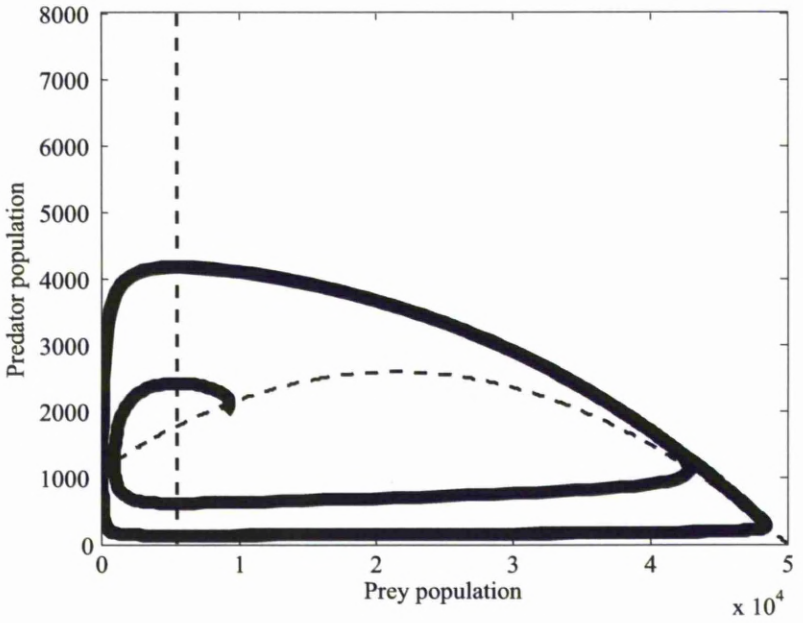

Figure 3.2: An example stable limit cycle for model (3.25, 3.26).

3.3.3 Numerical simulation

The above stability analysis highlights predator death rate (ν) and virion death rate (γ) as important parameters in determining stability of the equilibria. Figure 3.3 shows the five possible outcomes of model (3.1, 3.2, 3.3) and for which values of ν and γ they occur (based on the parameter values of Table 3.1). From equation (3.11), the vertical line in Figure 3.3 separating the regions where equilibrium 1 and equilibrium 2 are stable is given by $\gamma = \gamma_1$. Similarly, from equation (3.12), the stability boundary between equilibrium 1 and equilibrium 3 is given by the horizontal line $\nu = \nu_1$. From equation (3.15), the equilibrium 2 and equilibrium 3 stable solutions are separated by the curve $\nu = f(\gamma)$. Finally, from equation (3.15) and equation (3.19), there is a region which has no stable point equilibria, defined by $\nu < \min\{f(\gamma), \nu_2\}$. From section 3.3.2, we expect this region to contain predator-prey limit cycles. By numerical simulation, as indicated in Figure 3.3, we have determined that this region can be subdivided into two periodic long-term behaviours: predator-prey limit cycles and cyclic coexistence of virions, phytoplankton and predators, depicted by the shaded region in Figure 3.3. This shaded region was determined numerically, by systematically simulating the long term behaviour for $\nu < \min\{f(\gamma), \nu_2\}$ and $\gamma < 11$ (as this is the range of γ depicted in Figure 3.3). A resolution of 0.01 was used for the predator death rate, ν, and 0.1 for the virion decay rate, γ. The red asterisk shows parametric points on the boundary between (P, V, Z) coexistence and $(P, 0, Z)$ limit cycles, which were numerically computed to give (P, V, Z) coexistence in the long term. The straight line

plotted through these points is the line with equation $\nu = \frac{14}{9}(\gamma - 0.02)$.

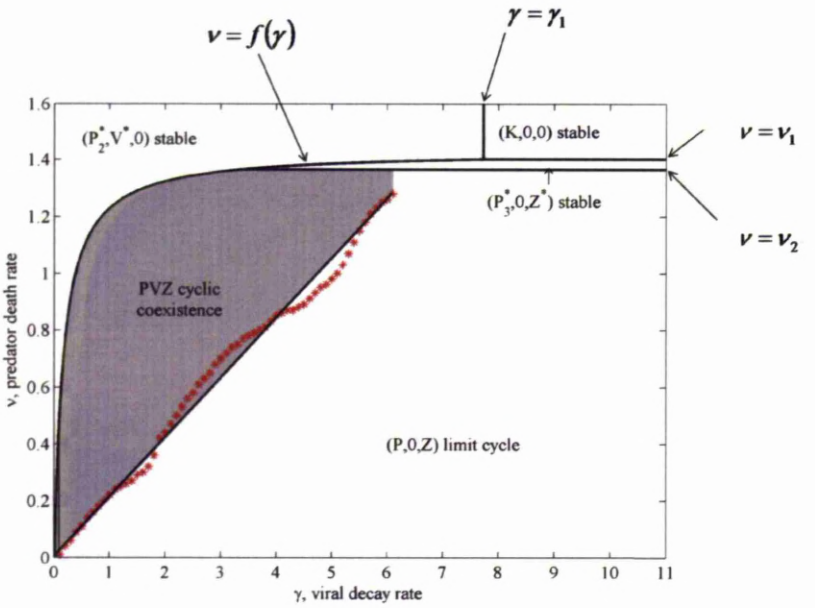

Figure 3.3: Plot depicting the five possible long-term dynamics of model (3.1, 3.2, 3.3) relative to the values of virion death rate and predator death rate. There are three possible stable equilibria and two further long-term dynamics. One is a phytoplankton-predator limit cycle and the other, represented by the shaded area, is a region where phytoplankton, virus and predator coexist. The '$*$' shows points on the boundary between (P, V, Z) coexistence and $(P, 0, Z)$ limit cycles, where (P, V, Z) coexistence was (numerically) found in the long term. The straight line plotted through these points is the line with equation $\nu = \frac{14}{9}(\gamma - 0.02)$. The quantities $\gamma_1, \nu_1, \nu_2, f(\gamma)$ are defined in equations (3.11), (3.12), (3.19), (3.15) respectively. The figure was computed using parameter values in Table 3.1.

We now consider the time evolution of model (3.1, 3.2, 3.3) to the four different long-term dynamics which have non-zero values for V or Z, by numerically simulating the model for different choices of predator death rate, ν, and viral decay rate, γ, taking all other parameters from Table 3.1. The final states do not depend on initial conditions, but the dynamics will be affected by our choice of initial conditions. In section 3.3.5, model (3.1, 3.2, 3.3) will be compared to observed data for *H. akashiwo* and its virus HaV and, separately, data for *H. akashiwo* and its predator *O. marina*. The initial conditions in these observed data sets are approximately $(P_0, V_0) = (9000, 10)\text{ml}^{-1}$ and $(P_0, Z_0) = (16000, 2000)\text{ml}^{-1}$ respectively. Following this, we take the initial concentrations for Figures 3.4 - 3.8 to be $(P_0, V_0, Z_0) = (9000, 10, 2000)$ per ml. This

isn't ideal since all three initial concentrations aren't from the same data set and, also, we have arbitrarily chosen the lower of the two P_0 values. It should also be noted that we are taking data from an annually repeating system and using it to represent initial conditions in an initial value problem, for a model that does not replicate this annually repeating behaviour. This lack of correlation between the data used in the model and the model itself may reduce the validity of transient behaviour in the following simulations, but won't affect the long term behaviour.

Figure 3.4 is the simulation where equilibrium 2, $(P_2^*, V^*, 0)$, is stable. The predator death rate is taken as $\nu = 1.2\text{d}^{-1}$, whilst the viral decay rate is $\gamma = 0.08\text{d}^{-1}$. The two dashed lines in Figure 3.4(b), along with the axes, are null-clines. The two visible null-clines intersect each other at the coexistence equilibrium, the point towards which the phase trajectory is spiralling. One null-cline intersects the horizontal axis at the carrying capacity of the phytoplankton. Figure 3.4 shows that the phytoplankton population repeatedly blooms in the presence of the virus, but each bloom is damped compared to the previous and eventually both populations become constant.

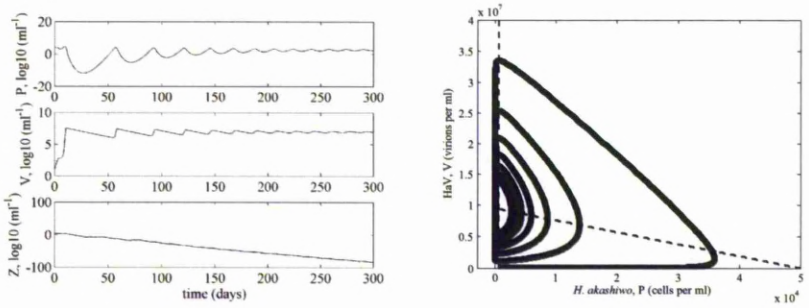

(a) Solution over time (b) Individual trajectory

Figure 3.4: $(P_2^*, V^*, 0)$ stable equilibrium, using parameter values as in Table 3.1 with $\nu = 1.2\text{d}^{-1}$ and $\gamma = 0.08\text{d}^{-1}$.

Figure 3.5 is the simulation where equilibrium 3, $(P_3^*, 0, Z^*)$, is stable. The viral decay rate is given by $\gamma = 6\text{d}^{-1}$, and predator death rate is $\nu = 1.38\text{d}^{-1}$. As with Figure 3.4(b), the two visible null-clines in Figure 3.5(b) intersect at the coexistence equilibrium and the solution tends to this point.

Figure 3.6 is the simulation where there is a $(P, 0, Z)$ limit cycle solution. The predator death rate is taken as $\nu = 0.2\text{d}^{-1}$ and virion decay rate as $\gamma = 6\text{d}^{-1}$. Figure 3.6(b) is a phase portrait of the system after allowing the initial dynamics to settle.

The final region of parameter space considered is that which exhibits long-term periodic behaviour of (P, V, Z) coexistence. Figure 3.7 shows (P, V, Z) during the initial transient stages on this region, whilst Figure 3.8 shows the system after allowing the initial dynamics to settle, revealing a (P, V, Z) limit cycle solution. Parameter values

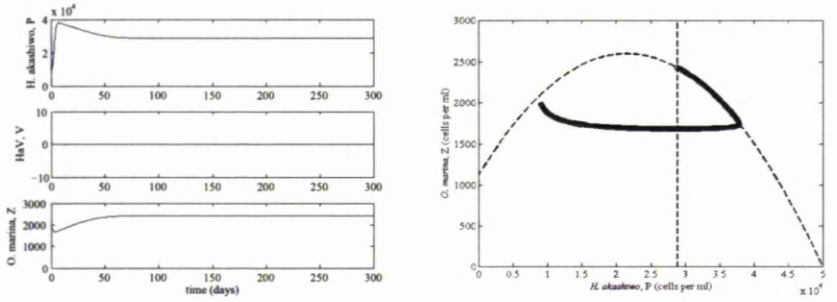

(a) Solution over time (b) Individual trajectory

Figure 3.5: $(P_3^*, 0, Z^*)$ stable equilibrium, using parameter values in Table 3.1 with $\nu = 1.38\text{d}^{-1}$ and $\gamma = 6\text{d}^{-1}$.

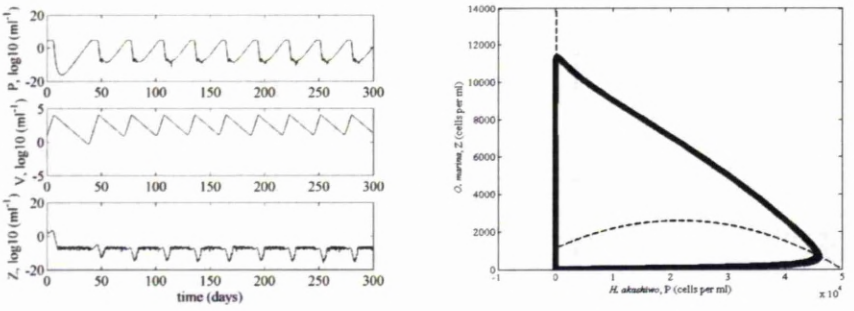

(a) Solution over time (b) Individual trajectory

Figure 3.6: $(P, 0, Z)$ limit cycle, using parameter values in Table 3.1 with $\nu = 0.2\text{d}^{-1}$ and $\gamma = 6\text{d}^{-1}$.

are as in Table 3.1, with $(\gamma, \nu) = (0.5, 0.45)\mathrm{d}^{-1}$.

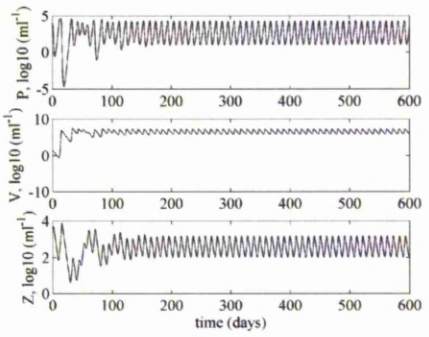

Figure 3.7: (P, V, Z) non-equilibrium coexistence, using parameter values in Table 3.1 with $\nu = 0.45\mathrm{d}^{-1}$ and $\gamma = 0.5\mathrm{d}^{-1}$.

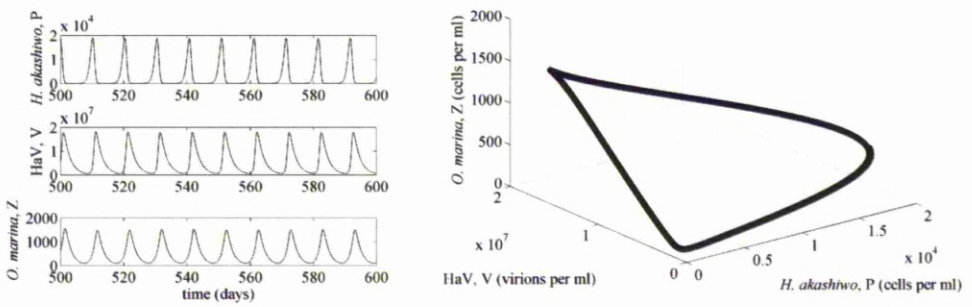

(a) Solution over time

(b) Individual trajectory

Figure 3.8: (P, V, Z) limit cycle, after allowing the dynamics to settle. Parameter values as in Table 3.1 with $\nu = 0.45\mathrm{d}^{-1}$ and $\gamma = 0.5\mathrm{d}^{-1}$.

3.3.4 Control of blooms by addition of viruses or grazers

This section addresses the scenario of having a phytoplankton community whose population size must be controlled. Phytoplankton control may be sought in order to preserve fish stocks, for example. Model (3.1, 3.2, 3.3), and its subsequent analysis, suggest that viruses or predators could be used to achieve this. At low concentrations, the behaviour of the system is much less predictable and the deterministic model (3.1, 3.2, 3.3) is no longer a good representation. This random, individual behaviour is referred to as stochasticity. The aim of this section is to either change the long-term behaviour so that the phytoplankton tends to an equilibrium lower than carrying capacity or to reduce the phytoplankton to low enough levels in the short term that this

stochasticity, or environmental factors, will prevent recovery. The critical community size (CSS), the smallest population size that doesn't suffer extinction (Keeling and Rohani, 2008), is therefore important. The critical concentration will depend on the environment. For example, in a test tube, a phytoplankton population less than one cell per ml would correspond to a very low total population, thus increasing the reliance on chance. However, less than one cell per ml in the field may still constitute a sizeable total population, reducing the likelihood of extinction. We will simply investigate how the phytoplankton concentration can be decreased by the addition of virions or grazers.

In reality, the short term transient behaviour may be more important since the environments phytoplankton reside in generally change on very short time scales, preventing long term system dynamics from being reached. However, our results regarding transient behaviour are dependent on the initial conditions used, although the effective controllability of HaV compared to *O. marina* will hold since we consider the initial conditions required for each to achieve a destruction of phytoplankton levels in the short term. We also consider the transient behaviour of a limit cycle system, where initial conditions will affect where in the cycle we start but won't alter maximum or minimum values.

Control of phytoplankton by altering the long-term dynamics

Here we consider lowering the long-term equilibrium phytoplankton concentration as a method of control. In the two-component phytoplankton-virus model (equations 3.1, 3.2, 3.3 in the absence of Z), $\gamma = \gamma_1 = c_v\sigma_1\lambda K$ (equation 3.11) separates the parameter region where phytoplankton exist alone at carrying capacity, K, and where the phytoplankton and virus coexist in stable equilibrium $(P, V) = (P_2^*, V^*)$ in the long-term, where $P_2^* < K$. Therefore, where a phytoplankton population exists alone at carrying capacity, adding even a small amount of the virus with $\gamma < \gamma_1$ will reduce the phytoplankton population from its carrying capacity down to its lower coexistence equilibrium. The phytoplankton coexistence equilibrium is defined as $P_2^* = \frac{\gamma}{c_v\sigma_1\lambda}$ (equation 3.13), therefore, smaller values of the virion decay rate, or larger values of c_v, σ_1 and λ, lead to lower phytoplankton equilibrium values. For the parameter values given in Table 3.1 for *H. akasiwo* and HaV, and $\gamma = 0.08\text{d}^{-1}$ (the value used in Figure 3.4), the *H. akashiwo* coexistence equilibrium occurs at 517 per ml (3sf). Figure 3.9(a) shows the effects of adding 10 HaV particles per ml after 100 days to a *H. akashiwo* population existing alone at carrying capacity. Parameter values are as in Table 3.1. There aren't any grazers in the system, but we set the predator death rate, $\nu = 1.5\text{d}^{-1}$ so that the system isn't unstable to predator growth. The figure shows the phytoplankton population being quickly reduced and experiencing small oscillations towards equilibrium.

Similarly, consider the two-component phytoplankton-predator system (model 3.1, 3.2, 3.3 in the absence of V). The addition of grazers with $\nu < \nu_1 = \frac{\mu_{\max}(K-p')}{K_{\mathrm{GR}}+K-p'}$ (equation 3.12) to a phytoplankton population existing alone at carrying capacity will remove the phytoplankton population from its carrying capacity in the long-term to a phytoplankton-predator coexistence stable steady state or, for lower values of ν, stable predator-prey limit cycles. Although the latter is undesirable since the phytoplankton periodically reach very high levels. Here, the phytoplankton coexistence equilibrium occurs at $P_3^* = \frac{\nu K_{\mathrm{GR}}}{\mu_{\max}-\nu} + p'$ (equation 3.16). Keeping all other parameters constant, decreasing the predator death rate, ν, will decrease the phytoplankton equilibrium. Using the parameter values in Table 3.1 for *H. akashiwo* and *O. marina* with $\nu = 1.38\mathrm{d}^{-1}$ (as in Figure 3.5), the phytoplankton coexistence equilibrium is calculated to be 28800 per ml (3sf). For the parameter values in Table 3.1, $\nu_2 = 1.36\mathrm{d}^{-1}$ (3sf). Thus, the lowest value of ν for which the system tends to $(P_3^*, 0, Z^*)$ stable is $1.36\mathrm{d}^{-1}$ (3sf). The lowest value of P_3^* for the parameters in Table 3.1 is therefore 20300 per ml (3sf). This suggests that HaV may be a better control of *H. akashiwo* than *O. marina* since the *H. akashiwo* coexistence equilibrium has the potential to be much lower. Figure 3.9(b) shows the effects of adding 10 *O. marina* cells per ml after 100 days to a *H. akashiwo* population existing alone at carrying capacity. Parameter values are as in Table 3.1, with $(\gamma, \nu) = (9, 1.38)\mathrm{d}^{-1}$. Notice how much longer *O. marina* takes to reduce *H. akashiwo* to equilibrium than HaV does.

We compare the efficiency of the virus at controlling the phytoplankton to the efficiency of the predator in aiming to allow a person seeking a control mechanism to balance the efficiency of a virus or predator against manufacturing costs, for example.

Thus, the addition of small amounts of virus or predator, whose death rates satisfy certain conditions, to a phytoplankton population existing alone at carrying capacity can shift the long term behaviour of the phytoplankton to either a $(P_2^*, V^*, 0)$ stable equilibrium, $(P_3^*, 0, Z^*)$ stable equilibrium or $(P, 0, Z)$ limit cycles. Similarly, the bifurcation plot of Figure 3.3 shows that, for the full phytoplankton-virus-predator system, addition of a virus with a small enough decay rate to a $(P_3^*, 0, Z^*)$ stable, or non-equilibrium, system may push the long term behaviour to $(P_2^*, V^*, 0)$ stable and vice-versa, P_2^* being considerably lower than P_3^* and K for *H. akashiwo*, HaV and *O. marina*. Figure 3.10 shows the effects of adding 10 HaV particles per ml, with $\gamma = 0.08\mathrm{d}^{-1}$, to a *H. akashiwo*-*O. marina* stable system, Figure 3.10(a), or a system undergoing *H. akashiwo*-*O. marina* limit cycles, Figure 3.10(b).

Control of phytoplankton by reduction to low levels in the short term

We now investigate how incorporation of virions and grazers affects the transient dynamics. Start by considering the simple case of adding virions to a phytoplankton community existing alone at carrying capacity. In Figure 3.9(a), the phytoplankton

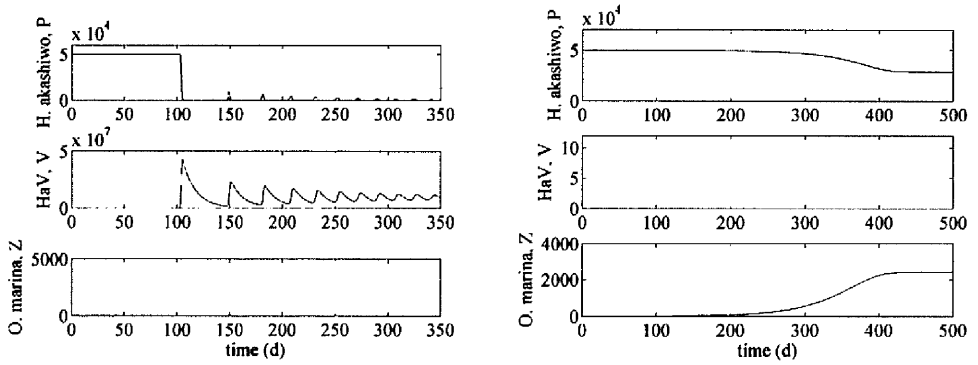

Figure 3.9: Control of *H. akashiwo* by adding 10 HaV particles per ml, Fig. (a), or 10 *O. marina* cells per ml, Fig. (b), to a *H. akashiwo* population existing alone at carrying capacity and shifting from this steady state to either phytoplankton-virus, Fig. (a), or phytoplankton-predator, Fig. (b), stable coexistence. Solved using parameter values in Table 3.1 with $(\gamma, \nu) = (0.08, 1.5)\mathrm{d}^{-1}$ for Fig. (a) and $(\gamma, \nu) = (9, 1.38)\mathrm{d}^{-1}$ for Fig. (b). The virions and grazers are added after 100 days.

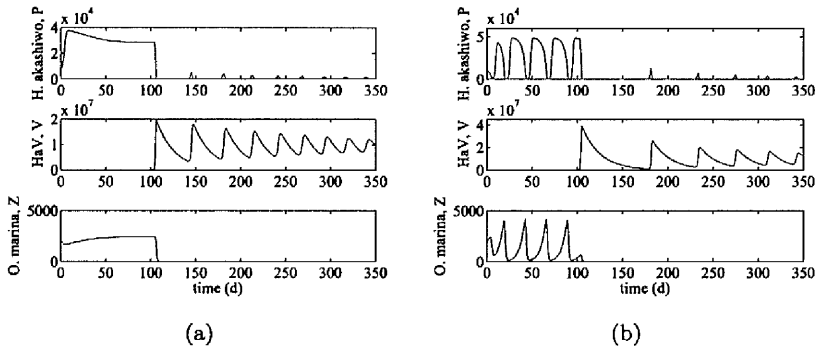

Figure 3.10: Control of *H. akashiwo* by adding 10 HaV particles per ml to a *H. akashiwo-O. marina* stable population, Fig. (a), or *H. akashiwo-O. marina* stable limit cycle behaviour, Fig. (b), and shifting to phytoplankton-virus stable coexistence. Solved using parameter values in Table 3.1 with $(\gamma, \nu) = (0.08, 1.38)\mathrm{d}^{-1}$ for Fig. (a) and $(\gamma, \nu) = (0.08, 1.2)\mathrm{d}^{-1}$ for Fig. (b). The virions and grazers are added after 100 days.

reached a minimum of 8.74×10^{-10} cells per ml (3sf) before recovering to a small bloom at day 148. This suggests that low concentrations could be added to a phytoplankton population and reduce it to very low levels in the short term. The phytoplankton are reduced to such low numbers that the population may not recover, and if they do, the population will still eventually be brought to equilibrium level (which has a value lower than the carrying capacity). Decreasing the virion decay rate decreases the minimum phytoplankton population level reached before they re-bloom, increases the time before the phytoplankton are able to re-bloom, decreases the height of subsequent blooms and increases the time before equilibrium is reached. Figure 3.9(b) shows that adding the same quantity of *O. marina* to a phytoplankton community existing alone at carrying capacity will reduce the phytoplankton to P_3^*, but not to a lower level prior to settling. A very high concentration of *O. marina* is needed to achieve this, again suggesting HaV to be a preferential control over *O. marina*. Decreasing the predator death rate decreases the time before the phytoplankton population reaches equilibrium. However, the range of values of ν for which the long term behaviour is $(P_3^*, 0, Z^*)$ stable steady state is small. Reducing ν below this range causes $(P, 0, Z)$ limit cycle behaviour. When $\nu = 1.2\text{d}^{-1}$, Figure 3.10(b) showed a virus being added to a phytoplankton-predator limit cycle system. However, the phytoplankton population was reduced to less than 0.1 cells per ml prior to the introduction of virions. It's therefore possible that the phytoplankton wouldn't recover from this and therefore the addition of virions could be unnecessary. Decreasing the predator death rate further, decreases the time before the first trough and decreases the minimum phytoplankton population reached. The latter effect is particularly desirable since reducing the phytoplankton to very low levels will allow stochasticity to become important and potentially stop the phytoplankton recovering. The number of cycles in a given time is increased.

The above analysis indicates that a shift in long-term behaviour may be unneccesary since the phytoplankton can potentially be reduced to very low levels in the short term, from which it may not recover. We thus investigate adding extra virions or grazers, with parameter values that don't alter the long term dynamics, to a $(P_2^*, V^*, 0)$ stable system and a $(P_3^*, 0, Z^*)$ stable system.

Consider a system tending to a $(P_2^*, V^*, 0)$ stable steady state in the long term, with phase portrait as in Figure 3.4(b). Above the diagonal null-cline intersecting the horizontal axis at $P = K$ in Figure 3.4(b), the phytoplankton concentration decreases in the short term. Therefore, ensuring the virus population satisfies

$$V > \frac{r(K-P)}{Kc\sigma_1\sigma_2}, \tag{3.27}$$

ensures the phytoplankton population decreases from the start. The deterministic model predicts that in the longer term the populations of phytoplankton and virus

will undergo decaying oscillations until the equilibrium solution is attained. Using the parameter values in Table 3.1 and taking P to be the initial phytoplankton concentration $P_0 = 9000\text{ml}^{-1}$, equation (3.27) says the number of virions per ml must be greater than 8×10^6 for the concentration of phytoplankton, in a $(P_2^*, V^*, 0)$ stable region of parameter space, to decrease in the short term. This quantity is likely to be unfeasibly high to manufacture and add to a phytoplankton community. Since Figure 3.4(b) shows that adding a smaller amount of the virus will still reduce the phytoplankton population, but only after allowing the phytoplankton to bloom, it may be best to let the bloom take place, knowing it will then be reduced. Determining the quantity of equation (3.27) may still be useful if, for example, the virus concentration was close to this quantity and extra virions could be added to speed up the bloom termination. Once the phytoplankton and virus populations reach equilibrium, adding extra virions or grazers can reduce the phytoplankton population in the short term, but it will recover to equilibrium unless very large quantities are added and the phytoplankton population gets too low to recover. Adding grazers to this system will reduce the phytoplankton in the short term, if the quantity added is large, before the phytoplankton returns to P_2^*. For instance, numerical simulation of model (3.1, 3.2, 3.3) using the parameter values of Table 3.1 and $(\gamma, \nu) = (0.08, 1.2)\text{d}^{-1}$ shows that the addition of 10^2 grazers per ml to a phytoplankton community existing at its P_2^* equilibrium of 517 per ml reduces the phytoplankton population to 455 per ml (3sf). Increasing the quantity of grazers added, decreases the minimum phytoplankton level achieved. The phytoplankton then increased to a maximum of 770 per ml (3sf), continuing to oscillate towards equilibrium.

Similarly, for a system tending to $(P_3^*, 0, Z^*)$ stable, Figure 3.5(b) shows that when the number of grazers added satisfies

$$Z > \frac{r(K_{\text{IR}} + P)}{I_{\max}} \left(1 - \frac{P}{K}\right), \tag{3.28}$$

the phytoplankton population will decrease in the short term. Equations (3.27) and (3.28) suggest that, for P close to K, a very small amount of viral particles or grazers would diminish very high phytoplankton population levels. In reality this is unrealistic since stochasticity becomes important. Again taking P to be the initial phytoplankton concentration $P_0 = 9000\text{ml}^{-1}$ and using the parameter values of Table 3.1, equation (3.28) determines the concentration of predators needed to reduce the phytoplankton population in the short term must be greater than $2.1 \times 10^3\text{ml}^{-1}$. Again, this may be too high a concentration to culture and add to a phytoplankton community. Similarly to the $(P_2^*, V^*, 0)$ stable case, it may be best to allow the grazer population to naturally oscillate with the phytoplankton (each phytoplankton bloom being damped compared to the previous). Adding a small quantity of extra grazers will reduce the time before the phytoplankton bloom. Adding virions to a phytoplankton community existing at

equilibrium with its grazers can create a dip in the phytoplankton population, with larger quantities of virions leading to a lower minimum. The phytoplankton then tend back towards their equilibrium of P_3^*.

For the non-equilibrium long term behaviour present in the phytoplankton-virus-predator system considered in Figures 3.6-3.8, the phytoplankton populations reached less than one cell per ml in the troughs. A further control mechanism may therefore be unnecessary, however, depending on the point in the cycle, the phytoplankton may bloom before being brought to such low levels.

In summary, we have found that addition of virions or grazers to a phytoplankton population existing alone at carrying capacity can alter the long term dynamics, reducing the phytoplankton from carrying capacity to some lower equilibrium concentration, the coexistence equilibrium of *H. akashiwo* with HaV, for the parameter values used here, being lower than that with *O. marina* suggesting HaV to be a better control mechanism. The long term behaviour achieved is dependent on the size of the virion or predator death rate relative to other parameters. The predator death rate is particularly sensitive to this since too low a value can change the long-term behaviour to phytoplankton-predator limit cycles. Even though the phytoplankton may be reduced during these cycles to levels from which it may not recover, in the event of recovery the phytoplankton population will bloom close to carrying capacity. Investigation of phytoplankton coexisting with a virus or predator found that addition of extra virions or grazers could reduce the phytoplankton population in the short term, but the population would always recover. A phytoplankton minimum low enough that we may not expect the population to recover from in the field was only found when very large quantities of virions or grazers were added. A formal representation of the quantity of virions or grazers needed to reduce the phytoplankton population in the short term is given in equations (3.27) and (3.28). However, the amount of these species required may be unfeasibly high.

3.3.5 Comparison with observed data

The idea of viral infection or predation terminating harmful algal blooms was first suggested due to observations rather than mathematical analysis. We have chosen two observational studies exploring control of *H. akashiwo* to consider. The first study, by Tarutani et al. (2000), observed viral infection of *H. akashiwo* in the field whilst the second study, by Jeong et al. (2003), observed predation of *H. akashiwo* in mesocosms. Figures from each paper, showing observed population levels, will be used to compare model (3.1,3.2,3.3) against.

H. akashiwo and its virus HaV

Figure 3.11(a), taken from Tarutani et al. (2000), shows observed population levels of *H. akashiwo* and HaV. Considering the surface particles, the authors describe the data in terms of three periods. The first period, taking place between the middle of May and early June, is characterised by a bloom of *H. akashiwo* whilst HaV remains at a nominal level. The second period depicts the disintegration of the phytoplankton bloom, whilst the viral population peaks before also declining. The final period shows a small secondary bloom in phytoplankton, but no real change in HaV.

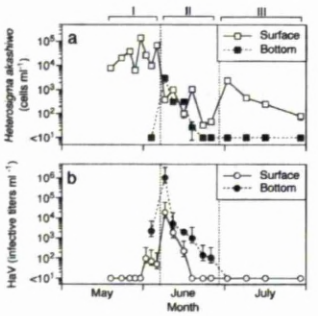

(a) Observed population levels, taken from Tarutani et al. (2000)

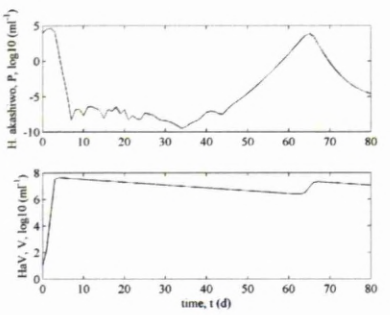

(b) Model solution

Figure 3.11: Comparison of phytoplankton-virus model, Figure (b), with observations made by Tarutani et al. (2000), Figure (a). The model solution is over an 80 day time period with initial conditions: $(P_0, V_0, Z_0) = (9000, 10, 0)$ cells per ml. Parameter values as in Table 3.1 with $\gamma = 0.05\text{d}^{-1}$ and $\nu = 1.4\text{d}^{-1}$.

Figure 3.11(b) shows the solution of model (3.1, 3.2, 3.3) over a two and a half month time period, using those values given in Table 3.1, taking $\nu = 1.4\text{d}^{-1}$ so that the system isn't unstable to predator growth and $\gamma = 0.05\text{d}^{-1}$. For the given choice of parameters for viral infection and phytoplankton growth, we are in the region where equilibrium $(P_2^*, V^*, 0)$, is stable. The initial conditions are estimated from the observed initial surface concentrations and are $(P_0, V_0, Z_0) = (9000, 10, 0)\text{ml}^{-1}$. There are some distinct differences between the observed data and the model solution. The minimum phytoplankton concentration levels are considerably less than those observed of between 10 and 10^2ml^{-1}. Tarutani et al. (2000) found that during this period the majority of *H. akashiwo* cells were resistant to the viruses, possibly explaining why the phytoplankton population in Figure 3.11(b), where only one cell-type is modelled, is driven to much lower concentrations. Secondly, the virus peaks at a higher abundance in Figure 3.11(b) and the secondary bloom in phytoplankton, which starts later in our plot, is also followed by a secondary peak in viral particles, which doesn't correlate with the observed populations. The observed secondary bloom in Figure 3.11(a) may

be due to low virus concentration, however, unless the viral population gets so low that it can't recover, we would expect the bloom in phytoplankton to be followed by a peak in viral abundance. An alternative suggestion, put forward by Tarutani et al. (2000), is that the resistant cells of the second period may be infected and lysed by viruses and thus wouldn't appear in Figure 3.11(b). Another point is that the phytoplankton and viral particles are not homogeneously distributed in space, as is evident from the difference in abundance between surface and bottom waters. Spatial transport, for example due to sinking or swimming will modify the model, and may also explain some of the differences between the model and the observed data. From Figure 3.4, Figure 3.11(b) is expected to oscillate and tend to a stable equilibrium over a longer time frame. However, in the model solution, phytoplankton concentration reaches a minimum of the order 10^{-9} cells per ml and so stochastic effects will become important.

H. akashiwo and its predator *O. marina*

Figure 3.12(a), taken from Jeong et al. (2003), shows observed population levels of *H. akashiwo* and its predator *O. marina*. Over a 73 hour time period the *H. akashiwo* population steadily declines. During this time, the *O. marina* population increases to peak between 50 and 60 hours, after which this population also diminishes.

To compare directly with Jeong et al. (2003), we also take $\nu = 0$, which, ensuring $\gamma > 0.02\text{d}^{-1}$ (from equation (3.18)), forces the long-term dynamics to be the $(P, 0, Z)$ limit cycle behaviour (see Figure 3.3). Figure 3.12(b) is a plot of model (3.1, 3.2, 3.3) over a 3 day time period, which can be compared with Figure 3.12(a). The initial conditions of $(P_0, V_0, Z_0) = (16000, 0, 2000)\text{ml}^{-1}$ are estimated from Figure 3.12(a). A striking difference is the length of time the predator takes to decay in the model solution, Figure 3.12(b), which suggests a problem in the model. Consider the dynamics of the predator when the prey concentration has been reduced to very low levels, $P \approx 0$. The equation describing the time evolution of the predator, equation (3.3), with $\nu = 0$ and $P = 0$ is given by

$$\frac{dZ}{dt} = -\frac{\mu_{\max} p'}{K_{\text{GR}} - p'} Z. \tag{3.29}$$

Therefore, $Z = Z_0 \exp\left(-\frac{\mu_{\max}}{(K_{\text{GR}} - p')} t\right)$. Substituting parameter values from Table 3.1 reveals $Z \approx Z_0 e^{-\frac{t}{10}}$, indicating that it will take just under 7 days for the predator population to halve in size [1]. However, in Figure 3.12(a), the predator population takes approximately 14 hours to halve in size. Therefore, there seems to be some discrepancy between the numeric response function of *O. marina* on *H. akashiwo*, which was fitted by Jeong et al. (2003) to observed data shown in Figure 2 of their paper, and the cell concentrations observed by Jeong et al. (2003) and shown in Figure

[1] $\exp\left(-\frac{t}{10}\right) = \frac{1}{2} \Rightarrow t = 10\ln(2) \approx 6.93$ days

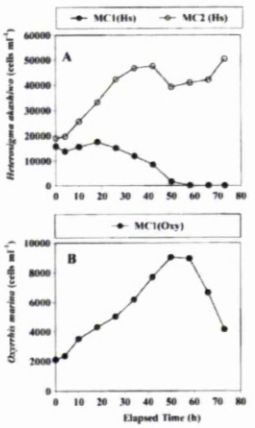

(a) Observed populations levels, taken from Jeong et al. (2003)

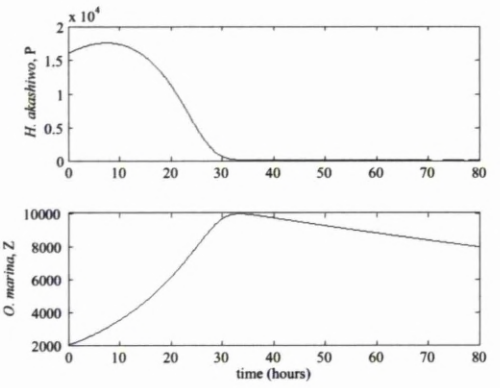

(b) Model solution

Figure 3.12: Figure (a) shows population levels of *H. akashiwo* and its predator *O. marina*, observed by Jeong et al. (2003). The top curve, labelled MC2(Hs), is the control population, showing *H. akashiwo* growth in the absence of *O. marina* and the bottom curve, labelled MC1(Hs), shows *H. akashiwo* growth in the presence of *O. marina*. Figure (b) shows the solution of model (3.1, 3.2, 3.3) over an 80 hour time period for comparison with the observed data. Parameter values are those in Table 3.1 with $(P_0, V_0, Z_0) = (16000, 0, 2000)\text{ml}^{-1}$, $\gamma = 0.05\text{d}^{-1}$ and $\nu = 0\text{d}^{-1}$.

4 of their paper (reproduced here in Figure 3.12(a)). Jeong et al. (2003) calculated the specific growth rate of *O. marina* by averaging the instantaneous growth rates for each sampling interval. The data for *O. marina* growth rates were then fitted to a Michaelis-Menten (or Holling Type II) equation, where specific growth rate $= \dfrac{\mu_{\max}(P-p')}{K_{\mathrm{GR}}+(P-p')}$.

Also, the peak size of the predator is higher in the model than observed, and the predator peaks sooner in Figure 3.12(b) than was observed by Jeong et al. (2003).

3.3.6 Changing the volume clearance rate

Here we investigate how changing the phytoplankton-virus or phytoplankton-predator volume clearance rates, due to phytoplankton swimming or turbulence for example, affects the long-term dynamics of model (3.1, 3.2, 3.3).

Phytoplankton-virus

In order to study the effects of changing the $P-V$ volume clearance rate, $\mathrm{c_v}$, define the dimensionless quantity

$$\beta = \frac{\gamma}{K\mathrm{c_v}\sigma_1\lambda}, \tag{3.30}$$

and summarise the stability criteria determined in section 3.3.1, in terms of β.

- Equilibrium 1: $P = K, V = Z = 0$.

  Stable if:

$$\beta > 1, \tag{3.31}$$

$$\nu > \frac{\mu_{max}(K-p')}{K_{\mathrm{GR}}+K-p'} = \nu_1. \tag{3.32}$$

- Equilibrium 2: $P = P_2^*, V = V^*, Z = 0$.

  The equilibrium concentrations are given by:

$$P_2^* = \beta K, \quad V^* = \frac{r}{\mathrm{c_v}\sigma_1\sigma_2}(1-\beta). \tag{3.33}$$

  Stable if:

$$\nu > \frac{\mu_{\max}(\beta K-p')}{K_{\mathrm{GR}}+\beta K-p'} = f(\beta). \tag{3.34}$$

- Equilibrium 3: $P = P_3^*, V = 0, Z = Z^*$. The equilibrium concentrations are given by:

$$P_3^* = \frac{\nu K_{\mathrm{GR}}}{\mu_{\max}-\nu} + p', \quad Z^* = \frac{r}{I_{\max}}(K_{\mathrm{IR}}+P_3^*)(1-\frac{P_3^*}{K}). \tag{3.35}$$

Stable if:

$$\nu < f(\beta), \tag{3.36}$$

$$\nu > \frac{\mu_{\max}(K - 2p' - K_{\mathrm{IR}})}{2K_{\mathrm{GR}} + K - 2p' - K_{\mathrm{IR}}} = \nu_2. \tag{3.37}$$

Altering the phytoplankton-virus volume clearance rate, c_v, will change stability criteria (3.31), (3.34) and (3.36). The P_2^* and V^* equilibria, along with $f(\beta)$, will change with c_v.

Figure 3.13 shows the long-term dynamics of model (3.1, 3.2, 3.3) relative to the predator death rate ν and the quantity $\beta = \frac{\gamma}{Kc_v\sigma_1\lambda}$. Varying the volume clearance rate c_v will alter the quantity β and potentially change the long term dynamics of the system. The value of c_v used so far is that in Table 3.1, $c_v = 7 \times 10^{-5}$ml d^{-1}. Figure 3.14 shows how changing the phytoplankton-virus volume clearance rate, c_v, can alter the long-term dynamics of the model. Increasing c_v decreases the quantity β. The dashed line in Figure 3.14 shows the possible long-term behaviour of the model for a particular volume clearance rate. Figure 3.14(b) shows the possible long-term dynamics when $c_v = 7 \times 10^{-5}$ml d^{-1}, as has been used thus far. Taking γ to be 5d^{-1}, $K = 5 \times 10^4$ml^{-1}, $\lambda = 22.1$ and $\sigma_1 = 0.1$, $\beta = 0.646$ when $c_v = 7 \times 10^{-5}$ml d^{-1}. Here, there are three possible outcomes: $(P_2^*, V^*, 0)$ stable, $(P_3^*, 0, Z^*)$ stable and non-equilibrium solutions. Figure 3.14(c) shows how halving the volume clearance rate will change the dynamics. Keeping all other parameters the same, β is now 1.29. There are still three possible outcomes, but the $(P_2^*, V^*, 0)$ stable state is no longer a possibility. However, the long-term behaviour can now tend to a $(K, 0, 0)$ stable equilibrium. Finally doubling the value of c_v in Table 3.1 gives $c_v = 14 \times 10^{-5}$ml d^{-1} and therefore $\beta = 0.323$. Figure 3.14(a) shows that there are only two possible long-term behaviours for this value of c_v : $(P_2^*, V^*, 0)$ stable and non-equilibrium solutions.

To increase the probability of the system tending to a $(P_2^*, V^*, 0)$ stable state, for example, one can increase the volume clearance rate. As discussed in section 2.3.1, the phytoplankton-virus volume clearance rate varies with diameter of both the host and virus, temperature, motility of the phytoplankton, and fluid motions, due to turbulence for example. Any one, or multiples, of these factors changing the value of c_v will affect what long-term dynamics the model is capable of.

Consider *H. akashiwo* and HaV specifically, using the parameter values of Table 3.1. In section 2.3.1, the volume clearance rate for motile *H. akashiwo* and HaV in still fluid was calculated to be $c_v = 5.4 - 9.8 \times 10^{-5}$ml d^{-1}, whereas the purely diffusional volume clearance rate is $c_v = 1.7 \times 10^{-5}$ml d^{-1}. Figure 3.15 shows the population dynamics of *H. akashiwo* and HaV. The three plots represent non-motile *H. akashiwo* ($c_v = 1.7 \times 10^{-5}$ml d^{-1}), *H. akashiwo* swimming at 20×10^{-4}cms^{-1} ($c_v = 5.4 \times 10^{-5}$ml d^{-1}) and *H. akashiwo* swimming at 160×10^{-4}cms^{-1} ($c_v = 9.8 \times 10^{-5}$ml d^{-1}). The figure shows that ability of *H. akashiwo* to swim doesn't change the long-term behaviour from $(P_2^*, V^*, 0)$

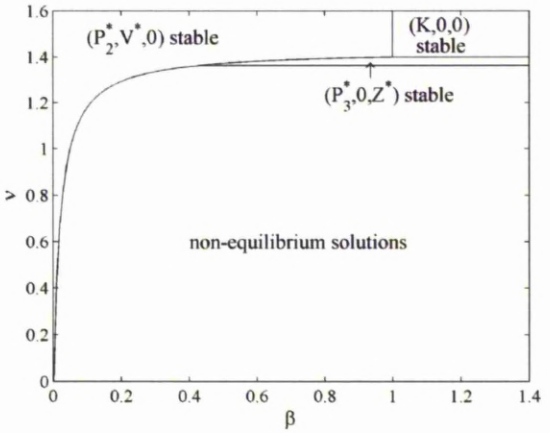

Figure 3.13: Plot depicting the long-term dynamics of model (3.1, 3.2, 3.3) relative to the values of predator death rate and the quantity $\beta = \frac{\gamma}{K c_v \sigma_1 \lambda}$. The quantities ν_1, ν_2 and $f(\beta)$ are defined in equations (3.32), (3.37) and (3.34) respectively. The figure was computed using parameter values in Table 3.1.

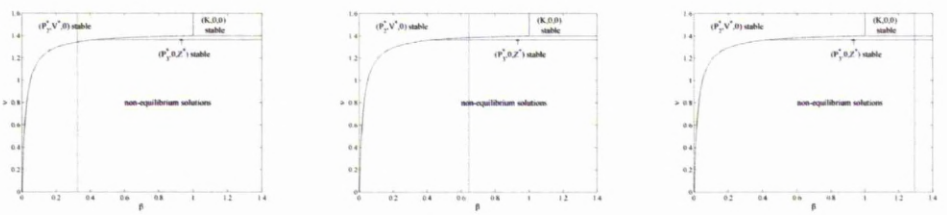

(a) $c_v = 14 \times 10^{-5}$ml d^{-1} (b) $c_v = 7 \times 10^{-5}$ml d^{-1} (c) $c_v = 3.5 \times 10^{-5}$ml d^{-1}

Figure 3.14: Figure depicting how altering the phytoplankton-virus volume clearance rate, c_v, affects the long-term dynamics of model (3.1, 3.2, 3.3). The dashed line in each plot represents the value of β when $c_v = 14 \times 10^{-5}, 7 \times 10^{-5}$ and 3.5×10^{-5}ml d^{-1} respectively.

stable for the parameters used, however, increasing phytoplankton swimming speed lowers the equilibrium levels of P and V, P_2^* and V^* respectively. The transient behaviour is also altered. Motility of *H. akashiwo* can prevent the phytoplankton reaching carrying capacity. For the phytoplankton swimming speed of $U_{\mathrm{P}} = 160 \times 10^{-4}\mathrm{cms}^{-1}$ in Figure 3.15, the first peak in the phytoplankton reaches a concentration of 4.4×10^4 cells per ml, compared to it reaching carrying capacity, 5×10^4 cells per ml, for $U_{\mathrm{P}} = 0\mathrm{cms}^{-1}$. Increasing swimming speed decreases the time before the bloom is terminated, decreases the minimum level of phytoplankton attained and allows more secondary blooms, but each is damped compared to the previous. The equilibrium level of both the phytoplankton and virus is reduced, which is to be expected given $(P_2^*, V^*) = \left(\frac{\gamma}{\mathrm{c_v}\sigma_1\lambda}, \frac{r}{\mathrm{c_v}\sigma_1\sigma_2}\left(1 - \frac{P_2^*}{K}\right)\right)$, remembering $\mathrm{c_v}$ increases as swimming speed increases. A value of γ could also be chosen so that the long-term behaviour changes with swimming speed as well as the transient dynamics. For example, keeping other parameters as used above, taking a value of $\gamma = 7\mathrm{d}^{-1}$ will allow the long-term behaviour to shift from $(K, 0, 0)$ stable to $(P_2^*, V^*, 0)$ stable as phytoplankton swimming speed increases from $20\mathrm{cms}^{-1}$ $160\mathrm{cms}^{-1}$, providing the predator death rate is greater than $1.38\mathrm{d}^{-1}$.

If we were to consider non-motile *H. akashiwo* and Hav in a turbulent regime, the results would be similar to Figure 3.15 except less pronounced since, for typical values of $\epsilon = 10^{-9}$ to $10^{-6}\mathrm{cm}^3\mathrm{s}^{-3}$ in the upper mixed layer, the volume clearance rate is in the range $2.0 - 3.1 \times 10^{-5}\mathrm{ml\ d}^{-1}$ (calculated in Chapter 2).

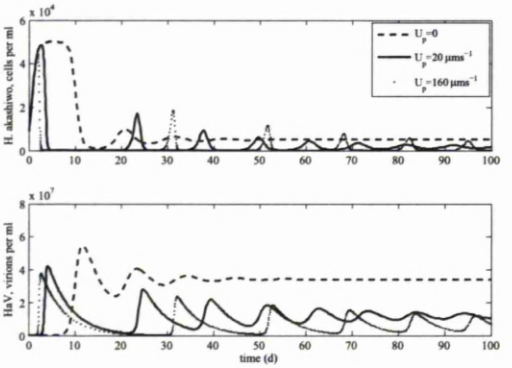

Figure 3.15: Effect of increasing phytoplankton swimming speed on the $P - V$ population dynamics. Parameter values are as in Table 3.1, with $\gamma = 0.2\mathrm{d}^{-1}$ and $(P_0, V_0) = (9000, 10)$ cells per ml.

Phytoplankton-predator

Consider the predation function of model equation (3.1) and write

$$\frac{dP}{dt} = -\frac{I_{\max}}{K_{\mathrm{IR}} + P} PZ, \tag{3.38}$$

the change in phytoplankton population over time in the absence of viral infection and for zero phytoplankton growth. We expect the right hand side of this equation to change when the phytoplankton-predator volume clearance rate changes, as suggested by equation (2.12). Relating this to the phytoplankton-predator volume clearance rate will be slightly more involved than when we related the phytoplankton-virus volume clearance rate to the viral transmission term in the model since the predation function is non-linear. When $P \ll K_{\mathrm{IR}}$,

$$\frac{dP}{dt} \approx -\frac{I_{\max}}{K_{\mathrm{IR}}} PZ. \tag{3.39}$$

Thus, for low levels of phytoplankton, the rate of consumption of the phytoplankton per predator is equal to $\frac{I_{\max}}{K_{\mathrm{IR}}} P$. For low values of P, we don't expect the predator to become satisfied and expect the maximum removal of phytoplankton per predator to be equal to the phytoplankton-predator volume clearance rate. Therefore,

$$\mathrm{c_z} = \frac{I_{\max}}{K_{\mathrm{IR}}}. \tag{3.40}$$

When $P \gg K_{\mathrm{IR}}$,

$$\frac{dP}{dt} \approx -I_{\max} Z. \tag{3.41}$$

For high levels of the phytoplankton population, we expect the contact rate to be so large that a predator consumes prey at its maximum ingestion rate, which is what equation (3.41) represents. The maximum ingestion rate represents intra-cellular processes such as time taken to handle and consume food, which we assume won't be affected by fluid motions. Therefore, $I_{\max}$ must be a fixed quantity. Therefore, from equation (3.40), we take the half saturation constant K_{IR} to be inversely proportional to $\mathrm{c_z}$. We also wish to reflect that changes in the volume clearance rate will alter the predator growth rate. Since K_{GR} plays a similar role to K_{IR}, by appearing in a similar way in the model and having a similar biological origin, we choose to also scale K_{GR} inversely proportional to $\mathrm{c_z}$.

The quantities $I_{\max}$ and K_{IR} have been estimated by Jeong et al. (2003) for *O. marina* and *H. akashiwo* in still fluid, and are stated in Table 3.1. This gives a volume clearance rate for *H. akashiwo* and *O. marina* to be $\mathrm{c_z} = 1.78 \times 10^{-3} \mathrm{ml\ d^{-1}}$.

If we now calculate the volume clearance rate for motile plankton in still fluid using Gerritsen and Strickler's (1977), we will be able to achieve an estimate of *O. marina's* perception radius. Continue to take *H. akashiwo* swimming speed to be in the range

$20 - 160\mu\text{ms}^{-1}$ (Smayda, 1998) and assume the swimming speed of *O. marina* in the presence of *H. akashiwo* to be $339\mu\text{ms}^{-1}$ (Menden-Deuer and Grünbaum, 2006), then the Gerritsen and Strickler (1977) expression for the volume clearance rate of motile *O. marina* and *H. akashiwo* in still fluid, equation (2.62), becomes:

$$\begin{aligned} c_z &= \pi R^2 \frac{(20 \text{ to } 160 \times 10^{-4}\text{cm s}^{-1})^2 + 3(339 \times 10^{-4}\text{cm s}^{-1})^2}{3(339 \times 10^{-4}\text{cm s}^{-1})^2} \\ &= (9211 \text{ to } 9884)R^2 \text{ ml d}^{-1} \end{aligned} \tag{3.42}$$

where R is the perception radius. Therefore, given we calculate Jeong et al. (2003) to have observed a volume clearance rate of $1.776 \times 10^{-3}\text{ml d}^{-1}$, this would suggest R is in the range 4.24 to 4.39×10^{-4}cm for *O. marina*. As expected, the perception radius of *O. marina*, which has a length of $\sim 13 \times 10^{-4}$cm (Menden-Deuer and Grünbaum, 2006), is significantly smaller than that of the copepod *C. furcatus*, which has length $\sim 10^3\mu$m and perception radius 4×10^{-2}cm (Uttieri et al., 2008).

Considering Figure 3.13, which shows the possible long-term dynamics of model (3.1, 3.2, 3.3) relative to the predator death rate, ν, and the dimensionless quantity β, it is clear that altering c_z will only affect the quantity ν_2 where (equation (3.37))

$$\nu_2 = \frac{\mu_{\max}(K - 2p' - K_{\text{IR}})}{2K_{\text{GR}} + K - 2p' - K_{\text{IR}}}. \tag{3.43}$$

This will lead to a change in the range of values of predator death rate, ν, for which a $(P_3^*, 0, Z^*)$ stable equilibrium is possible. However, halving c_z from $1.78 \times 10^{-3}\text{ml d}^{-1}$ (the value used throughout this chapter) to $8.9 \times 10^{-4}\text{ml d}^{-1}$, which causes K_{IR} and K_{GR} to double from 7040 to 14080 per ml and 1040 to 2080 per ml respectively, only changes ν_2 from 1.3637 to 1.3686. Similarly, doubling c_z from $1.78 \times 10^{-3}\text{ml d}^{-1}$ to $3.56 \times 10^{-3}\text{ml d}^{-1}$ changes ν_2 to 1.35. The equilibrium value of Z is increased when K_{IR} is increased, i.e. when c_z decreases.

If we take $R = 4.3 \times 10^{-4}$cm for *O. marina*, we calculated in section 2.4.2 the volume clearance rate for *H. akashiwo* in still fluid swimming at speeds in the range 20 to $160 \times 10^{-4}\text{cms}^{-1}$ to be in the range $1.70 \times 10^{-3}\text{ml d}^{-1}$ to $1.83 \times 10^{-3}\text{ml d}^{-1}$, and the volume clearance rate for non-motile *H. akashiwo* in still fluid to be 1.70×10^{-3}ml d^{-1}. Notice how the value for non-motile *H. akashiwo* is the same, to 2 d.p., as for one swimming at $20 \times 10^{-4}\text{cms}^{-1}$. Figure 3.16 shows the population dynamics of *O. marina* and *H. akashiwo*. There are two plots, representing non-motile *H. akashiwo* and *H. akashiwo* swimming at $160 \times 10^{-4}\text{cms}^{-1}$. However, the plots for the phytoplankton population are indistinguishable, indicating that the ability of *H. akashiwo* to swim doesn't alter the transient or long-term dynamics of its population. A slight difference can be seen in the predator population; an increased phytoplankton swimming speed lowers the equilibrium predator population.

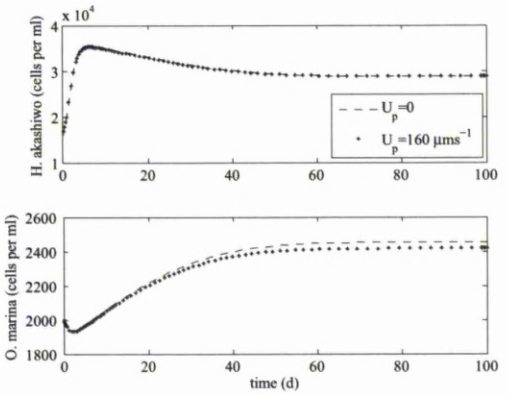

Figure 3.16: Effect of increasing phytoplankton swimming speed on the $P-Z$ population dynamics. Parameter values are as in Table 3.1, with $\nu = 1.38\text{d}^{-1}$ and $(P_0, V_0) = (16000, 2000)$ cells per ml.

Now consider the volume clearance rate for motile *H. akashiwo* in a turbulent environment, as calculated in section 2.4.2. Parameter values remain as above, with the inclusion of kinematic viscosity of water, $\nu = 10^{-2}\text{cm}^2\ \text{s}^{-2}$, structure function constant, $Sc = 2.411$, and energy dissipation rate, $\epsilon = 10^{-9}$ to $10^{-6}\text{cm}^2\text{s}^{-3}$. For *H. akashiwo* swimming at $20 \times 10^{-4}\text{cms}^{-1}$, the volume clearance rate is $\text{c}_\text{z} = 1.70 \times 10^{-3}\text{ml d}^{-1}$ (the same value, to 2 d.p., as for non-motile phytoplankton in still fluid) for ϵ between 10^{-9} and $10^{-6}\text{cm}^2\text{s}^{-3}$. For *H. akashiwo* swimming at $160 \times 10^{-4}\text{cms}^{-1}$, the volume clearance rate is $\text{c}_\text{z} = 1.83 \times 10^{-3}\text{ml d}^{-1}$ for ϵ in the range 10^{-9} to $10^{-6}\text{cm}^2\text{s}^{-3}$. Comparing with the values above for motile plankton in still fluid, we see that the introduction of this level of turbulence doesn't alter the phytoplankton-predator volume clearance rate and therefore won't affect the population dynamics. However, it should be remembered that this wasn't the case for the larger organism *C. furcatus*, as discussed in section 2.4.2.

3.3.7 Comparison of Viruses

Table 3.2 demonstrates the vast difference in parameter values between three of the *H. akashiwo* viruses isolated to date. This section shows how the overall dynamics differ for each virus and discusses choosing the most efficient virus for terminating a bloom. In chapter 2 we found that decreasing the diameter of the virus leads to an increase in the $P-V$ volume clearance rate. We therefore expect HaNIV and HaRNAV to have a higher volume clearance rate with *H. akashiwo* than HaV does. This is confirmed in our calculation of the volume clearance rate, c_v, below. The burst sizes of HaNIV and HaRNAV are much larger than that of HaV, further leading us to expect them to be a better control of *H. akashiwo* populations.

Referring to Figure 3.13, the data in Table 3.2 will only change the value of β, where $\beta = \frac{\gamma}{Kc_v\sigma_1(m\sigma_2-1)}$. The virus HaV has diameter $\approx 0.2 \times 10^{-4}$cm, which corresponds to a phytoplankton-virus volume clearance rate of $c_v = 9.7 \times 10^{-5}$ml d^{-1} for a host phytoplankton 15×10^{-4}cm in diameter, swimming at a speed of 50×10^{-4}cms^{-1} (a mid-range speed of those mentioned in Smayda (1998)) and residing in 20°C water. The virus has a burst size of 770. If γ were to lie in the range $0 - 10$d^{-1}, then the value of β would be in the range $0 - 0.93$ and four out of the five long-term dynamics would be possible (the $(K, 0, 0)$ stable equilibrium not being possible). The virus HaRNAV has a much smaller diameter of 25nm and therefore a volume clearance rate of $c_v = 6.3 \times 10^{-4}$ml d^{-1}. The burst size of this virus is 21000, much higher than that of HaV. For γ between $0 - 10$d^{-1}, β lies in the range $0 - 5.05 \times 10^{-3}$ (3sf) and the only possible long-term behaviour is the $(P_2^*, V^*, 0)$ stable equilibrium. Finally, HaNIV has a diameter of 30nm, similar to HaRNAV, but a burst size of the order 10^5. The volume clearance rate for this virus would be $c_v = 5.6 \times 10^{-4}$ml d^{-1}. Again, for γ in the range $0 - 10$d^{-1}, β is $0 - 1.19 \times 10^{-3}$ml^{-1}, which again only gives rise to a $(P_2^*, V^*, 0)$ stable equilibrium in the long-term.

A more general way to consider Figure 3.13 is to say, for example, $\beta = 1$ and $\nu = 1$. Here the system is in the non-equilibrium region. However, using a different virus which has a much larger burst size, for example, would decrease β and possibly push the long-term behaviour of the system into the $(P_2^*, V^*, 0)$ stable region. A virus with a higher contact rate or higher percentage of contacts achieving adsorption would also give this result.

	HaV	HaRNAV	HaNIV
Diameter (nm)	200	25	30
Burst size, m (per host cell)	770	21000	1×10^5
Source	Nagasaki et al. (1999)	Lawrence et al. (2006)	Lawrence et al. (2001)
Vol. clearance rate, c_v (ml d^{-1})	9.76×10^{-5}	6.32×10^{-4}	5.56×10^{-4}

Table 3.2: Data for three *H. akashiwo* viruses.

3.4 Discussion

Harmful algal blooms have serious ecological implications causing methods of control to be sought. Two such methods which have been proposed are predation and viral infection. Both have been considered here.

Model (3.1,3.2,3.3) has been proposed, to which there are five possible mathematical outcomes. There are three possible point stable steady states: phytoplankton and virus in the absence of predation, phytoplankton and predator in the absence of viral

infection or phytoplankton at carrying capacity with zero predator and virus. Another possible outcome is a phytoplankton-predator stable limit cycle, with zero viral infection. It was also found that phytoplankton, virus and predator can only coexist at equilibrium in the special case where $\nu = f(\gamma)$, but the steady state is always unstable. However, in nature, all three species do coexist. A numerical study showed that the model does allow for this since (P, V, Z) limit cycle behaviour was found in a region of parameter space.

Numerical simulations of the five situations were conducted. Both the predator and the virus were able to terminate the phytoplankton bloom and tend to stable population levels. However, in both cases, the phytoplankton were capable of recovery, dependent on initial conditions. For the region with $(P, 0, Z)$ and (P, V, Z) limit cycles, the blooms are terminated but repeatedly return to bloom.

We considered phytoplankton control more explicitly by adding virions or grazers to a phytoplankton community existing in stable equilibrium. For the parameter values used here, the phytoplankton had a lower equilibrium when coexisting with the virus as opposed to the predator, suggesting our virus to be a better control mechanism. Numerical simulation showed that a small concentration of virions was capable of swiftly reducing the phytoplankton from carrying capacity equilibrium to its much lower coexistence equilibrium. The virus could also be added to a $(P_3^*, 0, Z^*)$ stable system or $(P, 0, Z)$ limit cycles and change the long-term behaviour to $(P_2^*, V^*, 0)$ stable. Numerical simulation also showed a small concentration of grazers reduce a phytoplankton from carrying capacity to its coexistence equilibrium, but, for the parameters values used here, this equilibrium level was still high and the process of reducing the population a slow one. We also determined that introducing our virus to a virus-free system could reduce the phytoplankton to very low levels in the short term, from which the population may not recover in reality. This could also be achieved by adding grazers, but for our parameter values the quantity needed was very high. The phase portraits of the $(P_2^*, V^*, 0)$ and $(P_3^*, 0, Z^*)$ stable systems allowed formulae to be found that can be used to determine the amount of predator or virus needed to reduce the phytoplankton population in the short term. This allows us to calculate the extra quantity of virions or grazers needed in a system tending to $(P_2^*, V^*, 0)$ and $(P_3^*, 0, Z^*)$ stable, respectively, for the phytoplankton to be reduced in the short term to a level from which it can't recover. However, the quantity of grazers and virions needed is unfeasibly high.

The model predicts that for the stable phytoplankton-virus system, the virus is able to terminate the phytoplankton bloom. This is in agreement with Tarutani et al. (2000), although our model solution over time does differ to the observed data. The largest discrepancy, however, came when comparing the stable phytoplankton-predator system with Jeong et al. (2003). The model found the predator able to terminate the phytoplankton bloom as seen in Jeong et al. (2003). However, there is a striking

difference in the length of time the predator takes to decay in the model solution compared to that observed by Jeong et al. (2003). Closer inspection highlights a discrepancy between the numeric response function, which was fitted by Jeong et al. (2003) to observed data shown in Figure 2 of their paper, and the cell concentrations observed by Jeong et al. (2003) and shown in Figure 4 of their paper (reproduced in Figure 3.12(a) of this thesis).

We considered how changing the $P-V$ and $P-Z$ volume clearance rates altered the population dynamics. It was found that, for the parameter values used, changing the $P-V$ volume clearance rate from 14×10^{-5}ml d^{-1} to 3.5×10^{-5}ml d^{-1} removed the possibility of $P-V$ stable long-term behaviour. Changing the $P-Z$ volume clearance rate, via changing K_{IR}, altered the range of values of γ and ν for which $P-Z$ stable long-term behaviour was possible. However, changing the $P-Z$ volume clearance rate from 3.6×10^{-3}ml d^{-1} to 8.9×10^{-4}ml d^{-1} only changed the lower bound on ν (for $P-Z$ stable behaviour) from 1.3500 to 1.3686. The impact of altering the $P-Z$ volume clearance rate is thus limited, for the parameter values considered here. For *H. akashiwo* and HaV, increasing the phytoplankton swimming speed decreased the length of the initial peak in *H. akashiwo* and lowered the equilibrium levels of *H. akashiwo* and HaV, but increased the time taken to reach equilibrium. For *H. akashiwo* and *O. marina*, increasing the phytoplankton swimming speed didn't alter the population dynamics of *H. akashiwo*. The increase in phytoplankton swimming speed did, however, lower the equilibrium level of *O. marina*.

Finally, we considered how the dynamics may differ for different species of virus. We discussed three viruses, including HaV, all of which are known to infect *H. akashiwo*. The three viruses differ vastly in terms of diameter and burst size. By keeping all parameter values the same, except for virus diameter and burst size, we found the *H. akashiwo* volume clearance rate could change from 5.56×10^{-4}ml d^{-1} to 9.76×10^{-5}ml d^{-1} by considering a different virus.

Regarding the phytoplankton-predator system, it would be interesting to determine experimentally if/how K_{IR} changes with turbulence and phytoplankton swimming, and how this may alter other parameters in the model. An aspect of the phytoplankton-virus system which hasn't been considered here is the length of the lytic cycle (the time between a host becoming infected and lysing) and thus incorporation of an infected class of phytoplankton. This phytoplankton-virus system is the full model proposed by Bratbak et al. (1998), included here as model (1.21, 1.23, 1.23). Simulations in Bratbak et al. (1998) imply that increasing the length of the lytic cycle will increase the maximum population size of the phytoplankton and also increase the length of time before the phytoplankton population declines. Consideration of infected phytoplankton would enable further interesting dynamics to be explored. Reproduction by infected phytoplankton adding to the susceptible class could be considered, for instance. Also, removal of infected phytoplankton due to consumption by a predator, for example,

possibly consuming susceptible and infected phytoplankton at differing rates could be included.

A further area to consider is the incorporation of diversity into the model. The ability to model more than one strain of HaV, each infecting *H. akashiwo* with different viral infection characteristics, would allow greater comparison with the work of Tarutani et al. (2000). Equally, modelling more than one virus system infecting *H. akashiwo* would be an interesting adaptation of the model and would offer comparison with Lawrence et al. (2006). From the competitive exclusion principle, we don't expect two virus systems residing in the same environment "competing" to infect the same host to coexist. However, in Chapter 1, some limitations of the competitive exclusion principle were discussed. The original mathematical model (formulated by Volterra) that suggested coexistence of two or more species on one resource to be impossible is based on a number of assumptions. For example, a species specific growth rate dependent on more than the shared resource breaks one of these assumptions. Thus, more than one virus infecting the same species can coexist. Lack of coexistence in our system is a limitation of the model structure. Lawrence et al. (2006) have found two such viruses in coexistence: HaRNAV and OIs1, both of which infect *H. akashiwo*. The authors explain this coexistence by suggesting that one virus is temporarily favoured over the other on short time scales. For example, they explain that the shorter length of the lytic cycle of OIs1 offers it a competitive advantage when *H. akashiwo* density is high, whilst HaRNAV has a competitive advantage when the host density is low because of its large burst size.

Chapter 4

Effect of spatial heterogeneity on population dynamics

4.1 Introduction

This chapter considers how incorporating spatial variance, both explicitly and implicitly via key parameters, in the ODE model of Chapter 3, alters the population dynamics of a phytoplankton, virus and predator system. We model these dynamics using a system of 1-dimensional reaction-diffusion equations. The reaction terms represent growth, viral infection and predation, and are those of the ODEs studied in Chapter 3. The diffusion equation, which is used to model turbulence, considers the effects of the vertical, z, spatial component only, i.e. the system is modelled as a vertical water column. The diffusion terms involve an eddy diffusivity parameter, which we have utilised data presented in Sharples et al. (2001) to estimate. Thus, spatial heterogeneity of turbulence is incorporated via data profiles of eddy diffusivity.

It follows from incorporation of spatial heterogeneity into the eddy diffusivity parameter that the $P - V$ and $P - Z$ volume clearance rates will also vary spatially. Other key parameters such as the phytoplankton growth rate and carrying capacity don't vary in space in this thesis, but inclusion of this would make an important improvement in the future. However, keeping other parameters constant does have the benefit of allowing us clearly see how spatially variant turbulence affects the population dynamics. Utility of results would be improved by incorporation of spatial variance into other key parameters, but the results found here provide a good basis to consider the control of phytoplankton by a virus or predator in an environment with spatially varying turbulence.

An investigation into the use, and accuracy of, Matlab's PDE solver, pdepe, is conducted. We then consider each of the long-term behaviours studied in Chapter 3 to determine how a spatially heterogeneous water column may be structured. A systematic investigation of each long term behaviour is conducted, considering the

effects of spatially variant eddy diffusivity (and thus $P-V$ and $P-Z$ volume clearance rates) and a spatially variant initial phytoplankton population in turn. We investigate the possibility of different long-term behaviours occurring in different parts of the water column at the same time and we extend the work of section 3.3.4 by considering how the addition of a virus or predator to a heterogeneous phytoplankton community in turbulent fluid may act as a control mechanism.

4.2 Methodology

4.2.1 Model

We will now consider the population model of Chapter 3 in the presence of turbulence, by including a diffusion term in each population equation and allowing some key parameters to vary spatially:

$$\frac{\partial P}{\partial t} = rP\left(1-\frac{P}{K}\right) - \mathrm{c_v}\sigma_1\sigma_2 PV - \frac{I_{\max}PZ}{K_{\mathrm{IR}}+P} + \frac{\partial}{\partial z}\left(\kappa_z\frac{\partial P}{\partial z}\right); \tag{4.1}$$

$$\frac{\partial V}{\partial t} = \lambda \mathrm{c_v}\sigma_1 PV - \gamma V + \frac{\partial}{\partial z}\left(\kappa_z\frac{\partial V}{\partial z}\right); \tag{4.2}$$

$$\frac{\partial Z}{\partial t} = \frac{\mu_{\max}(P-p')}{K_{\mathrm{GR}}+P-p'}Z - \nu Z + \frac{\partial}{\partial z}\left(\kappa_z\frac{\partial Z}{\partial z}\right). \tag{4.3}$$

Recall that r represents phytoplankton growth, K is the carrying capacity of the phytoplankton, $\mathrm{c_v}$ is the phytoplankton-virus volume clearance rate, the quantities σ_1 and σ_2 represent the fraction of contacts resulting in adsorption and the fraction of those adsorbed that are infectious respectively and γ is the virion decay rate. The quantity λ is equal to $m\sigma_2 - 1$. The predation terms consist of $I_{\max}$, the predator ingestion rate, K_{IR} and K_{GR} the half saturation constants, $\mu_{\max}$ the maximum phytoplankton growth rate (from consumption of prey), p' the threshold prey concentration needed for the predator to sustain itself and ν is the predator death rate. Turbulence is modelled via the diffusion term, where κ_z represents eddy diffusivity. The spatial component, z, represents vertical movement. All parameters with a constant value throughout the chapter are summarised in Table 4.1. Both uniform and non-uniform values of the eddy diffusivity, κ_z, are considered. Values are based upon energy dissipation rate data presented in Sharples et al. (2001), which also determines the values of $\mathrm{c_v}$, K_{IR} and K_{GR}. Spatial variance of the phytoplankton growth rate, r, and phytoplankton carrying capacity, K, aren't considered here, but would make a useful future addition.

To aid numerical analysis, it is convenient to non-dimensionalise model (4.1, 4.2, 4.3). We non-dimensionalise on the equilibria, choosing to non-dimensionalise the phytoplankton population on P_2^*, thus set:

$$P = P_2^* \tilde{P},\ V = V^* \tilde{V},\ Z = Z^* \tilde{Z},\ t = \frac{\tilde{t}}{r},\ z = H\tilde{z},\ \kappa_z = rH^2\tilde{\kappa_z},\ \gamma = r\tilde{\gamma},\ \nu = r\tilde{\nu},$$

$$K = P_2^* \tilde{K},\ K_{\text{IR}} = P_2^* \tilde{K_{\text{IR}}},\ K_{\text{GR}} = P_2^* \tilde{K_{\text{GR}}},\ p' = P_2^* \tilde{p'}, \tag{4.4}$$

where tilde denotes a dimensionless quantity, H is the height of the water column and P_2^*, V^*, Z^* represent the equilibrium concentrations derived in Chapter 3:

$$P_2^* = \frac{\gamma}{c_v \sigma_1 \lambda}, \tag{4.5}$$

$$V^* = \frac{r}{c_v \sigma_1 \sigma_2}\left(1 - \frac{P_2^*}{K}\right), \tag{4.6}$$

$$Z^* = \frac{r}{I_{\max}}(K_{\text{IR}} + P_3^*)\left(1 - \frac{P_3^*}{K}\right), \tag{4.7}$$

where $P_3^* = \frac{\nu K_{\text{GR}}}{\mu_{\max} - \nu} + p'$. The model (4.1, 4.2, 4.3) therefore reduces to, dropping the tilde:

$$\frac{\partial P}{\partial t} = P\left(1 - \frac{P}{K}\right) - \alpha PV - \frac{\beta}{K_{\text{IR}} + P} PZ + \frac{\partial}{\partial z}\left(\kappa_z \frac{\partial P}{\partial z}\right); \tag{4.8}$$

$$\frac{\partial V}{\partial t} = \gamma V(P - 1) + \frac{\partial}{\partial z}\left(\kappa_z \frac{\partial V}{\partial z}\right); \tag{4.9}$$

$$\frac{\partial Z}{\partial t} = \frac{\mu_{\max}(P - p')}{r(K_{\text{GR}} + P - p')} Z - \nu Z + \frac{\partial}{\partial z}\left(\kappa_z \frac{\partial Z}{\partial z}\right); \tag{4.10}$$

where

$$\alpha = 1 - \frac{P_2^*}{K} = 1 - \frac{\gamma}{K c_v \sigma_1 \lambda}, \tag{4.11}$$

$$\beta = \frac{(P_2^* K_{\text{IR}} + P_3^*)}{P_2^*}\left(1 - \frac{P_3^*}{K}\right). \tag{4.12}$$

To complete the model we must define boundary and initial conditions. We impose no flux boundary conditions since, in real terms, it does not make sense for it to be possible for phytoplankton, virions, or predators to be transported through the upper and lower boundaries, i.e. the surface and bottom of the water column. Thus, setting $\mathbf{C} = (P, V, Z)$, the boundary equations for this non-dimensional system are:

$$\kappa_z \frac{\partial \mathbf{C}}{\partial z} = 0 \text{ at } z = 0,\ 1. \tag{4.13}$$

4.2.2 Numerical methods and parameters

The Matlab PDE solver pdepe has been used to solve model (4.8, 4.9, 4.10) for differing values of eddy diffusivity, κ_z. This solver discretises in space, using the method of

Skeel and Berzins (1990), leaving a set of time-dependent ODEs that are solved using Matlab's ode15s solver. Where possible, the solution has been compared to the solution of the ODEs which make up the reaction part of the model. The ODE solutions were computed using Matlab's ode45. We also solved model (4.8, 4.9, 4.10) using a modified version of Matlab's pdepe solver, which utilises ode45 rather than ode15s. When compared to the ode45 solution of the reaction part of the model, the modified PDE solver had a smaller percentage error than the original pdepe, as expected. However, for larger eddy diffusivity values and higher spatial resolution, the modified solver was extremely slow. Also, Figures 4.7, 4.8, demonstrate that pdepe captures the dynamics of the solution well when compared to ode45, even though the percentage error calculations are sometimes a little high. Therefore, Matlab's pdepe solver is used throughout the chapter, even though Matlab documentation describes the ode15s solver used within pdepe as being less accurate than ode45.

Parameter Estimation

Parameter values are those summarised in Table 4.1. For zero turbulence and phytoplankton swimming, $c_v = 1.74 \times 10^{-11}$ m^3 per day (3sf) and $K_{IR} = 7.35 \times 10^9$ cells per m^3 (3sf) are calculated as shown in Chapter 2 (with $c_z = \frac{I_{max}}{K_{IR}}$). For the large value of eddy diffusivity used later, $c_v = 1.84 \times 10^{-11}$ m^3 per day (3sf) and $K_{IR} = 7.35 \times 10^9$ cells per m^3 (3sf).

Data collected by Sharples et al. (2001), which includes turbulent energy dissipation rates, ϵ, and water density, ρ, at 22 different depths over a 25 hour time period in a well-stratified shelf region of the Western English Channel, has been provided by Prof. J. Sharples. As discussed in section 1.4.2, turbulence will be modelled using an eddy diffusivity parameter. We thus need to relate this eddy diffusivity to the data we have.

The energy equation for the mean flow can be written (Tennekes and Lumley, 1972):

$$U_j \frac{\partial}{\partial x_j}\left(\frac{1}{2}U_i U_i\right) = \frac{\partial}{\partial x_j}\left(-\frac{P}{\rho}U_j + 2\nu U_i S_{ij} - \overline{u_i u_j} U_i\right) - 2\nu S_{ij} S_{ij} + \overline{u_i u_j} S_{ij}, \quad (4.14)$$

where U is the mean flow and u is the fluctuating flow, P is the mean pressure, ν the kinematic viscosity, ρ the density and S the mean strain rate. The mean kinetic energy of the turbulent velocity fluctuations can be written (Tennekes and Lumley, 1972):

$$U_j \frac{\partial}{\partial x_j}\left(\frac{1}{2}\overline{u_i u_i}\right) = -\frac{\partial}{\partial x_j}\left(\frac{1}{\rho}\overline{u_j p} + \frac{1}{2}\overline{u_i u_i u_j} - 2\nu \overline{u_i s_{ij}}\right) - \overline{u_i u_j} S_{ij} - 2\nu \overline{s_{ij} s_{ij}}, \quad (4.15)$$

where p is the fluctuating pressure and s the fluctuating strain rate. The only term to appear in both energy equations is equal to the Reynolds stress multiplied by the mean strain:

$$\overline{u_i u_j} S_{ij}, \tag{4.16}$$

although the quantity has opposite sign in the two energy equations. Therefore, (4.16) exchanges kinetic energy between the mean flow and turbulence. From here we look to determine the dominant terms of equation (4.15) for the type of flow considered. In a steady, homogeneous, pure shear flow (in which all averaged quantities, except for the mean flow, are independent of position and the mean strain rate is a constant) equation (4.15) is reduced to (Tennekes and Lumley, 1972):

$$-\overline{u_i u_j} S_{ij} = 2\nu \overline{s_{ij} s_{ij}} = \epsilon, \tag{4.17}$$

i.e. production of turbulent energy by Reynolds stresses ($\overline{u_i u_j} S_{ij}$) equals the rate of viscous dissipation ($\epsilon = 2\nu \overline{s_{ij} s_{ij}}$). Making analogy to work in section 1.4.3 we make the relation:

$$-\overline{u_i u_j} \equiv \kappa_z \frac{\partial u_i}{\partial x_j}. \tag{4.18}$$

Thus, in a steady, homogeneous, pure shear flow, we assume eddy diffusivity to be proportional to the dissipation rate, ϵ. We will follow Sharples et al. (2001) to use the relationship proposed by Osborn (1980) for stratified oceanic systems:

$$\kappa_z = \frac{\mathrm{Rf}}{(1 - \mathrm{Rf})\, N^2} \epsilon, \tag{4.19}$$

where the flux Richardson number, Rf, is the ratio of buoyancy flux to turbulent production (Osborn, 1980), the Brunt-Vaisala frequency, N, is the frequency of gravity waves in a stable atmosphere (Tennekes and Lumley, 1972), in other words a measure of how stratified the system is, and ϵ is the dissipation rate. We also follow Osborn (1980) in taking the critical value of the flux Richardson number (the maximum value for which turbulence can be maintained in steady state) to be $\mathrm{Rf} \sim 0.15$. Therefore, if we take $\mathrm{Rf} = 0.15$, we can calculate the maximum eddy diffusivity (rounding the constant of proportionality to 1dp) using:

$$\kappa_z = 0.2 \frac{\epsilon}{N^2}. \tag{4.20}$$

Figure 4.1(a) shows the data points recorded for the energy dissipation rate, ϵ, at depths up to 100m below the surface, at one time point. These data points are represented by $\circ$ in the figure. We have interpolated the data using the Matlab functions interp1 and pchip, which performs piecewise cubic Hermite interpolation - a method of interpolating data points as a polynomial (Yang et al., 2005). The interpolation is shown by the curve in Figure 4.1(a). Figure 4 of Sharples et al. (2001) show the energy dissipation rate data at three time points with error bars marking the 95% confidence limits. The size of some of these error bars suggests we perhaps should have used a

more smoothing interpolation. This data will be used, via equation (4.20), to calculate the eddy diffusivity. We also require the Brunt-Vaisala frequency in order to make this calculation. The squared Brunt-Vaisala frequency, N^2, can be calculated using (Prinsenberg and Rattray, 1975):

$$N^2 \equiv -\frac{g}{\rho}\frac{d\rho}{dz}, \tag{4.21}$$

where g is the acceleration due to gravity, taken as 9.81ms^{-2}, ρ is the water density and z is depth. Figure 4.1(b) shows the data points, denoted by $\circ$, calculated for N^2 at each depth (that the density was measured at) and again the curve represents the interpolated values, found using Matlab's interp1 and pchip functions. The data of Figure 4.1 is used in equation (4.20) to calculate the eddy diffusivity as a function of depth, shown in Figure 4.2. It was shown in Chapter 2 how both the phytoplankton-virus and phytoplankton-predator volume clearance rates for non-motile phytoplankton in turbulent fluid depend on the energy dissipation rate, ϵ. Figure 4.3 shows the phytoplankton-virus (Figure (a)) and phytoplankton-predator (Figure (b)) volume clearance rates varying with depth, determined from the energy dissipation rates of Figure 4.1(a).

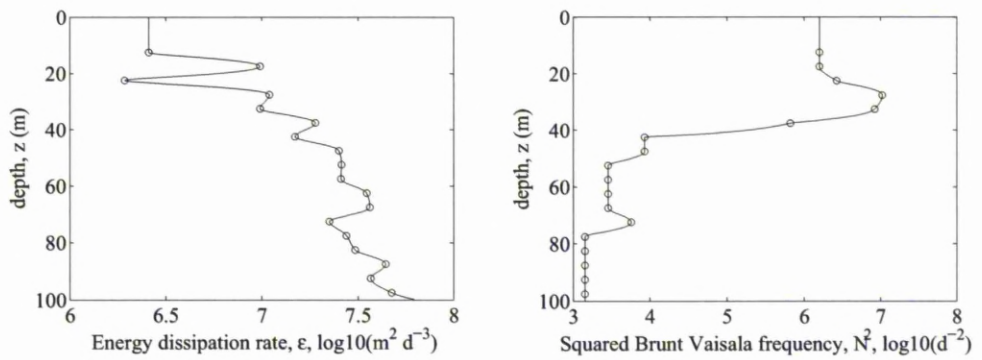

(a) (b)

Figure 4.1: Plot (a) shows the data points ($\circ$) and interpolated curve for the energy dissipation rate, ϵ, for the first 100m from the surface. Plot (b) shows the data points ($\circ$) and interpolated curve for the squared Brunt-Vaisala frequency, N^2, calculated using the water density at each depth, at the same time point as the ϵ data was recorded.

We will also use a second eddy diffusivity profile, where there is a more pronounced region of low turbulence, to compare the dynamics. The second profile is plotted from the same data set as the first, but represents a different time point. Figure 4.4 shows the energy dissipation rate, ϵ (Figure (a)), and squared Brunt Vaisala frequency, N^2 (Figure (b)), at this time point. Figure 4.5 then shows the corresponding eddy

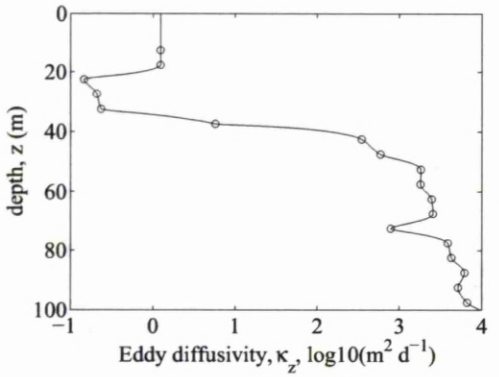

Figure 4.2: This is the first eddy diffusivity profile being considered, which is calculated from data provided by Prof. J. Sharples and forms part of a data set used in Sharples et al. (2001). The ○ represents a data point, while the curve shows the interpolated values.

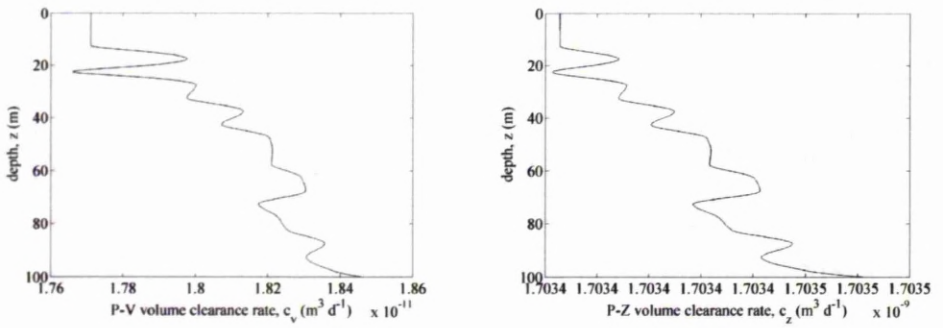

(a) (b)

Figure 4.3: Profiles of the $P - V$ and $P - Z$ volume clearance rates associated with the eddy diffusivity profile of Figure 4.2.

diffusivity profile. This log plot shoes a more clearly defined low eddy diffusivity region than the first, which exists between depths of approximately 20-50m. Figure 4.6 shows the phytoplankton-virus (Figure (a)) and phytoplankton-predator (Figure (b)) volume clearance rates, found using the energy dissipation rates of Figure 4.4(a). The presence of the low diffusivity region is apparent in these profiles also. Figure 2b of Sharples et al. (2001) shows there to be a peak in chlorophyll in the region of lowest diffusivity. Figure 4.6 demonstrates that the $P - V$ and $P - Z$ volume clearance rates are at a minimum when eddy diffusivity is at a minimum, supporting the increased phytoplankton concentrations seen in this region. We will thus test in this chapter the hypothesis of this chlorophyll maximum being due to turbulence modifying inter-species interactions.

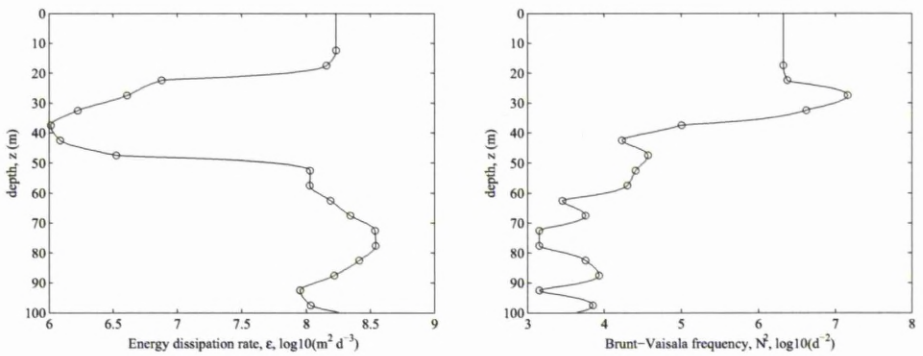

(a) (b)

Figure 4.4: Plot (a) shows the second set of data points (○) and interpolated curve for the energy dissipation rate, ϵ, for the first 100m from the surface. Plot (b) shows the second set of data points (○) and interpolated curve for the squared Brunt-Vaisala frequency, N^2, calculated using the water density at each depth, at the same time point as the ϵ data was recorded.

4.3 Results

Here we consider how the introduction of spatial heterogeneity affects the population dynamics. This heterogeneity is introduced via a spatially variant eddy diffusivity and initial phytoplankton distribution. On consideration of the stability criteria found for the ODEs in Chapter 3, we may expect that variance of c_v, K_{IR} and K_{GR}, which change with κ_z, to enable the possibility of different long term behaviours present in different regions of the water column. However, this behaviour isn't seen here. The values of c_v, K_{IR} and K_{GR} don't vary greatly over the range of eddy diffusivity values used, creating the need to lie near a boundary between different regimes in the $\gamma - \nu$

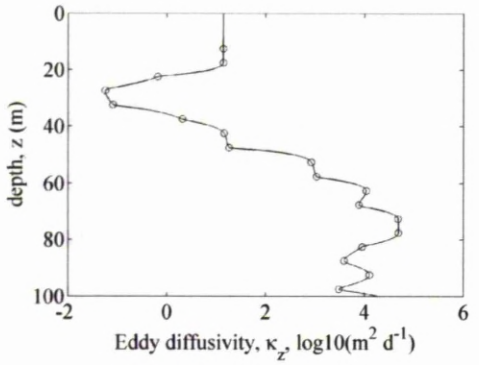

Figure 4.5: This is the second eddy diffusivity profile being considered, which is also calculated from data provided by Prof. J. Sharples. This forms part of a data set used in Sharples et al. (2001).

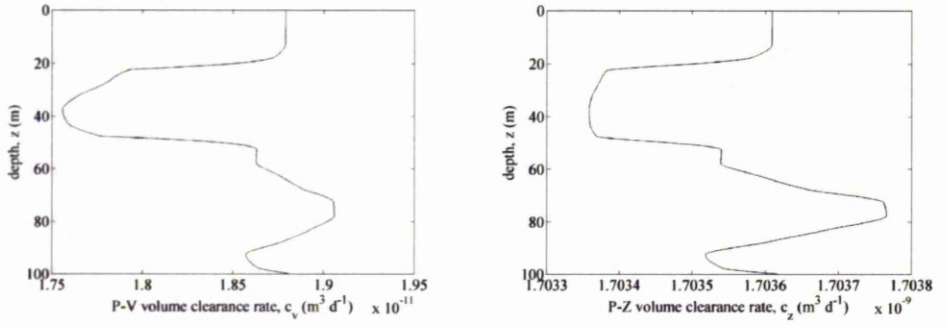

(a) (b)

Figure 4.6: Profiles of the $P - V$ and $P - Z$ volume clearance rates associated with the eddy diffusivity profile of Figure 4.5.

Symbol	Value	Source
r	2 d^{-1}	Estimated from Jeong et al. (2003)
K	5×10^{10} cells m^{-3}	Estimated from Jeong et al. (2003)
σ_1	10^{-1}	Bratbak et al. (1998)
σ_2	10^{-2}	Tarutani et al. (2006)
m	770 viruses $cell^{-1}$	Nagasaki et al. (1999)
$\lambda = m\sigma_2 - 1$	6.7 viruses $cell^{-1}$	Calculated from above
I_{max}	12.5 cells $grazer^{-1}$ d^{-1}	Jeong et al. (2003)
μ_{max}	1.43 d^{-1}	Jeong et al. (2003)
p'	8×10^7 cells m^{-3}	Jeong et al. (2003)

Table 4.1: Parameter values assumed constant and used in the spatial phytoplankton-virus-predator model throughout this chapter.

stability plot, Figure 3.3, to see this behaviour.

We conduct our study by considering four different long-term behaviours of model (4.8, 4.9, 4.10) separately: $(P_2^*, V^*, 0)$ stable, $(P_3^*, 0, Z^*)$ stable, $(P, 0, Z)$ stable limit cycle and (P, V, Z) coexistence. We will change from one type of long-term behaviour to another by changing the virus decay rate, γ, and predator death rate, ν, only. For each type of long-term behaviour, we investigate the effects of introducing turbulence (both uniform and heterogeneous in one dimension) and of introducing spatially heterogeneous (in 1D) initial phytoplankton populations. This is done by first validating Matlab's pdepe solver against its ode45 solver for zero eddy diffusivity and uniform initial conditions. We then do a second validation of the solver for uniform initial conditions and a large eddy diffusivity value. Two profiles of eddy diffusivity varying with depth are considered. The profiles are created from field data supplied by Prof. J. Sharples. They are shown in Figures 4.2 and 4.5. The profiles are first investigated for initially uniformly distributed phytoplankton, virus and predator populations. A non-uniform initial phytoplankton distribution, with constant eddy diffusivity followed by spatially variant eddy diffusivity, is then considered. The section closes with an investigation of phytoplankton control by the addition of virus or grazers, continuing the work of section 3.3.4.

4.3.1 $(P_2^*, V^*, 0)$ Stable

Here we consider the effects of spatial heterogeneity on the phytoplankton-virus- predator population dynamics in the parameter region where the long-term behaviour tends to a $(P_2^*, V^*, 0)$ stable equilibrium, which occurs at $(P, V, Z) = (1, 1, 0)$ for the non-dimensional model. We force this long-term behaviour by setting $(\gamma, \nu) = (0.08, 1.3)d^{-1}$. These values of γ and ν are used throughout this section.

4.3.1.1 Zero eddy diffusivity, uniform initial conditions

The uniform initial conditions used here are $(P_0, V_0, Z_0) = (9000 \times 10^6, 10 \times 10^6, 2000 \times 10^6)\text{m}^{-3}$, which is consistent with those used in Chapter 3. Non-dimensionalising P_0, V_0 and Z_0 on the equilibria P_2^*, V^*, Z^* respectively gives the initial conditions to be $(P_0, V_0, Z_0) = (1.365, 1.043 \times 10^{-7}, 0.8876)$ in non-dimensional values, to four significant figures. In section 2.3.1, we found the phytoplankton-virus volume clearance rate for non-motile phytoplankton in still fluid to be $c_v = 1.74 \times 10^{-11}\text{m}^3\ \text{d}^{-1}$ (3sf). This value of c_v will therefore be used in this section. The phytoplankton-predator volume clearance rate was calculated in section 2.4.2 to be $1.70 \times 10^{-9}\text{m}^3\ \text{d}^{-1}$ (3sf) in the absence of turbulence and phytoplankton swimming. As defined in section 3.3.6, the phytoplankton-predator volume clearance rate is taken to be:

$$c_z = \frac{I_{\max}}{K_{\text{IR}}}. \tag{4.22}$$

Since we keep $I_{\max}$ fixed at a value of 12.5 grazer^{-1}d^{-1} (as estimated by Jeong et al. (2003)), when $c_z = 1.70 \times 10^{-9}\text{m}^3\ \text{d}^{-1}$, $K_{\text{IR}} = 7.35 \times 10^9$ cells per m^3 (3sf). As we have chosen to change K_{GR} by the same proportion as K_{IR}, we use $K_{\text{GR}} = 1.09 \times 10^9$ cells per m^3 (3sf).

Figure 4.7 plots the solution of model (4.8, 4.9, 4.10) using these parameter values, and those in Table 4.1, to show the dynamics when there isn't any eddy diffusivity and initial conditions are uniform. This is therefore equivalent to the solution of the ODEs (3.1, 3.2, 3.3). There are three plots in Figure 4.7 representing the pdepe solution for two different spatial resolutions (red line = resolution 0.01, black line = resolution 0.1) and the ode45 solution (blue line) of the reaction terms in model (4.8, 4.9, 4.10), i.e. the model without the diffusive terms. The three solutions for the P, V and Z populations are indistinguishable in the figure. The largest percentage error between the pdepe solution and ode45 solution, over the first 150 days, occurs in the phytoplankton population and has a value of 7.55%, however, this doesn't appear to affect the transient or long-term dynamics. We were also able to determine that a spatial resolution of 0.1 is adequate, since the solutions for spatial resolutions of 0.1 and 0.01 were indistinguishable in Figure 4.7 and the largest percentage error had a value of 7.5×10^{-8}%, occurring in the predator population.

4.3.1.2 Large eddy diffusivity, uniform initial conditions

Continuing to use the non-dimensional, uniform, initial conditions $(P_0, V_0, Z_0) = (1.365, 1.043 \times 10^{-7}, 0.8876)$, we now solve model (4.8, 4.9, 4.10) for a large value of eddy diffusivity, κ_z, and compare the results found using Matlab's pdepe solver to those found using its ode45 solver. Since the initial conditions are uniform, the turbulent diffusion terms of model (4.8, 4.9, 4.10), which act to evenly distribute the populations over

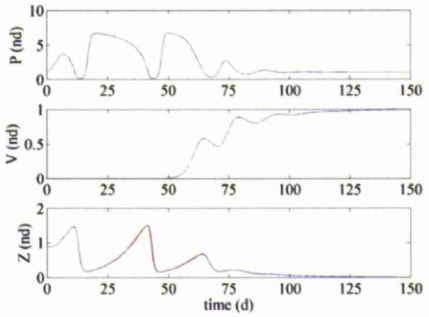

Figure 4.7: Validation of Matlab's pdepe solver against its ode45 solver for $(P_2^*, V^*, 0)$ stable long-term behaviour of model (4.8, 4.9, 4.10) with zero eddy diffusivity and uniform initial conditions of $(P_0, V_0, Z_0) = (1.365, 1.043 \times 10^{-7}, 0.8876)$, in non-dimensional values. Parameter values are as in Table 4.1, with $c_v = 1.74 \times 10^{-11}\text{m}^3$ d^{-1}, $K_{IR} = 7.35 \times 10^9\text{m}^{-3}$, $K_{GR} = 1.09 \times 10^9\text{m}^{-3}$, $\gamma = 0.08\text{d}^{-1}$ and $\nu = 1.3\text{d}^{-1}$. The solution is plotted using pdepe with resolutions 0.1 and 0.01, and using ode45. The three solutions are consistent, thus only one curve is clearly visible in the plots.

depth, won't affect the population dynamics. Thus we can, again, directly compare the solution of these PDEs to that of the ODEs (3.1, 3.2, 3.3). We do, however, expect the solution to differ from that for zero eddy diffusivity, Figure 4.7, since the values of the phytoplankton-virus and phytoplankton-predator volume clearance rates will change.

The value of eddy diffusivity used here is the maximum value seen in the first profile of eddy diffusivity varying with depth, shown in Figure 4.2. This maximal value of eddy diffusivity is $\kappa_z = 9.690 \times 10^3\text{m}^2\text{d}^{-1}$ (4sf), which is equal to 0.485 (3sf) in non-dimensional values. Considering dimensions of the diffusion equation, the species concentrations should spread over 100m with time $T = \dfrac{H^2}{\kappa_z} = \dfrac{100^2}{9.690 \times 10^3} = 1.03$ days (3sf). The eddy diffusivity values are calculated using data for the energy dissipation rate, ϵ. The value of ϵ corresponding to $\kappa_z = 9.690 \times 10^3\text{m}^2\text{d}^{-1}$ is $\epsilon = 6.250 \times 10^7\text{m}^2\ \text{d}^{-3}$ (4sf). This value of the energy dissipation rate is used to calculate the phytoplankton-virus volume clearance rate of non-motile *H. akashiwo* and HaV in a turbulent regime to be $c_v = 1.84 \times 10^{-11}\text{m}^3\ \text{d}^{-1}$ (3sf) and the *H. akashiwo*-*O. marina* volume clearance rate, in the same fluid regime with *O. marina* swimming at $339 \times 10^{-6}\text{ms}^{-1}$, to be $c_z = 1.70 \times 10^{-9}\text{m}^3\text{d}^{-1}$, which is the same as that for zero eddy diffusivity to three significant figures.

Remembering $I_{max} = 12.5$ grazer$^{-1}\text{d}^{-1}$, $K_{IR} = 7.35 \times 10^9$ cells per m^3 using equation (4.22) and $K_{GR} = 1.09 \times 10^9$ cells per m^3. Thus, Figure 4.8 shows the solution of model (4.8, 4.9, 4.10) for a large value of eddy diffusivity and uniform initial conditions. The

solution was found using the parameter values shown here and those in Table 4.1.

Again, Figure 4.8 shows two pdepe solutions: that for a resolution of 0.1 (black line) and also a resolution of 0.01 (red line). The largest percentage error, for the 150 days computed, between the two solutions is $6.33\times10^{-6}\%$, occurring in the phytoplankton population. No difference can be seen between the two plots in Figure 4.8. A third solution is plotted in Figure 4.8, that found using ode45 (blue line). The figure shows that, despite the largest percentage error between the pdepe solution (for a resolution of 0.01) and the ode45 solution being calculated to be 5.28% in the phytoplankton population, the less accurate ODE solver, ode15s, used in pdepe gives a solution in good agreement with ode45.

Comparison of Figure 4.7 with Figure 4.8 shows little discernible difference between zero eddy diffusivity and a large eddy diffusivity, with value $\kappa_z = 9.690\times10^3\text{m}^2\ \text{d}^{-1}$, for these parameter values and uniform initial conditions. The *H. akashiwo*-HaV volume clearance rate has increased from $c_v = 1.74 \times 10^{-11}\text{m}^3\ \text{d}^{-1}$ to $c_v = 1.84 \times 10^{-11}\text{m}^3\ \text{d}^{-1}$, whilst the *H. akashiwo*-*O. marina* volume clearance rate remains unchanged (to 3sf), when a large eddy diffusivity value is introduced. Even the increase in c_v is small and so the changes in population dynamics that were found in Figure 3.14, section 3.3.6, when considering the introduction of phytoplankton swimming aren't seen here for the introduction of turbulence.

We have also validated Matlab's pdepe solver against its ode45 solver for each of the other long term behaviours, finding pdepe to compare well to ode45. The full details are given in Appendix B.

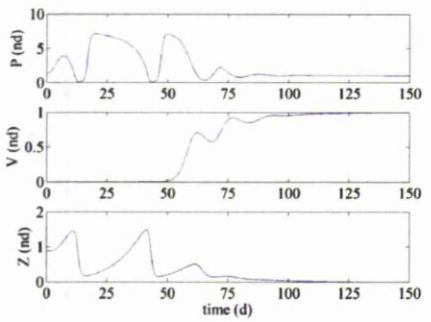

Figure 4.8: Validation of Matlab's pdepe solver against its ode45 solver for $(P_2^*, V^*, 0)$ stable long-term behaviour of model (4.8, 4.9, 4.10) with a large eddy diffusivity value of $\kappa_z = 9.690 \times 10^3\text{m}^2\ \text{d}^{-1}$ and uniform, non-dimensional, initial conditions of $(P_0, V_0, Z_0) = (1.365, 1.043 \times 10^{-7}, 0.8876)$. Parameter values: $c_v = 1.84 \times 10^{-11}\text{m}^3\ \text{d}^{-1}$, $K_{\text{IR}} = 7.35 \times 10^9\text{m}^{-3}$, $K_{\text{GR}} = 1.09 \times 10^9\text{m}^{-3}$, $\gamma = 0.08\text{d}^{-1}$ and $\nu = 1.3\text{d}^{-1}$. The solution is plotted using pdepe with resolutions 0.1 and 0.01, and using ode45. The three solutions are consistent, thus only one curve is clearly visible in the plots.

4.3.1.3 Variable eddy diffusivity, uniform initial conditions

We now incorporate eddy diffusivity varying with depth. We use two different eddy diffusivity profiles. The first being that of Figure 4.2 and the second, which has a more pronounced region of low eddy diffusivity, is shown in Figure 4.5.

Figure 4.9 shows the solution of model (4.8, 4.9, 4.10) for the first eddy diffusivity profile with the uniform non-dimensional initial conditions $(P_0, V_0, Z_0) = (1.365, 1.043 \times 10^{-7}, 0.8876)$. The phytoplankton-virus and phytoplankton-predator volume clearance rates now vary with depth, as shown in Figure 4.3. Parameters are defined in Table 4.1 with $K_{\mathrm{GR}} = 1.09 \times 10^9$ cells per m^3, $\gamma = 0.08\mathrm{d}^{-1}$ and $\nu = 1.3\mathrm{d}^{-1}$. Four separate plots are shown in Figure 4.9: space-time plots of phytoplankton, virus and predator, and time series solution for the three species. Due to using uniform initial conditions we may expect the solution to be uniform over all depths. However, since variable eddy diffusivity means variable energy dissipation rate and thus volume clearance rates (particularly $\mathrm{c_v}$), the ODE solution for each eddy diffusivity value will be slightly different, hence the slight heterogeneity present in the PDE solution. To confirm this hypothesis, Figure 4.10 shows the same simulation except the contact rates are kept at the constant minimum values of $\mathrm{c_v} = 1.79 \times 10^{-11}\mathrm{m}^3\mathrm{d}^{-1}$ and $K_{\mathrm{IR}} = 7.35 \times 10^9\mathrm{m}^{-3}$. The absence of heterogeneity in this Figure shows that the heterogeneity in Figure 4.9 is due to a spatially variant $P - V$ volume clearance rate, even though the change in $\mathrm{c_v}$ isn't particularly large.

Figure 4.11 shows solution of the full model for the second eddy diffusivity profile (Figure 4.5). Comparing with the solution for the first eddy diffusivity profile, shown in Figure 4.9, there is little difference between the overall dynamics of these two solutions, but there is more heterogeneity in the solution for the second eddy diffusivity profile. This heterogeneity is particularly apparent in the region of depths between 25 and 35m, an effect of the more pronounced low diffusivity region of the second eddy diffusivity profile.

4.3.1.4 Constant eddy diffusivity, non-uniform initial conditions

We now consider the initial phytoplankton distribution to vary with depth, as shown in Figure 4.12. This is an arbitrary Gaussian function. The maximum phytoplankton concentration is set to 1.365 in non-dimensional values, which is the value of the initial phytoplankton concentration used in the previous sections where uniform initial conditions were considered (to 4sf). The equation determining this distribution is thus:

$$P_0 = 1.365 \exp\left(\frac{-(z - 0.4H)^2}{50}\right), \tag{4.23}$$

where H is the height of the water column. In order to gauge the effect of non-uniform initial conditions, Figure 4.13 shows the solution of the model for zero eddy

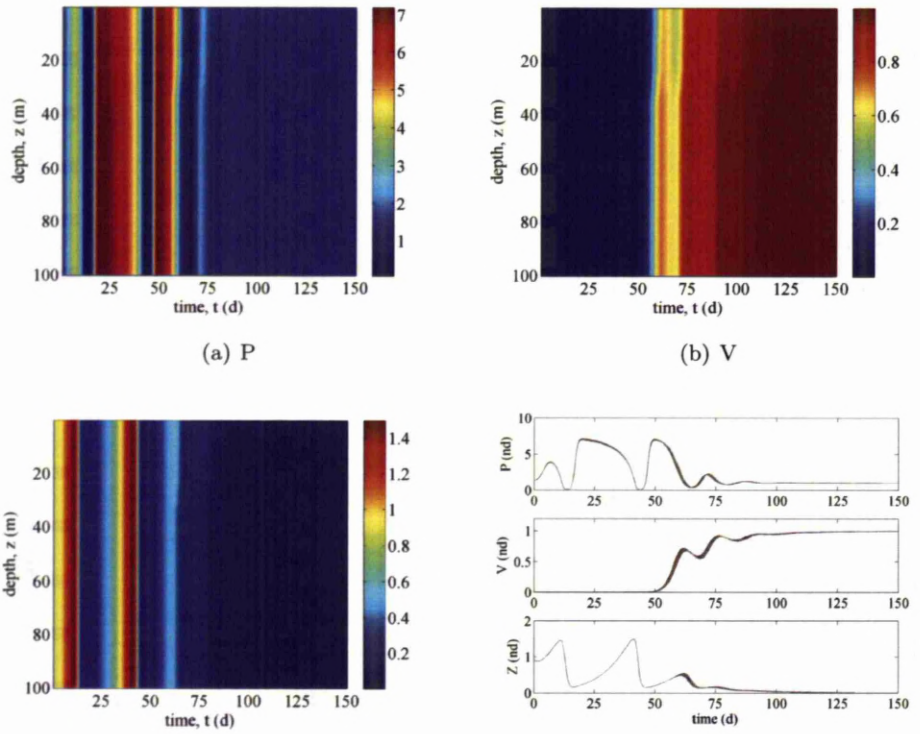

(a) P

(b) V

(c) Z

(d) Time series, all depths

Figure 4.9: Solution of model (4.8, 4.9, 4.10) for eddy diffusivity varying with the data set of Figure 4.2 and uniform initial conditions of $(P_0, V_0, Z_0) = (1.365, 1.043 \times 10^{-7}, 0.8876)$ in non-dimensional values, in the parameter region where the system tends to $(P_2^*, V^*, 0)$ stable in the long term. The $P - V$ and $P - Z$ volume clearance rate profiles are shown in Figure 4.3. Other parameters are as in Table 4.1 with $K_{\mathrm{GR}} = 1.09 \times 10^9 \mathrm{m}^{-3}$, $\gamma = 0.08\mathrm{d}^{-1}$ and $\nu = 1.3\mathrm{d}^{-1}$. Each figure shows the phytoplankton population, virus population, zooplankton population and the time series solution, over all depths, for each species, respectively.

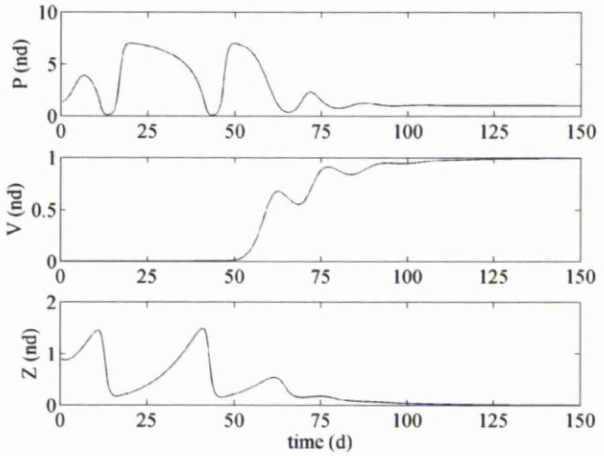

Figure 4.10: Solution of model (4.8, 4.9, 4.10) for eddy diffusivity varying with the data set of Figure 4.2 and uniform initial conditions of $(P_0, V_0, Z_0) = (1.365, 1.043 \times 10^{-7}, 0.8876)$ in non-dimensional values, in the parameter region where the system tends to $(P_2^*, V^*, 0)$ stable in the long term. The $P - V$ and $P - Z$ volume clearance rates are kept at the constant minimum values of $c_v = 1.79 \times 10^{-11} m^3 d^{-1}$ and $K_{IR} = 7.35 \times 10^9 m^{-3}$. Other parameters are as in Table 4.1 with $K_{GR} = 1.09 \times 10^9 m^{-3}$, $\gamma = 0.08 d^{-1}$ and $\nu = 1.3d{-}1$. The time series solution, for the full spatial resolution, of each population is shown.

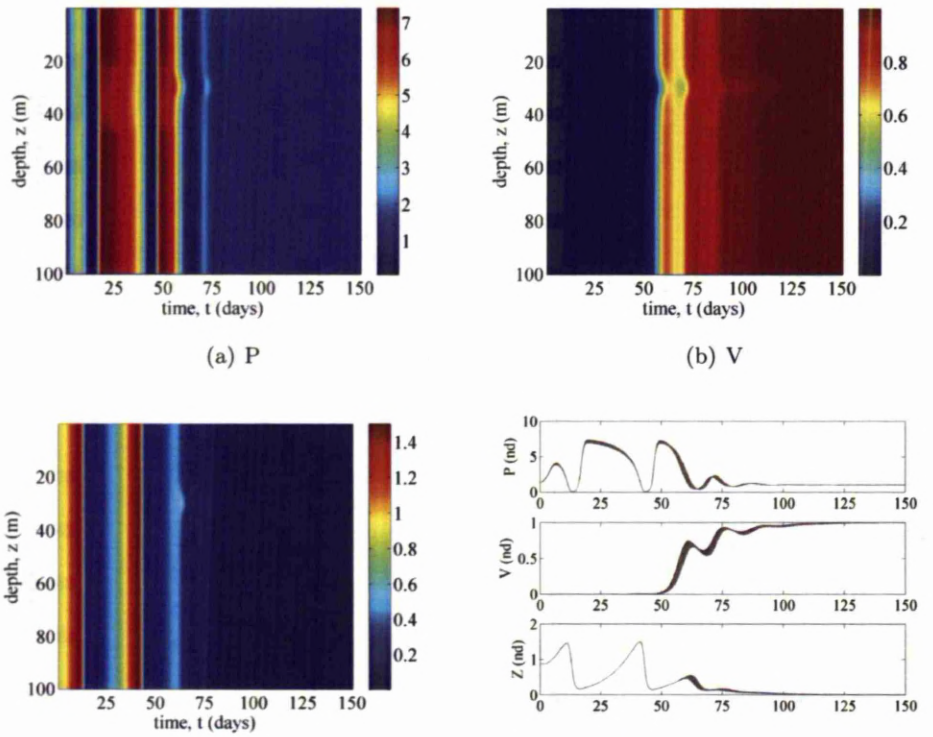

(a) P

(b) V

(c) Z

(d) Time series, all depths

Figure 4.11: Solution of model (4.8, 4.9, 4.10) in the parameter region where $(P_2^*, V^*, 0)$ is stable in the long term for eddy diffusivity varying with the data set of Figure 4.5 and uniform initial conditions of $(P_0, V_0, Z_0) = (1.365, 1.043 \times 10^{-7}, 0.8876)$ in non-dimensional values. Parameter values as in Table 4.1 with $K_{\mathrm{GR}} = 1.09 \times 10^9 \mathrm{m}^{-3}$, $\gamma = 0.08\mathrm{d}^{-1}$ and $\nu = 1.3\mathrm{d}^{-1}$. The $P - V$ and P_Z volume clearance rates as in Figure 4.6. Each figure shows the phytoplankton population, virus population, zooplankton population and the time series solution, for the full spatial resolution, of each population, respectively.

diffusivity. The initial phytoplankton distribution is that shown in Figure 4.12, whereas the initial virus and zooplankton populations remain at the uniform levels of $(V_0, Z_0) = (1.043 \times 10^{-7}, 0.8876)$, in non-dimensional values. Figures 4.13(a), 4.13(b), and 4.13(c) are space-time plots, showing the changes in population of the phytoplankton, virus and predator respectively. Figure 4.14 shows the time series solution of all three species, at three different depths: $z = 30$m, marked by a red line, 40m, marked by a blue line, and 80m, marked by a green line. There are two plots for each depth, per species: a full-line and a dashed line. The full-line marks the pdepe solution, whilst the dashed line shows the equivalent ode45 solution. For depths of 30m and 40m, there is a slight delay in the ode45 solution compared to pdepe, but pdepe does capture the overall dynamics well. The non-uniform initial conditions mean that each of these three depths has a different value for P_0, hence the different transient dynamics seen in the three time series solutions. This difference seen in the transient dynamics of the time series solution helps us to understand the patterning visible in the space-time plots of Figure 4.13. There are negative predator concentrations in the solution, most likely arising due to pdepe's handling of zero eddy diffusivity.

We have also computed the solution with these initial conditions, but eddy diffusivity taking the value of $9.690 \times 10^3 \mathrm{m}^2\mathrm{d}^{-1}$ as used in section 4.3.1.2. The parameter values are those in Table 4.1 with $c_v = 1.84 \times 10^{-11}\mathrm{m}^3\mathrm{d}^{-1}$, $K_{IR} = 7.35 \times 10^9\mathrm{m}^{-3}$, $K_{GR} = 1.09 \times 10^9\mathrm{m}^{-3}$, $\gamma = 0.08\mathrm{d}^{-1}$ and $\nu = 1.3\mathrm{d}^{-1}$. This solution is shown in Figure 4.15. This level of eddy diffusivity spreads the phytoplankton population evenly throughout the water column very quickly, thus not allowing any variance to emerge in the virus or zooplankton populations. Figure 4.15(b) highlights how quickly the phytoplankton population is made uniform. It takes approximately 1 day for the phytoplankton to be evenly distributed throughout the water column, as predicted by our calculation of the diffusion timescale, T, in the 'Large eddy diffusivity, uniform initial conditions' section. Although the transient dynamics of Figure 4.15 differ slightly to those in Figure 4.8, which shows the solution for uniform initial conditions and this large eddy diffusivity value, a non-uniform initial phytoplankton distribution makes little difference to the overall dynamics, when eddy diffusivity is large.

4.3.1.5 Variable eddy diffusivity, non-uniform initial conditions

Here we combine the non-uniform initial phytoplankton distribution of Figure 4.12 with the variable eddy diffusivities of Figures 4.2 and 4.5. The initial virus and predator populations remain constant with non-dimensional values $(V_0, Z_0) = (1.043 \times 10^{-7}, 0.8876)$. Figure 4.16 shows the solution of model (4.8, 4.9, 4.10) for the first eddy diffusivity profile (shown in Figure 4.2). The solution was also found for twice the resolution to confirm the resolution used is adequate. The phytoplankton-virus and phytoplankton-predator volume clearance rate profiles are those of Figure 4.3. Other parameters are as

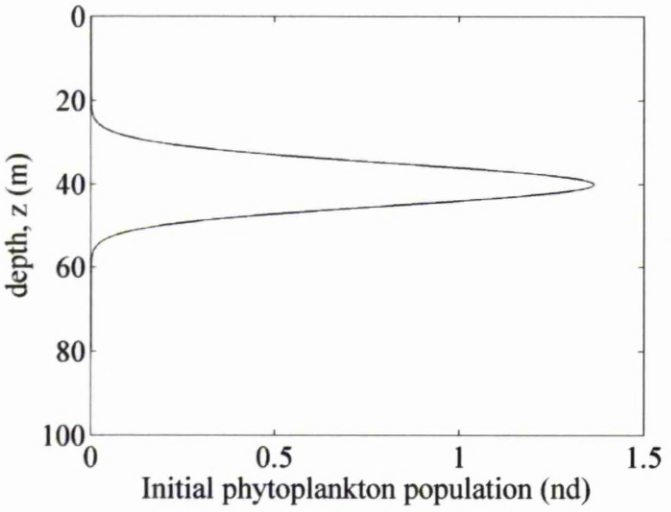

Figure 4.12: This is the initial phytoplankton distribution being considered, which is given in equation (4.23).

in Table 4.1, with $K_{\mathrm{GR}} = 1.09 \times 10^9 \mathrm{m}^{-3}$, $\gamma = 0.08\mathrm{d}^{-1}$ and $\nu = 1.3\mathrm{d}^{-1}$. Figures 4.18 and 4.19 depict the same solution, showing only the first few days since the initial behaviour is unclear in Figure 4.16. The long-term behaviour still tends to $(P, V, Z) = (1, 1, 0)$ stable, but the transient population dynamics now differ significantly to those seen previously. There is much more heterogeneity throughout the water column in each population. The predator population has very low levels in the top 25m of the water column, initially allowing the phytoplankton population to tend to carrying capacity level in this region. The largest concentration of the virus initially emerges in this region, quickly reducing the phytoplankton population. The virus population then spreads more evenly throughout the water column. Figure 4.17 shows the time series solution of the system at two depths. The red lines represent a depth of $z = 20$m and the blue lines a depth of $z = 40$m. The dashed-line shows the time series solution for $\mathrm{c_v}$ and $\mathrm{c_z}$ varying with κ_z, whilst the full-line shows the time series solution where $\mathrm{c_v}$ and $\mathrm{c_z}$ are kept at constant minimum values: $\mathrm{c_v} = 1.79 \times 10^{-11}\mathrm{m}^3$ per day and $K_{\mathrm{IR}} = 7.35 \times 10^9 \mathrm{m}^{-3}$. As there is very little difference between the dashed and full lines, we suggest the dynamics present are due to mixing rather than changes in the volume clearance rates.

During the time where the virus mainly populates the surface region, the phytoplankton population at lower depths seems to display oscillatory behaviour with the predator, but once the virus becomes evenly distributed, the phytoplankton population in the lower region is also quickly reduced. The predator population then becomes extinct.

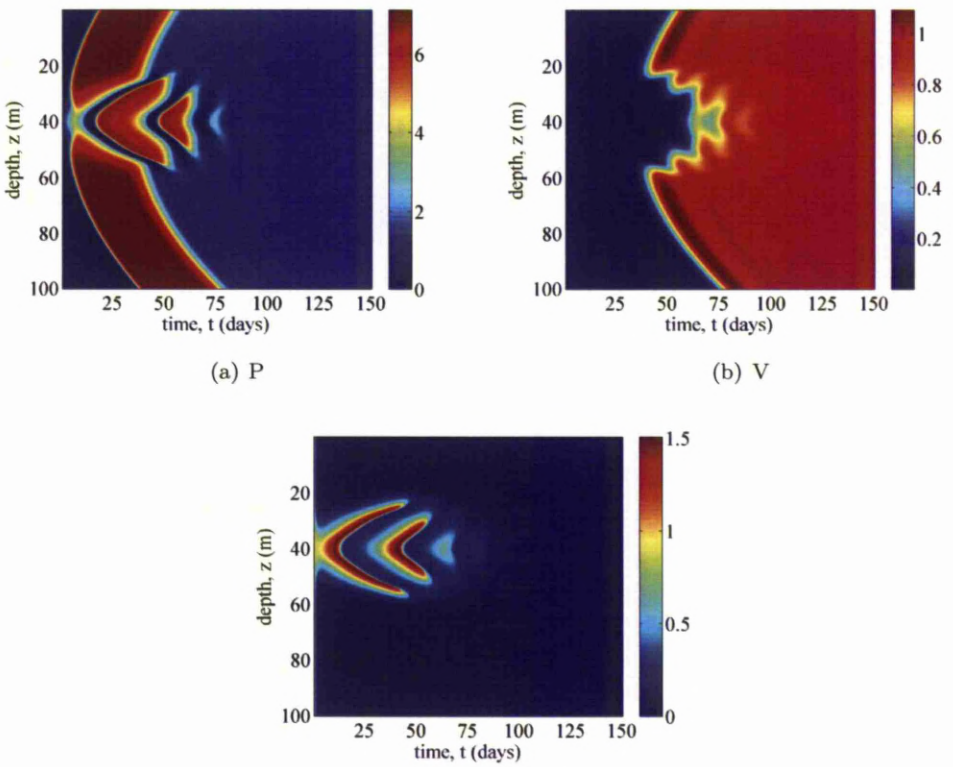

(a) P

(b) V

(c) Z

Figure 4.13: Solution of model (4.8, 4.9, 4.10) where $(P_2^*, V^*, 0)$ is stable in the long term for zero eddy diffusivity and initial conditions of $(V_0, Z_0) = (1.043 \times 10^{-7}, 0.8876)$, in non-dimensional values, and P_0 varying as shown in Figure 4.12. Other parameters are as in Table 4.1, $K_{\mathrm{GR}} = 1.09 \times 10^9 \mathrm{m}^{-3}$, $K_{\mathrm{IR}} = 7.35 \times 10^9 \mathrm{m}^{-3}$, $\mathrm{c_v} = 1.70 \times 10^{-11}$ $\mathrm{m}^3\mathrm{d}^{-1}$, $\gamma = 0.08\mathrm{d}^{-1}$ and $\nu = 1.3\mathrm{d}^{-1}$. Each figure shows the phytoplankton population, virus population and zooplankton population respectively.

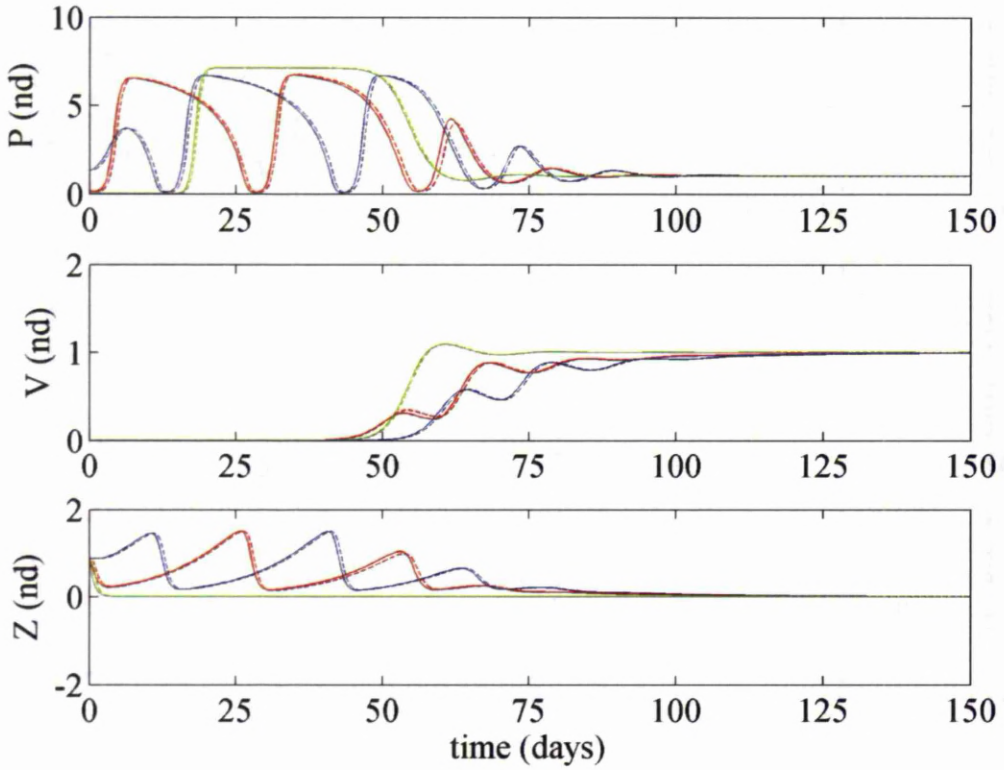

Figure 4.14: Solution of model (4.8, 4.9, 4.10) where $(P_2^*, V^*, 0)$ is stable in the long term for zero eddy diffusivity and initial conditions of $(V_0, Z_0) = (1.043 \times 10^{-7}, 0.8876)$, in non-dimensional values, and P_0 varying as shown in Figure 4.12. Other parameters are as in Table 4.1, $K_{\mathrm{GR}} = 1.09 \times 10^9 \mathrm{m}^{-3}$, $K_{\mathrm{IR}} = 7.35 \times 10^9 \mathrm{m}^{-3}$, $\mathrm{c_v} = 1.70 \times 10^{-11}$ $\mathrm{m}^3\mathrm{d}^{-1}$, $\gamma = 0.08\mathrm{d}^{-1}$ and $\nu = 1.3\mathrm{d}^{-1}$. The red lines represent $z = 30\mathrm{m}$, the blue line $z = 40\mathrm{m}$ and the green line $z = 80\mathrm{m}$. The full-line is the pdepe solution and the dashed line the equivalent ode45 solution.

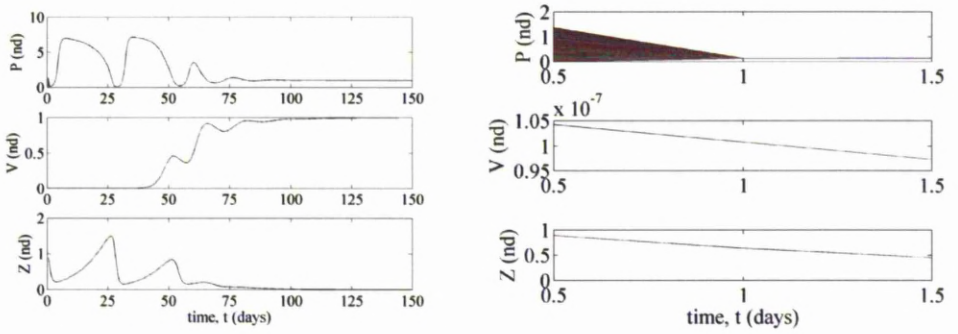

(a) (b)

Figure 4.15: Solution of model (4.8, 4.9, 4.10) in the parameter region where $(P_2^*, V^*, 0)$ stable in the long term for a large, uniform, eddy diffusivity and initial conditions of $(V_0, Z_0) = (1.043 \times 10^{-7}, 0.8876)$, in non-dimensional values, and P_0 varying as shown in Figure 4.12. Other parameters as in Table 4.1 with $c_v = 1.84 \times 10^{-11}$ $m^3 d^{-1}$, $K_{IR} = 7.35 \times 10^9 m^{-3}$, $K_{GR} = 1.09 \times 10^9 m^{-3}$ and $(\gamma, \nu) = (0.08, 1.3) d^{-1}$. Plot (a) shows the time series solution over 150 days, plot (b) showing just the first 1.5 days to highlight how quickly the phytoplankton population becomes uniform.

These dynamics can be compared with those in Figure 4.20, which solves the model using the second eddy diffusivity profile (that of Figure 4.5) Now, the phytoplankton-virus and phytoplankton-predator volume clearance rates are those in Figure 4.6. The other parameters continue to be those in Table 4.1 with $K_{GR} = 1.09 \times 10^9 m^{-3}$, $\gamma = 0.08 d^{-1}$ and $\nu = 1.3 d^{-1}$. Again, Figures 4.21 and 4.22 show the first few days. There is little difference in the population dynamics between the two eddy diffusivity profiles. Comparison of the dynamics over the first 5 days (Figures 4.18 and 4.21) shows variance between the two sets of dynamics more clearly. The predator population is larger in the low eddy diffusivity region for longer in Figure 4.21, where the eddy diffusivity follows profile 2. The virus concentration is larger over the first few days in Figure 4.18, where the first eddy diffusivity profile is considered.

4.3.2 $(P_3^*, 0, Z^*)$ Stable

We now investigate how turbulence and non-homogeneous initial conditions affect the population dynamics of a system tending to $(P_3^*, 0, Z^*)$ stable behaviour in the long-term. This long-term behaviour is achieved by setting $(\gamma, \nu) = (0.4, 1.38) d^{-1}$. The equilibrium, in non-dimensional values, occurs at $(P, V, Z) = (0.84, 0, 1)$, P being correct to 2sf for c_v corresponding to zero eddy diffusivity. The structure of this section will follow that of section 4.3.1. We consider how variable eddy diffusivity affects the

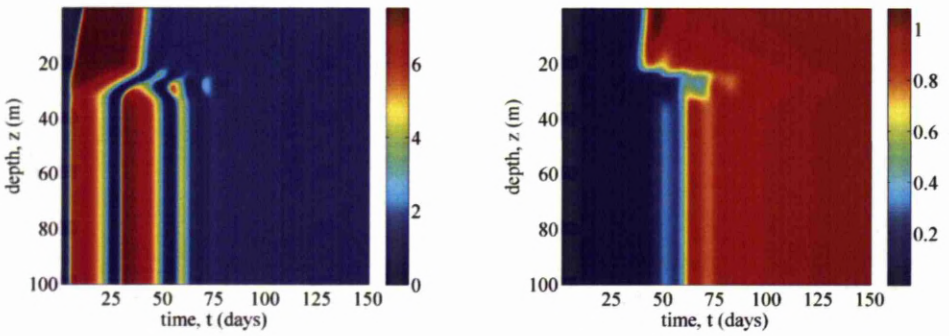

(a) P

(b) V

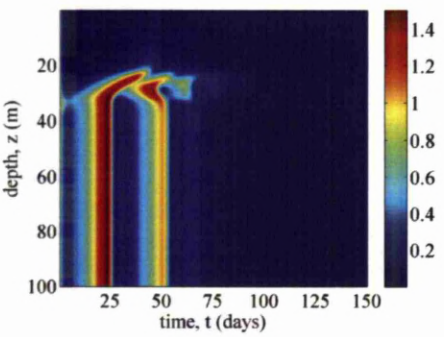

(c) Z

Figure 4.16: Solution of model (4.8, 4.9, 4.10) where $(P_2^*, V^*, 0)$ is stable in the long term for eddy diffusivity varying with the data set of Figure 4.2 and initial conditions of $(V_0, Z_0) = (1.043 \times 10^{-7}, 0.8876)$ in non-dimensional values and P_0 varying as shown in Figure 4.12. Parameter values as in Table 4.1 with $\gamma = 0.08\text{d}^{-1}$ and $\nu = 1.3\text{d}^{-1}$. Each figure shows the phytoplankton population, virus population and zooplankton population respectively.

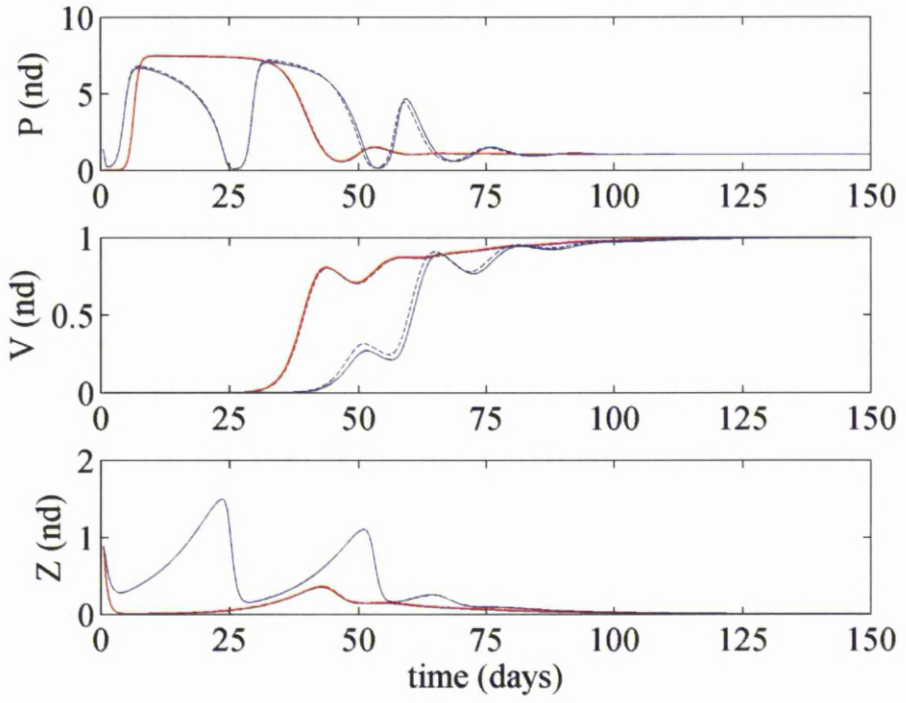

Figure 4.17: Solution of model (4.8, 4.9, 4.10) where $(P_2^*, V^*, 0)$ is stable in the long term for eddy diffusivity varying with the data set of Figure 4.2 and initial conditions of $(V_0, Z_0) = (1.043 \times 10^{-7}, 0.8876)$ in non-dimensional values and P_0 varying as shown in Figure 4.12. Parameter values as in Table 4.1 with $\gamma = 0.08\text{d}^{-1}$ and $\nu = 1.3\text{d}^{-1}$. The red lines represent a depth of $z = 20\text{m}$ and the blue lines a depth of $z = 40\text{m}$. The dashed-line shows the time series solution for c_v and c_z varying with κ_z, whilst the full-line shows the time series solution where c_v and c_z are kept at the constant minimum values of $\text{c}_\text{v} = 1.79 \times 10^{-11}\text{m}^3\text{d}^{-1}$ and $K_{\text{IR}} = 7.35 \times 10^9\text{m}^{-3}$.

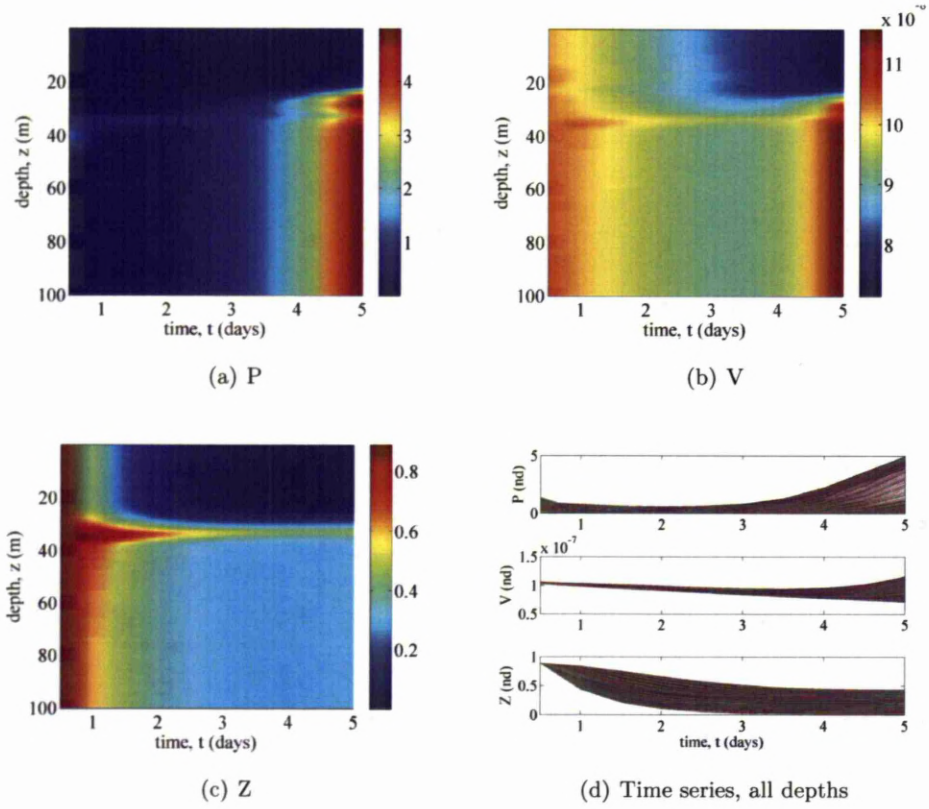

(a) P (b) V

(c) Z (d) Time series, all depths

Figure 4.18: This is the same as the solution shown in Figure 4.16, with just the first 5 days plotted, for the full spatial resolution.

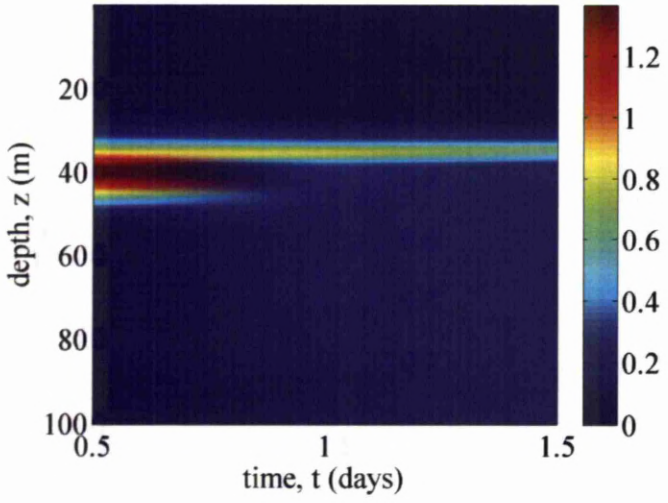

Figure 4.19: The same solution as in Figure 4.16, but just showing the phytoplankton population during the first 1.5 days.

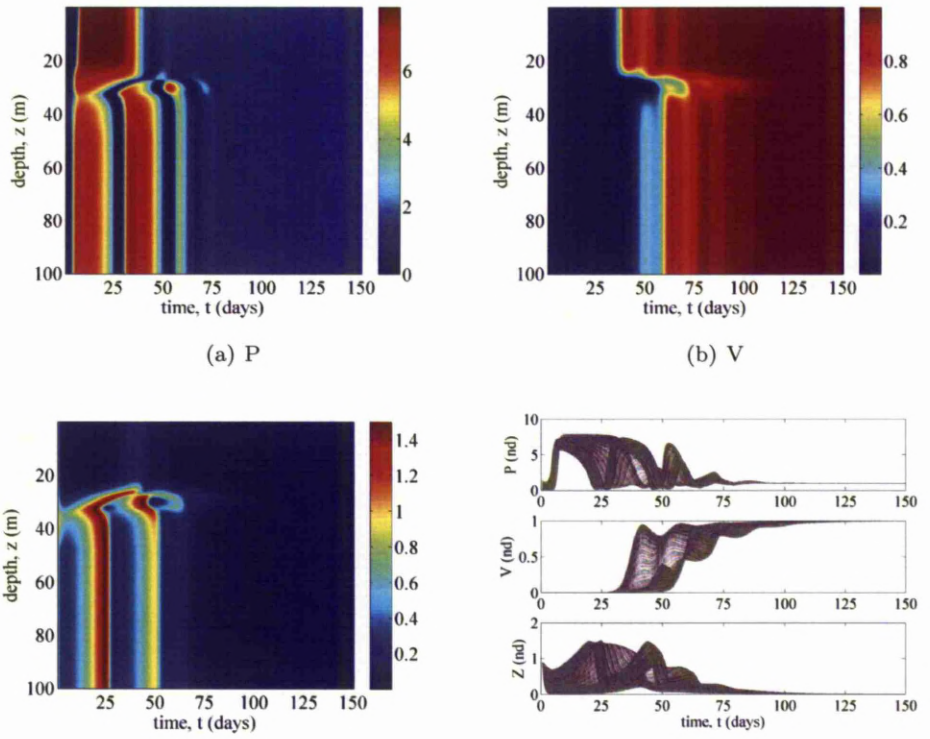

(a) P

(b) V

(c) Z

(d) Time series, all depths

Figure 4.20: Solution of model (4.8, 4.9, 4.10) where $(P_2^*, V^*, 0)$ is stable in the long term, for the second eddy diffusivity profile (Figure 4.5) and initial conditions of $(V_0, Z_0) = (1.043 \times 10^{-7}, 0.8876)$, in non-dimensional values and P_0 varying as shown in Figure 4.12. The $P-V$ and $P-Z$ profiles are those in Figure 4.3. Other parameters as in Table 4.1 with $K_{\mathrm{GR}} = 1.09 \times 10^9 \mathrm{m}^{-3}$, $\gamma = 0.08\mathrm{d}^{-1}$ and $\nu = 1.3\mathrm{d}^{-1}$. Each figure shows the phytoplankton population, virus population, zooplankton population and the time series solution, for the full spatial resolution, of each population respectively.

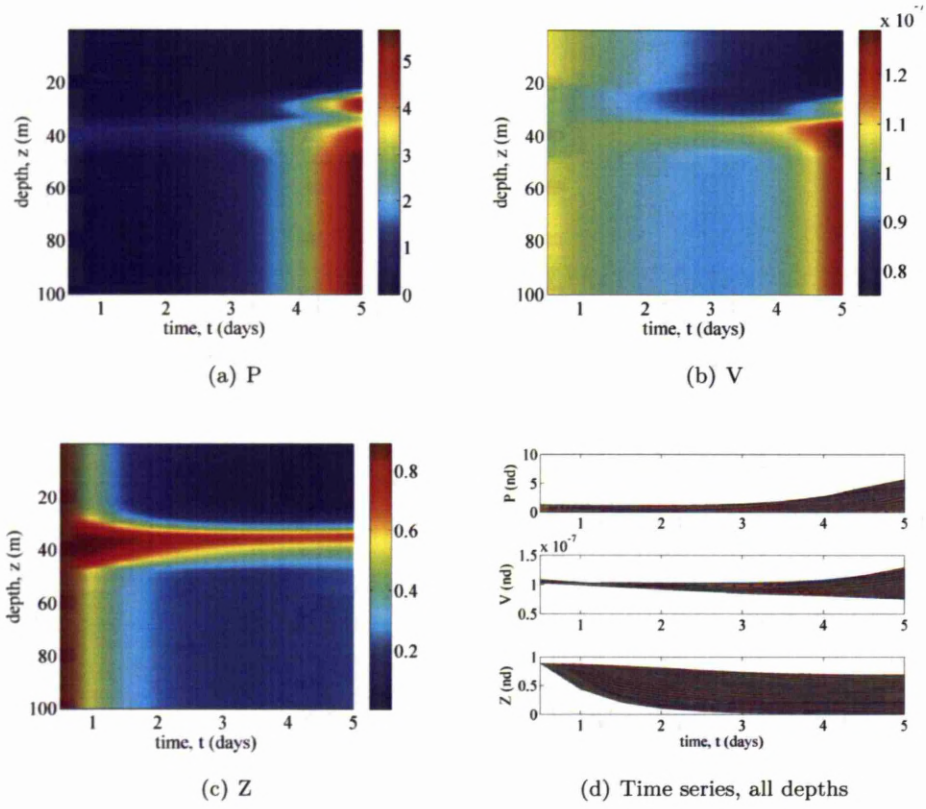

(a) P (b) V

(c) Z (d) Time series, all depths

Figure 4.21: The same solution as shown in Figure 4.20, just showing the first 5 days, for the full spatial resolution.

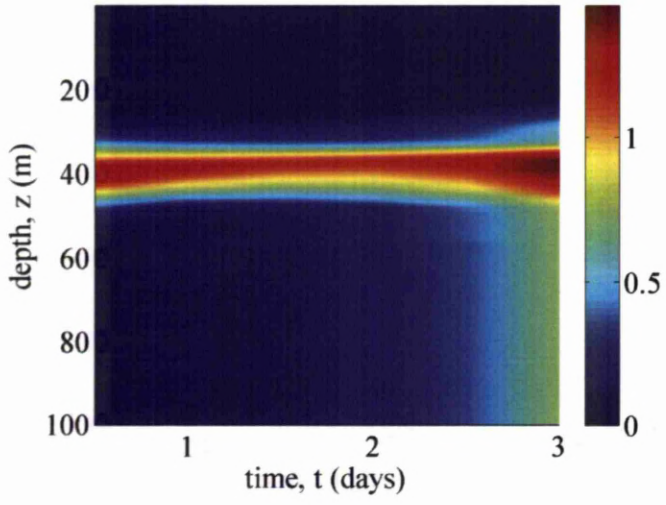

Figure 4.22: The solution is the same as in Figures 4.20 and 4.21, showing the phytoplankton population during the first 1.5 days.

dynamics before moving on to consider constant and variable eddy diffusivity with a non-uniform initial phytoplankton distribution.

4.3.2.1 Variable eddy diffusivity, uniform initial conditions

Similarly to the $(P_2^*, V^*, 0)$ stable system considered in section 4.3.1, we now consider the dynamics for two different eddy diffusivity profiles. The first is that shown in Figure 4.2 and the second is that shown in Figure 4.5. Figures 4.23 and 4.24 show the solution of model (4.8, 4.9, 4.10) for eddy diffusivity profiles 1 and 2 respectively, with uniform initial conditions of $(P_0, V_0, Z_0) = (1.365, 1.043 \times 10^{-7}, 0.8876)$ in non-dimensional values. Both figures include space-time plots for the phytoplankton, virus and predator populations, and also a time series solution of the three species. The second eddy diffusivity profile leads to a higher concentration of the virus in the surface waters, which is expected since the eddy diffusivity is slightly higher in this region for profile 2 than profile 1, and thus the energy dissipation rate, and therefore $P - V$ and $P - Z$ volume clearance rates, are increased. The maximum virus concentration is also increased for the second eddy diffusivity profile. There is no real change in the predator population for either eddy diffusivity profile. There is slightly more heterogeneity in the phytoplankton population for the second eddy diffusivity profile compared to the first, with most heterogeneity being present in the virus population. A region of low diffusivity is more apparent in Figure 4.24(a), there being a slightly lower phytoplankton concentration in this region, which is consistent with eddy diffusivity profile 2.

4.3.2.2 Constant eddy diffusivity, non-uniform initial conditions

Here we consider a non-uniform initial phytoplankton population. Firstly, the solution is found for zero eddy diffusivity and then large eddy diffusivity. These solutions can then be compared to Figures B.1 and B.2 respectively to gauge the effect of non-uniform initial conditions.

The initial phytoplankton population is distributed as in Figure 4.12. Figure 4.25 shows space-time plots of the solution of model (4.8, 4.9, 4.10) for this initial phytoplankton distribution, with zero eddy diffusivity. Figure 4.26 shows the time series solution at three depths: $z = 30$m, represented by a red line, $z = 40$m, represented by a blue line and $z = 80$m, represented by a green line. The full-line is the pdepe solution and the dashed line the equivalent ode45 solution. The largest value of P_0 is 1.365 (non-dimensional), which is the value used in the uniform P_0 sections. The $P - V$ volume clearance rate is $c_v = 1.74 \times 10^{-11}\text{m}^3\text{d}^{-1}$. Other parameters are as in Table 4.1, with $K_{GR} = 1.09 \times 10^9\text{m}^{-3}$, $\gamma = 0.4\text{d}^{-1}$ and $\nu = 1.38\text{d}^{-1}$. The initial virus and predator populations remain uniform with non-dimensional values of $(V_0, Z_0) = (1.043 \times 10^{-7}, 0.8876)$. As with the $(P_2^*, V^*, 0)$ stable case of section 4.3.1,

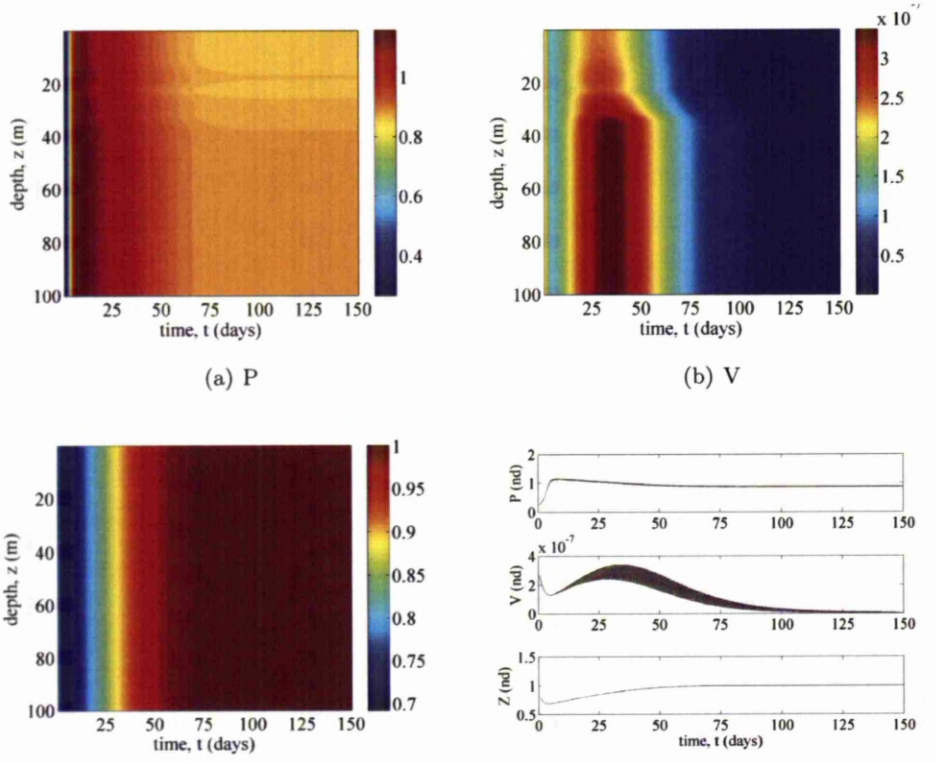

(a) P

(b) V

(c) Z

(d) Time series, all depths

Figure 4.23: Solution of model (4.8, 4.9, 4.10) for eddy diffusivity varying with the data set of Figure 4.2 (profile 1) and uniform initial conditions of $(P_0, V_0, Z_0) = (1.365, 1.043 \times 10^{-7}, 0.8876)$ in non-dimensional values. The $P - V$ and $P - Z$ volume clearance rates vary as in Figure 4.3. Other parameters are as in Table 4.1 with $K_{\mathrm{GR}} = 1.09 \times 10^9$ m^{-3}, $\gamma = 0.4\mathrm{d}^{-1}$ and $\nu = 1.38\mathrm{d}^{-1}$. The system tends to $(P_3^*, 0, Z^*)$ stable in the long-term. Each figure shows the phytoplankton population, virus population, zooplankton population and the time series solution, for the full spatial resolution, of each population respectively.

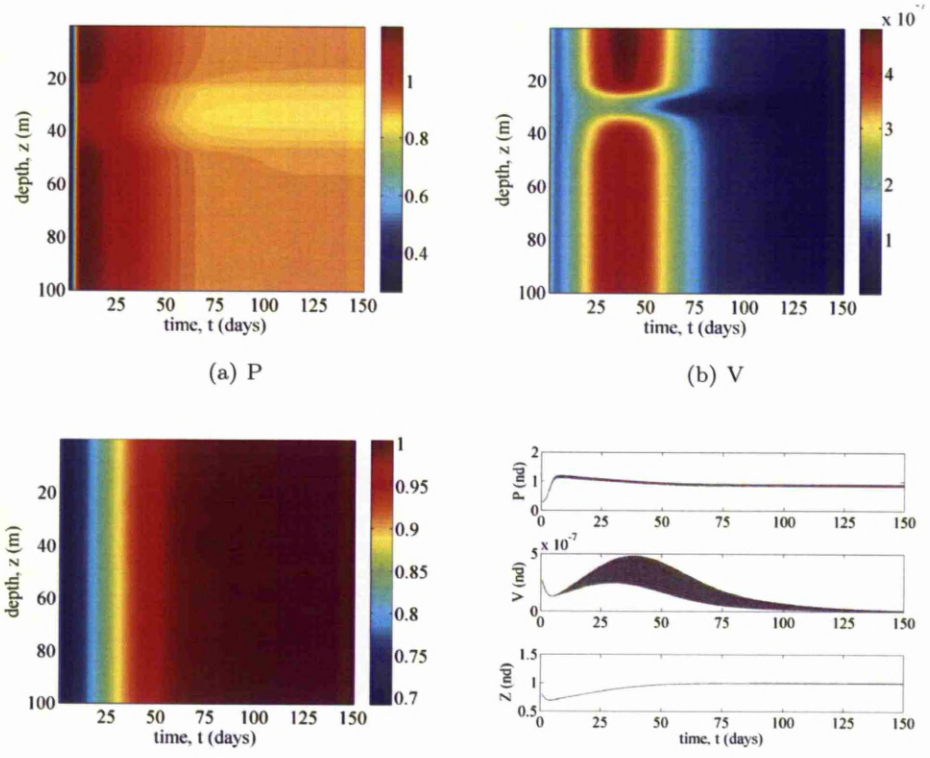

(a) P

(b) V

(c) Z

(d) Time series, all depths

Figure 4.24: Solution of model (4.8, 4.9, 4.10) for eddy diffusivity varying with the data set of Figure 4.5 (profile 2) and uniform initial conditions of $(P_0, V_0, Z_0) = (1.365, 1.043 \times 10^{-7}, 0.8876)$ in non-dimensional values, tending to $(P_3^*, 0, Z^*)$ stable in the long-term. Parameter values as in Table 4.1 with c_v and c_z varying as in Figure 4.6, $K_{GR} = 1.09 \times 10^9 m^{-3}$, $\gamma = 0.4 d^{-1}$ and $\nu = 1.38 d^{-1}$. Each figure shows the phytoplankton population, virus population, zooplankton population and the time series solution, for the full spatial resolution, of each population respectively.

there is numerical error, this time in both the virus and predator populations. Here, the predator population exists mainly in the low diffusivity region. Outside of this region, there is emergence of the virus after approximately 85 days. It takes in excess of 4000 days for the virus to be eradicated. The most striking difference compared to Figure B.1 is the large amount of heterogeneity in all three populations. The distribution of P_0 used allows the transient phytoplankton population to reach a higher level than seen in Figure B.1, at some depths. The heterogeneity in the phytoplankton population also allows a strong emergence of the virus, but only after a substantial amount of time.

Figure 4.27 shows the same solution, except the large value of eddy diffusivity, $\kappa_z = 9.690 \times 10^3 \mathrm{m}^2\mathrm{d}^{-1}$, is used. Here, $\mathrm{c_v} = 1.84 \times 10^{-11}\mathrm{m}^3\mathrm{d}^{-1}$, $K_{\mathrm{IR}} = 7.35 \times 10^9 \mathrm{m}^{-3}$, $K_{\mathrm{GR}} = 1.09 \times 10^9 \mathrm{m}^{-3}$, $\gamma = 0.4\mathrm{d}^{-1}$ and $\nu = 1.38\mathrm{d}^{-1}$. Other parameters are as in Table 4.1. Similarly to what was seen in section 4.3.1, the phytoplankton population is smoothed very quickly by the large eddy diffusivity value. This can be seen clearly in Figure 4.27(b), which shows the phytoplankton population to be smoothed at a rate consistent with the previously computed diffusion timescale of $T = 1.03\mathrm{d}$. The virus and predator populations therefore remain homogeneous since their initial conditions were uniform and the phytoplankton population quickly becomes uniform. The virus population emerges later and has a higher maximum value here than it did for large eddy diffusivity with uniform initial conditions, Figure B.2, but emerges sooner with a lower maximum value compared to zero eddy diffusivity with non-uniform initial conditions (Figure 4.25).

4.3.2.3 Variable eddy diffusivity, non-uniform initial conditions

Here we consider the full model (4.8, 4.9, 4.10) with the non-uniform initial phytoplankton population of Figure 4.12, and eddy diffusivity varying as in Figures 4.2 and 4.5. The virus and predator populations remain constant with non-dimensional values $(V_0, Z_0) = (1.043 \times 10^{-7}, 0.8876)$. Figure 4.28 shows the solution for the first eddy diffusivity profile, that of Figure 4.2, where $\mathrm{c_v}$ and $\mathrm{c_z}$ are as in Figure 4.3. Other parameters are as in Table 4.1, with $K_{\mathrm{GR}} = 1.09 \times 10^9 \mathrm{m}^{-3}$, $\gamma = 0.4\mathrm{d}^{-1}$ and $\nu = 1.38\mathrm{d}^{-1}$. Figures 4.29 and 4.30 show just the first few days of this solution. The largest predator concentrations exist in the region below approximately 30m, the concentrations tending to 1 over time. This allows large phytoplankton concentrations to exist in the surface waters. After approximately 80 days, the virus population emerges, predominantly at depths above 30m. Figure 4.31 also shows the solution of model (4.8, 4.9, 4.10) with non-uniform P_0, but now for eddy diffusivity varying with the second profile, that of Figure 4.5. The $P - V$ and $P - Z$ volume clearance rates are those in Figure 4.6. Other parameters are given in Table 4.1, with $K_{\mathrm{GR}} = 1.09 \times 10^9 \mathrm{m}^{-3}$, $\gamma = 0.4\mathrm{d}^{-1}$ and $\nu = 1.38\mathrm{d}^{-1}$. Again, Figures 4.32 and 4.33 show the first few days of the solution.

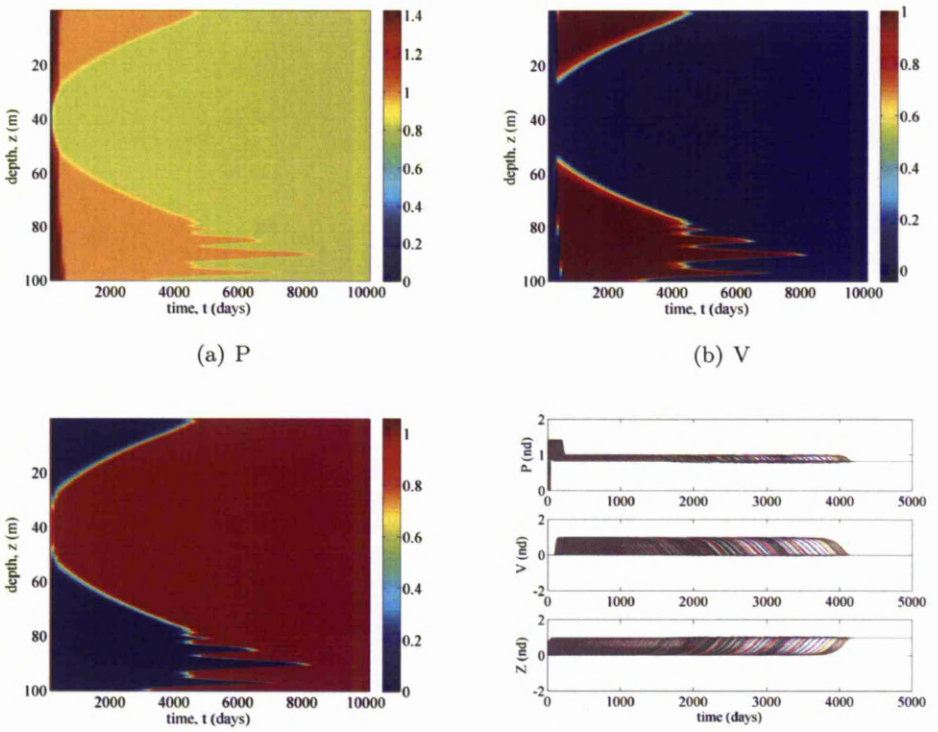

(a) P

(b) V

(c) Z

(d) Time series, all depths

Figure 4.25: Solution of model (4.8, 4.9, 4.10) for zero eddy diffusivity and initial conditions of $(V_0, Z_0) = (1.043\times10^{-7}, 0.8876)$ in non-dimensional values and P_0 varying as shown in Figure 4.12, in the parameter region tending to $(P_3^*, 0, Z^*)$ stable in the long term. Parameters as in Table 4.1 with $c_v = 1.74 \times 10^{-11}\text{m}^3\text{d}^{-1}$, $K_{IR} = 7.35 \times 10^9\text{m}^{-3}$, $K_{GR} = 1.09 \times 10^9\text{m}^{-3}$, $\gamma = 0.4\text{d}^{-1}$ and $\nu = 1.38\text{d}^{-1}$. Each figure shows the phytoplankton population, virus population, zooplankton population and time series respectively.

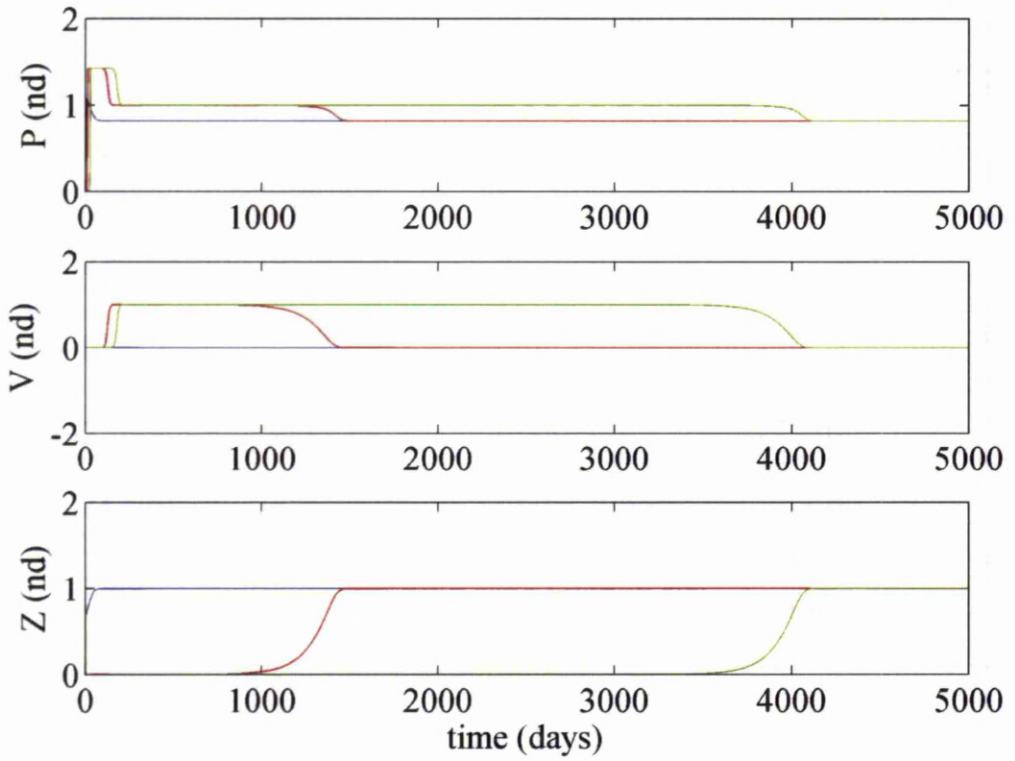

Figure 4.26: Solution of model (4.8, 4.9, 4.10) where $(P_3^*, 0, Z^*)$ is stable in the long term for zero eddy diffusivity and initial conditions of $(V_0, Z_0) = (1.043 \times 10^{-7}, 0.8876)$, in non-dimensional values, and P_0 varying as shown in Figure 4.12. Other parameters are as in Table 4.1, $K_{\mathrm{GR}} = 1.09 \times 10^9 \mathrm{m}^{-3}$, $K_{\mathrm{IR}} = 7.35 \times 10^9 \mathrm{m}^{-3}$, $\mathrm{c_v} = 1.74 \times 10^{-11}$ $\mathrm{m}^3\mathrm{d}^{-1}$, $\gamma = 0.4\mathrm{d}^{-1}$ and $\nu = 1.38\mathrm{d}^{-1}$. The red lines represent $z = 30\mathrm{m}$, the blue line $z = 40\mathrm{m}$ and the green line $z = 80\mathrm{m}$. The full-line is the pdepe solution and the dashed line the equivalent ode45 solution.

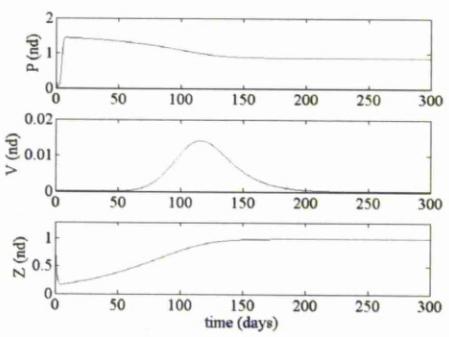

(a) Time series, all depths

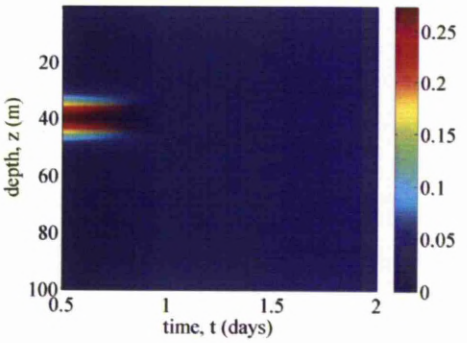

(b) P

Figure 4.27: Solution of model (4.8, 4.9, 4.10) for a maximum eddy diffusivity and initial conditions of $(V_0, Z_0) = (1.043 \times 10^{-7}, 0.8876)$ in non-dimensional values and P_0 varying as shown in Figure 4.12. Parameters as in Table 4.1 with $c_v = 1.84 \times 10^{-11}\text{m}^3\text{d}^{-1}$, $K_{\text{IR}} = 7.35 \times 10^9\text{m}^{-3}$, $K_{\text{GR}} = 1.09 \times 10^9\text{m}^{-3}$, $\gamma = 0.4\text{d}^{-1}$ and $\nu = 1.38\text{d}^{-1}$. The system tends to $(P_3^*, 0, Z^*)$ stable in the long term. Plot (a) shows the time series solution, for the full spatial resolution, over 150 days, plot (b) showing just the first 2 days of the phytoplankton population.

Both Figures 4.28 and 4.31 show the emergence of the virus, predominantly near the surface, so that P, V and Z coexist by the end time points plotted. The virus is eradicated after approximately 480 days. For the second eddy diffusivity profile, the virus emerges sooner. Otherwise, the dynamics between the two eddy diffusivity profiles are very similar. Comparison with the solution for non-uniform initial conditions, but uniform eddy diffusivity (Figures 4.25 and 4.27) shows more heterogeneity in all the populations for non-uniform eddy diffusivity than the large value used in Figure 4.27. However, there is less heterogeneity in the phytoplankton population for non-uniform eddy diffusivity compared to zero eddy diffusivity. Figures 4.28 and 4.31 show that for non-uniform eddy diffusivity, even though the whole system tends to $(P_3^*, 0, Z^*)$ stable behaviour in the long term, there is a transient period where the phytoplankton and virus coexist in the surface region of the water column whilst the phytoplankton and predator coexist in the bottom waters.

4.3.3 $(P, 0, Z)$ Stable limit cycle

We repeat the previous investigations into the effects of turbulence and a non-uniform initial phytoplankton distribution on the population dynamics, but here we consider $(P, 0, Z)$ stable limit cycle behaviour in the long-term. We force this long-term behaviour by setting $(\gamma, \nu) = (0.5, 0.8)$ per day.

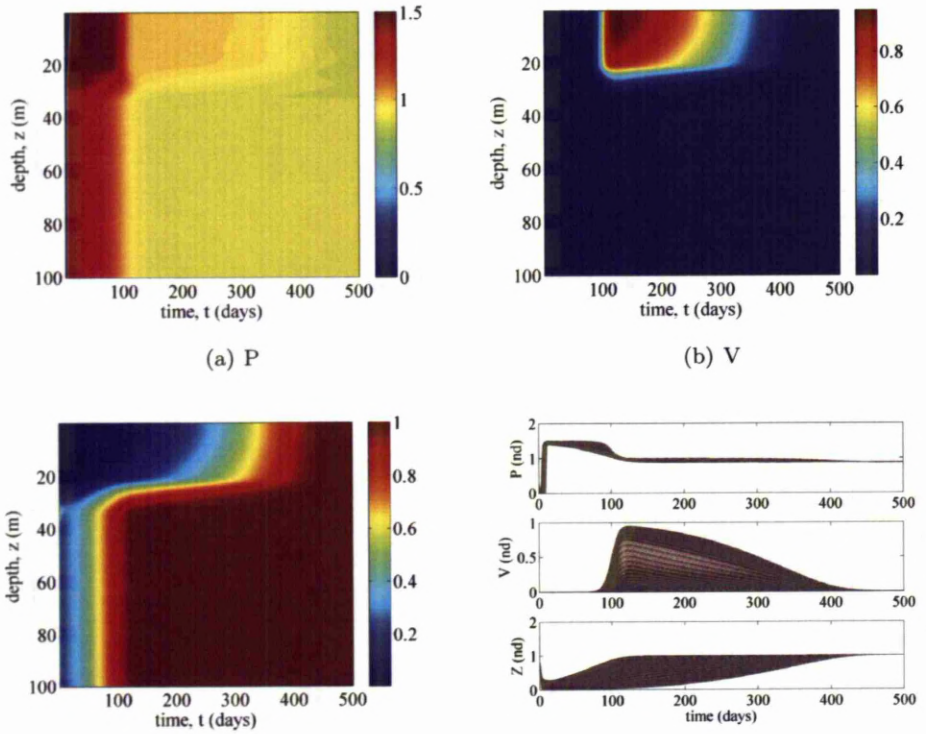

(a) P (b) V

(c) Z (d) Time series, all depths

Figure 4.28: Solution of model (4.8, 4.9, 4.10) for eddy diffusivity varying with the data set of Figure 4.2 and initial conditions of $(V_0, Z_0) = (1.043 \times 10^{-7}, 0.8876)$ in non-dimensional values and P_0 varying as shown in Figure 4.12. The system tends to $(P_3^*, 0, Z^*)$ stable in the long term due to $(\gamma, \nu) = (0.4, 1.38)\mathrm{d}^{-1}$, but this occurs after ~ 480 days. The volume clearance rates are those in Figure 4.3, $K_{\mathrm{GR}} = 1.09 \times 10^9 \mathrm{m}^{-3}$ and other parameters are stated in Table 4.1. Each figure shows the phytoplankton population, virus population, zooplankton population and the time series solution, for the full spatial resolution, of each population respectively.

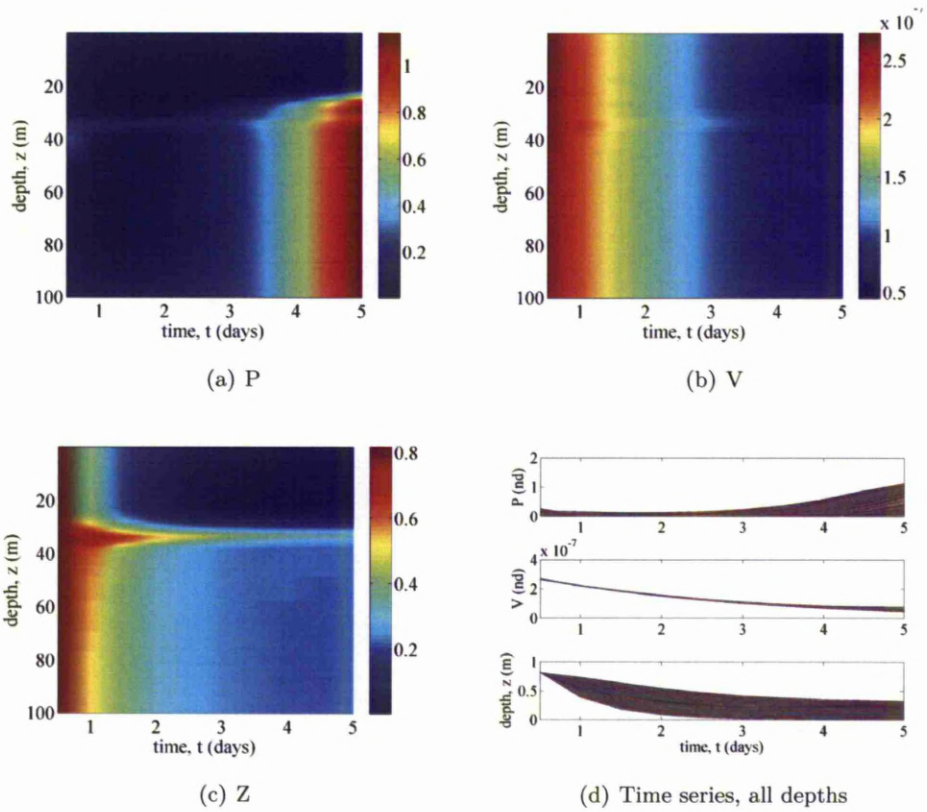

(a) P (b) V

(c) Z (d) Time series, all depths

Figure 4.29: The same solution as Figure 4.28, over the first 5 days, for the full spatial resolution.

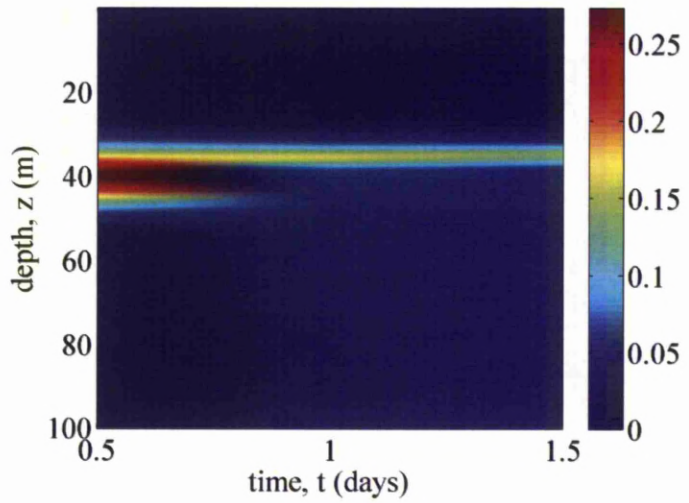

Figure 4.30: The same as Figure 4.28, but just showing the first 1.5 days of the phytoplankton population.

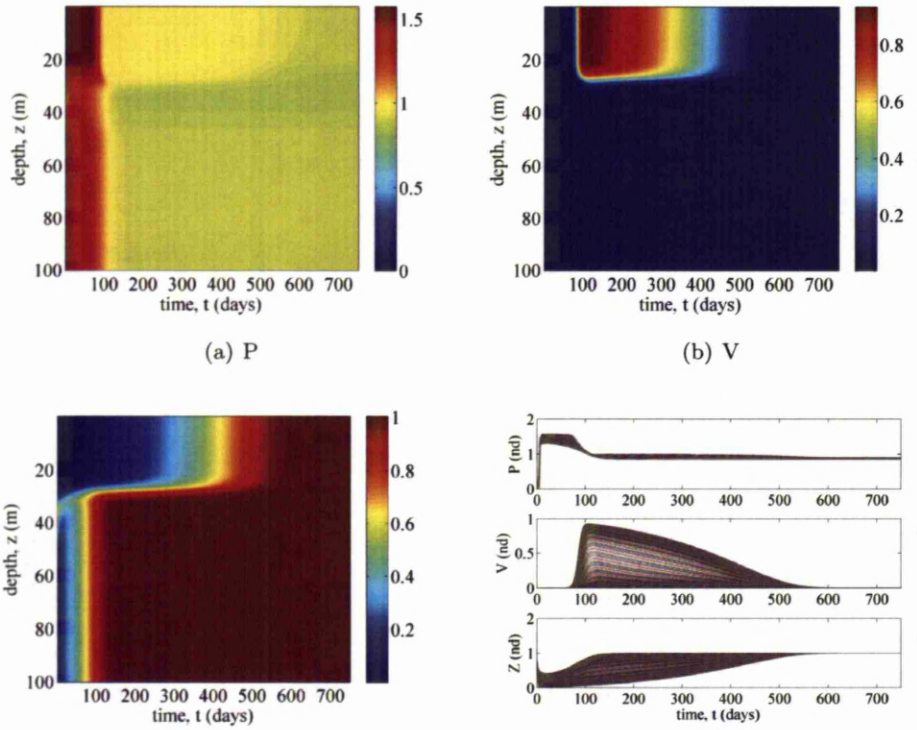

(a) P

(b) V

(c) Z

(d) Time series, all depths

Figure 4.31: Solution of model (4.8, 4.9, 4.10) for eddy diffusivity varying with the second data set, Figure 4.5. Initial conditions of $(V_0, Z_0) = (1.043 \times 10^{-7}, 0.8876)$ in non-dimensional values and P_0 varying as shown in Figure 4.12. Setting $(\gamma, \nu) = (0.4, 1.38)\mathrm{d}^{-1}$ forces the system to $(P_3^*, 0, Z^*)$ stable in the long term, but this occurs after $\sim$ 600 days. Parameters as in Table 4.1 with $\mathrm{c_v}$ and $\mathrm{c_z}$ given in Figure 4.6 and $K_{\mathrm{GR}} = 1.09 \times 10^9 \mathrm{m}^{-3}$. Each figure shows the phytoplankton population, virus population, zooplankton population and the time series solution, for the full spatial resolution, of each population respectively.

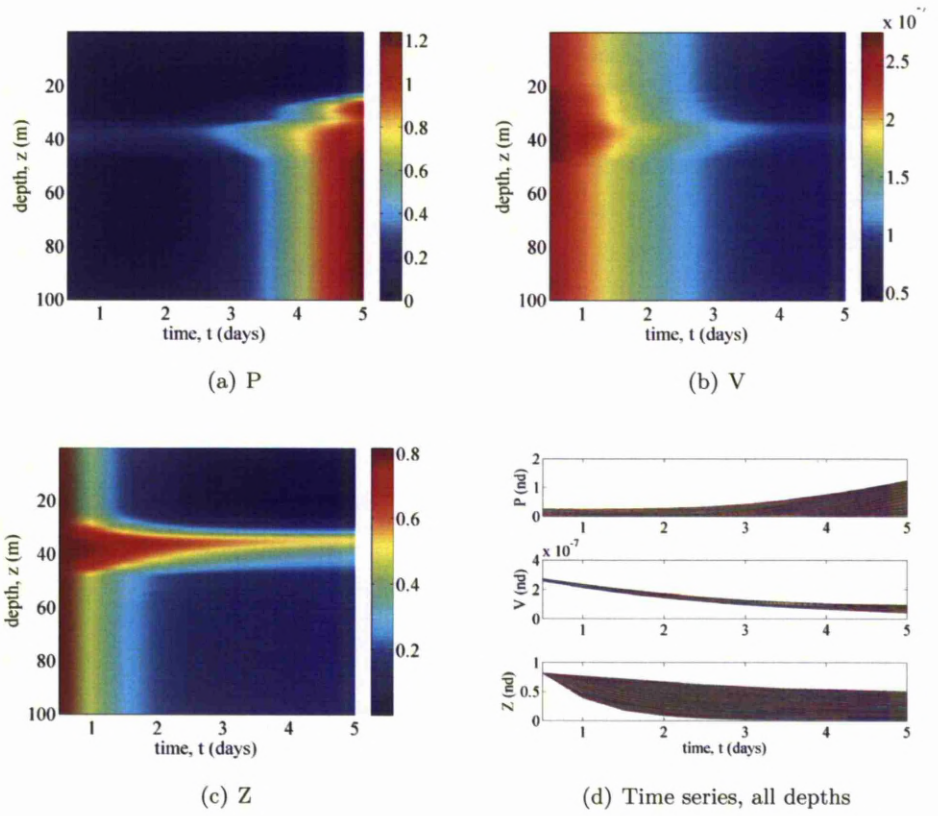

(a) P (b) V

(c) Z (d) Time series, all depths

Figure 4.32: The same solution as Figure 4.31, showing just the first 5 days, for the first spatial resolution.

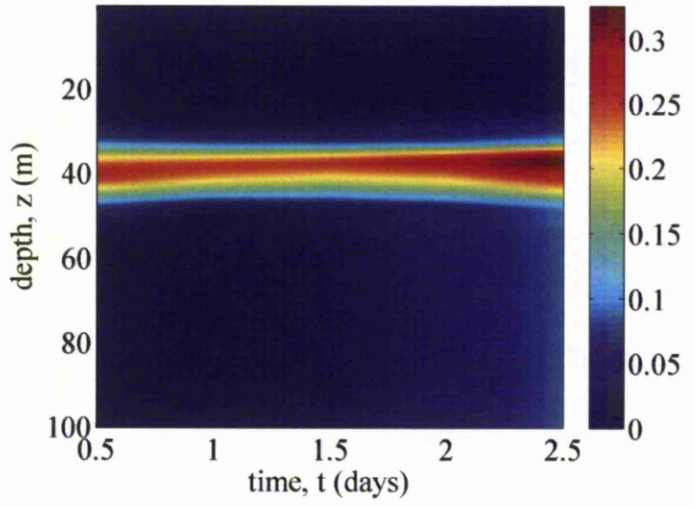

Figure 4.33: The same as Figure 4.31, but just showing the first 2.5 days of the phytoplankton population.

4.3.3.1 Variable eddy diffusivity, uniform initial conditions

Our next step is to consider eddy diffusivity varying with depth, keeping the initial conditions uniform. As previously, we consider two different eddy diffusivity profiles. Figure 4.34 solves model (4.8, 4.9, 4.10) for the first eddy diffusivity profile, that shown in Figure 4.2. The uniform initial conditions continue to be $(P_0, V_0, Z_0) = (1.365, 1.043 \times 10^{-7}, 0.8876)$ in non-dimensional values. The volume clearance rates are shown in Figure 4.3. Other parameters continue to be those of Table 4.1 and $(\gamma, \nu) = (0.5, 0.8)\text{d}^{-1}$. The population dynamics remain largely unchanged, except for a little heterogeneity in the phytoplankton maximum being evident in Figure 4.34(c). The maximum predator concentration is unaltered. Figure 4.35 solves the same system, except the second eddy diffusivity profile, shown in Figure 4.5, is now used. This alters the volume clearance rates to those of Figure 4.6. All other parameters are unchanged. The second eddy diffusivity profile is also unable to introduce any significant heterogeneity into this system although the difference in maximum phytoplankton concentrations is slightly more pronounced for the second eddy diffusivity profile, as can be seen in Figure 4.35(c).

4.3.3.2 Constant eddy diffusivity, non-uniform initial conditions

As previously, in order to consider the effects of non-uniform initial conditions we first study the dynamics where the eddy diffusivity is zero, followed by a large eddy diffusivity. In the next section, we will go on to consider variable eddy diffusivity. Figure 4.36 shows the solution of model (4.8, 4.9, 4.10) for zero eddy diffusivity. The initial phytoplankton concentration varies with depth, as shown in Figure 4.12. The initial virus and predator populations are uniform: $(V_0, Z_0) = (1.043 \times 10^{-7}, 0.8876)$ in non-dimensional values. The $P - V$ volume clearance rate is $\text{c}_\text{v} = 1.74 \times 10^{-11}\text{m}^3\text{d}^{-1}$ and $K_{\text{IR}} = 7.35 \times 10^9\text{m}^{-3}$. The death rates remain at $(\gamma, \nu) = (0.5, 0.8)\text{d}^{-1}$ with all other parameters given in Table 4.1. The same system with a large eddy diffusivity value is shown in Figure 4.37. The dynamics are very different to the zero eddy diffusivity case. Similarly to what was seen in previous sections, the large eddy diffusivity value quickly smooths the phytoplankton population causing the virus and predator populations to remain uniform also. The heterogeneity present for zero eddy diffusivity is therefore not seen here. There is a slight difference in the phytoplankton and predator populations in the first 12 days than was seen previously, but the overall dynamics remain unchanged from the uniform initial condition case.

4.3.3.3 Variable eddy diffusivity, non-uniform initial conditions

We now consider the same system as above except here the eddy diffusivity will vary with depth. Figure 4.38 shows how eddy diffusivity varying with profile 1 (Figure 4.2)

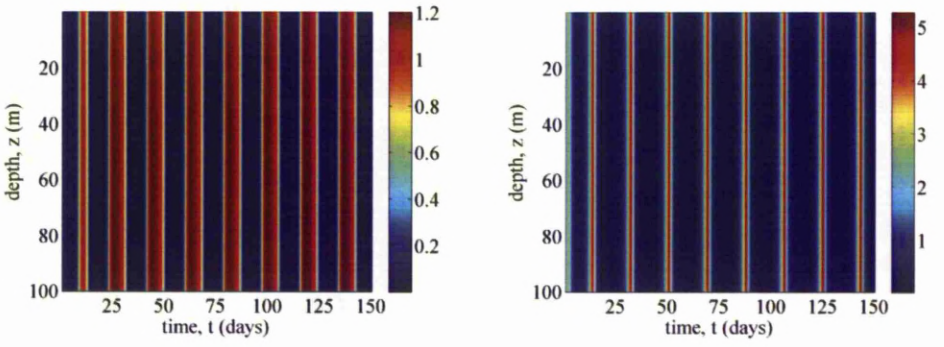

(a) P (b) Z

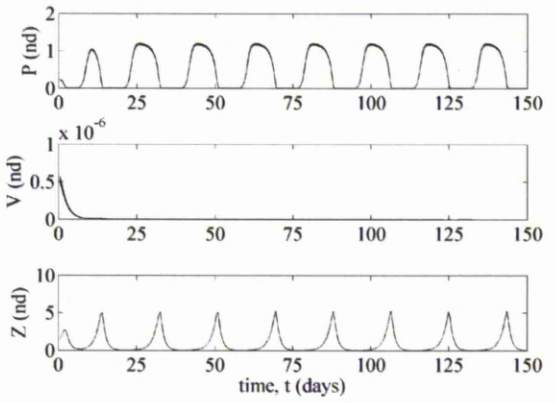

(c) Times series, all depths

Figure 4.34: Solution of model (4.8, 4.9, 4.10) for eddy diffusivity varying with the data set of Figure 4.2 and uniform initial conditions of $(P_0, V_0, Z_0) = (1.365, 1.043 \times 10^{-7}, 0.8876)$ in non-dimensional values. The $P-V$ and $P-Z$ volume clearance rates vary as in Figure 4.3. Parameters given in Table 4.1 with $K_{\text{GR}} = 1.09 \times 10^9 \text{m}^{-3}$ and $(\gamma, \nu) = (0.5, 0.8)\text{d}^{-1}$, forcing the long term behaviour to $(P, 0, Z)$ stable limit cycles. Each figure shows the phytoplankton population, zooplankton population and the time series solution, for the full spatial resolution, of each population respectively.

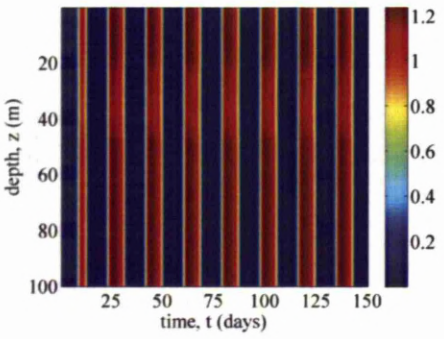

(a) P

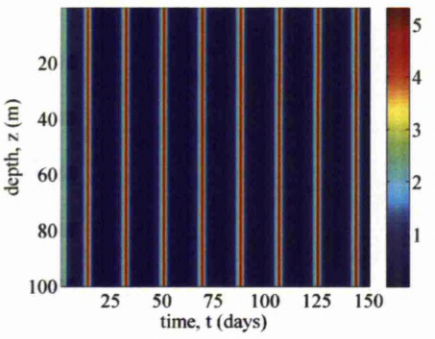

(b) Z

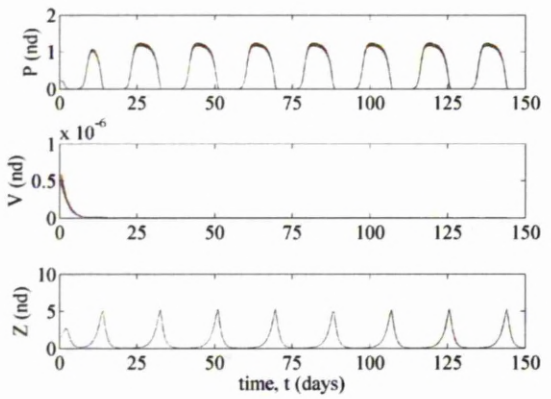

(c) Time series, all depths

Figure 4.35: Solution of model (4.8, 4.9, 4.10) for eddy diffusivity varying with the data set of Figure 4.5 and uniform initial conditions of $(P_0, V_0, Z_0) = (1.365, 1.043 \times 10^{-7}, 0.8876)$ in non-dimensional values. Parameters as in Table 4.1 with $(\gamma, \nu) = (0.5, 0.8)\mathrm{d}^{-1}$ and $K_{\mathrm{GR}} = 1.09 \times 10^{9}\mathrm{m}^{-3}$. The volume clearance rates are those of Figure 4.6. Each figure shows the phytoplankton population, zooplankton population and the time series solution, for the full spatial resolution, of each population respectively.

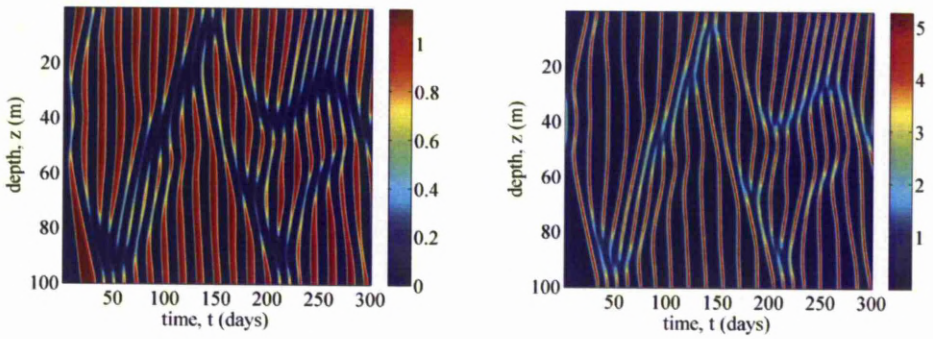

(a) P (b) Z

Figure 4.36: Solution of model (4.8, 4.9, 4.10) for zero eddy diffusivity and initial conditions of $(V_0, Z_0) = (1.043\times10^{-7}, 0.8876)$ in non-dimensional values and P_0 varying as shown in Figure 4.12. Parameters as in Table 4.1 with $c_v = 1.74 \times 10^{-11}m^3d^{-1}$, $K_{IR} = 7.35 \times 10^9 m^{-3}$, $K_{GR} = 1.09 \times 10^9 m^{-3}$ and $(\gamma, \nu) = (0.5, 0.8)d^{-1}$. Figure 4.36(a) shows the phytoplankton population and Figure 4.36(b) the zooplankton population.

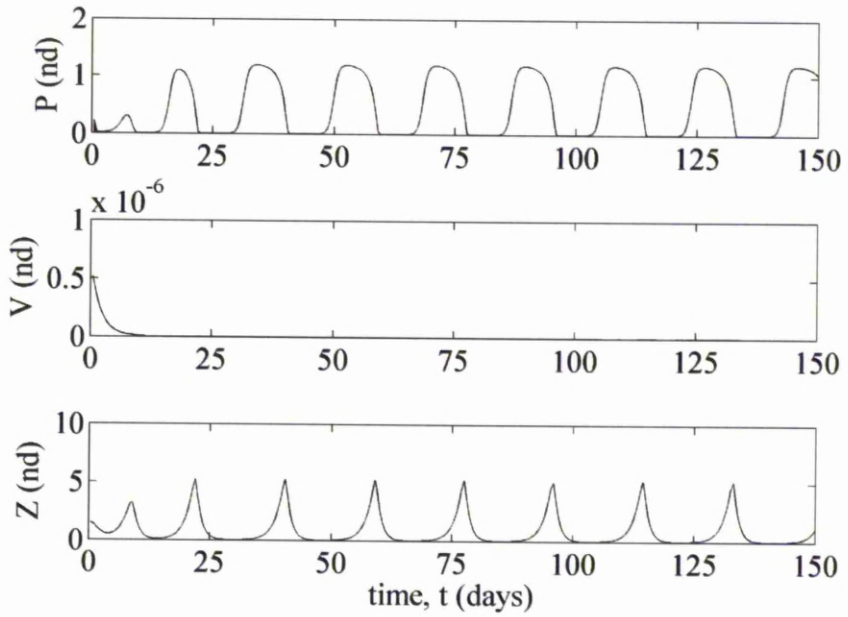

Figure 4.37: Solution of model (4.8, 4.9, 4.10) for a large eddy diffusivity and initial conditions of $(V_0, Z_0) = (1.043\times10^{-7}, 0.8876)$ in non-dimensional values and P_0 varying as shown in Figure 4.12. Other parameters as in Table 4.1 with $c_v = 1.81\times10^{-11}m^3d^{-1}$, $K_{IR} = 7.35 \times 10^9 m^{-3}$, $K_{GR} = 1.09 \times 10^9 m^{-3}$ and $(\gamma, \nu) = (0.5, 0.8)d^{-1}$.

affects the population dynamics, over a timescale where regular oscillations are present. The initial phytoplankton population still varies as in Figure 4.12, with initial virus and predator concentrations of $(V_0, Z_0) = (1.043 \times 10^{-7}, 0.8876)$ in non-dimensional values. The volume clearance rates are those in Figure 4.3. Other parameters are given in Table 4.1, with $K_{\mathrm{GR}} = 1.09 \times 10^{9}\mathrm{m}^{-3}$ and $(\gamma, \nu) = (0.5, 0.8)\mathrm{d}^{-1}$. There is now a large amount of heterogeneity in the phytoplankton and predator populations. Both populations have a peak in concentration between 20 and 30m before this high concentration spreads to other depths. The population then diminishes and continues to oscillate. Figure 4.39 shows the same system over the first 5 days showing that the phytoplankton is quickly smoothed by the turbulence, whilst the predator population peaks between 30 and 40m until around day 3 when the population is smoothed. There is then an increase in the phytoplankton population between 20 and 30m on days 4 and 5. As previously, we compare these findings with a second eddy diffusivity profile, defined in Figure 4.5, with corresponding volume clearance rates those of Figure 4.6. Figure 4.40 shows that there is little difference between the two eddy diffusivity profiles. For the second eddy diffusivity profile, the heterogeneity is restricted to the low diffusivity region. In Figure 4.38, showing the first eddy diffusivity profile, there is also some heterogeneity present above the low eddy diffusivity region. However, Figure 4.40 does appear to show the population settling to stable limit cycle behaviour within the timescale, which wasn't seen in Figure 4.38 for the first eddy diffusivity profile. Figure 4.41 shows the system for the first 5 days. The dynamics are again similar to the first eddy diffusivity profile, but there are some small differences. The range of depths over which the predator peaks is a little wider than for the first eddy diffusivity profile, also the phytoplankton population takes slightly longer to become evenly distributed with the second eddy diffusivity profile.

4.3.4 (P, V, Z) Coexistence

Finally, we consider the effects of turbulence and spatially variant initial conditions on the population dynamics where the phytoplankton, virus and predator populations coexist outside of equilibrium in the long term. This long-term behaviour is achieved by setting $(\gamma, \nu) = (0.1, 1)$ per day.

4.3.4.1 Variable eddy diffusivity, uniform initial conditions

As previously, we now consider how spatially variant eddy diffusivity affects the population dynamics by comparing two different eddy diffusivity profiles. For now, we will continue to use the uniform, non-dimensional, initial conditions: $(P_0, V_0, Z_0) = (1.365, 1.043 \times 10^{-7}, 0.8876)$. Figure 4.42 shows the population dynamics when the eddy diffusivity follows the first profile, that of Figure 4.2. The corresponding volume clearance rates are given in Figure 4.3. Other parameters are given in Table 4.1 and

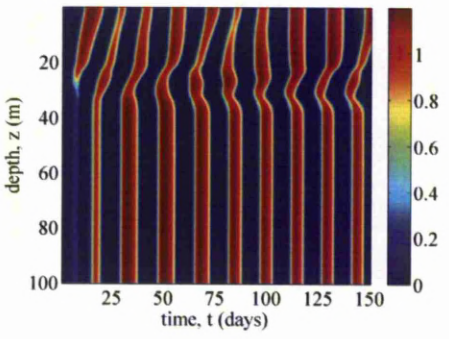

(a) P

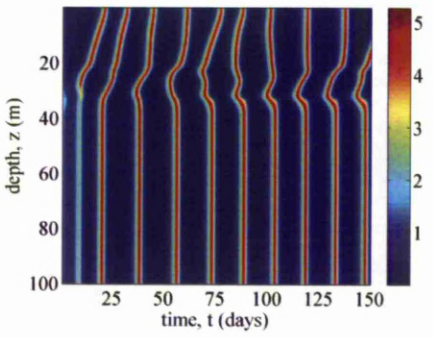

(b) Z

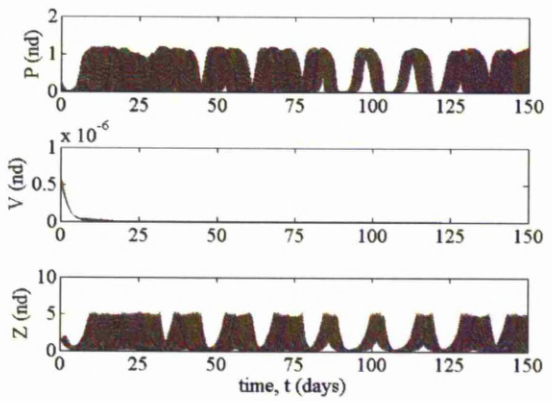

(c) Time series, all depths

Figure 4.38: Solution of model (4.8, 4.9, 4.10) for eddy diffusivity varying with the data set of Figure 4.2 and initial conditions of $(V_0, Z_0) = (1.043 \times 10^{-7}, 0.8876)$ in non-dimensional values and P_0 varying as shown in Figure 4.12. The system has settled to regular $(P, 0, Z)$ oscillations. The volume clearance rates are those of Figure 4.3. Other parameters are as in Table 4.1 with $(\gamma, \nu) = (0.5, 0.8)\mathrm{d}^{-1}$. Each figure shows the phytoplankton population, zooplankton population and the time series solution, for the full spatial resolution, of each population respectively.

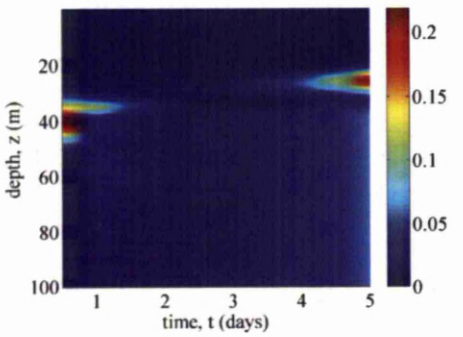

(a) P

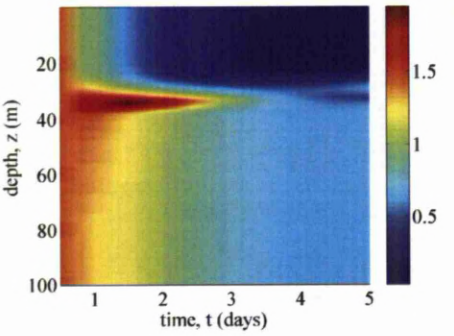

(b) Z

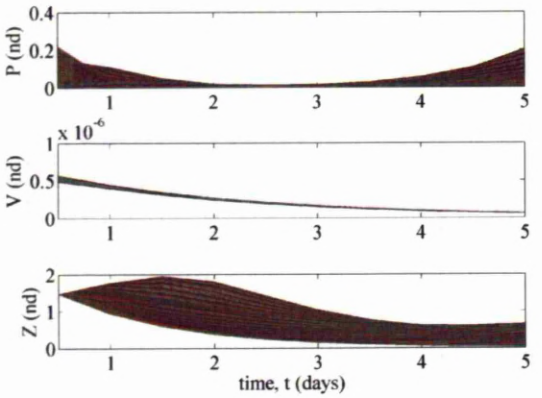

(c) Time series, all depths

Figure 4.39: The same solutions as Figure 4.38 is plotted, but just for the first 5 days, for the full spatial resolution.

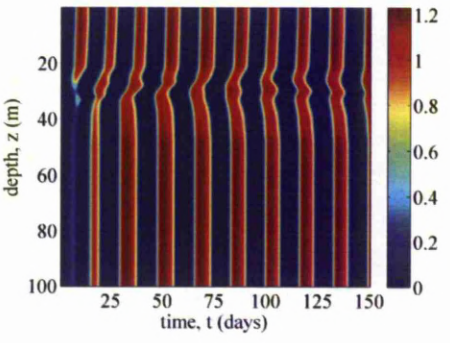

(a) P

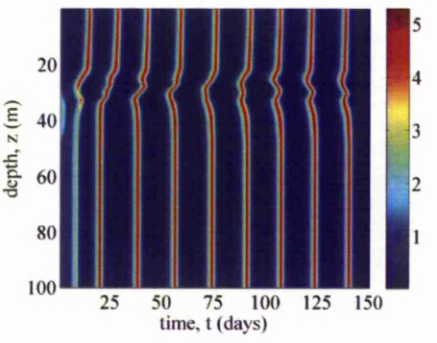

(b) Z

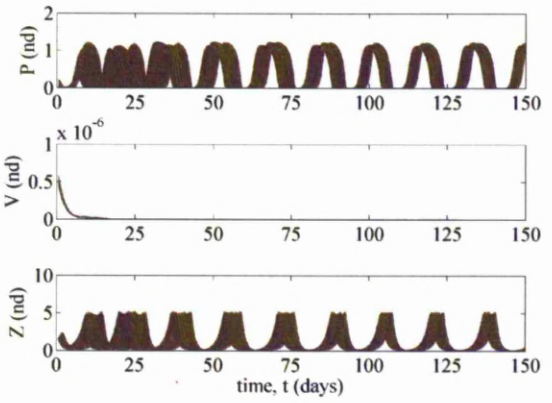

(c) Time series, all depths

Figure 4.40: Solution of model (4.8, 4.9, 4.10) for eddy diffusivity varying with the data set of Figure 4.5 and initial conditions of $(V_0, Z_0) = (1.043 \times 10^{-7}, 0.8876)$ in non-dimensional values and P_0 varying as shown in Figure 4.12. The volume clearance rates are those of Figure 4.6 and $(\gamma, \nu) = (0.5, 0.8)\text{d}^{-1}$, thus the system tends to $(P, 0, Z)$ stable limit cycles in the long term. Each figure shows the phytoplankton population, zooplankton population and the time series solution, for the full spatial resolution, of each population respectively.

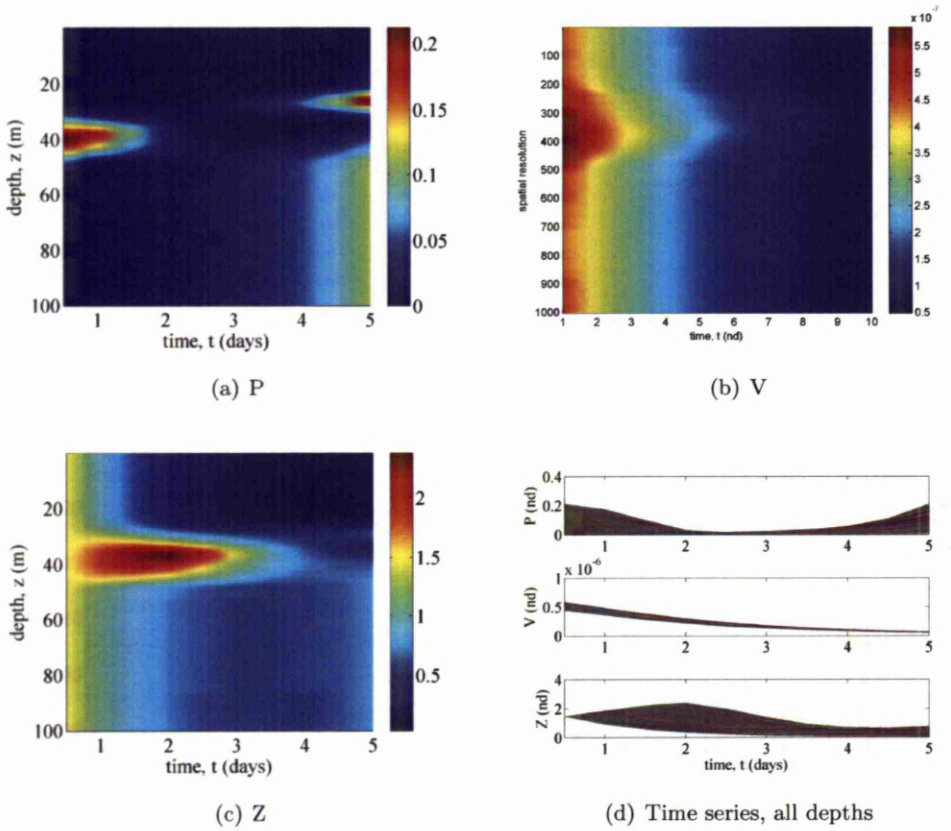

(a) P

(b) V

(c) Z

(d) Time series, all depths

Figure 4.41: The same solution as shown in Figure 4.40, but just over the first 5 days, for the full spatial resolution.

the death rates are $(\gamma, \nu) = (0.1, 1)\mathrm{d}^{-1}$. This variable eddy diffusivity introduces some heterogeneity into the population dynamics, but, overall, the time series solution remains consistent with Figure B.6. Figure 4.43 shows the same system with the second eddy diffusivity, that of Figure 4.5. Here, the volume clearance rates are those of Figure 4.6. All other parameters remain consistent with Figure 4.42. There is a little more heterogeneity in each population compared with the first eddy diffusivity profile, Figure 4.42, and the low diffusivity region is slightly more visible.

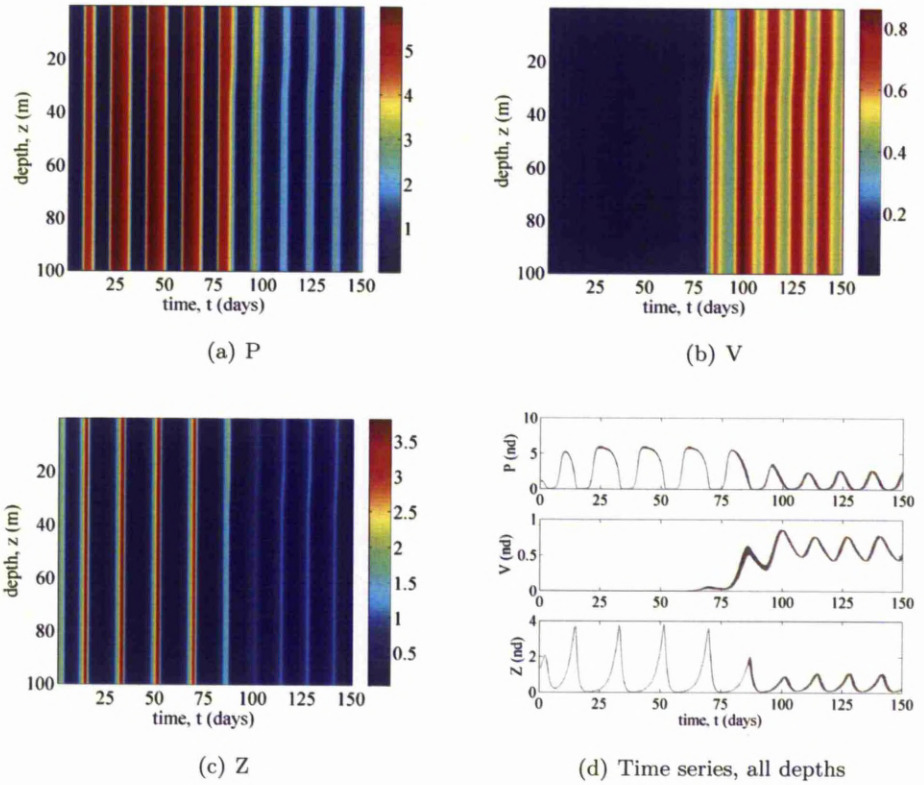

(a) P

(b) V

(c) Z

(d) Time series, all depths

Figure 4.42: Solution of model (4.8, 4.9, 4.10) for eddy diffusivity varying with the first data set, Figure 4.2, and uniform initial conditions of $(P_0, V_0, Z_0) = (1.365, 1.043 \times 10^{-7}, 0.8876)$ in non-dimensional values. The volume clearance rates are those of Figure 4.3. Other parameters in Table 4.1 with $K_{\mathrm{GR}} = 1.09 \times 10^{9}\mathrm{m}^{-3}$ and $(\gamma, \nu) = (0.1, 1)\mathrm{d}^{-1}$. Each figure shows the phytoplankton population, virus population, zooplankton population and the time series solution, for the full spatial resolution, of each population respectively.

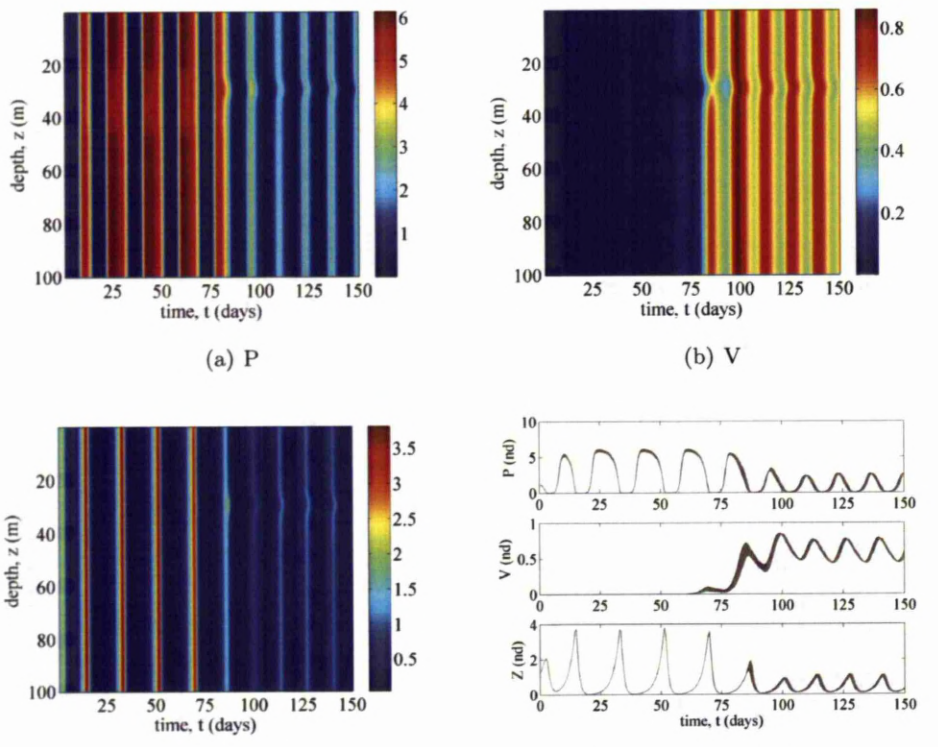

(a) P (b) V

(c) Z (d) Time series, all depths

Figure 4.43: Solution of model (4.8, 4.9, 4.10) for eddy diffusivity varying with the second data set, Figure 4.5, and uniform initial conditions of $(P_0, V_0, Z_0) = (1.365, 1.043 \times 10^{-7}, 0.8876)$ in non-dimensional values. The volume clearance rates are those of Figure 4.6. Other parameters are given in Table 4.1 with $K_{\mathrm{GR}} = 1.09 \times 10^9 \mathrm{m}^{-3}$ and $(\gamma, \nu) = (0.1, 1)\mathrm{d}^{-1}$. Each figure shows the phytoplankton population, virus population, zooplankton population and the time series solution, for the full spatial resolution, of each population respectively.

4.3.4.2 Constant eddy diffusivity, non-uniform initial conditions

Now return to consideration of uniform eddy diffusivity, both zero and large values, but with the inclusion of a non-uniform initial phytoplankton distribution. The initial phytoplankton distribution is that defined in Figure 4.12. The initial virus and predator populations remain uniform with non-dimensional values $(V_0, Z_0) = (1.043 \times 10^{-7}, 0.8876)$. Solution of model (4.8, 4.9, 4.10) when the eddy diffusivity is zero is shown in Figure 4.44. Parameter values are given in Table 4.1 with $c_v = 1.74 \times 10^{-11}\text{m}^3\text{d}^{-1}$, $K_{IR} = 7.35 \times 10^9\text{m}^{-3}$, $K_{GR} = 1.09 \times 10^9\text{m}^{-3}$ and $(\gamma, \nu) = (0.1, 1)\text{d}^{-1}$. The dynamics are significantly different to those for uniform initial conditions, shown in Figure B.5. As seen in previous sections, different transient dynamics at each depth give rise to the patterning seen in the space-time plots. Figure 4.45 shows solution of the model with a large eddy diffusivity value. Here, $\kappa_z = 9.690 \times 10^3\text{m}^2\text{d}^{-1}$, $c_v = 1.84 \times 10^{-11}\text{m}^3\text{d}^{-1}$. All other parameters are the same as for Figure 4.44. As seen in previous sections, the large eddy diffusivity value spreads the phytoplankton population very quickly, removing any heterogeneity from the population and preventing spatial variance developing in the virus or predator populations. Figure 4.45 is therefore very similar to that for large eddy diffusivity and uniform initial conditions, Figure B.6.

4.3.4.3 Variable eddy diffusivity, non-uniform initial conditions

We now combine non-uniform initial conditions and non-uniform eddy diffusivity, comparing the two eddy diffusivity profiles of Figures 4.2 and 4.5. Figure 4.46 shows the solution of model (4.8, 4.9, 4.10) for the initial phytoplankton population distributed as in Figure 4.12 and uniform non-dimensional initial conditions for the virus and predator of 1.043×10^{-7} and 0.8876 respectively with eddy diffusivity varying as in Figure 4.2. The dynamics are somewhere between those seen in Figures 4.44 and 4.45 for zero eddy diffusivity and large eddy diffusivity respectively, with non-uniform initial conditions. The overall dynamics are very similar to those for large eddy diffusivity, Figure 4.45, but with a large amount of heterogeneity, a separation appearing between the surface region and the rest of the water column. Figure 4.47 shows the same solution as Figure 4.46, but just over the first 5 days in order to see how the phytoplankton population is spread out initially. Heterogeneity appears in the predator population very early on. Figure 4.48 shows solution of the same model for the second eddy diffusivity profile, given in Figure 4.5. The volume clearance rate profiles now change to those of Figure 4.6, but all other parameters remain the same. We see more heterogeneity in Figure 4.48 compared to Figure 4.46. This is due to a more pronounced low diffusivity region present for the second eddy diffusivity profile. However, the dynamics above this low diffusivity region are more uniform for the second eddy diffusivity profile, Figure 4.48, compared to the first, Figure 4.46. Figure 4.49 shows just the first 5 days of the

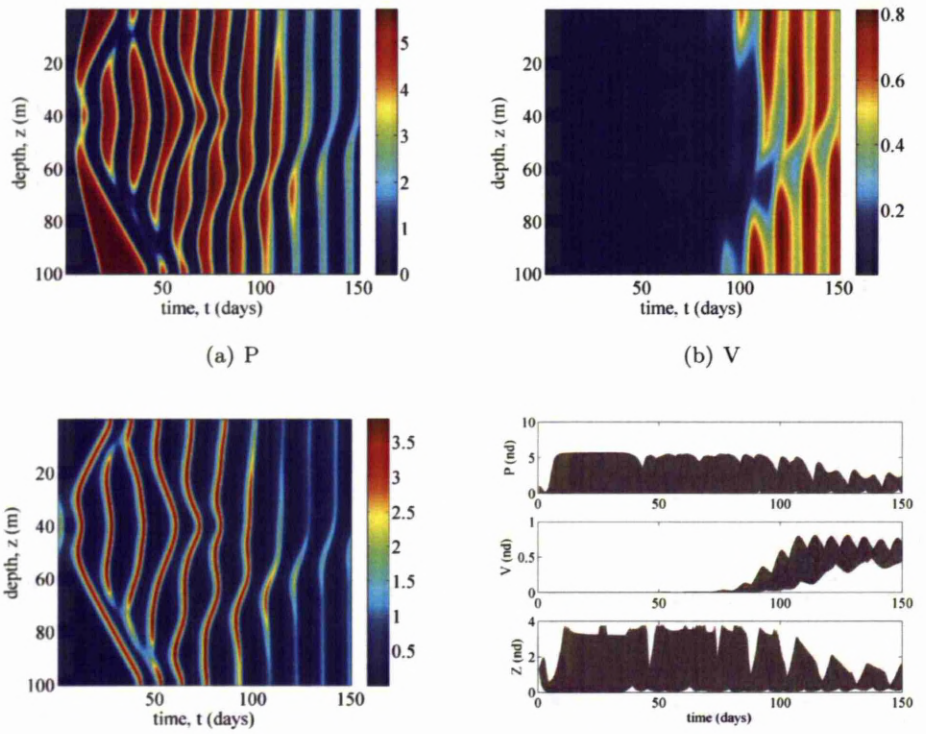

(a) P

(b) V

(c) Z

(d) Time series, few depths

Figure 4.44: Solution of model (4.8, 4.9, 4.10) for zero eddy diffusivity and initial conditions of $(V_0, Z_0) = (1.043 \times 10^{-7}, 0.8876)$ in non-dimensional values and P_0 varying as shown in Figure 4.12. Parameter values given in Table 4.1 with $c_v = 1.74 \times 10^{-11} m^3 d^{-1}$, $K_{IR} = 7.35 \times 10^9 m^{-3}$, $K_{GR} = 1.09 \times 10^9 m^{-3}$ and $(\gamma, \nu) = (0.1, 1) d^{-1}$. Each figure shows the phytoplankton population, virus population, zooplankton population and the time series solution, at all depths, of each population respectively.

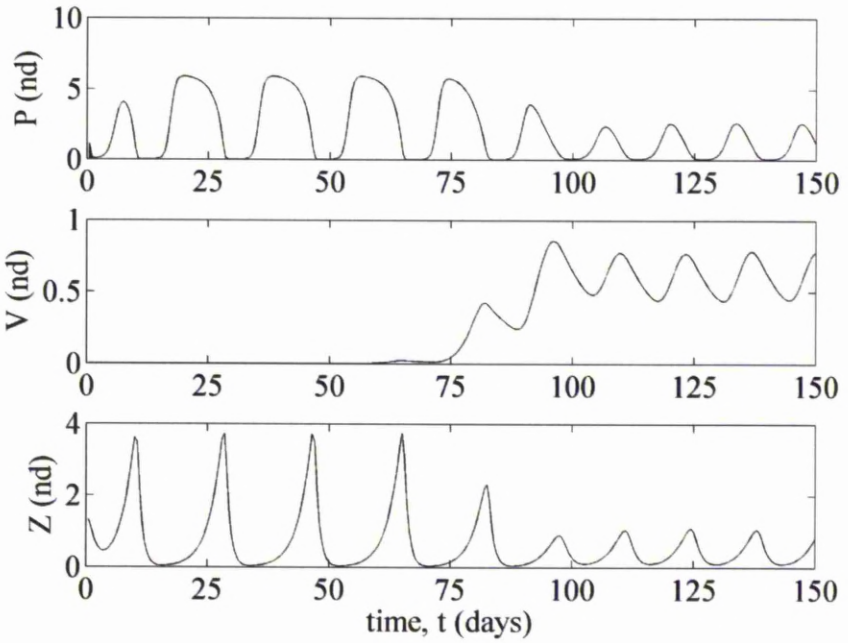

Figure 4.45: Solution of model (4.8, 4.9, 4.10) for a large eddy diffusivity of $\kappa_z = 9.690 \times 10^3 \mathrm{m^2 d^{-1}}$, which corresponds to $c_v = 1.84 \times 10^{-11} \mathrm{m^3 d^{-1}}$ and $K_{IR} = 7.35 \times 10^9 \mathrm{m^{-3}}$, and initial conditions of $(V_0, Z_0) = (1.043 \times 10^{-7}, 0.8876)$ in non-dimensional values and P_0 varying as shown in Figure 4.12. Other parameters are given in Table 4.1, with $K_{GR} = 1.09 \times 10^9 \mathrm{m^{-3}}$ and $(\gamma, \nu) = (0.1, 1)\mathrm{d^{-1}}$.

dynamics when the eddy diffusivity follows profile 2. The phytoplankton population is quickly smoothed before a variance emerges in the population around days 4 and 5. Heterogeneity appears in the predator population very quickly.

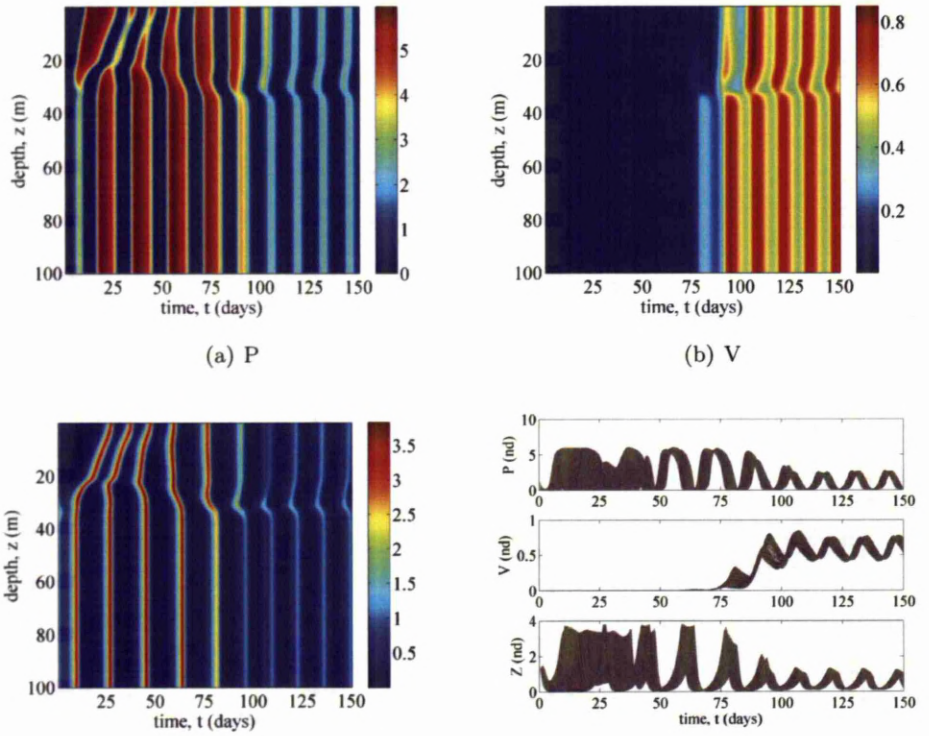

(a) P

(b) V

(c) Z

(d) Time series, all depths

Figure 4.46: Solution of model (4.8, 4.9, 4.10) for eddy diffusivity varying with the data set of Figure 4.2 and initial conditions of $(V_0, Z_0) = (1.043 \times 10^{-7}, 0.8876)$ in non-dimensional values and P_0 varying as shown in Figure 4.12. Volume clearance rates are given in Figure 4.3. Other parameters are as in Table 4.1 with $K_{\mathrm{GR}} = 1.09 \times 10^9 \mathrm{m}^{-3}$ and $(\gamma, \nu) = (0.1, 1)\mathrm{d}^{-1}$. Each figure shows the phytoplankton population, virus population, zooplankton population and the time series solution, for the full spatial resolution, of each population respectively.

4.3.5 Control of phytoplankton by addition of virions or grazers

We now continue the work of section 3.3.4 by investigating the addition of virions or grazers in order to control a phytoplankton community. The phytoplankton are initially distributed as in Figure 4.12. This section focuses on shifting the long term behaviour of the system, lowering the phytoplankton equilibrium level. We simulate the virus or predator being added to the surface of a water column. Figure 4.50 shows

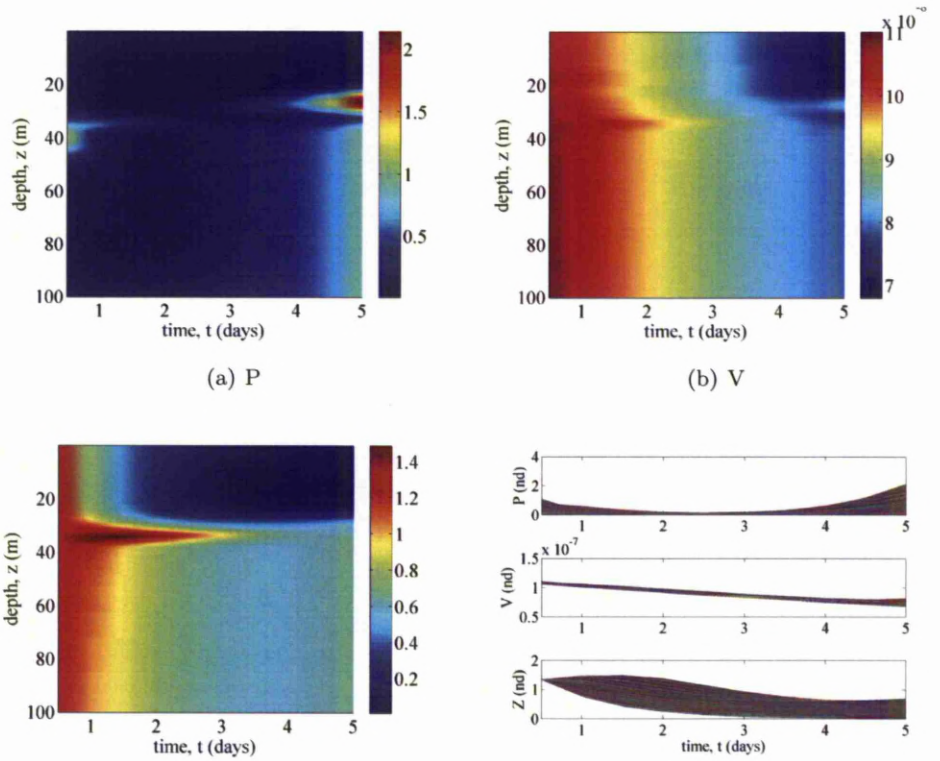

(a) P

(b) V

(c) Z

(d) Time series, all depths

Figure 4.47: The same solution as Figure 4.46, showing just the first 5 days, for the full spatial resolution.

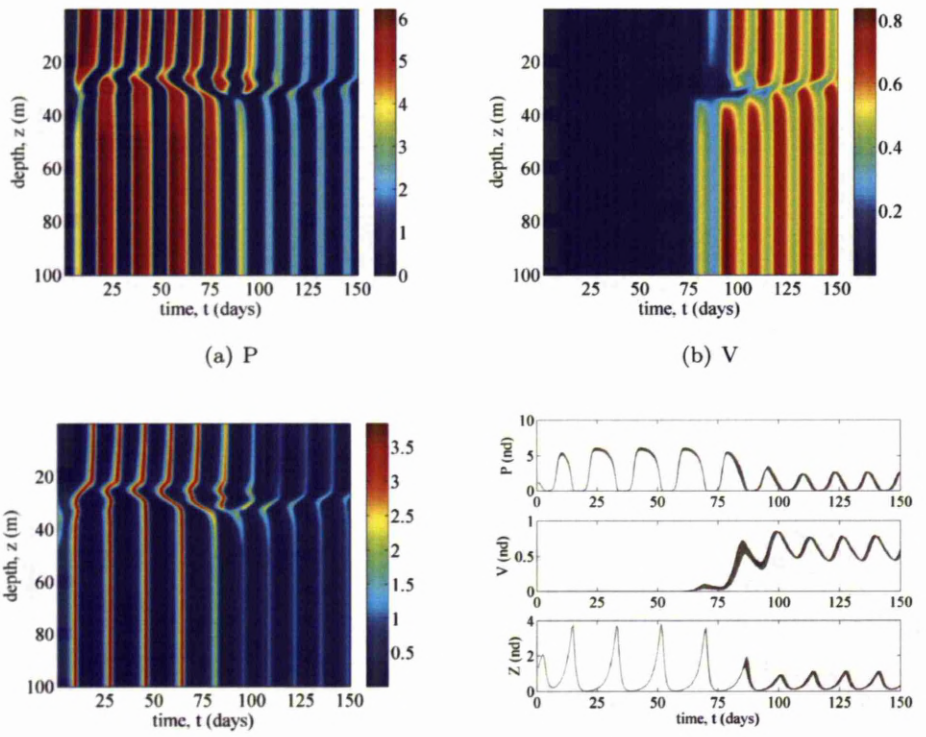

(a) P

(b) V

(c) Z

(d) Time series, all depths

Figure 4.48: Solution of model (4.8, 4.9, 4.10) for eddy diffusivity varying with the second data set, Figure 4.5, and initial conditions of $(V_0, Z_0) = (1.043 \times 10^{-7}, 0.8876)$ in non-dimensional values and P_0 varying as shown in Figure 4.12. The volume clearance rates are given in Figure 4.6. Other parameters are given in Table 4.1 with $K_{\mathrm{GR}} = 1.09 \times 10^{9}\mathrm{m}^{-3}$ and $(\gamma, \nu) = (0.1, 1)\mathrm{d}^{-1}$. Each figure shows the phytoplankton population, virus population, zooplankton population and the time series solution, for the full spatial resolution, of each population respectively.

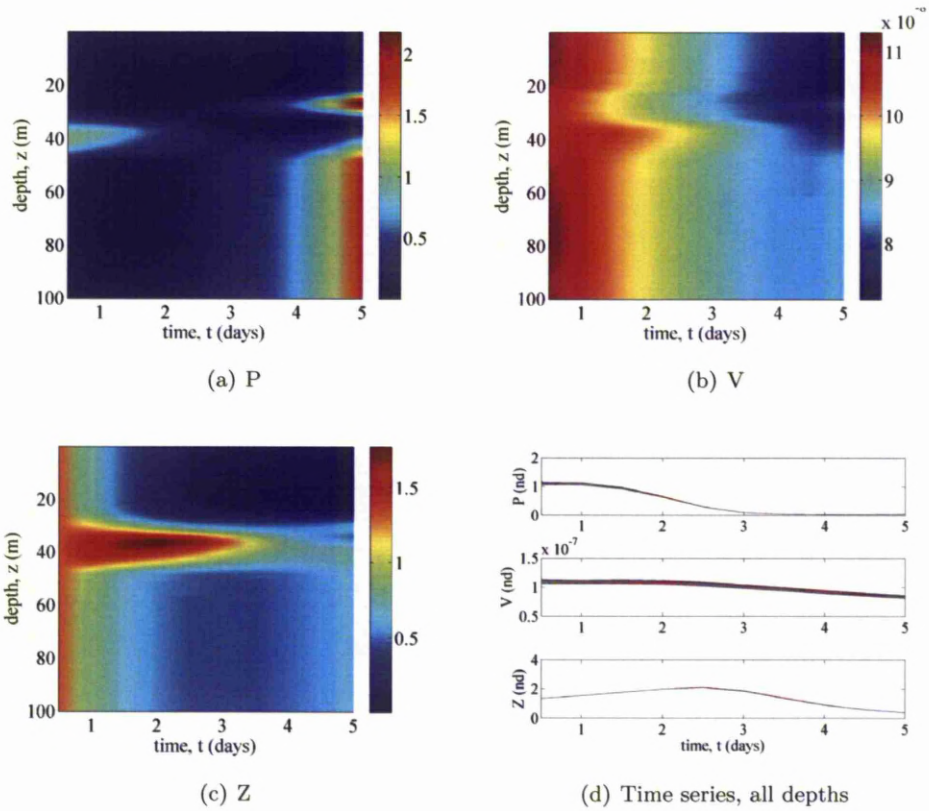

(a) P

(b) V

(c) Z

(d) Time series, all depths

Figure 4.49: The same solution as Figure 4.48, showing just the first 5 days, for the full spatial resolution.

the distribution of virus and predator added, which is given by

$$V, Z = 10^7 \exp\left(\frac{-(z - 0.0125H)^2}{100}\right) \tag{4.24}$$

for depths between 0 and 10m. For depths lower than 10m, the concentration of V or Z added is zero. The maximum concentration of either control mechanism added is $10^7 \mathrm{m}^{-3}$, equivalent to the 10 ml^{-1} added in section 3.3.4. The quantity 0.0125 was chosen arbitrarily. It should be noted that the natural ranges of micro-zooplankton and virus concentrations tend to differ by orders of magnitude and use of the same initial concentration here is thus somewhat paradoxical. However, the quantity of each species that can be manufactured may not reach anywhere near the concentrations found in the field and Figures 3.11(a) and 3.12(a) do show both HaV and *O. marina* to be more than capable of a $10\mathrm{ml}^{-1}$ natural concentration. We therefore consider adding the same small concentration of each in order to directly compare their controllability. Further investigation of what concentration of each species is reasonable to manufacture would, however, be desirable.

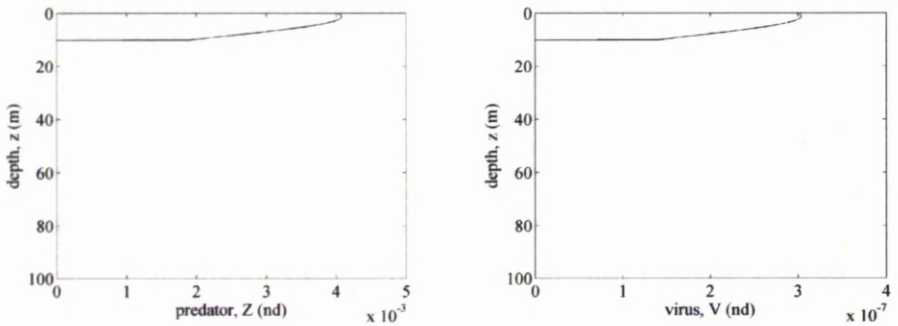

(a) (b)

Figure 4.50: Distribution of grazers and virions added as a control. In dimensional values, the maximum virus and predator concentration is $10^7 \mathrm{m}^{-3}$. Both the predator and virus populations are given by equation (4.24). The predator population in non-dimensionalised on Z^* (given in equation 4.7) and the virus population is non-dimensionalised on V^* (given by equation 4.6). This is consistent with the non-dimensionalisation of the full model in section 4.2.1.

Figure 4.51 considers shifting the long term dynamics of a phytoplankton community existing alone at carrying capacity to a phytoplankton-predator stable system. The phytoplankton is initially at carrying capacity with $(V_0, Z_0) = (0, 0)$. A predator, with death rate $\nu = 1.38\mathrm{d}^{-1}$, is added after 25 days with the distribution shown in Figure 4.50(a). The long term behaviour is shifted from $(K, 0, 0)$ stable to $(P_3^*, 0, Z^*)$ stable, where $P_3^* < K$. Figure 4.51 uses a spatially variant eddy diffusivity - that of

Figure 4.2. Figure 4.51 shows the whole system become $(P_3^*, 0, Z^*)$ stable in around 550 days, which is a long time frame in an actual aquatic system. The surface region is brought under control between 300 and 400 days. It then takes approximately 100 days for the grazers to spread through the low diffusivity region. However, once this is achieved, the whole water column is well mixed. Consideration of Figure 4.2 explains this behaviour. There is a barrier to mixing in the low κ_z region between $z = 20$ and 40m. There is close to a five order of magnitude difference between the eddy diffusivity in this region and that at depths below 40m, explaining the well mixed populations once the predator is below 40m. Figure 4.52 shows the same dynamics, but the largest predator concentration added is twice as large as that in Figure 4.50(a). Addition of these larger concentrations of the predator decreases the time taken to bring the phytoplankton to the lower level of P_3^* by approximately 25 days. Increasing the predator concentration added further continues to decrease the time before the coexistence equilibrium is reached.

We now consider a similar system, but using a virus as a control instead of predator. Again, the phytoplankton initially exist alone at carrying capacity. Figure 4.53 shows the system shifting from $(K, 0, 0)$ stable when a virus with decay rate $\gamma = 0.3\text{d}^{-1}$ is added 25 days into the simulation. The long term behaviour shifts to $(P_2^*, V^*, 0)$ stable, where $P_2^* < K$. By day 75, the system has reached $(P_2^*, V^*, 0)$ stable coexistence. Thus, for the parameter values used here, the virus is more efficient at shifting the phytoplankton to a lower equilibrium level than the predator. However, this efficiency will heavily depend on the virus and predator death rates. On the other hand, from Figure 3.3, there's a very narrow range of predator death rate values for which the system tends to $(P_3^*, 0, Z^*)$. Figure 4.53 uses the first eddy diffusivity profile, that of Figure 4.2. The low diffusivity region between 20 and 40m is also evident in these dynamics, but the virus has penetrated the sub-40m region within 25 days of being added.

We now investigate the situation of being at a coexistence equilibrium and shifting to a different coexistence equilibrium, where the phytoplankton concentration is lower, by the addition of a virus or predator. Figure 4.54 shows a system at $(P_2^*, V^*, 0)$ stable steady state, that is $(P, V, Z) = (1, 1, 0)$ in non-dimensional values, being shifted to $(P_3^*, 0, Z^*)$ upon addition of a predator. For the parameter values in Table 4.1 and $(\gamma, \nu) = (0.5, 1.38)\text{d}^{-1}$, $P_3^* < P_2^*$. The predator is added, with distribution as in Figure 4.50(a), after 25 days to a turbulent environment characterised by the eddy diffusivity profile in Figure 4.2. It is approximately day 400 when the phytoplankton near to the surface start to be brought under control. Again, the low diffusivity region between $z = 20$ and 40m slows the predator's descent. The predator population takes approximately 250 days to travel through this region.

By keeping parameter values as those in Table 4.1 and setting $(\gamma, \nu) = (0.08, 1.38)\text{d}^{-1}$, $P_2^* < P_3^*$. Therefore, consider a system at $(P_3^*, 0, Z^*) = (7.04, 0, 1)$, to 3sf in non-

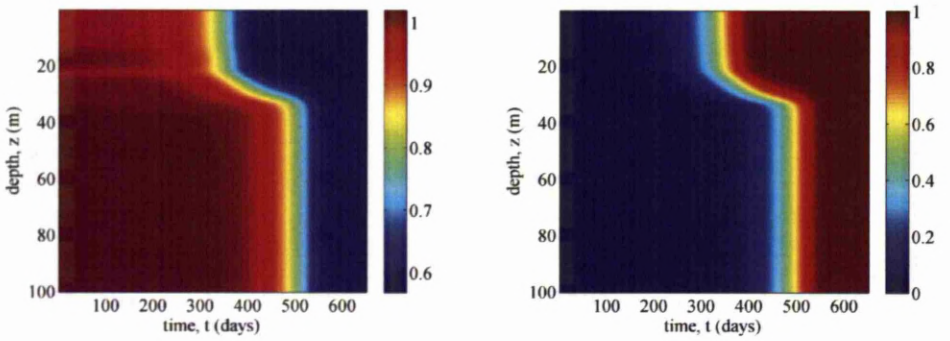

(a) P (b) Z

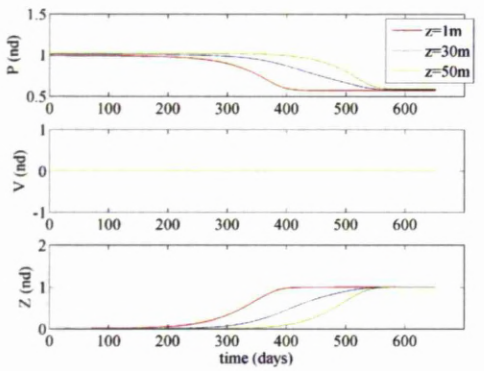

(c) Time series, few depths

Figure 4.51: Control, via addition of a predator to a phytoplankton community existing at carrying capacity, pushing the long-term behaviour to $(P_3^*, 0, Z^*)$ stable. Predator added after 25 days. The predator is added to the surface waters, with distribution shown in Figure 4.50(a). The eddy diffusivity is that of the first profile, Figure 4.2. Parameter values as in Table 4.1 with $(\gamma, \nu) = (0.6, 1.38)\text{d}^{-1}$. The top two figures show space-time plots of the phytoplankton and predator respectively, whilst the bottom plot is a time series solution of all three species at depths $z = 1\text{m}$, 30m and 50m. It should be noted that a propagating wave is present here, switching an unstable into a stable equilibrium, akin to the FPP-Fisher wave (although we have a two-component system here rather than one-component as in the KPP-Fisher equation).

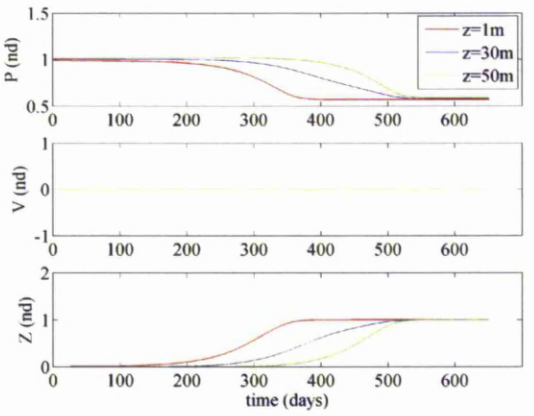

Figure 4.52: Control, via addition of a predator to a phytoplankton community existing at carrying capacity, pushing the long-term behaviour to $(P_3^*, 0, Z^*)$ stable. Predator added after 25 days. The predator is added to the surface waters, with the same distribution as shown in Figure 4.50(a), but with twice the maximum value. The eddy diffusivity is the first profile, Figure 4.2. Parameter values as in Table 4.1 with $(\gamma, \nu) = (0.6, 1.38)\mathrm{d}^{-1}$. The top two figures show space-time plots of the phytoplankton and predator respectively, whilst the bottom plot is a time series solution, for the full spatial resolution, of all three species.

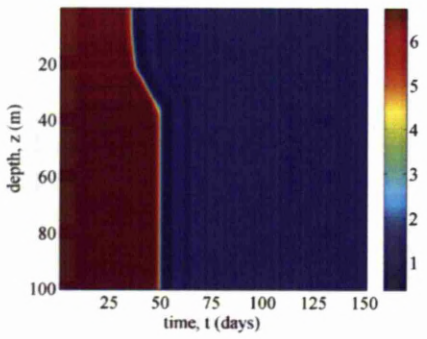

(a) P

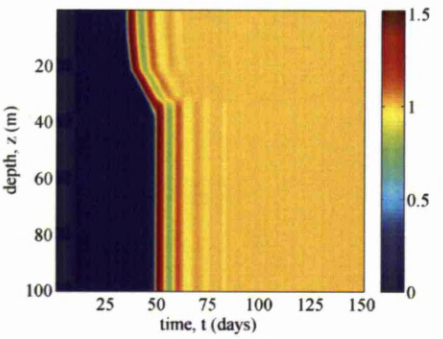

(b) V

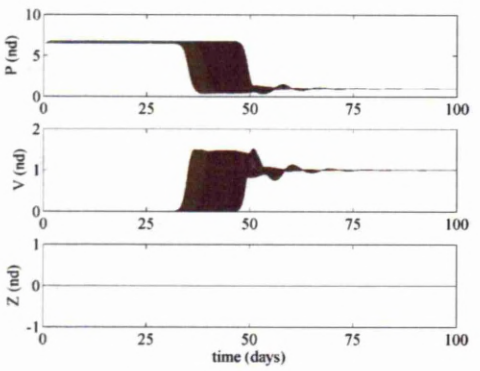

(c) Time series, all depths

Figure 4.53: Control, via addition of a virus to a phytoplankton community existing at carrying capacity, pushing the long-term behaviour to $(P_2^*, V^*, 0)$ stable. Virus added after 25 days. The virus is added to the surface waters, with distribution shown in Figure 4.50(b). The eddy diffusivity varies, as in Figure 4.2. Parameter values as in Table 4.1 with $(\gamma, \nu) = (0.3, 1.5)\mathrm{d}^{-1}$. The top two figures show space-time plots of the phytoplankton and virus respectively, whilst the bottom plot is a time series solution of all three species.

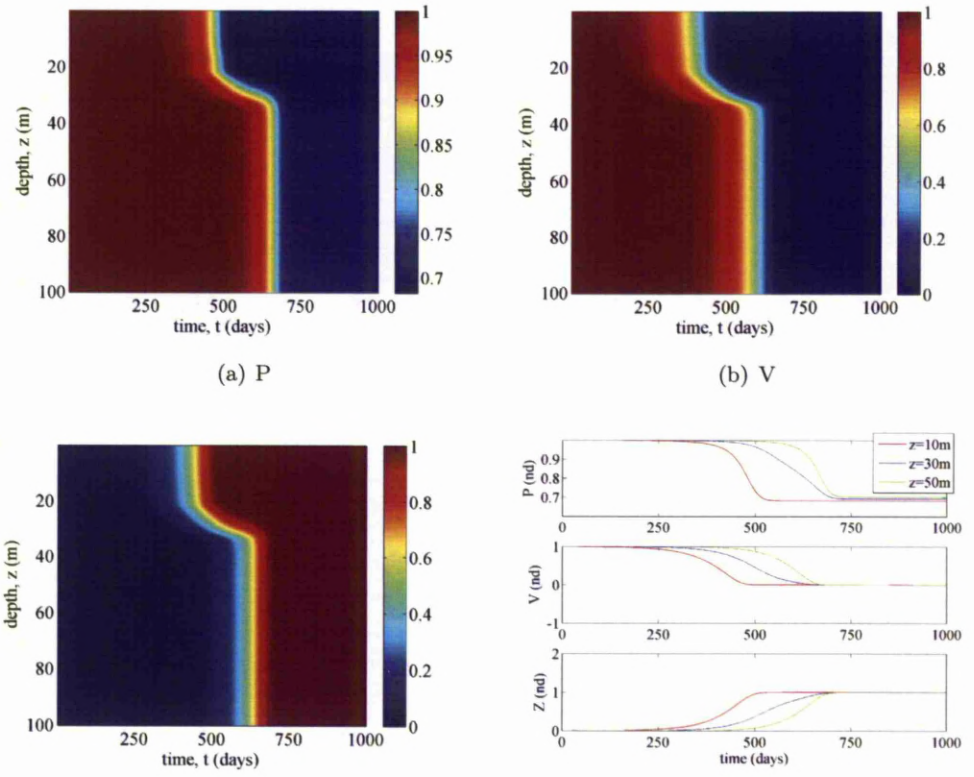

(a) P

(b) V

(c) Z

(d) Time series, few depths

Figure 4.54: Control, via addition of a predator to a $(P_2^*, V^*, 0) = (1, 1, 0)$ stable system, pushing the long-term behaviour to $(P_3^*, 0, Z^*)$ stable. Predator added after 25 days. The predator is added to the surface waters, with distribution shown in Figure 4.50(a). The eddy diffusivity profile is that of Figure 4.2. Other parameters are given in Table 4.1 with $(\gamma, \nu) = (0.5, 1.38)\mathrm{d}^{-1}$. The first three figures show space-time plots of the phytoplankton, virus and predator respectively. The fourth plot is a time series solution of all three species at depths $z = 10$, 30 and 50m.

dimensional values, steady state. Figure 4.55 shows the effects of adding a virus to this system after 25 days. Within the next 125 days, the phytoplankton is brought to its lower P_2^* equilibrium, where it coexists with the virus in the absence of predation. The eddy diffusivity profile is again that of Figure 4.2. The route of the virus to the lower part of the water column is again hampered by the low diffusivity region, taking about 25 days to penetrate.

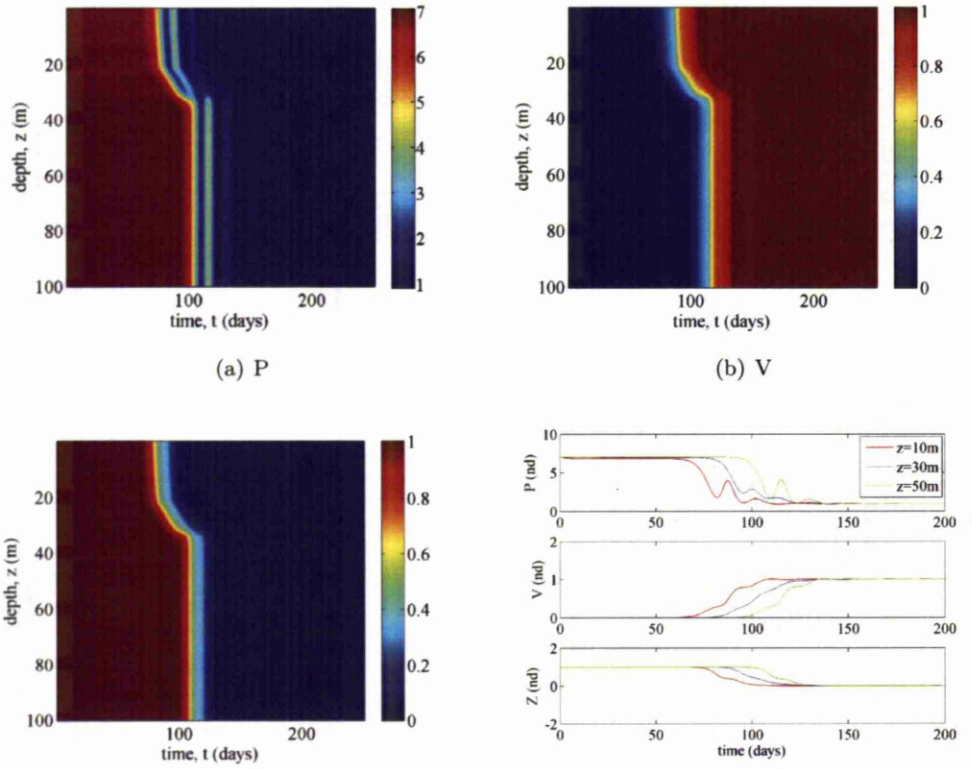

(a) P

(b) V

(c) Z

(d) Time series, few depths

Figure 4.55: Control, via addition of a virus to a $(P_3^*, 0, Z^*)$ stable system, pushing the long-term behaviour to $(P_2^*, V^*, 0)$ stable. Virus added after 25 days. The virus is added to the surface waters, with distribution shown in Figure 4.50(b). Initial conditions of P_0 varying as in Figure 4.12 and $(V_0, Z_0) = (0, 0.8876)$ in non-dimensional values. The eddy diffusivity is spatially variant, as shown in Figure 4.2. Parameter values as in Table 4.1 with $(\gamma, \nu) = (0.08, 1.38)\text{d}^{-1}$. The first three figures show space-time plots of the phytoplankton, virus and predator respectively, whilst the fourth plot is a time series solution of all three species at depths $z = 10$, 30 and 50m.

Another long term behaviour we may wish to alter is that of phytoplankton-predator limit cycles. By starting the simulation with the phytoplankton distributed as in Figure 4.12 with $(V_0, Z_0) = (0, 0.8876)$ in non-dimensional values, and by setting

$(\gamma, \nu) = (0.08, 1.3)\text{d}^{-1}$, the system will tend to $(P, 0, Z)$ stable limit cycle behaviour. Due to taking a long time to settle, we add the virus once regular oscillations are seen rather than stable limit cycles. The virus, with distribution as in Figure 4.50(b), is added after 100 days. Figure 4.56 shows the system, where the eddy diffusivity profile is that shown in Figure 4.2. Shortly after day 200 the oscillations have ceased. There is approximately a 50 day time delay between the surface region being reduced to $(P_2^*, V^*, 0)$ stable coexistence and the lower region being brought under control.

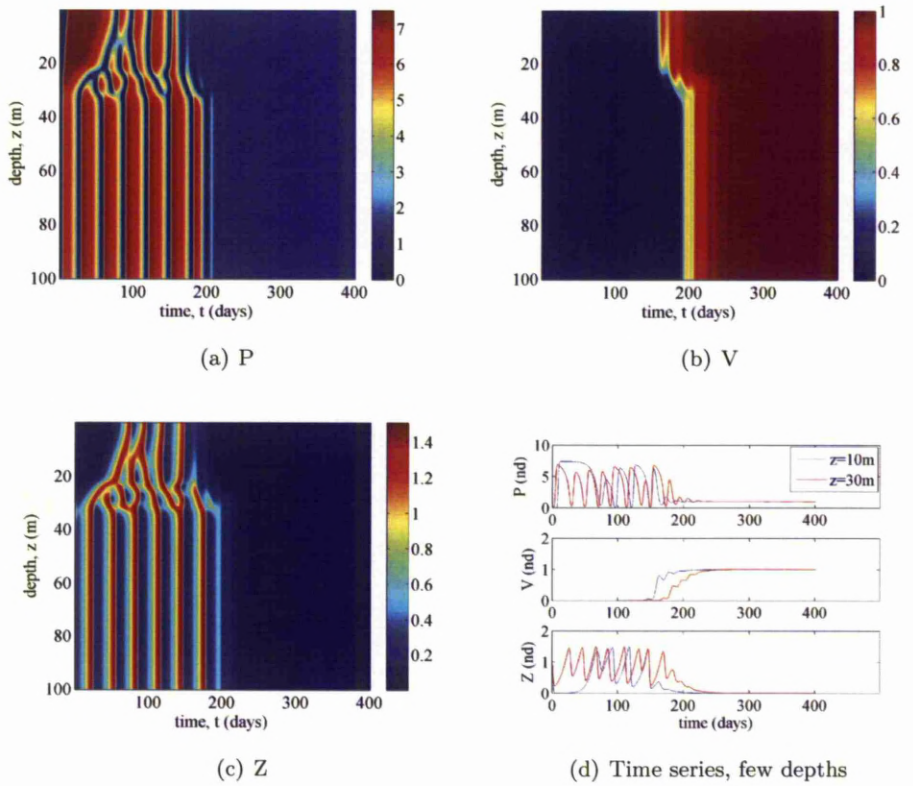

(a) P

(b) V

(c) Z

(d) Time series, few depths

Figure 4.56: Control, via addition of a virus to a $(P, 0, Z)$ oscillatory system, pushing the long-term behaviour to $(P_2^*, V^*, 0)$ stable. Virus added after 100 days. The virus is added to the surface waters, with distribution shown in Figure 4.50(b). Initial conditions of P_0 varying as in Figure 4.12 and $(V_0, Z_0) = (0, 0.8876)$ in non-dimensional values. The eddy diffusivity varies as in Figure 4.2. Parameter values as in Table 4.1 with $(\gamma, \nu) = (0.08, 1.3)\text{d}^{-1}$. The first three figures show space-time plots of the phytoplankton, virus and predator respectively, whilst the fourth plots is a time series solution of all three species at depths $z = 10\text{m}$ and $z = 30\text{m}$.

4.4 Discussion

In this chapter we have investigated how inclusion of spatial heterogeneity into the model of Chapter 3 affects the population dynamics. We tested Matlab's pdepe solver against its ode45 solver and then used this solver to simulate the population dynamics of a phytoplankton, virus and predator system. We investigated four long term behaviours of the system separately: $(P_2^*, V^*, 0)$ stable, $(P_3^*, 0, Z^*)$ stable, $(P, 0, Z)$ stable limit cycles and (P, V, Z) non-equilibrium coexistence. We initially incorporated spatially variant eddy diffusivity, comparing two profiles, whilst keeping the initial conditions uniform. We then explored the use of a non-uniform initial phytoplankton distribution, keeping other initial populations and eddy diffusivity uniform, before including non-uniform eddy diffusivity together with the non-uniform initial phytoplankton distribution. We close the results section with an investigation of the use of a virus or predator as a phytoplankton control mechanism, where the phytoplankton distribution is initially non-uniform, comparing a turbulent and still fluid environment.

We found Matlab's pdepe solver to give a good solution compared to ode45, for all four long term behaviours. The most marked difference in solution between the two solvers occurred where the system exhibited predator-prey limit cycles in the long term, with zero eddy diffusivity. For uniform initial conditions, there was no significant difference in solution for large or zero eddy diffusivity, as expected. Introducing a spatially variant eddy diffusivity to a system tending to phytoplankton-virus stable coexistence in the long term was able to generate a small amount of heterogeneity, even though initial conditions were uniform. Comparing the two eddy diffusivity profiles revealed slightly more heterogeneity in the system for the second eddy diffusivity profile, where the presence of a region of low eddy diffusivity was more pronounced. Inclusion of a spatially variant initial phytoplankton population generated a large amount of heterogeneity when the eddy diffusivity was zero or spatially variant. The large value of eddy diffusivity considered spread the phytoplankton population too quickly for any heterogeneity to occur in the other species populations.

For the system tending to phytoplankton-predator coexistence in the long term we saw emergence of the virus, which was driven to extinction as the phytoplankton and predator populations moved towards equilibrium. For uniform initial conditions, a spatially variant eddy diffusivity value generated heterogeneity in the virus population. The second diffusivity profile allowed more heterogeneity in the virus population than profile 1 and also allowed the virus to reach a higher maximum value. Incorporation of a non-uniform initial phytoplankton distribution increased the length of time before the virus was able to emerge, however, when the virus did emerge it was capable of much higher maximum values and took longer to become extinct. The space-time plots showed the virus predominantly existing where the predator population was minimal. The solution varied significantly between the two eddy diffusivity profiles when the

initial phytoplankton distribution was spatially variant. The virus existed solely in the surface water for the second profile, in the time frame considered, compared to it existing above and below the low diffusivity region for the first profile. There was also more heterogeneity in the phytoplankton population for the first eddy diffusivity profile.

When the system tended to phytoplankton-predator limit cycles in the long term, a spatially variant initial phytoplankton distribution was required before we saw any heterogeneity in the water column. This was similar for the system tending to phytoplankton -virus-predator non-equilibrium coexistence in the long term. A small amount of heterogeneity was present here for spatially variant eddy diffusivity with uniform initial conditions, but a non-uniform initial phytoplankton population introduced significant heterogeneity, except for when the large value of eddy diffusivity was considered and the phytoplankton population was smoothed too quickly for heterogeneity to appear.

Finally, we considered phytoplankton control by the addition of a virus or predator to the surface of the water column. We found both the virus and predator to be capable of altering the long term behaviour of the system. For the parameter values used, there was heterogeneity present once either the virus or predator had been added to a phytoplankton population existing alone at carrying capacity. Spatially variant eddy diffusivity allowed the virus or predator to be present throughout the water column, but it took a significant amount of time for either control mechanism to penetrate the low diffusivity region. This was particularly striking when adding a predator, in our simulations. We also considered altering the long term behaviour of the system from $(P_2^*, V^*, 0)$ stable to $(P_3^*, 0, Z^*)$ stable, and vice versa, and from $(P, 0, Z)$ limit cycle behaviour to $(P_2^*, V^*, 0)$ stable. We found all three examples to work as a control mechanism, with only a relatively small period where some regions of the water column had been brought under control whilst other regions still remained at their previous equilibrium level. As discussed in Chapter 3, the choice between altering the dynamics to $(P_2^*, V^*, 0)$ or $(P_3^*, 0, Z^*)$ stable is dependent on P_2^* being less than P_3^*, which is dependent on parameter values.

These results can be used to consider the use of a virus or predator as a harmful algal bloom control in a turbulent environment. Specifically, we have compared the controllability of HaV and *O. marina* and also considered the time taken for a virus or predator to penetrate the low diffusivity region, where Sharples et al. (2001) recorded a chlorophyll maximum, which is present in well-stratified environments. The model presented could be further used to investigate other species-specific systems and also to determine the turbulent conditions offering the virus or predator optimal controllability. Our use of space-varying turbulent parameters, whilst keeping other parameters uniform, offers a good insight into how the presence of a realistic turbulence profile alters the population dynamics. However, utility of results, in terms of comparison with

experimental results and virus or predator control investigations, would be improved by the inclusion of spatial variance into other parameters.

The data used here to determine the eddy diffusivity profiles is that used in Sharples et al. (2001). Their data is obtained at numerous time points, showing significant variation in the eddy diffusivity profile of the water column over time. Incorporation of time variance into this model would therefore make a good addition and would improve the ability to compare results of the model with observed data. Another improvement to this model would be the inclusion of non-uniform phytoplankton growth. Our current model is rather simplified, using a constant value throughout the water column. Phytoplankton growth is related to its capacity for photosynthesis, nutrient supply, respiration losses and time spent within the euphotic zone - the surface region of the ocean with sufficient light to allow photosynthesis (Ganf, 1974). Most phytoplankters face opposing vertical gradients in light versus nutrient supplies (Jäger et al., 2010) and also light is never homogeneously distributed (Huisman and Weissing, 1995), leading to spatial heterogeneity in the phytoplankton growth rate. Turbulence can also play a role in how phytoplankton growth varies with depth. Turbulence can reduce sedimentation losses but increases downward mixing of algae to more light-limited depths (Jäger et al. (2010) and references therein). Models investigating phytoplankton growth rate with depth already exist. For example, Huisman and Weissing (1995) developed a model to predict the outcome of competition for nutrients and light in a mixed water column. Huisman et al. (2004) developed a model that predicted changes in turbulent mixing to affect species composition of phytoplankton communities, which was supported by their field observations.

Chapter 5

Conclusions

In this thesis we have investigated the use of viral infection and predation in controlling phytoplankton population levels. Initially we considered the phytoplankton-virus and phytoplankton-predator contact rates, comparing the effects of phytoplankton swimming and turbulence. We analysed two published contact rate models in the context of virus-phytoplankton-predator interactions. We studied the phytoplankton-virus contact rate by adapting a previous diffusion model for nutrients. We verified asymptotic results expressing the phytoplankton-virus contact rate explicitly as a function of biological parameters (virus and phytoplankton diameter, phytoplankton swimming speed) and of physical parameters (temperature, fluid viscosity). Analysis of contact rates was extended to include the effects of ambient flows including steady shear and fluctuating shear; the latter being an appropriate approximation for turbulent flows at sufficiently small scales. Levels of turbulence intensity below which swimming can affect the contact rate were quantified. The second half of Chapter 2 studied the phytoplankton-predator contact rate, analysing previous work on encounter rates in turbulence. We re-examined two encounter rate derivations for predators and prey moving at fixed speeds, explicitly noting limitations of the models when applied to a specific phytoplankton-predator system. We re-examined how turbulence is included, again noting limitations when applied to a specific phytoplankton-predator system.

All of the above results were analysed for a range of biological parameters relevant to example HAB phytoplankton and a known virus and predator. We demonstrated that phytoplankton swimming ability can alter the phytoplankton-virus contact rate. For example, in still fluid for typical parameters, the ability to swim can cause up to a five-fold increase in contact rate from that predicted for a stationary phytoplankton cell. In contrast, calculations for typical values of turbulence show water motions do not have a significant effect on the phytoplankton-virus contact rates for non-motile phytoplankton. We calculated that, for relevant biological and physical parameters, there are turbulent regimes where swimming behaviour can still contribute to the phytoplankton-virus contact rate. We noted that several assumptions of the

phytoplankton-predator contact rate were either invalid or questionable for the primary phytoplankton-predator species considered: the radius of the perception sphere was much smaller than the Kolmogorov microscale, an assumption necessary in equation (2.74); it is not clear how appropriate the swept volume approach is at the low Reynolds numbers appropriate for the predator considered, *O. marina*, (in which the act of swimming drags a large quantity of fluid along with it). Subject to the previous caveats, we calculated that, for typical parameter values of *H. akashiwo* and *O. marina*, the ability of prey to swim doesn't significantly affect the phytoplankton-predator contact rate and that typical turbulence intensities also don't affect the contact rate. However, in contrast, for a larger example zooplankton predator (as opposed to the microzooplankton predator *O. marina*) and faster swimming prey, we demonstrated how the contact rate could increase with increasing turbulence intensity and swimming speeds.

In Chapter 3 we developed a phytoplankton-virus-predator model which couples a published free-living virus model, reduced to ignore the time delay associated with lysis, with a published model based on experimental data for the focal phytoplankton-predator species. Five possible long term dynamics of the model were determined using linear stability analysis, phase plane analysis and numerical simulation. Possible outcomes were graphically depicted on a diagram of predator death rate against viral decay rate.

We analysed possible control mechanisms to suppress phytoplankton blooms. For typical parameters, it was demonstrated how adding a small concentration of virions could rapidly degrade a phytoplankton bloom (phytoplankton alone at carrying capacity) whereas addition of predators was less successful. We noted the importance of stochastic effects in the possible extinction of a bloom. For example, in long-term cyclic behaviour, trough concentrations may be sufficiently low for stochastic events to eliminate the phytoplankton population. We calculated that unfeasibly large quantities of viruses or predators would be needed to prevent phytoplankton populations from increasing in the short term, thus preventing bloom initiation. Model results were compared to a field phytoplankton-virus study and mesocosm phytoplankton-predator study, and explanations for differences were proposed. We analysed how changes to the contact rate due to swimming and turbulence, as calculated in Chapter 2, altered the population dynamics and calculated how increasing the phytoplankton-virus contact rate could shift the long term dynamics. For example, shifting the phytoplankton from carrying capacity to a stable phytoplankton-virus system or eliminating the existence of a phytoplankton-predator stable equilibrium. We also found changing the phytoplankton-virus contact rate to alter the transient dynamics. Increasing the phytoplankton-virus contact rate was found to lower the phytoplankton-virus equilibrium level and reduce the initial peak in the phytoplankton population. We suggested how to modify the phytoplankton-predator grazing model so as to include changes

in the phytoplankton-predator contact rate. However, as noted in Chapter 2, the phytoplankton-predator contact rate was not significantly affected by typical values of swimming and turbulence. Chapter 3 closed with calculations of how the long term dynamics would change for different *H. akashiwo* viruses with published estimates of diameter and burst sizes.

Chapter 4 extended the ODE population model of Chapter 3 to allow for spatial variation in the phytoplankton-virus-predator populations. We analysed field data at two time points to obtain depth profiles for the energy dissipation rate to estimate the phytoplankton-predator and phytoplankton-virus contact rates as a function of depth, using results from Chapter 2, assuming the phytoplankton to be non-motile. We found less than a 10% variation in the phytoplankton-virus contact rate across the depths of the water column and even less variation in the phytoplankton-predator contact rate. The field data was re-analysed to provide a depth profile of the Brunt Vaisala frequency, and combined with the energy dissipation rate to obtain depth profiles for eddy diffusivity.

Numerical solution of the spatial dynamics for different choices of parameters yielded the following results. When the phytoplankton, virus and predator are initially uniformly distributed, some spatial heterogeneity is introduced prior to the system stabilising to a long term equilibrium. This is due to the variation in contact rate with depth (due to variable energy dissipation rates), as variation in eddy diffusion alone is not able to generate heterogeneity from an initially uniform distribution. When the phytoplankton population is initially non-uniformly distributed, a wide range of transient spatial dynamics are possible: Figures 4.16 and 4.20 demonstrate several transient peaks of the predator population in the lower part of the water column prior to the system stabilising to a phytoplankton-virus stable equilibrium; Figures 4.28 and 4.31 demonstrate a long transient period where the viral population dominates in the upper part of the water column and the predators dominate in the lower part before the long term phytoplankton-predator equilibrium is realised. Considerable spatial variation is also observed when considering transient dynamics which lead to long term cyclic behaviour. Finally, we calculated how addition of viruses or predators to the surface layer could control a phytoplankton bloom, either shifting the long term dynamics away from the phytoplankton existing alone at carrying capacity to phytoplankton-predator or phytoplankton-virus equilibrium, or shifting between phytoplankton-predator and phytoplankton-virus equilibria.

In summary, we have considered which parameters are key to the $P-V$ and $P-Z$ contact rates, both generally and for three specific species. We quantified levels of turbulence intensity below which swimming can affect the $P-V$ contact rate and found neither *H. akashiwo* swimming or typical turbulent intensities to affect the *H. akashiwo* - *O. marina* contact rate, both which have practical utility. We developed a population model that compared well with observed results, thus allowing it to be used

confidently when considering $P-V-Z$ systems. The vast majority of parameter values have good estimates for *H. akashiwo*, HaV and *O. marina* recited here allowing the system to be quickly and easily compared to experiments involving these species. We also extended the model to include spatial variation, which allows users to compare against field data rather than just lab. experiments. Certain results of the thesis could also be considered experimentally. For instance, our suggestion that HaNIV and HaRNAV would better control *H. akashiwo* than HaV could be investigated in the lab. Similarly, testing whether alteration of long term behaviour or reduction of the phytoplankton population in the short term is the most effective use of the virus or predator would allow comparison with our results. Experimental approximation of the $P-V$ and $P-Z$ volume clearance rates, in different fluid regimes, would also allow verification of our theoretical results from Chapter 2.

In terms of further research directions, incorporation of variable swimming velocity into the contact rate calculations of Chapter 2 would be more realistic. A gaussian plankton swimming distribution, and irregular predator trajectory, have already been considered for the $P-Z$ contact rate by Lewis and Pedley (2000) and Lewis and Bala (2006) respectively. Another key area for further work in Chapter 2 is that of the $P-V$ contact rate for motile phytoplankton in turbulent fluid. Ideally, more information regarding the enhancement of flux at low and intermediate values of Pe would be sought. Also, investigation of the small-scale interactions between swimming phytoplankton and microzooplankton using hydrodynamic models (e.g. solutions of Stokes equations) to investigate how the encounter rate is affected by swimming and imposed external flows could be conducted (e.g. Ishikawa et al., 2006). Continuing the work of Chapter 3 could involve experimentally determining if/how K_{IR} changes with turbulence and phytoplankton swimming, and how this may alter other parameters in the model. Determining how generic the phytoplankton-virus-predator dynamics are to the specific predation model and viral infection model used could be investigated. An aspect of the phytoplankton-virus system that hasn't been considered throughout the thesis is the length of the lytic cycle and thus incorporation of an infected class of phytoplankton. Simulations in Bratbak et al. (1998) imply that increasing the length of the lytic cycle will increase the maximum population size of the phytoplankton and also increase the length of time before the phytoplankton population declines. A study of the differences between our results and the previous results reviewed in Chapter 1 for $S-I$ type viral models and other predation models would make a valuable contribution. Incorporation of diversity into the models of Chapters 3 and 4, by inclusion of multiple virus strains for example, would enable greater comparison with published observations. However, our current model supports the competitive exclusion principle, which we have previously discussed to have limited applicability here. Experimentation to test our control of bloom ideas could be conducted. More analysis of stochastic levels/ minimum community size would also be valuable. Incorporation

of time dependence into the spatial model of Chapter 4 would also improve the ability to compare results of the model with observed data. Another major improvement to this model would be the inclusion of non-uniform phytoplankton growth, due to light and nutrients varying with depth (e.g. Huisman and Weissing, 1995).

Appendix A

Contact rates

A.1 Phytoplankton-Virus

A.1.1 Purely diffusional flux

A.1.1.1 Steady state equation

The dimensional diffusion equation:

$$\frac{\partial V}{\partial t} = D_v \nabla^2 V. \tag{A.1}$$

Find the steady state by setting $\frac{\partial V}{\partial t} = 0$. Writing $\nabla^2 V$ in spherical coordinates (r, ϕ, θ), the steady state diffusion equation is:

$$D_v \left(\frac{1}{r^2} \frac{\partial}{\partial r} \left(r^2 \frac{\partial V}{\partial r} \right) \right) = 0. \tag{A.2}$$

Integrating gives

$$r^2 \frac{\partial V}{\partial r} = c_1. \tag{A.3}$$

Rewriting as $\frac{\partial V}{\partial r} = \frac{c_1}{r^2}$ and integrating gives $V = -\frac{c_1}{r} + c_2$. Boundary conditions:

$$V = 0 \text{ at } r = r_0 : c_2 - \frac{c_1}{r_0} = 0 \Rightarrow c_1 = r_0 c_2; \tag{A.4}$$

$$V = V_\infty \text{ as } r \to \infty : -\frac{c_1}{(\infty)} + c_2 = V_\infty \Rightarrow c_2 = V_\infty \text{ and } \therefore c_1 = r_0 V_\infty. \tag{A.5}$$

The steady state of the diffusion equation, with boundary conditions (A.4, A.5) is therefore

$$V = V_\infty \left(1 - \frac{r_0}{r} \right). \tag{A.6}$$

A.1.1.2 Flux

Total flux:

$$\int D_v \frac{\partial V}{\partial r} dS. \tag{A.7}$$

In spherical coordinates (r, ϕ, θ),

$$dS = r^2 \sin\theta d\theta d\phi. \tag{A.8}$$

Differentiating equation A.6 with respect to r, the total flux (and thus the purely diffusional $P - V$ contact rate) becomes:

$$\begin{aligned}
\text{Total flux} &= D_v V_\infty \int_0^{2\pi} \int_0^{\pi} r^2 \sin\theta \frac{r_0}{r^2} d\theta d\phi && \text{(A.9)} \\
&= D_v V_\infty \int_0^{\pi} 2\pi r_0 \sin\theta d\theta && \text{(A.10)} \\
&= [-2\pi \cos\theta D_v r_0 V_\infty]_0^{\pi} && \text{(A.11)} \\
&= 4\pi D_v r_0 V_\infty. && \text{(A.12)}
\end{aligned}$$

A.1.2 Advection-diffusion equation in spherical coordinates

Non-dimensional advection-diffusion equation:

$$\mathrm{Pe}\,(\mathbf{U} \cdot \nabla V) = \nabla^2 V, \tag{A.13}$$

with boundary conditions:

$$\begin{aligned}
V &= 0 \text{ at } r = 1, \text{ and} && \text{(A.14)} \\
V &= 1 \text{ for } r \to \infty. && \text{(A.15)}
\end{aligned}$$

In spherical coordinates $\mathbf{U} = (U_r, 0, U_\theta)$,

$$\mathbf{U} \cdot \nabla V = U_r \frac{\partial V}{\partial r} + \frac{U_\theta}{r} \frac{\partial V}{\partial \theta}, \tag{A.16}$$

where

$$\begin{aligned}
U_r &= \frac{1}{r^2 \sin\theta} \frac{\partial \psi}{\partial \theta} = \left(1 - \frac{3}{2r} + \frac{1}{2r^3}\right) \cos\theta, && \text{(A.17)} \\
U_\theta &= -\frac{1}{r \sin\theta} \frac{\partial \psi}{\partial r} = -\left(1 - \frac{3}{4r} - \frac{1}{4r^3}\right) \sin\theta, && \text{(A.18)}
\end{aligned}$$

for Stokes flow:

$$\psi = \frac{1}{2}\left(r^2 - \frac{3r}{2} + \frac{1}{2r}\right)\sin^2\theta. \tag{A.19}$$

Hence,

$$\mathbf{U}\cdot\nabla V = \left(1 - \frac{3}{2r} + \frac{1}{2r^3}\right)\cos\theta\frac{\partial V}{\partial r} - \frac{\sin\theta}{r}\left(1 - \frac{3}{4r} - \frac{1}{4r^3}\right)\frac{\partial V}{\partial\theta}. \tag{A.20}$$

Similarly,

$$\nabla^2 V = \frac{1}{r^2}\frac{\partial}{\partial r}\left(r^2\frac{\partial V}{\partial r}\right) + \frac{1}{r^2\sin\theta}\frac{\partial}{\partial\theta}\left(\sin\theta\frac{\partial V}{\partial\theta}\right). \tag{A.21}$$

The non-dimensional advection-diffusion equation in spherical coordinates for Stokes flow is therefore:

$$\begin{aligned}&\frac{1}{r^2}\left\{\frac{\partial}{\partial r}\left(r^2\frac{\partial V}{\partial r}\right) + \frac{1}{\sin\theta}\frac{\partial}{\partial\theta}\left(\sin\theta\frac{\partial V}{\partial\theta}\right)\right\}\\ =\ &\mathrm{Pe}\left[\left(1 - \frac{3}{2r} + \frac{1}{2r^3}\right)\cos\theta\frac{\partial V}{\partial r} - \frac{\sin\theta}{r}\left(1 - \frac{3}{4r} - \frac{1}{4r^3}\right)\frac{\partial V}{\partial\theta}\right].\end{aligned} \tag{A.22}$$

A.1.3 Asymptotic expansion

We will first try to solve equation (2.18) in the limit $\mathrm{Pe} \gg 1$ by taking the regular asymptotic expansion (Leal, 2007):

$$V = V_0 + \sum_{n=1}^{N} F_n(\mathrm{Pe}^{-1})\, V_n, \tag{A.23}$$

where $F_n(\mathrm{Pe}^{-1})$ are unspecified gauge functions, except for the requirement that

$$\lim_{\epsilon\to 0}\frac{F_{n+1}(\epsilon)}{F_n(\epsilon)} \to 0 \text{ for all } n \tag{A.24}$$

is satisfied in the domain of interest. This is a necessary condition for asymptotic convergence (Leal, 2007). From equation (A.23), as $\mathrm{Pe}\to\infty$ then $V \to V_0$. Thus, in the limit $\mathrm{Pe}\to\infty$, equation (2.4) becomes:

$$\mathbf{U}\cdot\nabla V_0 = 0. \tag{A.25}$$

Therefore, ∇V_0 is perpendicular to $\mathbf{U}$ everywhere. By definition, the streamfunction, ψ, is also constant along lines parallel to $\mathbf{U}$ (Leal, 2007):

$$\mathbf{U}\cdot\nabla\psi = 0 \tag{A.26}$$

and comparing with equation (A.25) we can conclude that

$$V_0 = V_0(\psi), \tag{A.27}$$

that is, V_0 is constant on streamlines of the flow. In Stokes' solution for streaming flow past a sphere, all streamlines are open. That is, they begin "at infinity" on one side of the sphere and end "at infinity" on the other side (Leal, 2007). Since boundary condition (2.6) states that $V = 1$ far away from the phytoplankton, we can conclude $V = 1$ on every streamline. Therefore,

$$V = 1 \tag{A.28}$$

everywhere in the outer region. However, the boundary conditions state that $V_0 = 0$ at the phytoplankton surface and $V_0 = 1$ far from the cell surface. As both conditions cannot be satisfied, a regular expansion of the form (A.23) doesn't exist and we need to use matched asymptotics. Figure A.1 shows the region where these two solutions must be matched.

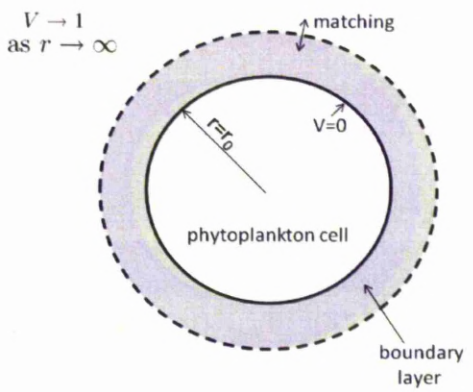

Figure A.1: Matching asymptotic approximations

In order to find equation (A.25) we assumed that the sphere radius was an appropriate characteristic length scale on which to nondimensionalise. The resultant nondimensional form of the advection-diffusion equation (2.4) implies diffusion can be neglected everywhere relative to advection for Pe large. However, molecular diffusion is the only mechanism for transport of viral particles across the phytoplankton cell wall. We must therefore conclude that the sphere radius is not an appropriate characteristic length scale near the sphere surface (Leal, 2007). A more appropriate characteristic length scale near the sphere surface may be the length scale over which diffusion takes place. In order to determine the characteristic length scale over which diffusion takes place, L, we must first consider the timescale characteristic of the diffusion process:

$$t^* = O\left(\frac{L^2}{D_v}\right), \tag{A.29}$$

where L is the length scale over which diffusion takes place and D_v is viral diffusivity. On the other hand, the characteristic timescale for a fluid element to move completely around the sphere, due to advection, is

$$\hat{t} = O\left(\frac{r_0}{U}\right), \tag{A.30}$$

where U is the relative velocity between the sphere and surrounding fluid (Leal, 2007). Thus, $\hat{t}$ provides an estimate of the time available within which diffusion must remove viral particles from the surrounding fluid. However, since U will rapidly decrease near the sphere surface, $\hat{t}$ is actually an underestimate. Substituting $\hat{t}$ for t^*, we find the characteristic length scale near the sphere surface to be:

$$L^2 \sim \frac{r_0 D_v}{U}, \tag{A.31}$$

which is the radial distance from the sphere over which it is expected viral particles will be taken across the cell wall by diffusion. This region is called the boundary layer. Nondimensionalising with respect to r_0 ($L^2 = r_0^2 \ell^2$):

$$\ell^2 \sim \left(\frac{D_v}{r_0 U}\right) = \mathrm{Pe}^{-1}. \tag{A.32}$$

As mentioned previously, $\hat{t}$ is an underestimate and so the accuracy of equation (A.32) is unknown. However, it does establish that the distance the boundary layer extends to from the sphere surface decreases as Pe increases (Leal, 2007). This will now be explored more rigorously.

Rescale equation (2.18) by setting

$$r - 1 = y \tag{A.33}$$

so y is a radial variable that is zero at the sphere surface. Since we are dealing with a very thin boundary layer it is desirable to rescale to a new nondimensional radial variable Y:

$$y = \mathrm{Pe}^{-m} Y. \tag{A.34}$$

Setting $m > 0$ makes Y larger than y. Now the radial distance is not so impossibly small and we can better judge the relative size of other terms in the full equation (2.18). Substituting (A.34) into the advection-diffusion equation (2.18) we can choose m to retain both advection and the largest diffusion terms. The Taylor expansion for $(r-1) = y \ll 1$ of U_r and U_θ is (Leal, 2007):

$$\begin{aligned} u_r &= u_r|_{r=1} + (r-1)\left(\frac{\partial u_r}{\partial r}\right)\Big|_{r=1} + \frac{(r-1)^2}{2}\left(\frac{\partial^2 u_r}{\partial r^2}\right)\Big|_{r=1} + \ldots + \\ &\sim \frac{3}{2}\cos\theta(r-1)^2 + O\left((r-1)^3\right) \end{aligned} \tag{A.35}$$

and

$$\begin{aligned} u_\theta &= u_\theta|_{r=1} + (r-1)\left(\frac{\partial u_\theta}{\partial r}\right)\Big|_{r=1} + \ldots + \\ &\sim \frac{3}{2}\sin\theta(r-1) + O\left((r-1)^2\right). \end{aligned} \tag{A.36}$$

Introducing the scaling (A.34) gives

$$u_r \sim \frac{3}{2}\cos\theta\left(\mathrm{Pe}^{-2m}Y^2\right) + O\left(\mathrm{Pe}^{-3m}Y^3\right), \tag{A.37}$$

$$u_\theta \sim \frac{3}{2}\sin\theta\left(\mathrm{Pe}^{-m}Y\right) + O\left(\mathrm{Pe}^{-2m}Y^2\right). \tag{A.38}$$

Now rescale the full advection-diffusion equation (2.18) using (A.37) and (A.38):

$$\begin{aligned} \frac{1}{\mathrm{Pe}}\left\{\frac{\partial^2 V}{\partial Y^2}\mathrm{Pe}^{2m} + \frac{2\mathrm{Pe}^m}{1+\mathrm{Pe}^{-m}Y}\frac{\partial V}{\partial Y} + \frac{1}{(1+\mathrm{Pe}^{-m}Y)^2\sin\theta}\frac{\partial}{\partial\theta}\left(\sin\theta\frac{\partial V}{\partial\theta}\right)\right\} \\ = \left[\frac{3}{2}Y^2\mathrm{Pe}^{-2m}\cos\theta + O\left(\mathrm{Pe}^{-3m}Y^3\right)\right]\mathrm{Pe}^m\frac{\partial V}{\partial Y} + \\ + \frac{1}{1+\mathrm{Pe}^{-m}Y}\left[\frac{3}{2}Y\mathrm{Pe}^{-m}\sin\theta + O\left(\mathrm{Pe}^{-2m}Y^2\right)\right]\frac{\partial V}{\partial\theta}. \end{aligned} \tag{A.39}$$

Retaining largest terms on both sides (for $\mathrm{Pe} \gg 1$):

$$\mathrm{Pe}^{2m-1}\frac{\partial^2 V}{\partial Y^2} + O\left(\mathrm{Pe}^{m-1}\right) = \frac{3}{2}\left[Y^2\cos\theta\frac{\partial V}{\partial Y} + Y\sin\theta\frac{\partial V}{\partial\theta}\right]\mathrm{Pe}^{-m} + O\left(\mathrm{Pe}^{-2m}Y^2\right). \tag{A.40}$$

To retain both diffusion and advection in the boundary layer region for $Pe \gg 1$, $2m - 1 = -m$, that is $m = \frac{1}{3}$. Thus the boundary layer thickness is of the order $\mathrm{Pe}^{-\frac{1}{3}}$ rather than the $\mathrm{Pe}^{-\frac{1}{2}}$ prediction of equation (A.32). The inner region solution is therefore

$$\frac{\partial^2 V}{\partial Y^2} = \frac{3}{2}\left[Y^2\cos\theta\frac{\partial V}{\partial Y} + Y\sin\theta\frac{\partial V}{\partial\theta}\right] + O\left(Pe^{-\frac{1}{3}}\right). \tag{A.41}$$

We thus have a solution near the sphere and in the far field. Now we must match the two solutions at the boundary between the inner and outer region. Since $V = 1$ everywhere in the outer region, it must still be true at the outer boundary of the inner region. Thus the outer boundary condition of the inner solution is that

$$V \to 1 \text{ for } Y \gg 1 \text{ as } \mathrm{Pe} \to \infty. \tag{A.42}$$

Equation (A.41) must now be solved subject to the boundary conditions:

$$V = 0 \text{ at } Y = 0, \tag{A.43}$$

$$V \to 1 \text{ for } Y \gg 1 \text{ as } \mathrm{Pe} \to \infty. \tag{A.44}$$

An analytic approximation of V can be found by introducing a similarity solution of the form (Leal, 2007):

$$V = V(\varsigma), \text{ where } \varsigma = \frac{Y}{g(\theta)}, \tag{A.45}$$

into equation (A.41). The function $g(\theta)$ determines the dependence of the boundary-layer thickness on θ. Leal (2007) shows the general solution to be:

$$V = c_1 + c_2 \int_0^{\varsigma} e^{-t^3} dt. \tag{A.46}$$

Applying the boundary conditions (A.43) and (A.44) allows c_1 and c_2 to be found, such that:

$$V = \frac{\int_0^{\varsigma} e^{-t^3} dt}{\int_0^{\infty} e^{-t^3} dt}. \tag{A.47}$$

A.2 Phytoplankton-Predator

A.2.1 Derivation of contact rate in still fluid

Since ω exists, the probability that it occurs within some solid angle element, $d\Omega$, is 1 (Gerritsen and Strickler, 1977):

$$\int_0^{\pi} \int_0^{2\pi} k \sin\theta_U d\phi_U d\theta_U = 1. \tag{A.48}$$

Therefore, $k = \dfrac{1}{4\pi}$ and

$$\mathrm{CR_z} = \frac{PR^2}{4} \int_0^{\pi} \int_0^{2\pi} U \sin(\theta_U)\, d\phi_U d\theta_U. \tag{A.49}$$

By the law of cosines, the relative speed, U, is given by

$$U = \sqrt{(\mathbf{U_z} - \mathbf{U_p}) \cdot (\mathbf{U_z} - \mathbf{U_p})} = \sqrt{U_p^2 + U_z^2 - 2U_p U_z \cos\theta_U}. \tag{A.50}$$

Using equation (A.50) and performing the integral of equation (A.49) for θ_U and ϕ_U, the encounter rate of a predator with its motile prey in a still fluid is given by (Gerritsen and Strickler, 1977):

$$\mathrm{CR_z} = \pi P R^2 \frac{\left(U_\mathrm{P}^2 + 3U_\mathrm{Z}^2\right)}{3U_\mathrm{Z}} \qquad U_\mathrm{Z} \geq U_\mathrm{P}. \tag{A.51}$$

A.2.2 Derivation of contact rate in turbulent fluid

In order to estimate (2.69) it is convenient to apply the following change of variables (Lewis and Pedley, 2000):

$$\mathbf{U}(\mathbf{x},\mathbf{r},t) = \mathbf{V_Z}(\mathbf{x},t) - \mathbf{V_P}(\mathbf{x}+\mathbf{r},t), \tag{A.52}$$

$$\mathbf{V}(\mathbf{x},\mathbf{r},t) = \frac{\sigma_{V_z}^2 \mathbf{V_P}(\mathbf{x}+\mathbf{r},t) + \sigma_{V_p}^2 \mathbf{V_Z}(\mathbf{x},t)}{\sigma_{V_z}^2 + \sigma_{V_p}^2}, \tag{A.53}$$

where $\sigma_{V_p}^2$ and $\sigma_{V_z}^2$ are the ensemble average variances of $\mathbf{V_P}$ and $\mathbf{V_Z}$ respectively:

$$\sigma_{V_p}^2 = \frac{1}{3}\left(<\mathbf{V_p}\cdot\mathbf{V_p}> - <\mathbf{V_p}>\cdot<\mathbf{V_p}>\right), \tag{A.54}$$

$$\sigma_{V_z}^2 = \frac{1}{3}\left(<\mathbf{V_z}\cdot\mathbf{V_z}> - <\mathbf{V_z}>\cdot<\mathbf{V_z}>\right), \tag{A.55}$$

and the corresponding Jacobian equals unity (see Appendix A.2.3), such that $\mathrm{d}\mathbf{V_p}\mathrm{d}\mathbf{V_z}$=$\mathrm{d}\mathbf{U}\mathrm{d}\mathbf{V}$. The use of <> refers to spatial averaging, i.e. $<\mathbf{V_Z}(\mathbf{x},t)>= \lim_{V\to\infty}\frac{1}{V}\int \mathbf{V_Z}(\mathbf{x},t)d\mathbf{x}$ where V is a large volume of space over which the averaging is performed (Lewis and Pedley, 2000). However, in the statistically steady, homogeneous turbulence considered, the spatial, time and ensemble averages all give the same result. Equation (2.69) then becomes

$$\mathrm{CR_z} = \frac{R^2 P}{4}\int_\mathbf{V}\int_\mathbf{U}\int_0^\pi\int_0^{2\pi} U(\mathbf{R}) p_{\mathrm{U,V}}(\mathbf{U},\mathbf{V}|\mathbf{R})\sin(\theta_R)d\phi_R d\theta_R d\mathbf{U}d\mathbf{V}, \tag{A.56}$$

where $p_{\mathrm{U,V}}(\mathbf{U},\mathbf{V}|\mathbf{R})$ is the conditional joint probability distribution for $\mathbf{U}$ and $\mathbf{V}$ at a vector separation $\mathbf{R}$. Limited information is known regarding this probability distribution, but it is possible to postulate a plausible approximation. The following binormal distribution was suggested by Lewis and Pedley (2000):

$$p_{\mathrm{U,V}}(\mathbf{U},\mathbf{V}|\mathbf{R}) = \frac{\det A^{-1}(\mathbf{R})}{(2\pi)^3}\exp\left\{-\frac{1}{2}[\mathbf{U},\mathbf{V}]A^{-1}(\mathbf{R})[\mathbf{U},\mathbf{V}]^T\right\}, \tag{A.57}$$

where $[\mathbf{U},\mathbf{V}] = (U_1,U_2,U_3,V_1,V_2,V_3)$ and $A(\mathbf{R})$ is the matrix of covariances of $\mathbf{U}$ and $\mathbf{V}$, this type of distribution having been successfully used to model turbulent diffusion by Thomson in 1987 (Lewis and Pedley, 2000). However, calculations by Lewis and Pedley (2000) found the diagonal elements of matrix A to be dominant. For simplicity, they set all non-diagonal elements to zero. Equation (A.57) thus reduces to:

$$p_{\mathrm{U,V}}(\mathbf{U},\mathbf{V}) = \frac{1}{[2\pi\sigma_U\sigma_V(1-\varsigma^2)^{\frac{1}{2}}]^3}\exp\left[\left\{-\frac{1}{2(1-\varsigma^2)}\right\}\left\{\frac{(\mathbf{V}-<\mathbf{V}>)^2}{\sigma_V^2} + \frac{(\mathbf{U}-<\mathbf{U}>)^2}{\sigma_U^2} - \frac{2\varsigma(\mathbf{V}-<\mathbf{V}>)\cdot(\mathbf{U}-<\mathbf{U}>)}{\sigma_U\sigma_V}\right\}\right], \quad \text{(A.58)}$$

where $\varsigma = \frac{\mathbf{U}\cdot\mathbf{V}}{3\sigma_U\sigma_V}$, which lies between -1 and 1. The quantities σ_U and σ_V are ensemble-average variances of the components $\mathbf{U}$ and $\mathbf{V}$, respectively. It is the, now zero, terms of equation (A.57) that contain information about the influence of $\mathbf{R}$. It is thus assumed that equation (A.58) is valid at the vector separation $\mathbf{R}$. In order to evaluate the contact rate (A.56) using this binormal distribution, it is convenient to make a further change of variables. Let

$$\mathbf{p} = \frac{\mathbf{U}-<\mathbf{U}>}{\sigma_U}, \quad \text{(A.59)}$$

$$\mathbf{q} = \frac{1}{(1-\varsigma^2)^{\frac{1}{2}}}\left(\frac{\mathbf{V}-<\mathbf{V}>}{\sigma_V} - \frac{\varsigma(\mathbf{U}-<\mathbf{U}>)}{\sigma_U}\right). \quad \text{(A.60)}$$

Applying this change of variables to equation (A.56) gives (see Appendix A.2.4):

$$\mathrm{CR_z} = \frac{\pi PR^2}{(2\pi)^3 2}\int_0^\pi\int_p\int_q U(\mathbf{R})e^{\frac{-p^2}{2}}e^{\frac{-q^2}{2}}\sin(\theta_R)d\mathbf{q}d\mathbf{p}d\theta_R. \quad \text{(A.61)}$$

It follows from equation (A.59) that $\mathbf{U} = \sigma_U\mathbf{p} + <\mathbf{U}>$. Therefore,

$$\begin{aligned} U^2 &= \mathbf{U}\cdot\mathbf{U} \quad \text{(A.62)}\\ &= (\sigma_U\mathbf{p}+<\mathbf{U}>)\cdot(\sigma_U\mathbf{p}+<\mathbf{U}>)\\ &= \sigma_U^2p^2 + <U>^2 + 2\sigma_U\mathbf{p}\cdot<\mathbf{U}>. \end{aligned}$$

Therefore, equation (A.61) becomes:

$$\mathrm{CR_z} = \frac{PR^2}{16\pi^2}\int_0^\pi\int_p\int_q\left[\sigma_U^2p^2 + <U>^2 + 2\sigma_U\mathbf{p}\cdot<\mathbf{U}>\right]^{\frac{1}{2}}e^{\frac{-p^2}{2}}e^{\frac{-q^2}{2}}\sin(\theta_R)d\mathbf{q}d\mathbf{p}d\theta_R. \quad \text{(A.63)}$$

It is assumed that the orientation of the predator and prey remains fixed over all space, such that $<\mathbf{U_Z}> = \mathbf{U_Z}$ and $<\mathbf{U_P}> = \mathbf{U_P}$. The relative velocity is $\mathbf{U(R)} = \mathbf{V_Z} - \mathbf{V_P}$, thus the average relative velocity is:

$$\begin{aligned} <\mathbf{U(R)}> &= <\mathbf{V_Z}> - <\mathbf{V_P}>\\ &= <\mathbf{U_Z}(\mathbf{x}+\mathbf{R},t)> + <\mathbf{w}(\mathbf{x}+\mathbf{R},t)> - <\mathbf{U_P}(\mathbf{x},t)> - <\mathbf{w}(\mathbf{x},t)>\\ &= \mathbf{U_Z} - \mathbf{U_P}. \quad \text{(A.64)} \end{aligned}$$

We solve (A.63) by first performing the simpler integral, that over $\mathbf{q}$. We can use the standard result (see Appendix A.2.5 for the full working solution):

$$\int_q e^{-\frac{q^2}{2}} d\mathbf{q} = 4\pi\sqrt{\frac{\pi}{2}}. \tag{A.65}$$

Substitute this result into equation (A.63) and define $\mathbf{p}$ in spherical coordinates; $\mathbf{p} = p\,(\sin\theta_p\cos\phi_p, \sin\theta_p\sin\phi_p, \cos\theta_p)$ and $d\mathbf{p} = p^2\sin\theta_p dp d\theta_p d\phi_p$. Then,

$$\begin{aligned} \mathrm{CR_z} &= \frac{PR^2}{4\pi}\sqrt{\frac{\pi}{2}}\int_0^{\pi}\int_0^{2\pi}\int_0^{\pi}\int_0^{\infty}\left[\sigma_U^2 p^2 + < U >^2\right. \\ &+ \left. 2\sigma_U \mathbf{p}\cdot < \mathbf{U} >\right]^{\frac{1}{2}} p^2 e^{\frac{-p^2}{2}} \sin\theta_R \sin\theta_p dp d\theta_p d\phi_p d\theta_R. \end{aligned} \tag{A.66}$$

Perform the integral over ϕ_p and use $2\sigma_U\mathbf{p}\cdot < \mathbf{U} >= 2\sigma_U p < U > \cos\theta_p$, θ_p being the angle between $\mathbf{p}$ and $< \mathbf{U} >$ if we choose, without loss of generality, the z-axis to lie parallel to $< \mathbf{U} >$ in p space (Lewis and Pedley, 2000).

Integrating over θ_p we obtain:

$$\begin{aligned} \mathrm{CR_z} = \frac{PR^2}{2}\sqrt{\frac{\pi}{2}}\int_0^{\pi}\int_0^{\infty} e^{\frac{-p^2}{2}}\left[\left(-\frac{p^2\sin\theta_R}{3\sigma_U p < U >}\right)\right. & \left|\sigma_U^2 p^2 + < U >^2\right. \\ & \left.\left. + 2\sigma_U p < U > \cos\theta_p\right|^{\frac{3}{2}}\right]_0^{\pi} dp d\theta_R. \end{aligned} \tag{A.67}$$

Note that $(\sigma_U^2 p^2 + < U >^2 + 2\sigma_U p < U > \cos\theta_p)^{\frac{1}{2}} = U$, and thus can't be a negative quantity, hence the modulus sign. By evaluating

$$\left[\left(-\frac{p^2\sin\theta_R}{3\sigma_U p < U >}\right)\left|\sigma_U^2 p^2 + < U >^2 + 2\sigma_U p < U > \cos\theta_p\right|^{\frac{3}{2}}\right]_0^{\pi}$$

equation (A.67) becomes:

$$\begin{aligned} \mathrm{CR_z} = \frac{PR^2}{6}\sqrt{\frac{\pi}{2}}\int_0^{\pi}\int_0^{\infty} e^{\frac{-p^2}{2}}\left(\frac{p\sin\theta_R}{\sigma_U < U >}\right)\left[(\sigma_U p + < U >)^3\right. & \\ \left. - \left|\sigma_U p - < U >\right|^3\right] dp d\theta_R. & \end{aligned} \tag{A.68}$$

The integral over p can now be performed in two stages, for $p < \frac{<U>}{\sigma_U}$ and $p > \frac{<U>}{\sigma_U}$. When $p < \frac{<U>}{\sigma_U}$:

$$\begin{aligned} (\sigma_U p + < U >)^3 - |\sigma_U p - < U >|^3 &= (\sigma_U p + < U >)^3 - (< U > - \sigma_u p)^3 \\ &= 2\sigma_U^3 p^3 + 6\sigma_U p < U >^2, \end{aligned} \tag{A.69}$$

and when $p > \frac{<U>}{\sigma_U}$:

$$
\begin{aligned}
(\sigma_U p + < U >)^3 - |\sigma_U p - < U >|^3 &= (\sigma_U p + < U >)^3 - (\sigma_U p - < U >)^3 \\
&= 6\sigma_U^2 p^2 < U > + 2 < U >^3 . \qquad \text{(A.70)}
\end{aligned}
$$

The contact rate is now:

$$
\begin{aligned}
\mathrm{CR}_z = &\frac{PR^2}{6}\sqrt{\frac{\pi}{2}}\int_0^{\pi}\int_0^{\frac{<U>}{\sigma_U}} e^{-\frac{p^2}{2}}\left(\frac{p\sin\theta_R}{\sigma_U < U >}\right)\left(2\sigma_U^3 p^3 + 6\sigma_U p < U >^2\right) dp d\theta_R \\
&+\frac{PR^2}{6}\sqrt{\frac{\pi}{2}}\int_0^{\pi}\int_{\frac{<U>}{\sigma_U}}^{\infty} e^{-\frac{p^2}{2}}\left(\frac{p\sin\theta_R}{\sigma_U < U >}\right)\left(6\sigma_U^2 p^2 < U > + 2 < U >^3\right) dp d\theta_R .
\end{aligned}
$$

Standard results are invoked to perform the following integrals with respect to p:

$$
\begin{aligned}
\int_0^{\frac{<U>}{\sigma_U}} p^2 e^{-\frac{p^2}{2}} dp &= \sqrt{\frac{\pi}{2}}\mathrm{erf}\left(\frac{< U >}{\sigma_U\sqrt{2}}\right) - \frac{< U >}{\sigma_U} e^{-\frac{<U>^2}{2\sigma_U^2}} , \\
\int_0^{\frac{<U>}{\sigma_U}} p^4 e^{-\frac{p^2}{2}} dp &= 3\sqrt{\frac{\pi}{2}}\mathrm{erf}\left(\frac{< U >}{\sigma_U\sqrt{2}}\right) - \left(\frac{3 < U >}{\sigma_U} + \frac{< U >^3}{\sigma_U^3}\right) e^{-\frac{<U>^2}{2\sigma_U^2}} , \\
\int_{\frac{<U>}{\sigma_U}}^{\infty} p e^{-\frac{p^2}{2}} dp &= e^{-\frac{<U>^2}{2\sigma_U^2}} , \\
\int_{\frac{<U>}{\sigma_U}}^{\infty} p^3 e^{-\frac{p^2}{2}} dp &= e^{-\frac{<U>^2}{2\sigma_U^2}}\left(2 + \frac{< U >^2}{\sigma_U^2}\right) .
\end{aligned}
$$

The expression $\mathrm{erf}(z) = \frac{2}{\sqrt{\pi}}\int_0^z e^{-t^2} dt$ is the error function (Kreyszig, 1962). Thus, for predator and prey swimming at constant speeds U_Z and U_P respectively, the contact rate (A.56) reduces to the integral:

$$
\begin{aligned}
\mathrm{CR}_\mathbf{z} = PR^2\sqrt{\frac{\pi}{2}}\int_0^{\pi}\Bigg\{&\sqrt{\frac{\pi}{2}}\mathrm{erf}\left(\frac{< U >}{\sigma_U\sqrt{2}}\right)\left[< U > + \frac{\sigma_U^2}{< U >}\right] \\
&+ \sigma_U \exp\left(-\frac{< U >^2}{2\sigma_U^2}\right)\Bigg\}\sin\theta_R d\theta_R . \qquad \text{(A.71)}
\end{aligned}
$$

A.2.3 Changing variables from $(\mathbf{V_Z}, \mathbf{V_P})$ to $(\mathbf{U}, \mathbf{V})$

Let

$$
\begin{aligned}
\mathbf{U} &= \mathbf{V_z} - \mathbf{V_p}, \qquad \text{(A.72)} \\
\mathbf{V} &= \alpha\mathbf{V_p} + \beta\mathbf{V_z}, \qquad \text{(A.73)}
\end{aligned}
$$

where $\alpha = \frac{\sigma_{V_z}^2}{\sigma_{V_z}^2 + \sigma_{V_p}^2}$ and $\beta = \frac{\sigma_{V_p}^2}{\sigma_{V_z}^2 + \sigma_{V_p}^2}$, such that $\alpha + \beta = 1$. Let the Jacobian be given by:

$$\mathbf{J}(\mathbf{U},\mathbf{V}) = \begin{vmatrix} \frac{\partial U_1}{\partial V_{Z1}} & \frac{\partial U_1}{\partial V_{Z2}} & \frac{\partial U_1}{\partial V_{Z3}} & \frac{\partial U_1}{\partial V_{P1}} & \frac{\partial U_1}{\partial V_{P2}} & \frac{\partial U_1}{\partial V_{P3}} \\ \frac{\partial U_2}{\partial V_{Z1}} & \frac{\partial U_2}{\partial V_{Z2}} & \frac{\partial U_2}{\partial V_{Z3}} & \frac{\partial U_2}{\partial V_{P1}} & \frac{\partial U_2}{\partial V_{P2}} & \frac{\partial U_2}{\partial V_{P3}} \\ \frac{\partial U_3}{\partial V_{Z1}} & \frac{\partial U_3}{\partial V_{Z2}} & \frac{\partial U_1}{\partial V_{Z3}} & \frac{\partial U_3}{\partial V_{P1}} & \frac{\partial U_3}{\partial V_{P2}} & \frac{\partial U_3}{\partial V_{P3}} \\ \frac{\partial V_1}{\partial V_{Z1}} & \frac{\partial V_1}{\partial V_{Z2}} & \frac{\partial V_1}{\partial V_{Z3}} & \frac{\partial V_1}{\partial V_{P1}} & \frac{\partial V_1}{\partial V_{P2}} & \frac{\partial V_1}{\partial V_{P3}} \\ \frac{\partial V_2}{\partial V_{Z1}} & \frac{\partial V_2}{\partial V_{Z2}} & \frac{\partial V_2}{\partial V_{Z3}} & \frac{\partial V_2}{\partial V_{P1}} & \frac{\partial V_2}{\partial V_{P2}} & \frac{\partial V_2}{\partial V_{P3}} \\ \frac{\partial V_3}{\partial V_{Z1}} & \frac{\partial V_3}{\partial V_{Z2}} & \frac{\partial V_3}{\partial V_{Z3}} & \frac{\partial V_3}{\partial V_{P1}} & \frac{\partial V_3}{\partial V_{P2}} & \frac{\partial V_3}{\partial V_{P3}} \end{vmatrix}$$

The Jacobian is therefore

$$\mathbf{J} = \begin{vmatrix} 1 & 0 & 0 & -1 & 0 & 0 \\ 0 & 1 & 0 & 0 & -1 & 0 \\ 0 & 0 & 1 & 0 & 0 & -1 \\ \beta & 0 & 0 & \alpha & 0 & 0 \\ 0 & \beta & 0 & 0 & \alpha & 0 \\ 0 & 0 & \beta & 0 & 0 & \alpha \end{vmatrix}$$

which is equal to one. Thus $d\mathbf{V_p}d\mathbf{V_z}$=$d\mathbf{U}d\mathbf{V}$.

A.2.4 Changing variables from $(\mathbf{U},\mathbf{V})$ to $(\mathbf{p},\mathbf{q})$

Given the following relationship between $(\mathbf{U},\mathbf{V})$ and $(\mathbf{p},\mathbf{q})$:

$$\mathbf{p} = \frac{\mathbf{U} - <\mathbf{U}>}{\sigma_U}, \tag{A.74}$$

$$\mathbf{q} = \frac{1}{(1-\varsigma^2)^{\frac{1}{2}}}\left(\frac{\mathbf{V} - <\mathbf{V}>}{\sigma_V} - \frac{\varsigma(\mathbf{U} - <\mathbf{U}>)}{\sigma_U}\right), \tag{A.75}$$

then

$$q^2+p^2 = \frac{1}{(1-\varsigma^2)}\left(\frac{(\mathbf{V} - <\mathbf{V}>)^2}{\sigma_V^2} + \frac{(\mathbf{U} - <\mathbf{U}>)^2}{\sigma_U^2} - \frac{2\varsigma(\mathbf{V} - <\mathbf{V}>)\cdot(\mathbf{U} - <\mathbf{U}>)}{\sigma_U\sigma_V}\right). \tag{A.76}$$

The binormal distribution approximating $p_{\mathrm{U,V}}(\mathbf{U},\mathbf{V}|\mathbf{R})$, which is given by

$$\begin{aligned} p_{\mathrm{U,V}}(\mathbf{U},\mathbf{V}) &= \frac{1}{[2\pi\sigma_U\sigma_V(1-\varsigma^2)^{\frac{1}{2}}]^3}\exp\left[\left\{-\frac{1}{2(1-\varsigma^2)}\right\}\left\{\frac{(\mathbf{V} - <\mathbf{V}>)^2}{\sigma_V^2}\right.\right. \\ &+ \left.\left.\frac{(\mathbf{U} - <\mathbf{U}>)^2}{\sigma_U^2} - \frac{2\varsigma(\mathbf{V} - <\mathbf{V}>)\cdot(\mathbf{U} - <\mathbf{U}>)}{\sigma_U\sigma_V}\right\}\right], \end{aligned} \tag{A.77}$$

now reduces to

$$p_{\mathrm{U,V}}(\mathbf{U},\mathbf{V}) = \frac{1}{[2\pi\sigma_U\sigma_V(1-\varsigma^2)^{\frac{1}{2}}]^3}\exp\left\{-\frac{1}{2}\left(q^2+p^2\right)\right\}. \tag{A.78}$$

Since the Jacobian is equal to $\sigma_U^3\sigma_V^3(1-\varsigma^2)^{\frac{3}{2}}$,

$$d\mathbf{U}d\mathbf{V} = \left(\sigma_U^3\sigma_V^3(1-\varsigma^2)^{\frac{3}{2}}\right) d\mathbf{p}d\mathbf{q}. \tag{A.79}$$

The contact rate,

$$\mathrm{CR}_z = P\frac{R^2}{4}\int_V\int_U\int_0^\pi\int_0^{2\pi} U(\mathbf{R})p_{\mathrm{U,V}}(\mathbf{U},\mathbf{V}|\mathbf{R})\sin(\theta_R)d\phi_R d\theta_R d\mathbf{U}d\mathbf{V}, \tag{A.80}$$

then becomes, in terms of $(\mathbf{p},\mathbf{q})$,

$$\mathrm{CR}_z = \frac{\pi PR^2}{(2\pi)^32}\int_0^\pi\int_p\int_q U(\mathbf{R})e^{\frac{-p^2}{2}}e^{\frac{-q^2}{2}}\sin(\theta_R)d\mathbf{q}d\mathbf{p}d\theta_R. \tag{A.81}$$

A.2.5 Integrate over q

Integrate equation (A.81) over $\mathbf{q}$ by defining $\mathbf{q}$ in spherical coordinates (q,θ_q,ϕ_q), the volume element being $d\mathbf{q} = q^2\sin\theta_q dq d\theta_q d\phi_q$, such that:

$$\begin{aligned}
\int_q e^{-\frac{q^2}{2}}d\mathbf{q} &= \int_0^{2\pi}\int_0^\pi\int_0^\infty q^2e^{-\frac{q^2}{2}}\sin\theta_q dq d\theta_q d\phi_q \\
&= [-\cos\theta_q]_0^\pi\int_0^{2\pi}\int_0^\infty q^2e^{-\frac{q^2}{2}}dq d\phi_q \\
&= 2\,[\phi]_0^{2\pi}\int_0^\infty q^2e^{-\frac{q^2}{2}}dq \\
&= 4\pi\int_0^\infty q^2e^{-\frac{q^2}{2}}dq = \frac{4\pi\sqrt{2}\sqrt{\pi}}{2} \\
&= 4\pi\sqrt{\frac{\pi}{2}}.
\end{aligned} \tag{A.82}$$

A.2.6 Evaluation of σ_U^2

Consider

$$\sigma_U^2(\mathbf{R}) = \frac{1}{3}\left[6W^2 - 2 < \mathbf{w}(\mathbf{x},t)\cdot\mathbf{w}(\mathbf{x}+\mathbf{R},t) >\right], \tag{A.83}$$

where $W^2 = \frac{<\mathbf{w}(\mathbf{x},t)\cdot\mathbf{w}(\mathbf{x},t)>}{3}$. Thus,

$$\sigma_U^2(\mathbf{R}) = \frac{2}{3}\left[< \mathbf{w}(\mathbf{x},t)\cdot\mathbf{w}(\mathbf{x},t) > - < \mathbf{w}(\mathbf{x},t)\cdot\mathbf{w}(\mathbf{x}+\mathbf{R},t) >\right]. \tag{A.84}$$

Given the identity

$$\frac{1}{2} < \mathbf{w}(\mathbf{x},t)\cdot\mathbf{w}(\mathbf{x}+R,t) >= \int_0^\infty E(k,t)\frac{\sin(kR)}{kR}dk, \tag{A.85}$$

where $E(k,t)$ is the kinetic energy spectrum (Davidson, 2006), a function of wave number, k and time, t, and reducing to give

$$\frac{1}{2} < \mathbf{w}(\mathbf{x},t) \cdot \mathbf{w}(\mathbf{x},t) >= \int_0^\infty E(k,t)dk, \tag{A.86}$$

the ensemble average variance of **U** therefore becomes

$$\sigma_U^2(R) = \frac{4}{3}\int_0^\infty E(k,t)\left(1 - \frac{\sin(kR)}{kR}\right)dk. \tag{A.87}$$

In order to evaluate the integral, the energy spectrum is assumed to be proportional to $k^{\frac{-5}{3}}$. This is true for intermediate values of the wave number, but not for very small and very large k. However, it is widely used as an approximation and is based on many experimental observations (Tennekes and Lumley, 1972). If $R \gg \eta$, $E(k,t)$ can be approximated by (Lewis and Pedley (2000) and references therein):

$$E(k,t) = \frac{3}{2} < \epsilon >^{\frac{2}{3}} k^{-\frac{5}{3}}, \quad k \in \left[\approx \frac{1}{L}, \approx \frac{1}{\eta}\right]. \tag{A.88}$$

Assuming that $E(k,t)$ makes little contribution to equation (A.87) outside the range $\left[\frac{1}{L}, \frac{1}{\eta}\right]$ and $L \gg \eta$:

$$\sigma_U^2(R) \approx 2 < \epsilon >^{\frac{2}{3}} \int_{\frac{1}{L}}^{\frac{1}{\eta}} k^{-\frac{5}{3}}\left(1 - \frac{\sin(kR)}{kR}\right)dk. \tag{A.89}$$

Let $\tilde{k} = k\eta$:

$$\sigma_U^2(R) \approx 2 < \epsilon >^{\frac{2}{3}} \int_0^1 (\tilde{k}\eta)^{-\frac{5}{3}}\left(1 - \frac{\sin(\frac{\tilde{k}R}{\eta})}{\frac{\tilde{k}R}{\eta}}\right)\frac{d\tilde{k}}{\eta}. \tag{A.90}$$

Making the substitution $u = \frac{\tilde{k}R}{\eta}$, $du = \left(\frac{R}{\eta}\right)d\tilde{k}$:

$$\sigma_U^2(R) \approx 2 < \epsilon >^{\frac{2}{3}} \eta^{\frac{2}{3}}\left(\frac{\eta}{R}\right)\int_0^{\frac{R}{\eta}} \left(\frac{\eta u}{R}\right)^{-\frac{5}{3}}\left(1 - \frac{\sin(u)}{u}\right)dk. \tag{A.91}$$

Rewriting the integral as $\int_0^{\frac{R}{\eta}} = \int_0^\infty - \int_{\frac{R}{\eta}}^\infty$ and simplifying, we obtain:

$$\sigma_U^2(R) \approx < \epsilon >^{\frac{2}{3}} R^{\frac{2}{3}}\left[Sc - \frac{3\eta^{\frac{2}{3}}}{R^{\frac{2}{3}}} + 2\int_{\frac{R}{\eta}}^\infty \frac{\sin(x)}{x^{\frac{8}{3}}}dx\right], \tag{A.92}$$

where the structure function, $Sc = 2\int_0^\infty u^{-\frac{5}{3}}\left(1 - \frac{\sin(u)}{u}\right)du = \frac{9}{10}\Gamma\left(\frac{1}{3}\right) = 2.411$ (Lewis and Pedley, 2000).

The last two terms of equation (A.92) tend to be small, so $\sigma_U^2(R) \approx < \epsilon >^{\frac{2}{3}} R^{\frac{2}{3}} Sc$.

A.2.7 Matlab code to calculate CR_z

A.2.7.1 CRz_calculation.m

```
global R eta L eps Sc U_p U_z

R=4.3e-6; %m
nu=((60*60*24)^2)*1e-6; %m^2/d^2
Sc=2.411;
U_p=0; %m/d
U_z=(60*60*24)*339e-6; %m/d
eps=6.2501e7;

eta=(nu^3/eps)^(1/4);
L= R/eta;

QQ = quadgk(@CZ_eqns,0,pi);
cz=R^2*sqrt(pi/2)*QQ;
```

A.2.7.2 CRz_eqns.m

```
function z = CZ_eqns(theta)

global R eta L eps Sc U_p U_z

U2 = U_p^2 + U_z^2 - 2*U_p*U_z*cos(theta);

U=sqrt(U2);

Q = quadgk(@LP_int1a,L,inf);

sig = (eps^(2/3)*R^(2/3)*(Sc - 3*eta^(2/3)/R^(2/3) + 2*Q))^(1/2);

yy = U./(sig*sqrt(2));

Y = erf(yy);

z=(sqrt(pi/2)*Y.*(U+sig^2./U)+sig*exp(-U2/(2*sig^2))).*sin(theta);
```

A.2.7.3 LP_int1a.m

```
function y = LP_int1a(x)
```

```
y =(sin(x)./x.^(8/3));
```

Appendix B

Spatial heterogeneity

B.1 Validation of pdepe for $(P_3^*, 0, Z^*)$ stable

B.1.0.1 Zero eddy diffusivity, uniform initial conditions

Similarly to section 4.3.1, we validate Matlab's pdepe solver against its ode45 solver. Here we take eddy diffusivity to be zero and uniform, non-dimensional, initial conditions of $(P_0, V_0, Z_0) = (1.365, 1.043 \times 10^{-7}, 0.8876)$. As stated previously, when the eddy diffusivity, $\kappa_z = 0$, the phytoplankton-virus volume clearance rate is $c_v = 1.74 \times 10^{-11} m^3 d^{-1}$ and the phytoplankton-predator volume clearance rate is $c_z = 1.70 \times 10^{-9} m^3 d^{-1}$, giving $K_{IR} = 7.35 \times 10^9$ m^{-3} and $K_{GR} = 1.09 \times 10^9$ m^{-3}.

Figure B.1 shows the solution of model (4.8, 4.9, 4.10) for these parameter values. There is a black line representing a spatial resolution of 0.1, a red line representing a spatial resolution of 0.01 and a blue line showing the ode45 solution of the model without the diffusion terms. Figure B.1 shows the three solutions to be consistent with each other. There is some numerical error in the pdepe solutions, with the minimum virus population having a negative value. However, the value is very small and doesn;t appear to adversely affect the rest of the solution.

B.1.0.2 Large eddy diffusivity, uniform initial conditions

Again, we validate pdepe against ode45 for uniform, non-dimensional, initial conditions of $(P_0, V_0, Z_0) = (1.365, 1.043 \times 10^{-7}, 0.8876)$. We use the large eddy diffusivity value of $\kappa_z = 9.690 \times 10^3 m^2$ d^{-1}, which is calculated from $\epsilon = 6.250 \times 10^7 m^2$ d^{-3} in the first eddy diffusivity profile of section 4.3.1, shown in Figure 4.2. The corresponding volume clearance rates are then $c_v = 1.84 \times 10^{-11} m^3$ d^{-1} and $c_z = 1.70 \times 10^{-9} m^3 d^{-1}$. Then $K_{IR} = 7.35 \times 10^9$ cells per m^3 and $K_{GR} = 1.09 \times 10^9$ cells per m^3.

Figure B.2 shows the dynamics of model (4.8, 4.9, 4.10) for the parameter values stated above, and those in Table 4.1. Again, there are three plots within the figure: a black line representing the pdepe solution with a spatial resolution of 0.1, a red

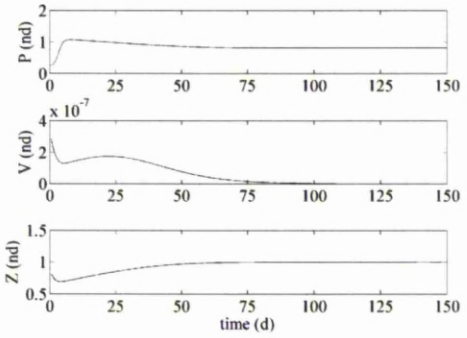

Figure B.1: Validation of Matlab's pdepe solver against its ode45 solver for $(P_3^*, 0, Z^*)$ stable long-term behaviour of model (4.8, 4.9, 4.10) with zero eddy diffusivity and uniform initial conditions of $(P_0, V_0, Z_0) = (1.365, 1.043 \times 10^{-7}, 0.8876)$ in non-dimensional values. Parameter values are as in Table 4.1, with $c_v = 1.74 \times 10^{-11}$ $m^3 d^{-1}$, $K_{IR} = 7.35 \times 10^9 m^{-3}$, $K_{IR} = 1.09 \times 10^9 m^{-3}$, $\gamma = 0.4 d^{-1}$ and $\nu = 1.38 d^{-1}$. The blue line represents the ode45 solution, the red line represents the pdepe solution with resolution 0.01, and there is also a black line showing the pdepe solution with resolution 0.1.

line showing the pdepe solution with spatial resolution 0.01 and a blue line showing the ode45 solution. The latter solves the reaction part of model (4.8, 4.9, 4.10), i.e. diffusion is neglected. This enables the ODE to be solved and should give a solution comparable to that of pdepe since the initial conditions are constant. The effects of eddy diffusivity are incorporated into the ODE via the $P-V$ and $P-Z$ contact rates. Similarly to the case of zero eddy diffusivity shown above, the three solutions are indistinguishable from one another in the figure. The pdepe solution still has a negative minimum virus population, but this doesn't appear to adversely affect the rest of the solution since it continues to tally with the ode45 solution. Comparison with Figure B.1 shows that the large eddy diffusivity doesn't significantly alter the population dynamics, when uniform initial conditions are used, even though the phytoplankton-virus volume clearance rate is slightly larger for eddy diffusivity than zero eddy diffusivity.

B.2 Validation of pdepe for $(P, 0, Z)$ stable limit cycles

B.2.0.1 Zero eddy diffusivity, uniform initial conditions

As discussed previously, for zero eddy diffusivity, $c_v = 1.74 \times 10^{-11} m^3$ d^{-1}, $c_z = 1.70 \times 10^{-9} m^3$ d^{-1} and thus $K_{IR} = 7.35 \times 10^9 m^{-3}$. The initial conditions are uniform with non-dimensional values of $(P_0, V_0, Z_0) = (1.365, 1.043 \times 10^{-7}, 0.8876)$. Figure B.3 shows the solution of model (4.8, 4.9, 4.10), for these parameter values and those in

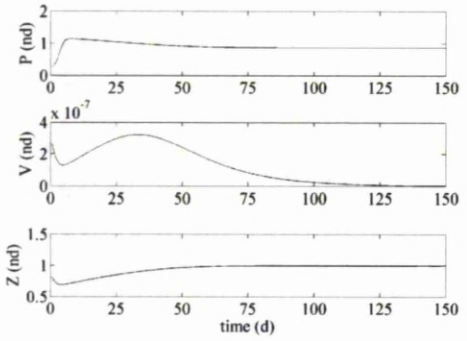

Figure B.2: Validation of Matlab's pdepe solver against its ode45 solver for $(P_3^*, 0, Z^*)$ stable long-term behaviour of model (4.8, 4.9, 4.10) with a large eddy diffusivity value of $\kappa_z = 9.6904 \times 10^3 \mathrm{m}^2\ \mathrm{d}^{-1}$ and uniform initial conditions of $(P_0, V_0, Z_0) = (1.365, 1.043 \times 10^{-7}, 0.8876)$ in non-dimensional values. Parameters are as in Table 4.1 with $\mathrm{c_v} = 1.81 \times 10^{-11}\ \mathrm{m^3 d^{-1}}$, $K_{\mathrm{IR}} = 7.35 \times 10^9 \mathrm{m}^{-3}$, $K_{\mathrm{GR}} = 1.09 \times 10^9 \mathrm{m}^{-3}$, $\gamma = 0.4 \mathrm{d}^{-1}$ and $\nu = 1.38 \mathrm{d}^{-1}$. The blue line represents the ode45 solution, the red line represents the pdepe solution with resolution 0.01, and there is also a black line showing the pdepe solution with resolution 0.1.

Table 4.1, in the region where there is a $(P, 0, Z)$ limit cycle in the long-term. Figure B.3(a) shows the solution using pdepe, spatial resolution 0.1 (black line) and 0.01 (red line), and the solution using ode45 (blue line). Figure B.3(b) shows the predator population during the latter half of the time series, which is where the pdepe solution becomes "out of step" with the ode45 solution.

The last cycle sees the two different pdepe solutions separate out also. Having found the solution with a resolution of 0.005 to be indistinguishable from that with a resolution of 0.01, we accept this latter resolution as adequate. The ode45 solution is still represented by a blue line. There is a slight improvement in the percentage error between pdepe, spatial resolution 0.005, and ode45 compared with the percentage error between pdepe, spatial resolution 0.01, and ode45. Also, there is numerical error in the virus population with the minimum concentration being negative in the pdepe solution, for all spatial resolutions discussed. However, the pdepe solutions do capture the overall transient and long-term dynamics well, for the 150 days plotted.

B.2.0.2 Large eddy diffusivity, uniform initial conditions

As previously, we will also validate pdepe against ode45 when the eddy diffusivity is large. The value of eddy diffusivity used continues to be $\kappa_z = 9.690 \times 10^3 \mathrm{m}^2\ \mathrm{d}^{-1}$, which corresponds to an energy dissipation rate of $\epsilon = 6.250 \times 10^7 \mathrm{m}^2\ \mathrm{d}^{-3}$. The associated volume clearance rates are $\mathrm{c_v} = 1.84 \times 10^{-11} \mathrm{m}^3\ \mathrm{d}^{-1}$ and $\mathrm{c_z} = 1.70 \times 10^{-9} \mathrm{m^3 d^{-1}}$.

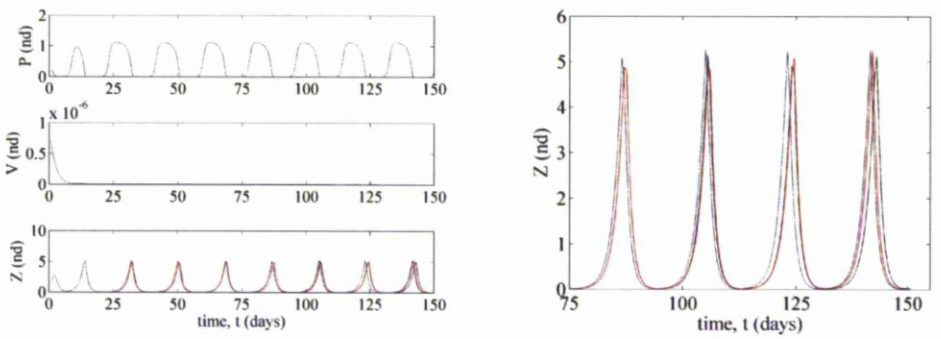

(a) (b)

Figure B.3: Validation of Matlab's pdepe solver against its ode45 solver for $(P, 0, Z)$ limit cycle long-term behaviour of model (4.8, 4.9, 4.10) with zero eddy diffusivity and uniform initial conditions of $(P_0, V_0, Z_0) = (1.365, 1.043 \times 10^{-7}, 0.8876)$ in non-dimensional values. Other parameters are given in Table 4.1, with $c_v = 1.74 \times 10^{-11} m^3 d^{-1}$, $K_{IR} = 7.35 \times 10^9 m^{-3}$, $K_{GR} = 1.09 \times 10^9 m^{-3}$ and $(\gamma, \nu) = (0.5, 0.8) d^{-1}$. In Figures (a) and (b) the black line shows the pdepe solution with resolution 0.1 and the red line represents the pdepe solution with resolution 0.01. The blue line represents the ode45 solution. Figure (b) shows a larger image of Z, during the second half of the time points displayed in (a) in order to see the difference in solution.

It follows that $K_{\mathrm{IR}} = 7.35 \times 10^9 \mathrm{m}^{-3}$. Other parameters are as in Table 4.1 and $(\gamma, \nu) = (0.5, 0.8)\mathrm{d}^{-1}$. The initial conditions remain uniform with non-dimensional values $(P_0, V_0, Z_0) = (1.365, 1.043 \times 10^{-7}, 0.8876)$.

Figure B.4 shows the solution of model (4.8, 4.9, 4.10) for these parameter values. The solutions found using pdepe agree more closely with ode45 for large eddy diffusivity than was seen for zero eddy diffusivity. It makes sense that pdepe may be more accurate when eddy diffusivity is non-zero, since this is what pdepe was designed to solve. Figure B.4(b) shows a larger image of the predator population in order to better see the difference between solutions. As previously, the black line represents pdepe with a spatial resolution of 0.1, the red line represents pdepe with a spatial resolution of 0.01 and the blue line represents ode45. Also note that there are no negative virus populations for this value of eddy diffusivity (true for both spatial resolutions discussed), which is in contrast with what we found for zero eddy diffusivity.

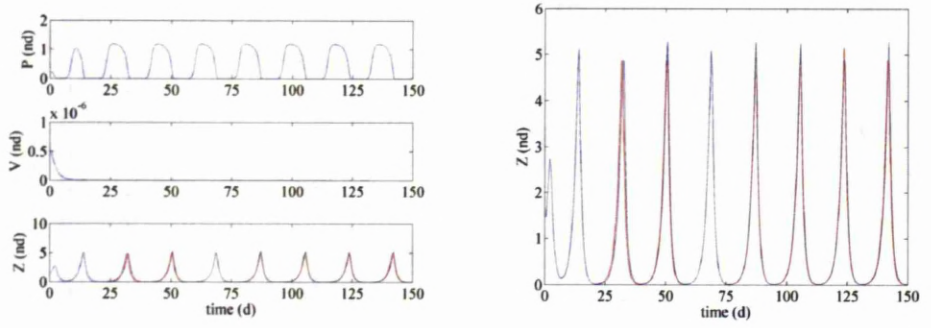

(a) (b)

Figure B.4: Validation of Matlab's pdepe solver against its ode45 solver for $(P, 0, Z)$ limit cycle long-term behaviour of model (4.8, 4.9, 4.10) with a large eddy diffusivity value of $\kappa_z = 9.6904 \times 10^3 \mathrm{m}^2\ \mathrm{d}^{-1}$ and uniform initial conditions of $(P_0, V_0, Z_0) = (1.365, 1.043 \times 10^{-7}, 0.8876)$ in non-dimensional values. Parameters as in Table 4.1, with $\mathrm{c_v} = 1.84 \times 10^{-11} \mathrm{m}^3\mathrm{d}^{-1}$, $K_{\mathrm{IR}} = 7.35 \times 10^9 \mathrm{m}^{-3}$, $K_{\mathrm{GR}} = 1.09 \times 10^9 \mathrm{m}^{-3}$ and $(\gamma, \nu) = (0.5, 0.8\mathrm{d}^{-1}$. The blue line represents the ode45 solution, the red line represents the pdepe solution with resolution 0.01, and there is also a black line showing the pdepe solution with resolution 0.1. Figure (b) shows a larger image of Z in order to see the difference in solution.

B.3 Validation of pdepe for (P, V, Z) non-equilibrium coexistence

B.3.0.1 Zero eddy diffusivity, uniform initial conditions

We follow the same structure as previously, firstly validating the pdepe solver against ode45 using uniform initial conditions and zero eddy diffusivity throughout the water column. The uniform initial conditions are $(P_0, V_0, Z_0) = (1.365, 1.043 \times 10^{-7}, 0.8876)$ in non-dimensional values. The phytoplankton-predator volume clearance rate is $c_z = 1.70 \times 10^{-9} m^2 d^{-1}$, thus $K_{IR} = 7.35 \times 10^9$ cells per m^3, and the phytoplankton-virus volume clearance rate is $c_v = 1.74 \times 10^{-11} m^3\ d^{-1}$, when $\kappa_z = 0$. Figure B.5 demonstrates that the pdepe solution of model (4.8, 4.9, 4.10) in the region where the long-term behaviour is (P, V, Z) coexistence is in good agreement with the ode45 solution of the same system, neglecting diffusion. The largest difference is seen in the predator population. Figure B.5(b) shows a larger image of the predator population in order to clearly see the difference between solutions. The two pdepe solutions are in very good agreement. The black line represents a spatial resolution of 0.1, whilst the red line a spatial resolution of 0.01.

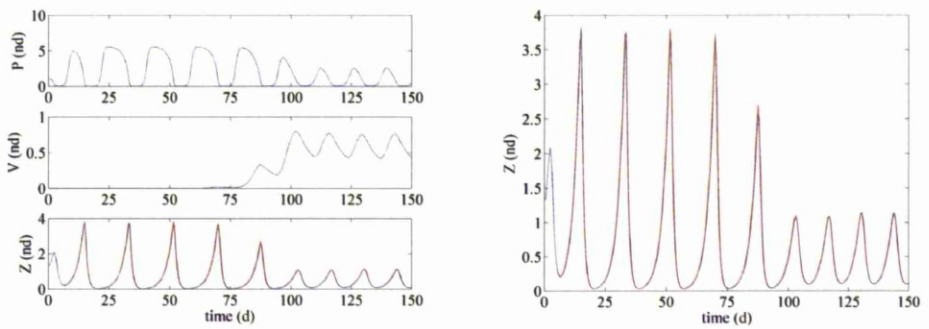

(a) (b)

Figure B.5: Validation of Matlab's pdepe solver against its ode45 solver for PVZ coexistence long-term behaviour of model (4.8, 4.9, 4.10) with zero eddy diffusivity and uniform initial conditions of $(P_0, V_0, Z_0) = (1.365, 1.043 \times 10^{-7}, 0.8876)$ in non-dimensional values. The blue line represents the ode45 solution, the red line represents the pdepe solution with resolution 0.01, and there is also a black line showing the pdepe solution with resolution 0.1. Figure (b) shows a larger image of Z in order to see the difference in solution. Parameter values are those in Table 4.1, $c_v = 1.74 \times 10^{-11} m^3 d^{-1}$, $K_{IR} = 7.35 \times 10^9 m^{-3}$, $K_{GR} = 1.09 \times 10^9 m^{-3}$ and $(\gamma, \nu) = (0.1, 1) d^{-1}$.

B.3.0.2 Large eddy diffusivity, uniform initial conditions

Here, continue to consider the uniform initial conditions: $(P_0, V_0, Z_0) = (1.365, 1.043 \times 10^{-7}, 0.8876)$ in non-dimensional values, but now with a large uniform eddy diffusivity value. As previously, we take $\kappa_z = 9.690 \times 10^3 \mathrm{m}^2\mathrm{d}^{-1}$, which corresponds to $\epsilon = 6.250 \times 10^7 \mathrm{m2\ d}^{-3}$. The values of K_{IR} and $\mathrm{c_v}$ are then $K_{\mathrm{IR}} = 7.35 \times 10^9\ \mathrm{m}^{-3}$ and $\mathrm{c_v} = 1.84 \times 10^{-11}\mathrm{m}^3\ \mathrm{d}^{-1}$.

Figure B.6 shows good agreement between the pdepe solution with resolution 0.01 (the red line) and the ode45 solution (the blue line).The solutions differ slightly in the predator population, as shown more clearly in Figure B.6(b). However, pdepe does capture the overall dynamics of the ode45 solution well, even in the predator population, and so, as previously, we will continue to use pdepe to investigate spatially variant eddy diffusivity and initial conditions. There is a slight alteration in the transient dynamics between large and zero eddy diffusivity, but, for uniform initial conditions, introduction of turbulence doesn't significantly affect the (P, V, Z) coexistence population dynamics.

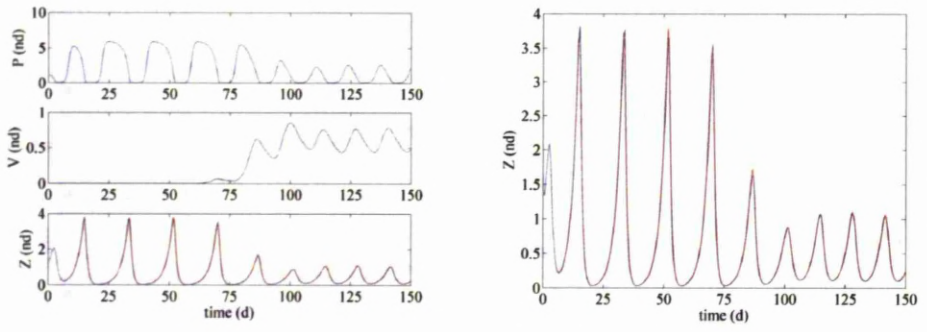

(a) (b)

Figure B.6: Validation of Matlab's pdepe solver against its ode45 solver for PVZ coexistence long-term behaviour of model (4.8, 4.9, 4.10) with a large eddy diffusivity value of $\kappa_z = 9.690 \times 10^3\mathrm{m}^2\ \mathrm{d}^{-1}$ and uniform initial conditions of $(P_0, V_0, Z_0) = (1.365, 1.043 \times 10^{-7}, 0.8876)$ in non-dimensional values. The blue line represents the ode45 solution, the red line represents the pdepe solution with resolution 0.01, and there is also a black line showing the pdepe solution with resolution 0.1. Figure (b) shows a larger image of Z in order to see the difference in solution. Parameter values are given in Table 4.1 with $\mathrm{c_v} = 1.84 \times 10^{-11}\mathrm{m}^3\mathrm{d}^{-1}$, $K_{\mathrm{IR}} = 7.35 \times 10^9\mathrm{m}^{-3}$, $K_{\mathrm{GR}} = 1.09 \times 10^9\mathrm{m}^{-3}$ and $(\gamma, \nu) = (0.1, 1)\mathrm{d}^{-1}$.

Appendix C

Licenses

C.1 License for Figure 3.11(a)

This is a License Agreement between Nicola Lloyd ("You") and American Society for Microbiology ("American Society for Microbiology") provided by Copyright Clearance Center ("CCC"). The license consists of your order details, the terms and conditions provided by American Society for Microbiology, and the payment terms and conditions.

All payments must be made in full to CCC. For payment instructions, please see information listed at the bottom of this form.

License Number: 2283650960675

License date: Oct 07, 2009

Licensed content publisher: American Society for Microbiology

Licensed content publication: Applied and Environmental Microbiology

Licensed content title: Viral Impacts on Total Abundance and Clonal Composition of the Harmful Bloom-Forming Phytoplankton Heterosigma akashiwo

Licensed content author: Kenji Tarutani, Mineo Yamaguchi

Licensed content date: Nov 1, 2000

Volume: 66

Issue: 11

Start page: 4916

End page: 4920

Type of Use: Dissertation/Thesis

Format: Print and electronic

Portion: Figures/tables/images

Number of figures/tables: 1

Title of your thesis / dissertation: Viral infection and predation of phytoplankton residing in a turbulent environment

Expected completion date: Mar 2010

Estimated size(pages): 200

Total: 0.00 GBP

Terms and Conditions

The publisher for this copyrighted material is the American Society for Microbiology (ASM). By clicking "accept" in connection with completing this licensing transaction, you agree that the following terms and conditions apply to this transaction (along with the Billing and Payment terms and conditions established by Copyright Clearance Center, Inc. ("CCC"), at the time that you opened your Rightslink account and that are available at any time at http://myaccount.copyright.com).

ASM hereby grants to you a non-exclusive license to use this material. Licenses are for one-time use only with a maximum distribution equal to the number that you identified in the licensing process; any form of republication must be completed within 1 year from the date hereof (although copies prepared before then may be distributed thereafter); any permission for electronic format posting is limited to the edition/volume of that online publication. The copyright of all material specified remains with ASM, and permission for reproduction is limited to the formats and products indicated in your license. The text may not be altered in any way without the express permission of the copyright owners.

The licenses may be exercised anywhere in the world.

You must include the copyright and permission notice in connection with any reproduction of the licensed material, i.e. Journal name, year, volume, page numbers, DOI and reproduced/amended with permission from American Society for Microbiology. The following conditions apply to photocopies: (a) The copies must be of high quality and match the standard of the original article, (b) The copies must be a true reproduction word for word, (c) No proprietary/trade names may be substituted, (d) No additional text, tables or figures may be added to the original text, (e) The integrity of the article should be preserved, i.e., no advertisements will be printed on the article, (f) The above permission does NOT include rights for any electronic reproduction - CD ROM, diskette or in any other format.

The following conditions apply to translations: (a) The translation must be of high

quality and match the standard of the original article, (b) The translation must be a true reproduction word for word, (c) All drug names must be generic; no proprietary/trade names may be substituted, (d) No additional text, tables or figures may be added to the translated text, (e) The integrity of the article should be preserved, i.e., no advertisements will be printed on the article, (f) The permission does NOT include rights for any electronic reproduction - CD - ROM, diskette or in any other format, (g) The translated version of ASM material must also carry a disclaimer in English and in the language of the translation. The two versions (English and other language) of the disclaimer MUST appear on the inside front cover or at the beginning of the translated material as follows: The American Society for Microbiology takes no responsibility for the accuracy of the translation from the published English original and is not liable for any errors which may occur. No responsibility is assumed, and responsibility is hereby disclaimed, by the American Society for Microbiology for any injury and/or damage to persons or property as a matter of product liability, negligence or otherwise, or from any use or operation of methods, products, instructions or ideas presented in the Journal. Independent verification of diagnosis and drug dosages should be made. Discussions, views, and recommendations as to medical procedures, choice of drugs and drug dosages are the responsibility of the authors, (h) This license does NOT apply to translations made of manuscripts published ahead of print as "[ASM Journal] Accepts" papers. Translation permission is granted only for the final published version of the ASM article. Furthermore, articles translated in their entirety must honor the ASM embargo period, and thus may not appear in print or online until 6 months after the official publication date in the original ASM journal.

E-Books must be password protected. E-Book permission is only granted for those requests that meet ASM's definition of an E-Book, as follows: An E-Book is the electronic version of a textbook that can be ordered on-line and used instead of the printed text. Students are given a pass-code and they are allowed to download it once to their desktop. Restricted access means that students are not permitted to share an account. No other electronic book uses are permitted.

While you may exercise the rights licensed immediately upon issuance of the license at the end of the licensing process for the transaction, provided that you have disclosed complete and accurate details of your proposed use, no license is finally effective unless and until full payment is received from you (either by ASM or by CCC) as provided in CCC's Billing and Payment terms and conditions. If full payment is not received on a timely basis, then any license preliminarily granted shall be deemed automatically revoked and shall be void as if never granted. In addition, permission granted is contingent upon author permission, which you MUST obtain, and appropriate credit (see item number 3 for details). If you fail to comply with any material provision of this license, ASM shall be entitled to revoke this license immediately and retain fees paid for the grant of the license. Further, in the event that you breach any of these

terms and conditions or any of CCC's Billing and Payment terms and conditions, the license is automatically revoked and shall be void as if never granted. Use of materials as described in a revoked license, as well as any use of the materials beyond the scope of an unrevoked license, may constitute copyright infringement and ASM reserves the right to take any and all action to protect its copyright in the materials.

ASM reserves all rights not specifically granted in the combination of (i) the license details provided by you and accepted in the course of this licensing transaction, (ii) these terms and conditions and (iii) CCC's Billing and Payment terms and conditions.

ASM makes no representations or warranties with respect to the licensed material and adopts on its own behalf the limitations and disclaimers established by CCC on its behalf in its Billing and Payment terms and conditions for this licensing transaction.

You hereby indemnify and agree to hold harmless ASM and CCC, and their respective officers, directors, employees and agents, from and against any and all claims arising out of your use of the licensed material other than as specifically authorized pursuant to this license.

This license is personal to you, but may be assigned or transferred by you to a business associate (or to your employer) if you give prompt written notice of the assignment or transfer to the publisher. No such assignment or transfer shall relieve you of the obligation to pay the designated license fee on a timely basis (although payment by the identified assignee can fulfill your obligation).

This license may not be amended except in a writing signed by both parties (or, in the case of ASM, by CCC on ASM 's behalf).

Objection to Contrary terms: ASM hereby objects to any terms contained in any purchase order, acknowledgment, check endorsement or other writing prepared by you, which terms are inconsistent with these terms and conditions or CCC's Billing and Payment terms and conditions. These terms and conditions, together with CCC's Billing and Payment terms and conditions (which are incorporated herein), comprise the entire agreement between you and ASM (and CCC) concerning this licensing transaction. In the event of any conflict between your obligations established by these terms and conditions and those established by CCC's Billing and Payment terms and conditions, these terms and conditions shall control.

The following terms and conditions apply to Commercial Photocopy and Commercial Reprint requests and should be considered by requestors to be additional terms. All other ASM terms and conditions indicating how the content may and may not be used also apply.

Limitations of Use:

The Materials you have requested permission to reuse in a commercial reprint or commercial photocopy are only for the use that you have indicated in your request, and they MAY NOT be used for either resale to others or republication to the public.

Further, you may not decompile, reverse engineer, disassemble, rent, lease, loan, sell, sublicense, or create derivative works from the Materials without ASM's prior written permission.

Revocation: This license transaction shall be governed by and construed in accordance with the laws of Washington, DC. You hereby agree to submit to the jurisdiction of the federal and state courts located in Washington, DC for purposes of resolving any disputes that may arise in connection with this licensing transaction. ASM or Copyright Clearance Center may, within 30 days of issuance of this License, deny the permissions described in this License at their sole discretion, for any reason or no reason, with a full refund payable to you. Notice of such denial will be made using the contact information provided by you. Failure to receive such notice will not alter or invalidate the denial. In no event will ASM or Copyright Clearance Center be responsible or liable for any costs, expenses or damage incurred by you as a result of a denial of your permission request, other than a refund of the amount(s) paid by you to ASM and/or Copyright Clearance Center for denied permissions. v1.4

Gratis licenses (referencing $0 in the Total field) are free. Please retain this printable license for your reference. No payment is required.

If you would like to pay for this license now, please remit this license along with your payment made payable to "COPYRIGHT CLEARANCE CENTER" otherwise you will be invoiced within 30 days of the license date. Payment should be in the form of a check or money order referencing your account number and this license number 2283650960675. If you would prefer to pay for this license by credit card, please go to http://www.copyright.com/creditcard to download our credit card payment authorization form.

Make Payment To: Copyright Clearance Center Dept 001 P.O. Box 843006 Boston, MA 02284-3006

If you find copyrighted material related to this license will not be used and wish to cancel, please contact us referencing this license number 2283650960675 and noting the reason for cancellation.

Questions? customercare@copyright.com or +1-877-622-5543 (toll free in the US) or +1-978-646-2777.

C.2 License for Figure 3.12(a)

Dear Nicola

Thank you for your email request. Permission is granted for you to use the material below for your thesis/dissertation subject to the usual acknowledgements and on the understanding that you will reapply for permission if you wish to distribute or publish your thesis/dissertation commercially.

Kind Regards

Katie B Wade

Permissions Assistant Wiley-Blackwell 9600 Garsington Road Oxford OX4 2DQ UK Tel: +44 (0) 1865 476149 Fax: +44 (0) 1865 471158 Email: katie.wade@wiley.com

From: Lloyd, Nicola [mailto:N.Lloyd@liverpool.ac.uk] Sent: 07 October 2009 14:20 To: Permission Requests - UK Subject: Permission to reprint material

I am seeking permission to reprint Figure 4 from the article:

Title: Feeding by the Heterotrophic Dinoflagellate Oxyrrhis Marina on the Red-Tide Raphidophyte Heterosigma akashiwo: a Potential Biological Method to Control Red Tides Using Mass-Cultured Grazers.

Authors: Hae Jin Jeong, Jae Seong Kim, Yeong Du Yoo, Seong Taek Kim, Tae Hoon Kim, Myung Gil Park, Chang Hoon Lee, Kyeong Ah Seong, Nam Seon Kang and Jae Hyung Shim.

Journal: Journal of Eukaryotic Microbiology, Volume: 50, Issue: 4, Year: 2003, Pages: 274-282.

I wish to include the figure within my PhD thesis. I expect to finish my PhD during early 2010. The title will be: Viral infection and predation of phytoplankton residing in a turbulent environment.

I don't wish to edit or amend the figure.

Thanks

Nikki Lloyd

Bibliography

Abbott, M. B. and Basco, D. R. (1989), *Computational fluid dynamics: an introduction for engineers*, Longmans scientific and technical, Harlow.

Acrivos, A. and Goddard, J. D. (1965), 'Asymptotic expansions for laminar forced-convection heat and mass transfer', *Journal of fluid mechanics* **23**, 273 – 291.

Acrivos, A. and Taylor, T. D. (1962), 'Heat and mass transfer from single spheres in Stokes flow', *Physics of fluids* **5**(4), 387 – 394.

Anderson, G. C., Comita, G. W. and Engstromheg, V. (1955), 'A note on the phytoplankton-zooplankton relationships in 2 lakes in Washington', *Ecology* **36**(4), 757 – 759.

Anderson, R. M. and May, R. M. (1981), 'The population-dynamics of micro-parasites and their invertebrate hosts', *Philosophical transactions of the royal societ of London series B-biological sciences* **291**(1054), 451 – 524.

Bailey, K. M. and Batty, R. S. (1983), 'A laboratory study of predation by *Aurelia aurita* on larval herring (*Clupea harengus*) - experimental observations compared with model predictions', *Marine biology* **72**(3), 295 – 301.

Batchelor, G. K. (1967), *An introduction to fluid dynamics*, Cambridge University Press.

Batchelor, G. K. (1979), 'Mass-transfer from a particle suspended in fluid with a steady linear ambient velocity distribution', *Journal of fluid mechanics* **95**.

Batchelor, G. K. (1980), 'Mass-transfer from small particles suspended in turbulent fluid', *Journal of fluid mechanics* **98**.

Bearon, R. N. and Grünbaum, D. (2008), 'From individual behaviour to population models: A case study using swimming algae', *Journal of theoretical biology* **251**(4), 679 – 697.

Bearon, R. N., Grünbaum, D. and Cattolico, R. A. (2004), 'Relating cell-level swimming behaviors to vertical population distributions in *Heterosigma akashiwo*

(Raphidophyceae), a harmful alga', *Limnology and oceanography* **49**(2), 607 – 613.

Bearon, R. N., Grünbaum, D. and Cattolico, R. A. (2006), 'Effects of salinity structure on swimming behavior and harmful algal bloom formation in *Heterosigma akashiwo*, a toxic Raphidophyte', *Marine ecology-progress series* **306**, 153 – 163.

Beltrami, E. and Carroll, T. O. (1994), 'Modeling the role of viral disease in recurrent phytoplankton blooms', *Journal of mathematical biology* **32**(8), 857 – 863.

Bergh, O., Borsheim, K. Y., Bratbak, G. and Heldal, M. (1989), 'High abundance of viruses found in aquatic environments', *Nature* **340**(6233), 467 – 468.

Boney, A. D. (1989), *Phytoplankton*, second edn, Edward Arnold.

Bradie, B. (2006), *A friendly introduction to numerical analysis*, Pearson.

Bratbak, G., Egge, J. K. and Heldal, M. (1993), 'Viral mortality of the marine alga *Emiliania huxleyi* (haptophyceae) and termination of algal blooms', *Marine ecology-progress series* **93**(1-2), 39 – 48.

Bratbak, G., Jacobsen, A., Heldal, M., Nagasaki, K. and Thingstad, F. (1998), 'Virus production in *Phaeocystis pouchetii* and its relation to host cell growth and nutrition', *Aquatic microbial ecology* **16**(1), 1 – 9.

Britton, N. F. (2003), *Essential mathematical biology*, Springer-Verlag, London.

Brussaard, C. P. D. (2004), 'Viral control of phytoplankton populations - a review', *Journal of eukaryotic microbiology* **51**(2), 125 – 138.

Buskey, E. J. (2008), 'How does eutrophication affect the role of grazers in harmful algal bloom dynamics?', *Harmful algae* **8**(1), 152 – 157.

Carpenter, S. R., Cottingham, K. L. and Stow, C. A. (1994), 'Fitting predator-prey models to time-series with observation errors', *Ecology* **75**(5), 1254 – 1264.

Chattopadhyay, J. and Pal, S. (2002), 'Viral infection on phytoplankton-zooplankton system - a mathematical model', *Ecological modelling* **151**(1), 15 – 28.

Clift, R., Grace, J. R. and Weber, M. E. (1978), *Bubbles, drops and particles*, Academic Press, New York.

Clough, J. and Strom, S. (2005), 'Effects of *Heterosigma akashiwo* (Raphidophyceae) on protist grazers: laboratory experiments with ciliates and heterotrophic dinoflagellates', *Aquatic microbial ecology* **39**, 121 – 134.

Coveney, M. F., Cronberg, G., Enell, M., Larsson, K. and Olofsson, L. (1977), 'Phytoplankton, zooplankton and bacteria - standing crop and production relationships in a eutrophic lake', *Oikos* **29**(1), 5 – 21.

Cropp, R. and Norbury, J. (2009), 'Simple predator-prey interactions control dynamics in a plankton food web model', *Ecological modelling* **220**(13-14), 1552 – 1565.

Davidson, P. A. (2006), *Turbulence: an introduction for scientists and engineers*, Oxford University Press.

Demir, E., Coyne, K. J., Doblin, M. A., Handy, S. M. and Hutchins, D. A. (2008), 'Assessment of microzooplankton grazing on *Heterosigma akashiwo* using a species-specific approach combining quantitative real-time PCR (QPCR) and dilution methods', *Microbial ecology* **55**(4), 583 – 594.

Dionysiou, D. (2010), 'Overview: Harmful algal blooms and natural toxins in fresh and marine waters - exposure, occurrence, detection, toxicity, control, management and policy.', *Toxicon* **55**(5), 907 – 8.

Dodds, J. A. (1979), 'Viruses of marine-algae', *Experientia* **35**(4), 440 – 442.

Dubois, D. M. (1975), 'A model of patchiness for prey predator plankton populations', *Ecological Modelling* 1(1), 67 – 80.

Edelstein-Keshet, L. (2005), *Mathematical models in biology*, Philadelphia : S. I. A. M.

Elliott, J. A. and Thackeray, S. J. (2004), 'The simulation of phytoplankton in shallow and deep lakes using PROTECH', *Ecological Modelling* **178**(3-4), 357 – 369.

Evans, G. T. (1989), 'The encounter speed of moving predator and prey', *Journal of plankton research* **11**(2), 415 – 417.

Evans, T., Bowers, R. G. and Mortimer, M. (2007), 'Modelling the stability of Stx lysogens', *Journal of theoretical biology* **248**(2), 241 – 250.

Falkowski, P. G. and Wilson, C. (1992), 'Phytoplankton productivity in the north pacific-ocean since 1900 and implications for absorption of anthropogenic CO2', *Nature* **358**(6389), 741 – 743.

Ganf, G. G. (1974), 'Diurnal mixing and vertical distribution of phytoplankton in a shallow equatorial lake (Lake George, Uganda)', *Journal of ecology* **62**(2), 611 – 629.

Gao, K. S., Guan, W. C. and Helbling, E. W. (2007), 'Effects of solar ultraviolet radiation on photosynthesis of the marine red tide alga *Heterosigma akashiwo* (Raphidophyceae)', *Journal of photochemistry and photobiology B-biology* **86**(2), 140 – 148.

Gerritsen, J. and Strickler, J. R. (1977), 'Encounter probabilities and community structure in zooplankton - mathematical-model', *Journal of the fisheries research board of Canada* **34**(1), 73 – 82.

Gons, H. J., Hoogveld, H. L., Simis, S. G. H. and Tijdens, M. (2006), 'Dynamic modelling of viral impact on cyanobacterial populations in shallow lakes: implications of burst size', *Journal of the marine biological association of the united kingdom* **86**(3), 537 – 542.

Graham, L. E. and Wilcox, L. W. (2000), *Algae*, Prentice Hall.

Graham, S. L. and Strom, S. L. (2010), 'Growth and grazing of microzooplankton in response to the harmful alga *Heterosigma akashiwo* in prey mixtures', *Aquatic microbial ecology* **59**(2), 111 – 124.

Gunter, G., Williams, R. H., Davis, C. C. and Smith, F. G. W. (1948), 'Catastrophic mass mortality of marine animals and coincident phytoplankton bloom on the west coast of Florida, November 1946 to August 1947', *Ecological monographs* **18**(3), 309 – 324.

Haigh, J. and Smith, J. M. (1972), 'Can there be more predators than prey', *Theoretical population biology* **3**(3), 290 – 299.

Hardin, G. (1960), 'Competitive exclusion principle', *Science* **131**(3409), 1292 – 1297.

Hays, G. C., Richardson, A. J. and Robinson, C. (2005), 'Climate change and marine plankton', *Trends in ecology & evolution* **20**(6), 337 – 344.

Heinbokel, J. F. (1978), 'Studies on functional role of tintinnids in southern-california bight .1. grazing and growth-rates in laboratory cultures', *Marine biology* **47**(2), 177 – 189.

Holling, C. S. (1959), 'The components of predation as revealed by a study of small mammal predation of the European Pine Sawfly', *Canadian entomologist* **91**, 293 – 320.

Holmes, R. W., Williams, P. M. and Eppley, R. W. (1967), 'Red water in La Jolla bay 1964-1966', *Limnology and oceanography* **12**(3), 503 – 512.

Huisman, J., Sharples, J., Stroom, J. M., Visser, P. M., Kardinaal, W. E. A., Verspagen, J. M. H. and Sommeijer, B. (2004), 'Changes in turbulent mixing shift competition for light between phytoplankton species', *Ecology* **85**(11), 2960 – 2970.

Huisman, J. and Sommeijer, B. (2002), 'Population dynamics of sinking phytoplankton in light-limited environments: simulation techniques and critical parameters', *Journal of sea research* **48**(2), 83 – 96.

Huisman, J. and Weissing, F. J. (1995), 'Competition for nutrients and light in a mixed water column - a theoretical-analysis', *American naturalist* **146**(4), 536 – 564.

Hutchinson, G. E. (1961), 'The paradox of the plankton', *American naturalist* **95**(882), 137 – 145.

Ishikawa, T., Simmonds, M. P. and Pedley, T. J. (2006), 'Hydrodynamic interaction of two swimming model micro-organisms', *Journal of fluid mechanics* **568**, 119 – 160.

Jäger, C. G., Diehl, S. and Emans, M. (2010), 'Physical determinants of phytoplankton production, algal stoichiometry, and vertical nutrient fluxes.', *American naturalist* **175**(4), E91 – E104.

Jeong, H. J., Kim, J. S., Yeong, D. Y., Kim, S. T., Kim, T. H., Park, M. G., Lee, C. H., Seong, K. A., Kang, N. S. and Shim, J. H. (2003), 'Feeding by the heterotrophic dinoflagellate *Oxyrrhis marina* on the red-tide Raphidophyte *Heterosigma akashiwo*: a potential biological method to control red tides using mass-cultured grazers', *Journal of eukaryotic microbiology* **50**(4), 274 – 282.

Jiang, H. S., Meneveau, C. and Osborn, T. R. (2002), 'The flow field around a freely swimming copepod in steady motion. part II: Numerical simulation', *Journal of plankton research* **24**(3), 191 – 213.

Kamykowski, D., Reed, R. E. and Kirkpatrick, G. J. (1992), 'Comparison of sinking velocity, swimming velocity, rotation and path characteristics among 6 marine dinoflagellate species', *Marine biology* **113**(2), 319 – 328.

Karp-Boss, L., Boss, E. and Jumars, P. A. (1996), 'Nutrient fluxes to planktonic osmotrophs in the presence of fluid motion', *Oceanography and marine biology* **34**, 71 – 107.

Keeling, M. J. and Rohani, P. (2008), *Modeling infectious diseases in humans and animals*, Princeton University Press.

Kemp, W. M. and Mitsch, W. J. (1979), 'Turbulence and phytoplankton diversity - general-model of the paradox of plankton', *Ecological modelling* **7**(3), 201 – 222.

Kimmance, S. A., Atkinson, D. and Montagnes, D. J. S. (2006), 'Do temperature-food interactions matter? responses of production and its components in the model heterotrophic flagellate oxyrrhis marina', *Aquatic microbial ecology* **42**(1), 63 – 73.

Kiorboe, T. and Visser, A. W. (1999), 'Predator and prey perception in copepods due to hydromechanical signals', *Marine ecology-progress series* **179**, 81 – 95.

Kreyszig, E. (1962), *Advanced engineering mathematics*, 8th edn, Wiley, New York.

Kubo, R. (1965), *Statistical mechanics: an advanced course with problems and solutions*, North-Holland, Amsterdam.

Lanerolle, L. W. J., Tomlinson, M. C., Gross, T. F., Aikman, F., Stumpf, R. P., Kirkpatrick, G. J. and Pederson, B. A. (2006), 'Numerical investigation of the effects of upwelling on harmful algal blooms off the west Florida coast', *Estuarine coastal and shelf science* **70**(4), 599 – 612.

Lawrence, J. E., Brussaard, C. P. D. and Suttle, C. A. (2006), 'Virus-specific responses of *Heterosigma akashiwo* to infection', *Applied and environmental microbiology* **72**(12), 7829 – 7834.

Lawrence, J. E., Chan, A. M. and Suttle, C. A. (2001), 'A novel virus (HaNIV) causes lysis of the toxic bloom-forming alga *Heterosigma akashiwo* (Raphidophyceae)', *Journal of phycology* **37**(2), 216 – 222.

Lazier, J. R. N. and Mann, K. H. (1989), 'Turbulence and the diffusive layers around small organisms', *Deep-sea research part A-oceanographic research papers* **36**(11), 1721 – 1733.

Leal, L. G. (2007), *Advanced transport phenomena: fluid mechanics and convective transport processes*, Cambridge University Press.

Lewis, D. M. (2003), 'Planktonic encounter rates in homogeneous isotropic turbulence: the case of predators with limited fields of sensory perception', *Journal of theoretical biology* **222**(1), 73 – 97.

Lewis, D. M. and Bala, S. I. (2006), 'Plankton predation rates in turbulence: A study of the limitations imposed on a predator with a non-spherical field of sensory perception', *Journal of theoretical biology* **242**, 44 – 61.

Lewis, D. M. and Pedley, T. J. (2000), 'Planktonic contact rates in homogeneous isotropic turbulence: Theoretical predictions and kinematic simulations', *Journal of theoretical biology* **205**(3), 377 – 408.

Lewis, D. M. and Pedley, T. J. (2001), 'The influence of turbulence on plankton predation strategies', *Journal of theoretical biology* **210**(3), 347 – 365.

Mackenzie, B. R. and Leggett, W. C. (1991), 'Quantifying the contribution of small-scale turbulence to the encounter rates between larval fish and their zooplankton prey - effects of wind and tide', *Marine ecology-progress series* **73**(2-3), 149 – 160.

Magar, V., Goto, T. and Pedley, T. J. (2003), 'Nutrient uptake by a self-propelled steady squirmer', *Quarterly journal of mechanics and applied mathematics* **56**, 65 – 91.

Magar, V. and Pedley, T. J. (2005), 'Average nutrient uptake by a self-propelled unsteady squirmer', *Journal of fluid mechanics* **539**, 93 – 112.

Malchow, H., Hilker, F. M., Sarkar, R. R. and Brauer, K. (2005), 'Spatiotemporal patterns in an excitable plankton system with lysogenic viral infection', *Mathematical and computer modelling* **42**(9-10), 1035 – 1048.

Mariani, P., Botte, V. and d'alcala, M. R. (2005), 'An object-oriented model for the prediction of turbulence effects on plankton', *Deep-sea research part II-topical studies in oceanography* **52**(9-10), 1287 – 1307.

Martinez, R., Orive, E., Laza-Martinez, A. and Seoane, S. (2010), 'Growth response of six strains of *Heterosigma akashiwo* to varying temperature, salinity and irradiance conditions', *Journal of plankton research* **32**(4), 529 – 538.

Matsuyama, Y., Miyamoto, M. and Kotani, Y. (1999), 'Grazing impacts of the heterotrophic dinoflagellate *Polykrikos kofoidii* on a bloom of *Gymnodinium catenatum*', *Aquatic microbial ecology* **17**(1), 91 – 98.

May, R. M. (1974), *Stability and complexity in model ecosystems*, second edn, Princeton University Press, Princeton.

Mazzocchi, M. G. and Paffenhofer, G. A. (1999), 'Swimming and feeding behaviour of the planktonic copepod clausocalanus furcatus', *Journal of plankton research* **21**(8), 1501 – 1518.

Menden-Deuer, S. and Grünbaum, D. (2006), 'Individual foraging behaviors and population distributions of a planktonic predator aggregating to phytoplankton thin layers', *Limnology and oceanography* **51**(1), 109 – 116.

Metcalfe, A. M., Pedley, T. J. and Thingstad, T. F. (2004), 'Incorporating turbulence into a plankton food-web model', *Journal of marine systems* **49**(1-4), 105 – 122.

Moin, P. and Mahesh, K. (1998), 'Direct numerical simulation: A tool in turbulence research', *Annual review of fluid mechanics* **30**, 539 – 578.

Montagnes, D. J. S. (1996), 'Growth responses of planktonic ciliates in the genera strobilidium and strombidium', *Marine ecology-progress series* **130**(1-3), 241 – 254.

Muelbert, J. H., Lewis, M. R. and Kelley, D. E. (1994), 'The importance of small-scale turbulence in the feeding of herring larvae', *Journal of plankton research* **16**(8), 927 – 944.

Murray, A. G. and Jackson, G. A. (1992), 'Viral dynamics - a model of the effects of size, shape, motion and abundance of single-celled planktonic organisms and other particles', *Marine ecology-progress series* **89**(2-3), 103 – 116.

Murray, J. D. (2003), *Mathematical biology 1: an introduction*, third edn, New York. Springer.

Nagasaki, K., Ando, M., Imai, I., Itakura, S. and Ishida, Y. (1994), 'Virus-like particles in *Heterosigma akashiwo* (Raphidophyceae) - a possible red tide disintegration mechanism', *Marine biology* **119**(2), 307 – 312.

Nagasaki, K., Ando, M., Itakura, S., Imai, I. and Ishida, Y. (1994), 'Viral mortality in the final stage of *Heterosigma akashiwo* (Raphidophyceae) red tide', *Journal of plankton research* **16**(11), 1595 – 1599.

Nagasaki, K., Tarutani, K. and Yamaguchi, M. (1999), 'Growth characteristics of *Heterosigma akashiwo* virus and its possible use as a microbiological agent for red tide control', *Applied and environmental microbiology* **65**(3), 898 – 902.

Nagasaki, K. and Yamaguchi, M. (1997), 'Isolation of a virus infectious to the harmful bloom causing microalga *Heterosigma akashiwo* (Raphidophyceae)', *Aquatic microbial ecology* **13**(2), 135 – 140.

Nybakken, J. W. and Bertness, M. D. (2005), *Marine biology: an ecological approach*, sixth edn, Pearson Education Inc., publishing as Benjamin Cummings.

Okubo, A. and Levin, S. A. (2002), *Diffusion and ecological problems - modern perspectives*, second edn, Springer - Verlag.

Orszag, S. A. and Patterson, G. S. (1972), 'Numerical simulation of 3-dimensional homogeneous isotropic turbulence', *Physical review letters* **28**(2), 76 – 79.

Osborn, T. R. (1980), 'Estimates of the local-rate of vertical diffusion from dissipation measurements', *Journal of physical oceanography* **10**(1), 83 – 89.

Pasquero, C. (2005), 'Differential eddy diffusion of biogeochemical tracers', *Geophysical research letters* **32**(17).

Pecseli, H. L., Trulsen, J. K. and Fiksen, O. (2010), 'Predator-prey encounter rates in turbulent water: Analytical models and numerical tests', *Progress in oceanography* **85**(3-4), 171 – 179.

Pennington, W. (1941), 'The control of the numbers of freshwater phytoplankton by small invertebrate animals', *Journal of ecology* **29**, 204 – 211.

Pingree, R. D., Pugh, P. R., Holligan, P. M. and Forster, G. R. (1975), 'Summer phytoplankton blooms and red tides along tidal fronts in approaches to English-Channel', *Nature* **258**(5537), 672 – 677.

Platt, T. (1972), 'Local phytoplankton abundance and turbulence', *Deep-sea research* **19**(3), 183 – 187.

Plumb, R. A. (1979), 'Eddy fluxes of conserved quantities by small-amplitude waves', *Journal of atmospheric sciences* **36**(9), 1699 – 1704.

Porter, K. G. (1976), 'Enhancement of algal growth and productivity by grazing zooplankton', *Science* **192**(4246), 1332 – 1334.

Prinsenberg, S. J. and Rattray, M. (1975), 'Effects of continental slope and variable Brunt-Vaisala frequency on coastal generation of internal tides', *Deep-sea research* **22**(4), 251 – 263.

Purcell, E. M. (1977), 'Life at low Reynolds-number', *American journal of physics* **45**(1), 3 – 11.

Rejas, D. and Muylaert, K. (2010), 'Bottom-up and top-down control of phytoplankton growth in an amazonian varzea lake', *Fundamental and applied limnology* **176**(3), 225 – 234.

Rhodes, C. J. and Anderson, R. M. (2008), 'Contact rate calculation for a basic epidemic model', *Mathematical biosciences* **216**(1), 56 – 62.

Rhodes, C. J. and Martin, A. P. (2010), 'The influence of viral infection on a plankton ecosystem undergoing nutrient enrichment.', *Journal of theoretical biology* **265**(3), 225 – 237.

Rhodes, C. J., Truscott, J. E. and Martin, A. P. (2008), 'Viral infection as a regulator of oceanic phytoplankton populations', *Journal of marine systems* **74**(1-2), 216 – 226.

Ross, O. N. and Sharples, J. (2004), 'Recipe for 1-D Lagrangian particle tracking models in space-varying diffusivity', *Limnology and oceanography-methods* **2**, 289 – 302.

Rothschild, B. J. and Osborn, T. R. (1988), 'Small-scale turbulence and plankton contact rates', *Journal of plankton research* **10**(3), 465 – 474.

Sauer, T. (2006), *Numerical analysis*, Pearson.

Sharples, J., Moore, C. M., Rippeth, T. P., Holligan, P. M., Hydes, D. J., Fisher, N. R. and Simpson, J. H. (2001), 'Phytoplankton distribution and survival in the thermocline', *Limnology and oceanography* **46**(3), 486 – 496.

Shertzer, K. W., Ellner, S. P., Fussmann, G. F. and Hairston, N. G. (2002), 'Predator-prey cycles in an aquatic microcosm: testing hypotheses of mechanism', *Journal of animal ecology* **71**(5), 802 – 815.

Shikata, T., Yoshikawa, S., Matsubara, T., Tanoue, W., Yamasaki, Y., Shimasaki, Y., Matsuyama, Y., Oshima, Y., Jenkinson, I. R. and Honjo, T. (2008), 'Growth dynamics of *Heterosigma akashiwo* (Raphidophyceae) in Hakata Bay, Japan', *European journal of phycology* **43**(4), 395 – 411.

Sieber, M., Malchow, H. and Schimansky-Geier, L. (2007), 'Constructive effects of environmental noise in an excitable prey-predator plankton system with infected prey', *Ecological complexity* **4**(4), 223 – 233.

Singh, B. K., Chattopadhyay, J. and Sinha, S. (2004), 'The role of virus infection in a simple phytoplankton zooplankton system', *Journal of theoretical biology* **231**(2), 153 – 166.

Skeel, R. D. and Berzins, M. (1990), 'A method for the spatial discretization of parabolic equations in one space variable', *SIAM journal on scientific and statistical computing* **11**(1), 1 – 32.

Smayda, T. J. (1998), *Ecophysiology and blooms dynamics of Heterosigma akashiwo (Raphidophyceae). In: Anderson, D. M., Cembella, A. D. and Hallegraeff, G. M. (eds.), Physiological Ecology of Harmful Algal Blooms*, Springer-Verlag.

Stelzer, C. P. (1998), 'Feeding behaviour of the rotifer *Ascomorpha ovalis*: functional response, handling time and exploitation of individual Ceratium cells', *Journal of plankton research* **20**(6), 1131 – 1144.

Strom, S. L., Macri, E. L. and Olson, M. B. (2007), 'Microzooplankton grazing in the coastal Gulf of Alaska: Variations in top-down control of phytoplankton', *Limnology and oceanography* **52**(4), 1480 – 1494.

Suttle, C. A. (2000), *Ecological, evolutionary, and geochemical consequences of viral infection of cyanobacteria and eukaryotic algae. In: Hurst, C.J. (ed.), Viral Ecology*, Academic Press.

Suttle, C. A. (2007), 'Marine viruses - major players in the global ecosystem', *Nature reviews microbiology* **5**(10), 801 – 812.

Suttle, C. A., Chan, A. M. and Cottrell, M. T. (1990), 'Infection of phytoplankton by viruses and reduction of primary productivity', *Nature* **347**(6292), 467 – 469.

Tai, V., Lawrence, J. E., Lang, A. S., Chan, A. M., Culley, A. I. and Suttle, C. A. (2003), 'Characterization of HaRNAV, a single-stranded RNA virus causing lysis of *Heterosigma akashiwo* (Raphidophyceae)', *Journal of phycology* **39**(2), 343 – 352.

Tarutani, K., Nagasaki, K. and Yamaguchi, M. (2000), 'Viral impacts on total abundance and clonal composition of the harmful bloom-forming phytoplankton *Heterosigma akashiwo*', *Applied and environmental microbiology* **66**(11), 4916 – +.

Tarutani, K., Nagasaki, K. and Yamaguchi, M. (2006), 'Virus adsorption process determines virus susceptibility in *Heterosigma akashiwo* (Raphidophyceae)', *Aquatic microbial ecology* **42**(3), 209 – 213.

Tennekes, H. and Lumley, J. L. (1972), *A first course in turbulence*, M.I.T Press.

Thorn, G. J. and Bearon, R. N. (2010), 'Transport of spherical gyrotactic organisms in general three-dimensional flow fields', *Physics of fluids* **22**(4).

Thyrhaug, R., Larsen, A., Thingstad, T. F. and Bratbak, G. (2003), 'Stable coexistence in marine algal host-virus systems', *Marine ecology-progress series* **254**, 27 – 35.

Tomas, C. R. (1979), '*Olisthodiscus luteus* (Chrysophyceae) .3. uptake and utilization of Nitrogen and Phosphorus', *Journal of phycology* **15**(1), 5 – 12.

Truscott, J. E. and Brindley, J. (1994), 'Ocean plankton populations as excitable media', *Bulletin of mathematical biology* **56**(5), 981 – 998.

Uttieri, M., Paffenhofer, G. A. and Mazzocchi, M. G. (2008), 'Prey capture in *Clausocalanus furcatus* (Copepoda : Calanoida). The role of swimming behaviour', *Marine biology* **153**(5), 925 – 935.

Uttieri, M., Sabia, L., Cianelli, D., Strickler, J. R. and Zambianchi, E. (2010), 'Lagrangian modelling of swimming behaviour and encounter success in co-occurring copepods: *Clausocalanus furcatus* vs. *Oithona plumifera*', *Journal of marine systems* **81**(1-2), 112 – 121.

Vargo, G. A. (2009), 'A brief summary of the physiology and ecology of *Karenia brevis* Davis (G. Hansen and Moestrup comb. nov.) red tides on the West Florida Shelf and of hypotheses posed for their initiation, growth, maintenance, and termination', *Harmful algae* **8**(4), 573 – 584.

Visser, A. W. (2001), 'Hydromechanical signals in the plankton', *Marine ecology-progress series* **222**, 1 – 24.

Visser, A. W., Mariani, P. and Pigolotti, S. (2009), 'Swimming in turbulence: zooplankton fitness in terms of foraging efficiency and predation risk', *Journal of plankton research* **31**(2), 121 – 133.

Willey, J. M., Sherwood, L. and Woolverton, C. J. (2007), *Prescott, Harley, and Klein's microbiology*, New York ; London : McGraw-Hill Higher Education.

Yang, W. Y., Cao, W., Chung, T. and Morris, J. (2005), *Applied numerical methods using Matlab*, Wiley-Interscience.

Yin, K. D., Song, X. X., Liu, S., Kan, J. J. and Qian, P. Y. (2008), 'Is inorganic nutrient enrichment a driving force for the formation of red tides? A case study of the dinoflagellate *Scrippsiella trochoidea* in an embayment', *Harmful algae* **8**(1), 54 – 59.